Molecularly Imprinted Polymer-Based Sensors for Halal food Control

CHEHASAN CHEUBONG

(Degree)
博士（学術）

(Date of Degree)
2022-03-25

(Date of Publication)
2024-03-25

(Resource Type)
doctoral thesis

(Report Number)
甲第8359号

(URL)
https://hdl.handle.net/20.500.14094/D1008359

Doctoral Dissertation

Molecularly Imprinted Polymer-Based Sensors for Halal food Control
(ハラール食品管理用の分子インプリントポリマーを用いたセンサー)

January 2022

Graduate School of Engineering,

Kobe University

CHEHASAN CHEUBONG

博士論文

Molecularly Imprinted Polymer-Based Sensors for Halal Food Control

(ハラール食品管理用の分子インプリントポリマーを用いたセンサー)

令和 4 年 1 月

神戸大学大学院工学研究科

CHEHASAN CHEUBONG

"And mankind has not been given of knowledge

except a little"

Al-Quran; Al-Isra 17:85

Acknowledgements

"In the name of Allah, the most gracious and the most merciful"

I would first like to thank Allah for giving me everything to complete my Ph.D. study. I would also like to express my gratitude to the most respectable person, Prophet Mohammed (Peace be upon him).

Working in the field of molecular imprinting polymers are challenges for me owing to many interesting ideas to be investigated. For this, it's an honor for me to have a great advisor, Prof. Toshifumi Takeuchi, who has guided me and opened the way for me to comprehend those fields. I really appreciate for your favor, patience, time, and all supports from you during my study. And I would like to express my thankfulness to the nice advisor, Prof. Hideto Minami for your really kind supports me to accomplish my Ph.D. course.

I would like to extend my appreciation to Associate Prof. Hirobumi Sunayama and Assistant Prof. Yukiya Kitayama who have taught and guided me how to perform molecularly imprinted polymers synthesis based on molecular imprinting and post-imprinting modification methods. It was wonderful to have fruitful discussions with you during my Ph.D. course. I also really thank you for helping me preparing documents needed for the completion of my study.

I would like to humbly express my gratitude to, Prof. Ogino and Associate Prof. Ooya for their beneficial suggestions to improve the quality of my Ph.D. dissertation.

I wish to express my gratitude to the Rajamangala University of technology Thanyaburi, Thailand for supporting my Ph.D. funding courses during the Ph.D. study program.

I would never complete my study without full support of my wife, Sumaida Cheubong, and my two beloved kids, Haneen and Haneef Cheubong. "Dear you all! we have done a thousand miles away of going forward together through the hard times and made the fantastic sweet memories of our life together".

I will not forget to express my sincere gratitude to my late father, beloved mother and two older sisters as well as my family members for their prayer day and night.

Lastly, I would like to acknowledge all my colleagues in Takeuchi's laboratory as well as all staff members at administration office of faculty of engineering of Kobe university for their help and support during my study.

Abstract

Molecularly Imprinted Polymer-Based Sensors for Halal Food Control

CHEHASAN CHEUBONG

In this dissertation, I have presented the new strategies to develop the highly selective and sensitive molecularly imprinted polymer (MIP)-based sensors for detection of pork contamination in halal food control.

MIPs are artificial receptors which obtains affinities and low cross-reactivities comparable to those of biological receptors such as antibodies or enzymes. Due to their high stability, easy synthesis, and low costs for production, MIP-based sensors have become attractive because they have the potential to be used as a simple, powerful, and accurate method to detect pork contamination for halal food control.

This dissertation consists of 6 chapters. In the first chapter, I summarized the motivation of this work and the importance for development of facile and rapid sensor for detection of pork contamination in halal food. The halal food industry is important worldwide, owing to the wide distribution of Muslims. Halal food products must be free from non-halal materials, including alcohol, blood, and pork. Nevertheless, many Muslims are concerned that halal meat products might be contaminated with pork or pork derivatives, which are prohibited for Muslims to consume. The contamination of beef products by pork is a cost advantage for manufacturers because pork costs less than beef. Thus, there is a need for tools to ensure that beef is free from pork contamination. These tools must involve highly effective analytical methods, with high sensitivity, rapid detection, and good specificity for detecting pork contamination in halal meats.

In the second chapter, I described the background of this study including halal food control with halal food market and several developed analytical methods for detection of pork contamination in meat extract. And provides interesting examples of MIP-based sensor applications in any areas with their good selectivity.

In the third chapter, I developed a label-free MIP-based QCM sensor for detection of pork contamination. Emulsifier-free precipitation polymerization method is utilized to synthesize molecularly imprinted polymer nanogels (MIP-NGs), capable of porcine serum albumin (PSA) recognition as artificial molecular recognition elements. For the incorporation

of interacting group in the MIP-NGs, pyrrolidyl acrylate (PyA) was used as a functional monomer. After purification of obtained MIP-NGs by ion-exchnage chromatography, the MIP-NGs were then immobilized on quartz crystal microbalance (QCM) sensor for detection of PSA in meat extract samples. The MIP-NGs-based QCM sensors exhibited high affinity (K_a = 6.7×10^7 M^{-1}) and excellent selectivity toward PSA compared to other animal serum albumins but the sensitivity was considerably lower than that of immunosensors. The high PSA specificity of MIP-NGs led to the detection of pork contamination with a detection limit of 1 wt% in real beef extract samples. Thus, the developed sensor provides a new label-free MIP-NGs based QCM sensor to detect pork contamination in halal raw meat samples with high selectivity.

In the fourth chapter, I aimed to investigate and develop a highly sensitive MIP-NGs fluorescence-based sensor for rapid PSA detection with introducing fluorescent reporter molecules (ATTO 647N) into the PSA-imprinted cavities via post-imprinting modifications (PIMs). For the purpose, 4-[2-(*N*- methacrylamido) ethylaminomethyl] benzoic acid (MABA) was used as a functional monomer, in which consist of benzoic acid moiety for interacting with target protein and secondary amine group for conjugation with fluorescent reporter dye as a PIM. The MIP-NGs was prepared by emulsifier-free precipitation polymerization method and purified by a size exclusion chromatography and ion-exchange chromatography. In PIM, obtained MIP-NGs were reacted with ATTO 647N NHS ester to introduce fluorescent signaling property, yielding fluorescent signaling MIP-NGs (F-MIP-NGs). After immobilization of F-MIP-NGs on gold coated sensor chip, the fluorescence response was measured by a custom-made fluorescence microscope equipped with a liquid handling robot. Under the optimum conditions, the developed F-MIP-NGs-based sensor exhibited extremely high sensitivity, with the detection limit of 40 pM, good affinity (K_a=1.6×10^8 M^{-1}) and high selectivity for PSA in comparison to the potentially interfering proteins. The good analytical performance, high recovery rate in real meat extract samples was observed, where the recovery range for PSA was 93–116%. These results indicated that F- MIP-NGs displayed high accuracy in recognizing the target protein PSA, even in real meat extract samples. Moreover, fast detection and very low detection limit of pork contamination indicate great potential ability of the proposed sensor to detect PSA for pork contamination in halal meat samples.

In the fifth chapter, I have successfully developed a sensitive assay using MIP-NGs for the selective detection of pork adulteration in halal food This assay was capable of measuring PSA in PBS and real meat extract. The sensitivity of the assay was better than those of methods

descrived in the three and fourth chapters. The developed assay displayed good repeatability, stability, and selectivity for PSA, compared with four animal serum albumins (BSA, GSA, SSA and RSA). For pork adulteration in halal meat extracts, the assay can detect very low level of contaminated pork. When compared to the conventional ELISA detection, the performance of this assay was better for the detection of pork adulteration in lamb extract samples, and was comparable in beef extract sample. Therefore, the proposed assay is promising for sensitive and rapid detection of pork adulteration in halal meat extracts, make it an attractive alternative to traditional immunoassay.

In sixth chapter as conclusions, I have first developed a novel biosensor using MIP-NGs as artificial antibody for detection of pork contamination in halal meat extracts with excellent sensitivity and selectivity. These MIP-NGs based sensing system were based on synthetic polymer which are stable for chemical/physical stimuli, easy to mass production, and low cost. Therefore, it shows a potential to be alternatives to conventional detection system based on naturally occuring materials such as antibodies and enzymes which are high specificity but low stability. I believe that the proposed sensor is a great potential ability as a new candidate in biosensor applications for halal food control, and should be a powerful tool for other food analysis areas as well. Furthermore, the insights obtained through this study would be a trigger to realize synthetic polymer receptors capable of specific molecular recognition which are beyond natural antibodies.

Table of Contents

List of Schemes and Figures

Schemes

Figures

Figure 5.5 SDS-PAGE analysis of purified Fc domain. Lane 1: Protein marker (Bio-Rad), Lane 2-3: IgG, Lane 4-5: Digested IgG, Lane 6-7: 1st purified Fc domain, Lane 8-9: 2rd purified Fc domain and Lane 10-11: purified deglyocosylated Fc domain.

Figure 5.6 CD spectra of Fc domain (100 nM in 10 mM phosphate buffer, pH 7.4) native (red line) and after incubation (blue line) at 50°C for 12 h.

Figure 5.7 A typical chromatogram of MIP-NGs with the fluorescence intensities of MTRB in MIP-NGs (λ_{ex}: 548 nm at λ_{em}: 570 nm) after two steps purification by size exclusion (Sephadex-G100) and ion-exchange chromatography (DEAE-sephadex).

Figure 5.8 Fluorescence spectra at λ_{ex}: 280 nm of tryptophan residues in MIP-NGs for Fc domain before and after purification by two-steps purification. Fluorescence intensities of tryptophan residues of Fc domain at λ_{em}: 350 nm before and after purification were 218 and 41, respectively. The concentration of obtained MIP-NGs before and after purification was 500 µg/mL.

Figure 5.9 Particle size distributions of MIP-NGs and NIP-NGs after purification by size exclusion chromatography and ion-exchange chromatography determined by DLS. (a): MIP-NGs after purification; Z-average particle size: 21 nm (b): NIP-NGs after purification; Z-average particle size: 18 nm.

Figure 5.10 Fluorescence intensity of the ATTO 647N NHS-ester in MIP-NGs and NIP-NGs after PIM treatment (λex: 647 nm and λem: 668 nm).

Figure 5.11 Fluorescence intensity of the gold-coated glass substrate before (red) and after (blue) the immobilization of F-MIP-NGs.

Figure 5.12 The binding isotherms of fluorescent Fc-MIP-MGs and fluorescent NIP-NGs for Fc domain. The various concentrations of Fc domain (0–1,600 nM) was incubated on NGs-immobilized gold-coated sensors. The error bars were obtained from triplicate experiments.

Figue 5.13 Affinity constants (Ka) for the binding of Fc doamin to fluorescent Fc-MIP-NGs and NIP-NGs, estimated from the relative fluorescence intensity measurements data.

Figure 5.14 Affinity constants (K_a) for the binding of F-MIP-NGs to whole IgG and *deglycosylated Fc domain* estimated from the relative fluorescence intensity measurements data.

Figure 5.15 Relative fluorescence intensities of fluorescent Fc-MIP-NGs (a) and fluorescent NIP-NGs (b) for Fc domain and four competitive proteins: deglycosylated Fc domain, whole IgG and PSA. The protein concentrations were 100 nM. The error bars were obtained from triplicate experiments.

Figure 5.16 Optimization of the blocking reagents on the biomimetic immunosensor of blank (PBS) analysis. The experiments were conducted in triplicate.

Figure 5.17 Optimization of the different concentrations of anti-PSA as a detection antibody (a). Optimization of the different concentrations of fluorescent Fc-MIP-NGs as a fluorescent secondary antibody mimic (b). The concnetration of PSA was 1 nM. The error bars were obtained from triplicate experiments.

Figure 5.18 Optimization of the binding times. The concnetration of PSA was 10 nM. The error bars were obtained from triplicate experiments.

Figure 5.19 The binding isotherm of developed sensor with step-by-step immobilization for PSA (0-100 nM) shows a linear calibration range of 0.01–10 nM (r^2 = 0.998).

Figure 5.20 The relative fluorescence intensity of PSA binding using the premix solution immobization and step-by-step immobilization. The PSA concentration was 0-100 nM.

Figure 5.21 The binding isotherm of developed sensor for PSA (0-100 nM) shows a linear calibration range of 0.01–10 nM (r^2 = 0.969). The error bars were obtained from triplicate experiments.

Figure 5.22 (a) The binding isotherms of developed biotic/abiotic antibody sandwich assay for PSA on the various concentrations from 0 to 100 nM. (b) The selectivity factor of developed biotic/abiotic antibody sandwich assay for PSA and four animal serum albumins (BSA, GSA, SSA and RSA) at the protein concentration of 10 nM. The error bars were obtained from triplicate.

Figure 5.23 Analytical performances of developed biotic/abiotic antibody sandwich assay for PSA. (a) The stability of developed sensor and (b) PSA binding isotherms (0-100 nM) in PBS and real meat extract for developed assay. The error bars were obtained from triplicate.

Figure 5.24 The relative fluorescence intensities of spiked 1 nM of PSA into diluted beef extract samples (PBS, 1, 10, 100 and 500-fold dilutions) binding to F-MIP-NGs. Error bars were obtained from triplicate experiments.

Figure 5.25 Relative fluorescence intensities to the developed assay of pork contaminated halal meat extract samples (beef and goat) in various concentrations (0–100 wt%) (a).; The absorbance at 450 nm of ELISA assay for detection of pork contamination in halal beef extract samples (b). The error bars were obtained from triplicate experiments.

Figure 5.26 The absorbance at 450 (nm) of ELISA assay. (a) the calibration curve of determined for a range of PSA protein standards from 0-300 ng/mL (r^2=0.9959), (b) the ELISA results from various pork contamination in PBS buffer.

List of Tables

Tables

Chapter 1

General Introduction

General Introduction

1.1 Background and Aim of this Dissertation

The halal industry including halal food, pharmaceuticals, cosmetic, and health products is currently expanding due to the rapid growth increase of the world's Muslim population. Moreover, halal food is not only fit for Muslim but also non-Muslim to be consume since it is the hygienic food for consumption. With halal food becoming mainstream consumer good, pork contamination is increasingly concerned for the global market of halal foods because the costumers always use pork instead of beef to reduce the production cost. In order to verify the halal certification of non-pork contamination food products, easy-to-use, sensitive, and reliable method is necessary to analyse pork contamination in halal food products. For decade, various developed sensors using the biological receptors such as protein-based method (immunosensor) and DNA-based method (DNA sensor) have been rapidly employed to promote the fast-growing halal market and to evaluate the validity of halal food quality products. However, the primary disadvantage of theses sensors is cumbersome procedures, low stability, and high costs of using biological receptors. To overcome these drawbacks, MIPs are biomimetic receptors which obtains affinities and low cross-reactivities comparable to those of biological receptors. Due to their high stability, easy synthesis, and low costs, MIPs-based sensers have become attractive as they can be potentially used as a simple, powerful, and accurate method to detect pork contamination for halal food control. MIPs, which are prepared through a template polymerization process, developing recognition capably in sizes and shapes of template molecules, have been attracted a great attention to be used as artificial antibodies to recognize the target interests.

The aim of this dissertation was to develop a new simple strategy to synthesize a highly sensitive and good selective MIP-NGs capable of PSA that would be an excellent candidate MIP-based sensor for halal food control analysis. To reach this goal, the proposed sensor should detect the pork contamination even in the real meat extract samples.

1.2 Outline of this Dissertation

This Ph.D. dissertation is composed of five chapters: one general introduction chapter followed by one literature review chapter and two results chapters. The experimental section is provided in specific for each result chapter. Finally, the final conclusions and some perspectives for further studies is proposed.

Chapter 1 provides a general introduction of the background and aim of this dissertation including a short brief of strategies to develop MIP-NGs and the proposed sensor.

Chapter 2 provides a literature review on halal food control with halal food market and several developed analytical methods for detection of pork contamination in meat extract. And provides interesting examples of MIP-based sensor applications in any areas with their good selectivity.

Chapter 3 describe the emulsifier-free precipitation polymerization synthesis of MIP-NGs capable of highly specific recognition for PSA by emulsifier-free precipitation polymerization with pyrrolidyl acrylate (PyA) as a functional monomer. The purification of MIP-NGs was carried out by ion-exchange chromatography. The immobilization method of MIP-NGs on the carboxyl functionalized surface of QCM sensor chips was conducted using an amine coupling reaction. The resulting MIP-NGs shows good characteristics and morphologies with the nano-sized MIPs, and exhibits excellent affinity and high selectivity, appropriate to be an artificial antibody instead of natural antibodies. Due to high affinity and selectivity of MIP-NGs, the label-free MIP-NGs-based QCM sensor is capable to detect PSA in the real meat extract samples, which renders it suitable for detection of pork contamination in halal food control.

Chapter 4 presents my work to improve the sensitivity of MIP-NGs-based sensor by post-imprinting modifications (PIMs). F-MIP-NGs were synthesized using molecular imprinting with 4-[2-(*N*- methacrylamido) ethylaminomethyl] benzoic acid (MABA) as a functional monomer and PIMs by introducing of fluorescence ATTO-647 dye into nano-cavities of MIP-NGs. The two-step purification procedure was used to purify nanogels before PIMs. The resulting F-MIP-NGs were immobilized on the amine functionalized surface of gold

coated sensor chips via the covalent conjugation. This fluorescence MIP-NGs-based sensor is performed to detection of PSA in meat extract samples. The proposed sensor provides more sensitive than that of label-free MIP-NGs-based QCM sensor with good affinity as a result it is potential to be a candidate for detection of pork contamination in halal meat extract.

Chapter 5 presents my work to develop a biotic/abiotic antibody sandwich assay using Fluorescent MIP-NGs capable of Fc domain (Fc-MIP-NGs) as fluorescent secondary antibody mimics for detection of pork contamination in halal biomarker sensing application. The fluorescent Fc-MIP-NGs was prepared using molecular imprinting and PIM. The proposed materials exhibited good affinity and selectivity of Fc domain over the whole IgG, deglycosylated Fc-IgG and PSA and is great potential to be an alternative secondary antibody mimics for halal sensing application. Next, the biotic/abiotic antibody sandwich assay for detection of pork contamination in halal met extract was demonstrated. This assay was can detect very low level of contaminated down to 0.01 wt% with rapid detection time for 30 min, after immobilization of capture PSA MIP-NGs. When compared to the ELISA results, the performance of this assay for detection of pork contamination was better in lamb extract samples 0.1 wt%, and was comparable in meat extract samples with limit of detection of 0.01 wt%. Therefore, the biotic/abiotic antibody sandwich assay is promising for sensitive and rapid detection of pork contamination in halal meat extracts, make it an attractive alternative to traditional immunoassay frequently used in ELISA.

Chapter 6 provides general conclusions and perspectives of MIP-NGs synthesis and MIP-NGs based sensor developing and applications.

Chapter 2

Molecularly Imprinted Polymer-Based Sensors for Halal food Control

A Literature Review

A Literature Review

2.1 Halal Food

2.1.1 Halal food market

Halal is the Arabic word, which means permitted and allowed. Halal is not only related to food but also includes politics, attires, logistics, economic transactions, and finance. The global halal industry is currently the fastest growing consumer segments in the world. It has become a powerful market force with Muslims and non-Muslims who are looking for high quality, ethical, and safe products. However, halal food industry is the most preferred in the global halal market. The halal food market can easily grow up of the world trade in food products as Muslims are expected to reach 31% of the world's population by 2060 as reported by The Pew Research Center.[1] (Figure 2.1)

Size and projected growth of major religious groups, 2015-2060

	Projected 2015 population	% of world population in 2015	Projected 2060 population	% of world population in 2060	Population growth 2015-2060
Christians	2,276,250,000	31.2%	3,054,460,000	31.8	778,210,000
Muslims	1,752,620,000	24.1	2,987,390,000	31.1	1,234,770,000
Unaffiliated	1,165,020,000	16.0	1,202,300,000	12.5	37,280,000
Hindus	1,099,110,000	15.1	1,392,900,000	14.5	293,790,000
Buddhists	499,380,000	6.9	461,980,000	4.8	-37,400,000
Folk religions	418,280,000	5.7	440,950,000	4.6	22,670,000
Other religions	59,710,000	0.8	59,410,000	0.6	-290,000
Jews	14,270,000	0.2	16,370,000	0.2	2,100,000
World	**7,284,640,000**	**100.0**	**9,615,760,000**	**100.0**	**2,331,120,000**

Source: Pew Research Center demographic projections. See Methodology for details.
"The Changing Global Religious Landscape"

PEW RESEARCH CENTER

Figure 2.1 The prediction of the world's population. Reprinted from [The Pew Research Center, 2015]

Nurrachmi (2017) reported that the market size of halal food segment in many developed countries such as United Kingdom, Australia and Japan has achieved USD 1 million as indicated in Table 2.1, resulting from an increasing demand for halal food products of Muslim and non-Muslim in their contries.[2] From the report, the halal food market has significant impact to the economy development not only developing countries but also

developed countries.

Table 2.1 Halal food market in selected developed countries. Reprinted from [Nurrachmi, 2017]

Developed Countries	Japan	Australia	UK
Number of Moslem	0.14% from 127.3 million	2.25% from 23.1 million	4.8% from 64.1 million
Market size for Halal Food Industry (2014)	USD 888,352 (JPY 120 million)	USD 1,016 million (AUD 1,420 million)	USD 1,462 million (1 billion UK pound)
Source of Halal Food	Self-production	Self-production	Self-production
Ecosystem	Focus on providing Halal food menu at university, international airport Export Halal food & drink to ASEAN	Focus on meat production Exporters for Halal red meat to Organization Islamic Committee (OIC) countries	Focus on meat and poultry production
Supply Chain Management	Mostly Commercial farms	Mostly Commercial farms	Mostly Commercial farms
Halal Certification	JHA uses JAKIM Malaysia's standard	Australia Government Authorized Halal Program (AGAHP)	The Halal Food Authority (HFA)

Currently, Brazil, New Zealand and Australia are the three largest exporter and producer of halal food products in the world including halal meat, poultry, and dairy products. Hence, halal food market has a great potential to be a new attractive segment in the global halal market as stated in Figure 2.2.[3]

2.1.2 Halal meat products

Halal meats is the meats fit for Muslim consumption and permitted by permissible and lawful. The Muslim halal law requires meat products free from pork and its derivatives. According to the Holy Qur'an, God said that "You are forbidden to eat the meat of any animal that dies by itself (dead body), blood, the flesh of pork."(Qur'an, chapter 5 verse 3).[4] Therefore, meat that contain pork or pork derivative are categorized as haram, prohibited for Muslims to be consumed. Halal meat product is one of the largest halal food export markets in the world. With the increasing of Muslim population in the world, the demand of halal meat products must be increased. For saving the cost, the costumers are often mixed pork into beef since the pork price is cheaper than the beef. As reported by The Food and Agriculture Organization (FAO) in 2021, the beef price is nearly doubled to the pork price as a result contamination of

pork in halal raw meats has become a worryingly regular occurrence.[5] (Figure 2.3)

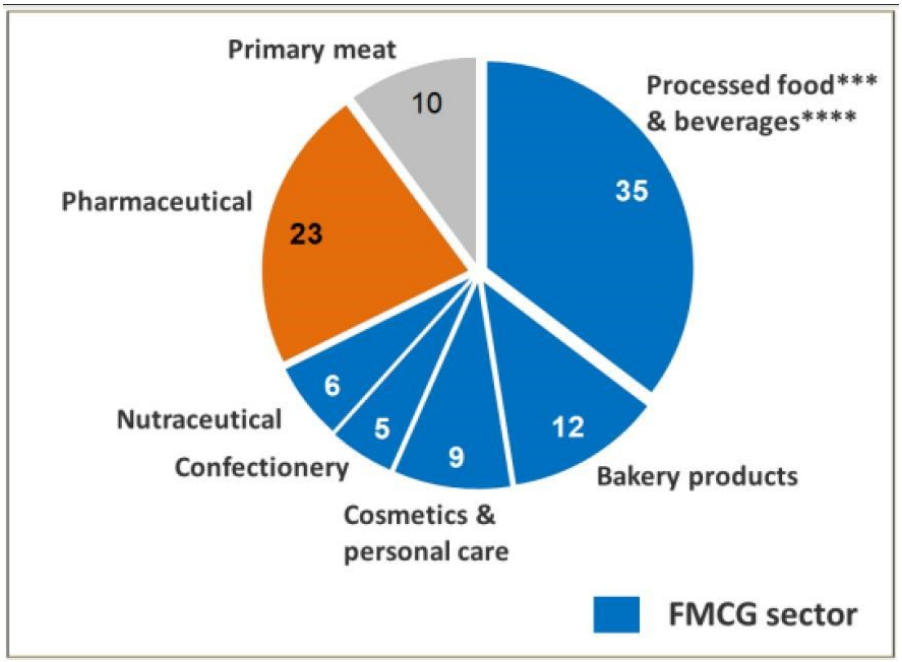

Figure 2.2 The global halal market for potential halal food products. Reprinted from [Hassan, 2014]

BOVINE MEAT PRICES

		AUSTRALIA[1/]	USA[2/]	BRAZIL[3/]
		US $ / ton		
2009		2562	4130	3257
2010		3272	4585	4093
2011		3944	5093	5078
2012		4176	5885	4765
2013		4009	6314	4527
2014		5016	7361	4712
2015		4699	7195	4320
2016		4171	6390	4053
2017		4463	6676	4196
2018		4198	7118	4045
2019		4873	7119	4119
2020	Jan	4929	7220	4900
2020	Feb	4545	7011	4469
2020	Mar	4394	7010	4407
2020	Apr	4462	6792	4374
2020	May	5071	6837	4400
2020	June	4972	7082	4299
2020	July	4688	6790	4081
2020	August	4707	6795	4008
2020	September	4666	6804	4096
2020	October	4387	6833	4251

1/ Australia: Cow 90CL export prices to the USA (FAS)
2/ USA : Meat of bovine (Fresh, Chilled Or Frozen), export unit value
3/ Brazil : Meat of bovine (Fresh, Chilled Or Frozen), export unit value

PIG MEAT PRICES

		USA[1/]	BRAZIL[2/]	GERMANY[3/]
		US $ / ton		
2009		2548	2107	2035
2010		2851	2647	1913
2011		3036	2941	2169
2012		2952	2700	2233
2013		2981	2797	2311
2014		3233	3411	2106
2015		2669	2482	1582
2016		2648	2129	1682
2017		2687	2475	1871
2018		2587	1959	1728
2019		2626	2245	1989
2020	Jan	2717	2572	2113
2020	Feb	2684	2465	2152
2020	Mar	2643	2463	2210
2020	Apr	2620	2448	2026
2020	May	2549	2372	1845
2020	June	2471	2159	1927
2020	July	2411	2123	1766
2020	August	2380	2236	1802
2020	September	2371	2315	1608
2020	October	2366	2396	1550

1/ USA: Meat of Swine (Fresh, Chilled Or Frozen), export unit value
2/ Brazil: Meat of Swine (Fresh, Chilled Or Frozen), export unit value
3/ Germany: Monthly market price for Grade E pig carcasses

Figure 2.3 The meat price in the three largest exporters in the world. [Source: The Food and Agriculture Organization (FAO), 2021]

Therefore, the most effective and accurate methods for detection of pork and pork derivatives are important in order to avoid pork contamination in halal raw meat and to evaluate halal authenticity for halal food control.

2.2 Biosensor for Pork Contamination Detection

The analytical authentication of halal meat products has the aim to solve the problem of pork contamination that are highly concerned for halal food control. Biosensor is a good potentials analytical devise for detection of pork and pork derivatives contamination in halal meat products with the use of advance biotechnology analyses. Nowadays, there are numerous analytical methods available for detecting pork contamination in halal meat products, and two molecular biomarkers commonly used for analyses are proteins and DNA. For decade, the Protein-based and DNA-based methods have increasingly been developed in biosensor applications due to their high affinity and specificity. Particularly, protein-based method using immunotechniques such as an enzyme-linked immunosorbent assay (ELISA) and a label-free immunosensor are considered the potential methods for detection of pork contamination in halal meat products due to timesaving and their simplicity of preparation comparing to the DNA-based methods. In contrast, the primary advantage of DNA-based methods such as species-specific polymerase chain reaction (PCR) and loop-mediated isothermal amplification (LAMP) are more sensitive and reliable for detection of pork contamination in cooked, heated, or processed meat products owing to a good stability of DNA at high temperature.

2.2.1 DNA-based methods

Sakalar and Kaynak (2016) developed a low-cost duplex-detection technique with a specific and rapid detection of pork gene in meat products using a real-time polymerase chain reaction assay based on fluorescence (EvaGreen as a DNA intercalating dye). (Scheme 2.1) This method exhibited high sensitivity presented by the lower limit of detection DNA target in sausage samples (0.01 ng/mL), confirming that this method is reliable to be a great tool for identification of pork contamination in meat products. [6]

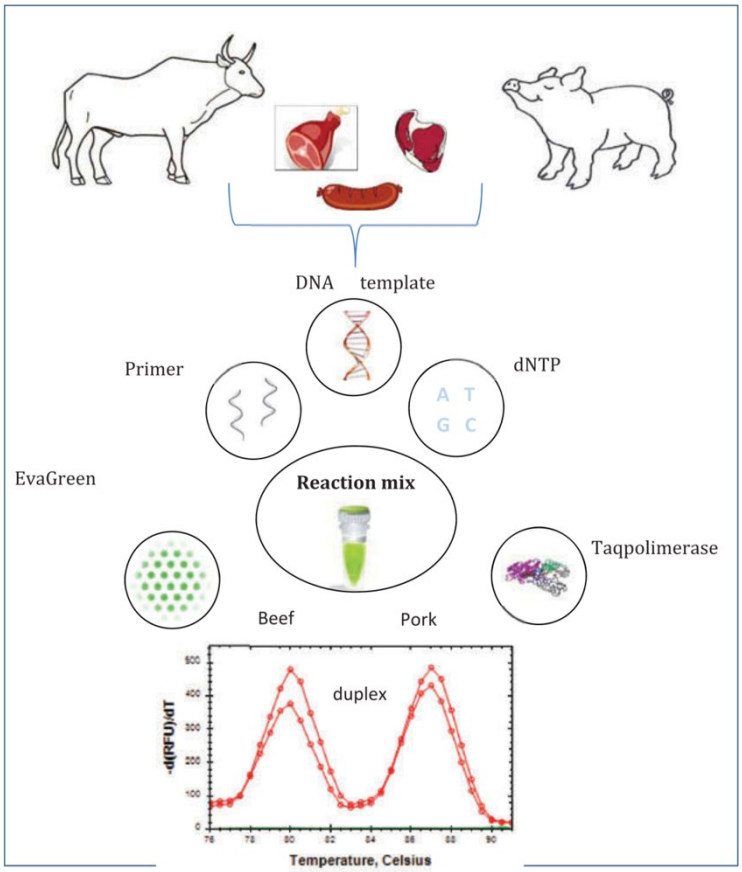

Scheme 2.1 Schematic overview of determination of meat species by EvaGreen based duplex real time PCR method. Reprinted from [Sakalar and Kaynak, 2016]

In another important study, Lee et al., (2016) developed on-site detection method with simple equipment for sensitive and rapid detection of pork contamination in processed meat products by reliable loop-mediated isothermal amplification (LAMP) method. The pork specific primers for the LAMP and the endogenous control in this study were designed based on the mitochondrial D-loop regions and the 18S rRNA gene, respectively as stated in Table 2.2. The developed method showed high sensitivity, a detection limit of 1pg in raw pork DNA and 0.1% of pork in meat extract sample, and rapid detection of pork contamination in meat products within 30 min. [7]

Table 2.2 Sequences of oligonucleotide primers used in this study. Reprinted with modified from [Lee et al., 2016]

Species	Genes	Primer	Sequence (5′ – 3′)
Sus scrofa	Mitochondrial D-loop	F3	GCAGGTAAATTATTAGCTCATTCA
		B3	AAATCTAGGGGGGTAGGT
		FIP	CTTTGTTTTTGGGGTTTGGCAAG TTACCCCCCATTAAACTTATGC
		BIP	AACATTTAACAACACAAACCACCAT TGCTTTCGTAGCACGTATT
Eukaryotes	18S rRNA	F3	GACCCATTCGAACGTCTG
		B3	GTTATTTTTCGTCACTACCTCC
		FIP	GAACCCTGATTCCCCGTCAC CCCTATCAACTTTCGATGGT
		BIP	CGGAGAGGGAGCCTGAGAAA GGAGTGGGTAATTTCGCG

Al-Kahtani et al., (2017) reported that they have successfully detected pork DNA in binary meat mixtures such as beef, chicken, rabbit, goat, sheep, and camel by both conventional and real-time PCR (RT-PCR) methods. The results of this study showed that the RT-PCR method provides more sensitive, simple, reliable, and accurate for detection of pork contamination in meat mixtures and commercial food products compared to conventional PCR method.[8]

In another interesting study reported by Cai and colleagues (2017), quantification and detection of pork materials in meat products were performed using a novel cost-effective method as duplex droplet digital PCR (dddPCR). The specific primers and probes for multiplex dPCR experiment in this study were shown in Table 2.3. This method can identify the source of meat in meat mixture samples in a single digital PRC tube with acceptable limit of detection (LOD) and limit of quantification (LOQ). The results confirmed that this method is suitable for detection of pork contamination in meat products.[9]

Table 2.3 Sequences of oligonucleotide primers and probes for multiplex dPCR experiment. Reprinted from [Cai et al., 2017]

Primer/Probe	Sequence/labeling
Bos-ACTB-63bp-F	GCGGCCTCGGAGTGTGTA
Bos-ACTB-63bp-R	CCCCAGAATGAGGTTCACTTCA
Bos-ACTB-63bp-P	FAM-TCAGTAGGTGCACAGTAC-MGB
Sus-ACTB-97bp-F	CGTAGGTGCACAGTAGGTCTGAC
Sus-ACTB-97bp-R	GGCCAGACTGGGGACATG
Sus-ACTB-97bp-P	VIC-CCAGGTCGGGGAGTC-MGB[16]

Amaral et al., (2017) developed a highly sensitive methods to detect pork contamination in processed meat products using EvaGreen real-time PCR. The specific primers for RT-PCR were designed based on mitochondrial *cytb* gene. This method showed excellent sensitivity to detect pork DNA as low as 0.0001% (w/w) in binary meat mixtures. Hence, the developed methodology can be a powerful tool for detecting low levels of pork contamination.[10]

In another important study reported by Kuswandi and colleagues (2017), a simple colorimetric based on gold nanoparticles DNA biosensor have successfully developed for detection of pork contamination in processed meat products. With aggregation property of 20 nm gold nanoparticles (AuNPs), the colour was easily observed after hybridization between complementary targets DNA toward porcine DNA probe as indicated in Scheme 2.2. The result indicated that the developed colorimetric DNA-based sensor provided a simple and rapid detection of pork contamination in beef meatballs.[11]

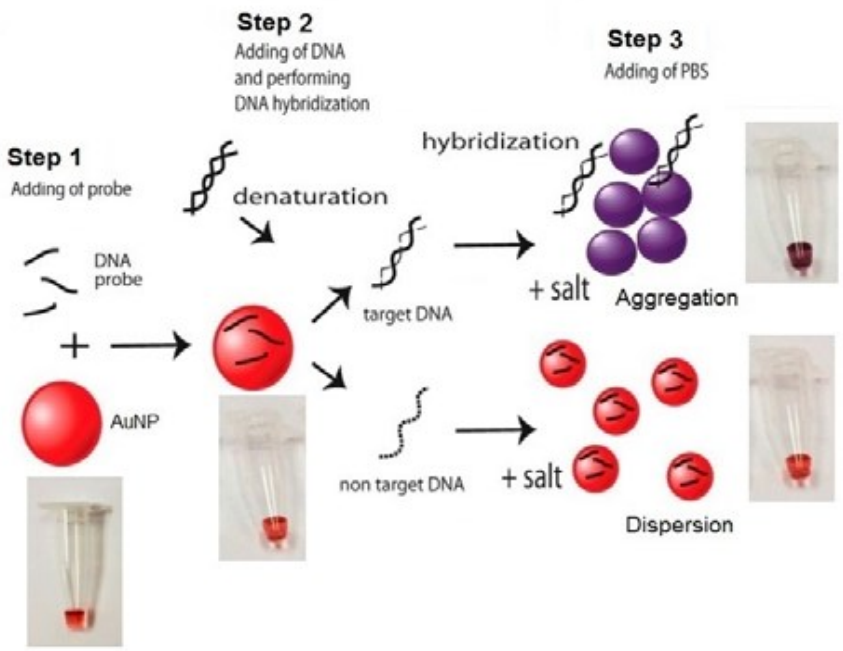

Scheme 2.2 Schematic representation of a colorimetric pork DNA detection based on AuNPs. Reprinted from [Kuswandi et al., 2017]

In a reported study, Cahyadi et al., (2020), developed a novel multiplex-PCR method to detect pork contamination in meatball. The mitochondrial 12S rRNA gene were used to design specific primers in this study. This designed primers successfully amplified pork DNA

in meatball products. This novel DNA-based method could be an alternative method to detection of pork contamination in processed meat products.[12]

2.2.2 Protein-based methods

Lim and Ahmed (2016) have demonstrated a novel label-free electrochemical immunosensor was developed for sensitive detection of porcine serum albumin (PSA) as a protein marker in halal raw meats. The PSA antibody was conjugated onto the electrode using covalent bonding, and the response was constructed by electrochemically reducing 4-corboxyphenyl diazonium salt, which was electrografted on an electrode surface as shown in Scheme 2.3. This developed sensor demonstrated a highly sensitive for detection of PSA in buffer solution, the detection limit of 0.5 pg/mL, and provided excellent specificity against albumins from other animal species.[13]

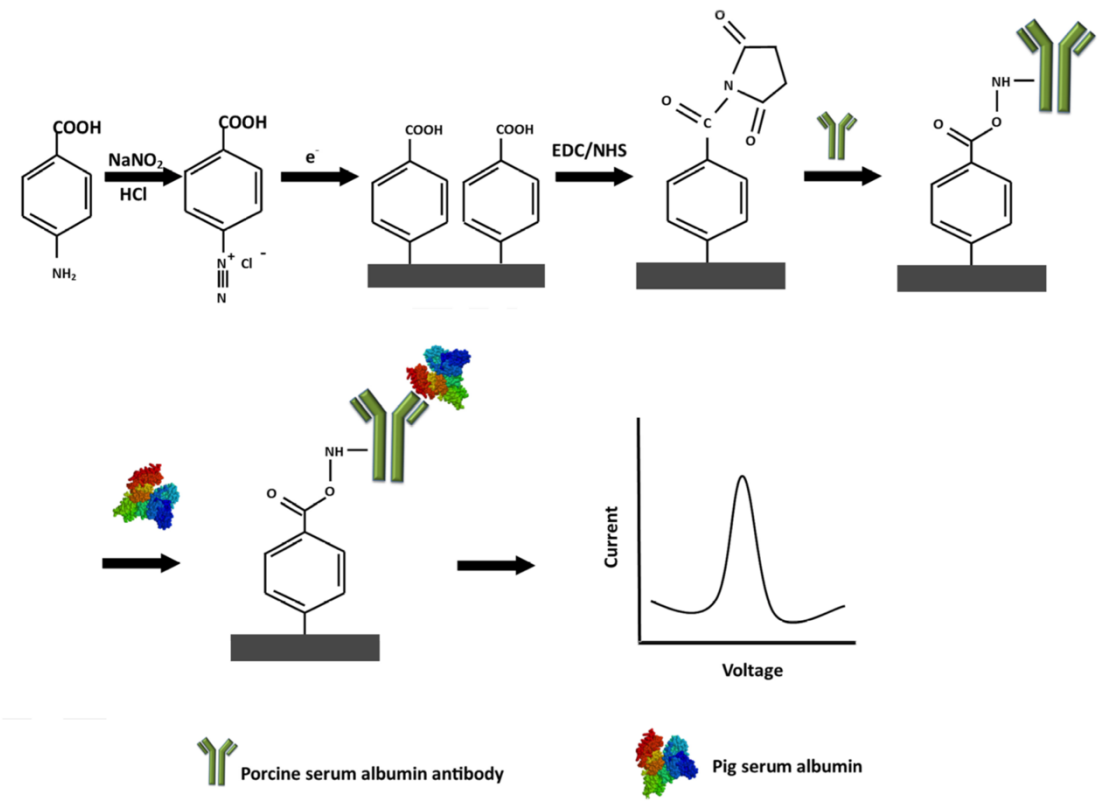

Scheme 2.3 Schematic overview of modification of a sandwich lateral flow electrochemical immunosensor. Reprinted from [Lim and Ahmed, 2016]

In another research by Kuswandi et al., (2017), a sensitive and rapid immuno strip test for detection of pork contamination in processed meats using conjugated gold nanoparticles with a high-affinity anti-Swine IgG polyclonal antibody have demonstrated. In this study, the developed sensor as a sandwich type lateral flow immunosensor is based on immunochromatographic construction, where antigen-antibody interaction is indicated by a colour band of attached nanoparticles as shown in Scheme 2.4. The immuno strip test exhibited high sensitivity and fast detection of presented by the lower limit of detection, LOD (0.1% w/w) and response time of 5 min, respectively. Moreover, the developed method can be applied to detect low-levels of pork contamination in beef meatballs. The results indicated that the developed immuno strip is a simple method to detect pork contamination in meat products with high potential and reliability.[14]

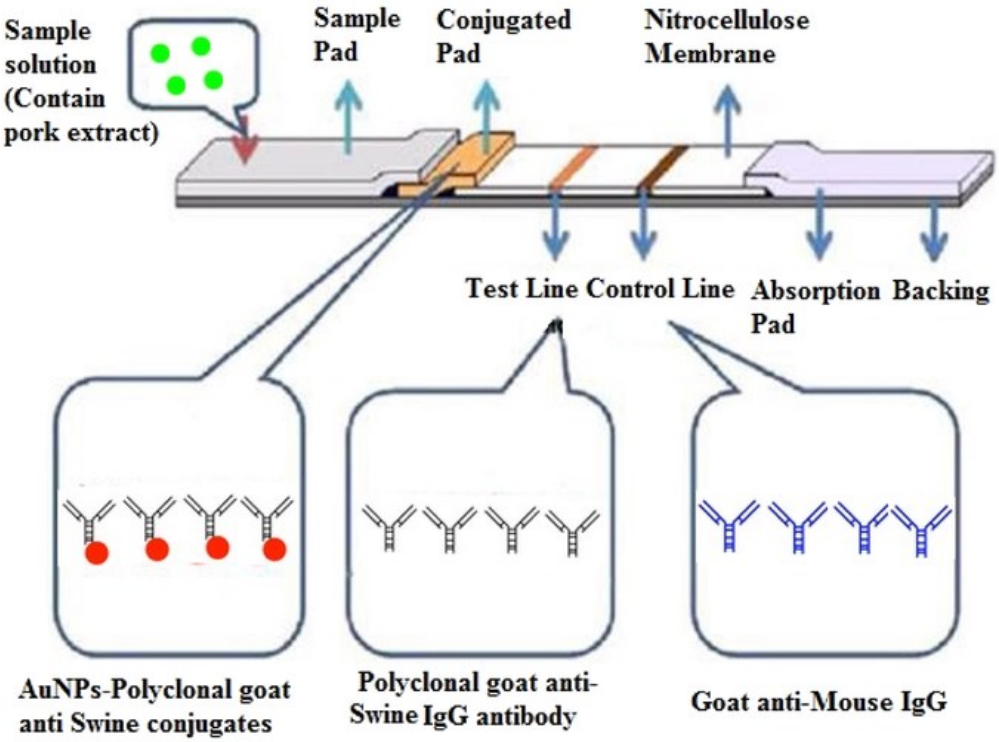

Scheme 2.4 Schematic illustration of determination of pork contamination by sandwich type lateral flow strips based on gold nanoparticles. Reprinted from [Kuswandi, 2017]

In an interesting study published by Mandli and colleagues (2018), an enzyme immunoassay (ELISA immunosensor) using HRP conjugated anti-pig IgG polyclonal antibody was prepared for highly sensitive detection of pork contamination in processed meats as shown in Scheme 2.5. Due to high affinity of anti-pig IgG polyclonal antibody with extracted pork IgG, this ELISA/immuno sensor exhibited a rapid, sensitive, and selective detection of low level of pork contamination in beef extracts. With the competitive immunosensor type, the sensor showed an excellent sensitivity presented by the lower limit of detection (LOD) of 0.01% pork contamination in beef extracts. The results confirmed that the developed sensor has potential to be a power tool for evaluate of pork contamination in halal food control.[15]

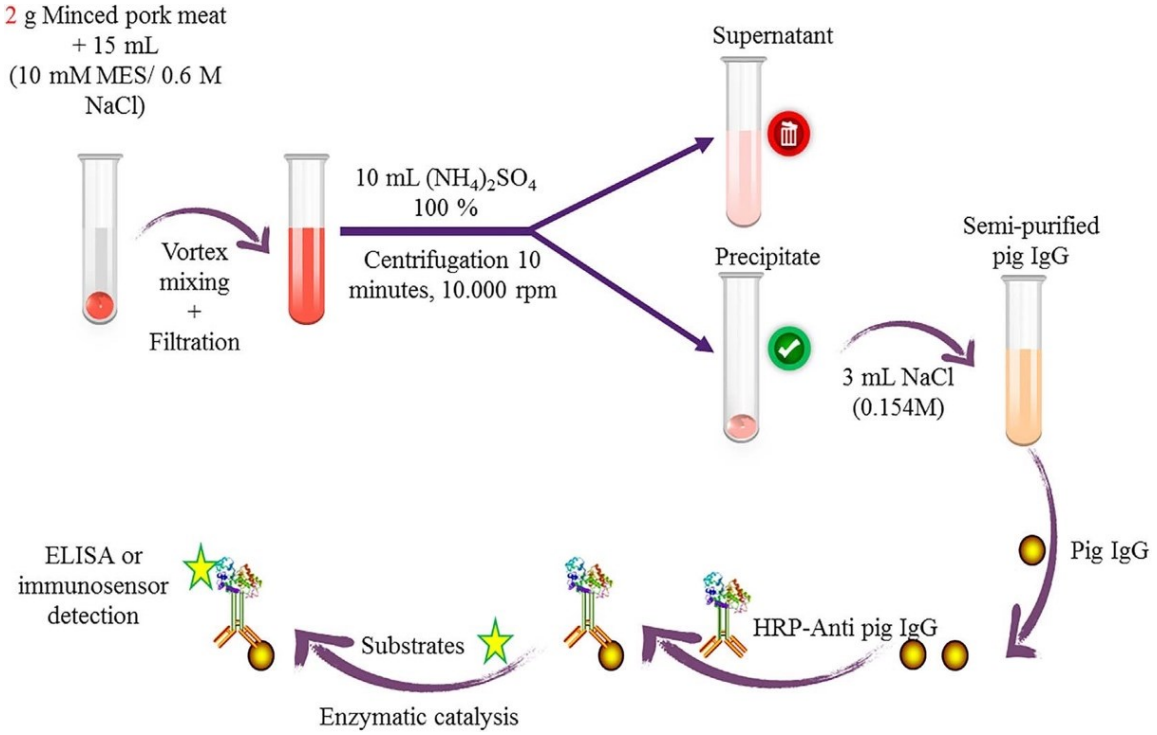

Scheme 2.5 Schematic representation of preparation of a rapid immunoenzymatic method for detection of pork contamination in meat extract samples. Reprinted from [Mandli et al., 2018]

In an important study published by Thienes and Masiri (2018), they also developed a sandwich ELISA method for detection horse contamination in cooked meats such as pork, chicken, goat, lamb, and beef meats. This method showed high sensitivity with the detection limit down to 0.05% (w/v) of cooked meats. The assay can be finished in 1 h and 10 min without any cross-reactivity.[16]

In a reported study (2018), Pan et al., developed an accurate method for detection of pork contamination in meat mixtures using parallel reaction monitoring (PRM) mass spectroscopy. In this study, the species-specific peptide biomarkers of myosin were identified by MS-based method as stated in Table 2.4. Then, the five selected peptides from myosin were performed for detection of pork contamination in meat extract samples including chicken, sheep, and beef. With the highly sensitive peptide, the method showed an excellent sensitivity presented by the low of the detection limit of 0.5% with acceptable the relative standard division, %RSD (4-15%). The results indicated that the developed method have a potential to detect pork contamination in meat mixtures.[17]

Table 2.4 The myosin-derived marker peptides. Reprinted with modified from [Pan et al., 2018]

Pork	Peptide
Myosin-4	HKYEETQAELEASQK
	NLTEEMAGLDENIAK
	KLETDISQIQGEMEDIVQEAR
	LETDISQIQGEMEDIVQEAR
	IAEKDEEIDQMK
Myosin-1	KLETDISQIQGEMEDIIQEAR
	LETDISQIQGEMEDIIQEAR
Myosin light chain	VLGNPSNEEMNAK

Han et al., (2020) developed a low-cost a rapid method for detection of pork contamination in raw beef using an electronic nose (E-nose) based on colorimetric sensor. In this study, chemometric algorithms of Fisher linear discriminant analysis (LDA) and extreme learning machine (ELM) were performed for identification of meat species via E-nose system and the colorimetric sensor array was used to convert the chemical information of the volatile organic compounds (VOCs) present in the meat to the electrical signals via its color changes as seen in Figure 2.4(a) and 2.4 (b). The results showed that the ELM model built was better than that of the Fisher LDA model with higher identification rates of 87.5% in the prediction sets. For the adulteration level prediction, the root-mean-square error and the correlation coefficient were acceptable. The results suggested that the low-cost electronic nose based on colorimetric sensors coupled with chemometrics has a great potential in rapid detection of beef adulterated with pork.[18]

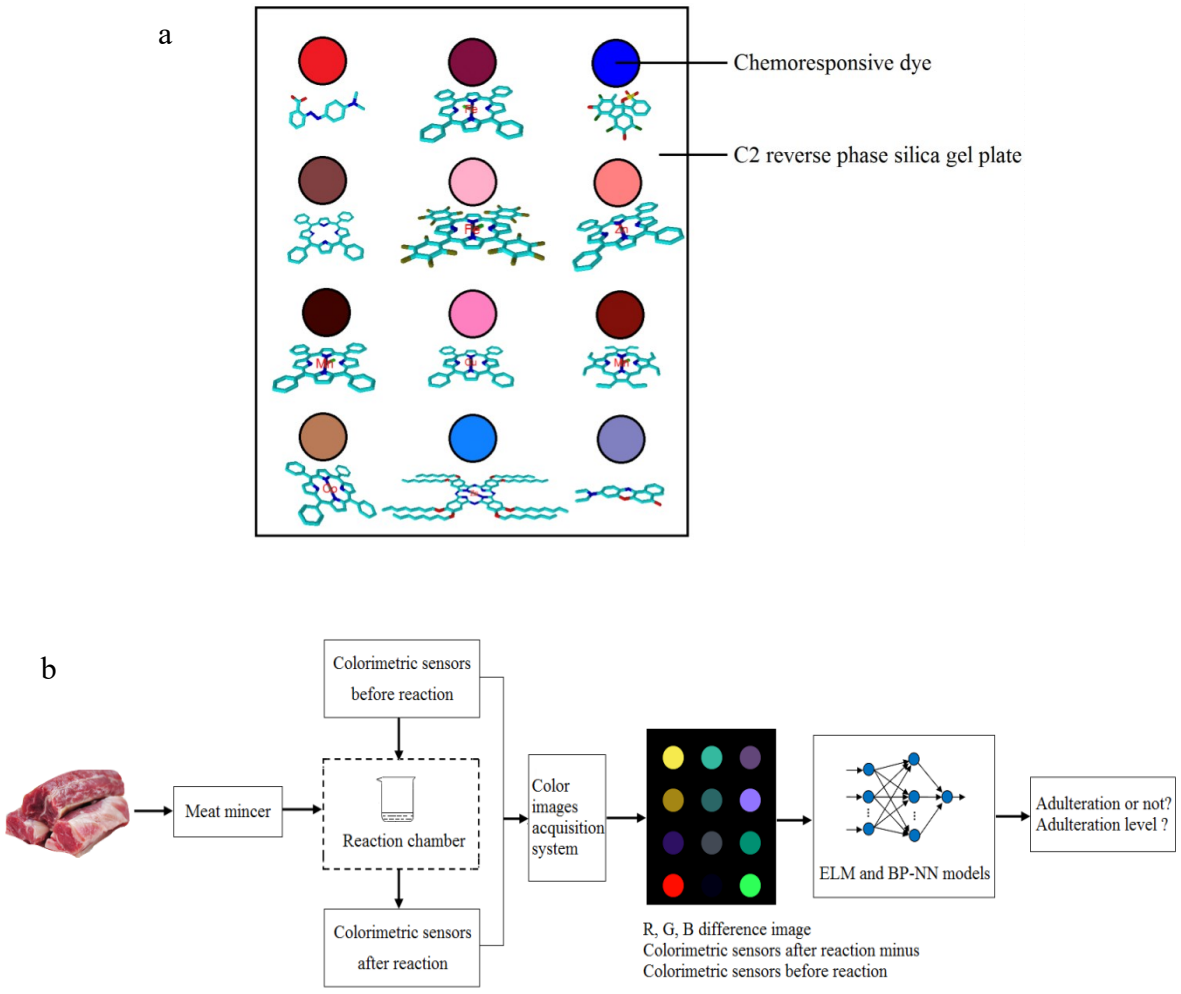

Figure 2.4 The schematic representation of (a) the fabricated colorimetric sensor arrays. (b) The overview of the measurement methods. Reprinted with modified from [Han, 2020]

Although both of DNA and protein-based sensor exhibited a high sensitivity and specificity for detection of pork contamination in halal meat products but there are high cost consuming of needed DNA primers, DNA probes, and antibodies. As well, a low stability of natural receptors is disadvantaging the alternative artificial antibody as a molecularly imprinted polymers (MIPs), which are high stability, easy synthesis, and low costs production. Therefore, MIPs-based sensor is a great candidate to be a potential powerful method for detection of pork contamination in halal meat products.

2.3 Recent Advance in MIPs-based Sensor

Molecularly imprinted polymers (MIPs) as an artificial selective receptor were prepared using molecular imprinting technique, where the particles are generated by copolymerization of cross-linker and functional monomer in the presence of a template molecule. Upon removal of the template molecule, imprinting cavities or recognition site are formed in the polymer matrix, which are complementary in shape and size to the template molecules and able to rebind with the template molecule as shown in Scheme 2.6.[19] Historically, Wulff and Sarhan first reported the example of the molecular imprinting technique in 1972.[20] Currently, there are several techniques used to synthesize MIPs such as ground bulk polymer, core shell particle, precipitation polymerization, iniferter polymerization, and emulsion polymerization as seen in Figure 2.5.

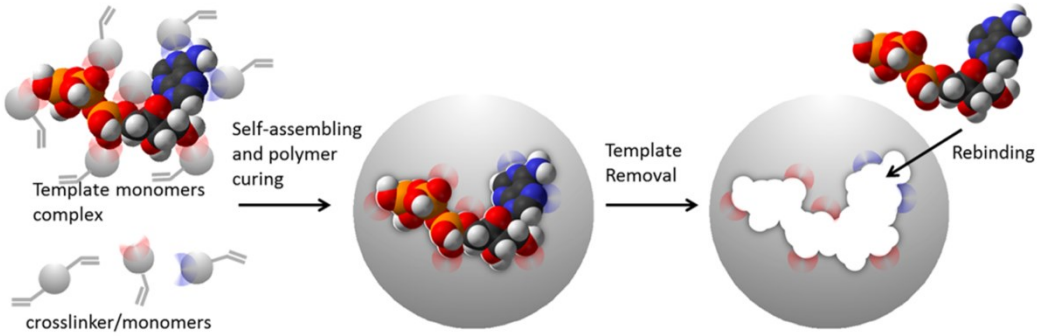

Scheme 2.6 Schematic overview of molecular imprinting technique. Reprinted from [Wackerlig and Schirhagl, 2016]

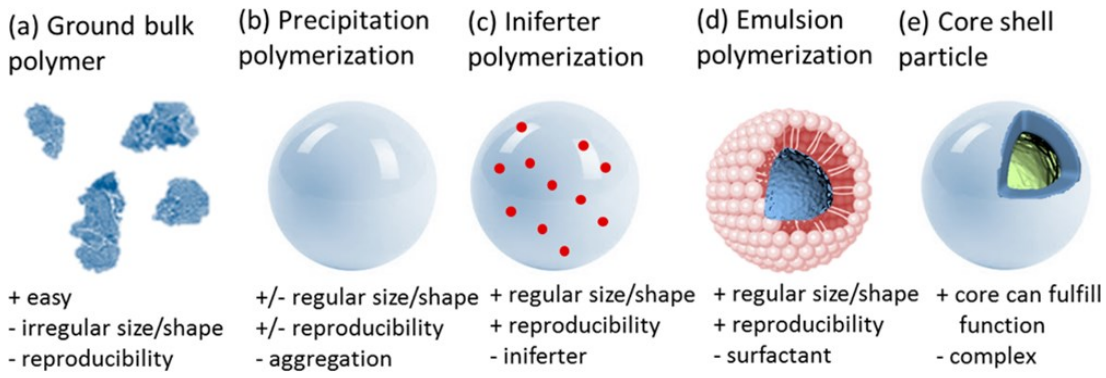

Figure 2.5 Comparison of the different methods to synthesis MIPs. Reprinted from [Wackerlig and Schirhagl, 2016]

Among all procedures above, precipitation polymerization is better to control size and shape of molecular particles than that of the other methods. Moreover, this method is a fast, simple, and potential strategy for obtaining monodispersed nanoparticles with good yields. Generally, this method is prepared the polymeric reaction in a homogenous phase with high dilution condition. During polymerization, the particles was precipitated when the expanding polymer becomes insoluble. Takeuchi et al., 2017, prepared nanometer-sized MIP particles as molecularly imprinted polymer nanogels (MIP-NGs) capable of human serum albumin (HSA) using emulsifier-free precipitation method, which provided a small particle size (35) nm and good monodispersity particles. In their study, MIP-NGs exhibited a good affinity for HSA, allowing them to form an albumin-rich protein corona as indicated in Figure 2.6.[21] The nano-sized MIPs have a primary advantage to presents a large total surface area per unit of polymer particles so that the imprinted cavities are more easily capable of the analytes.

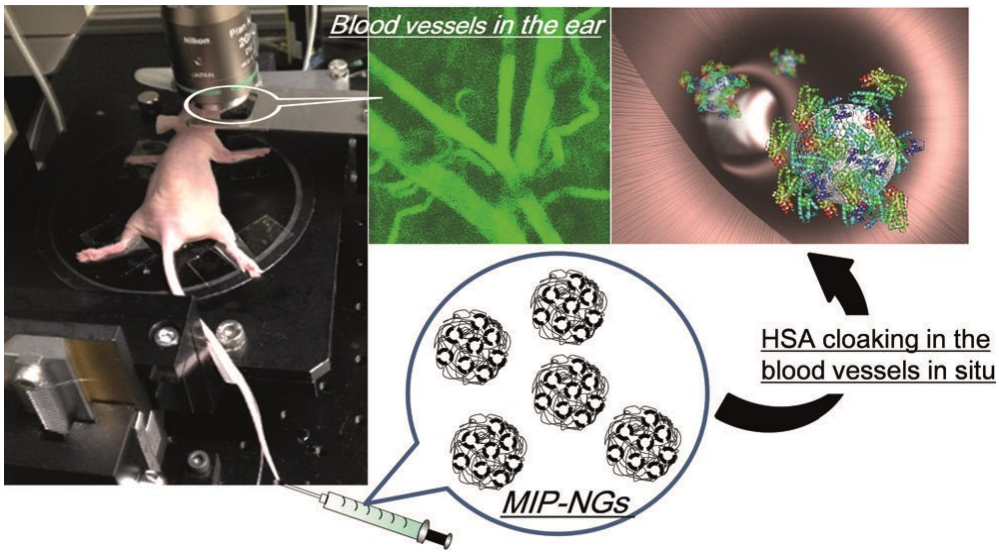

Figure 2.6 Schematic illustration of MIP-NGs to be cloaked through the formation of an albumin-rich protein corona. Reprinted from [Takeuchi et al., 2017]

Normally, the molecular imprinting presented an effective method for molecules of low molecular weight as lower than 1,500 Da. However, the molecular imprinting of biological macromolecules such as DNA, enzymes, and proteins is currently increasing owing to their widely application areas as artificial receptor instead of using natural receptors in practical use. Hence, the developing of sensitive and selectivity MIPs for proteins is extremely challenges for researchers including template characterization, monomer selection, template removal and washing methods, and quantification of the rebinding.[22]

For decade**,** a novel approach known as post-imprinting modifications (PIMs) was developed in order to achieve more sensitive and selective of MIPs for proteins. This procedure is like a natural biomechanism of post-translation modification in protein biosynthesis for cells, where modification was performed by conjugation of non-protein prosthetic groups and cofactors after translation process. After imprinting process, the resulting MIPs is also applicable for modification through a chemical-modification strategy. The combination of molecular imprinting and PIMs is attractive method to generate more sensitive MIPs than that of using only molecular imprinting process. Matsumoto et al., (2019) developed MIPs by molecular imprinting and post-imprinting modification strategies for the recognition of prostate-specific antigen (PSA) as a biomarker for prostate cancer. The MIPs were prepared using a non-covalent molecular imprinting approach combined with a PIM-based capping treatment as seen in Scheme 2.7. The results in their study showed that the developed method exhibited high sensitivity and selectivity for the recognition of PSA.[23]

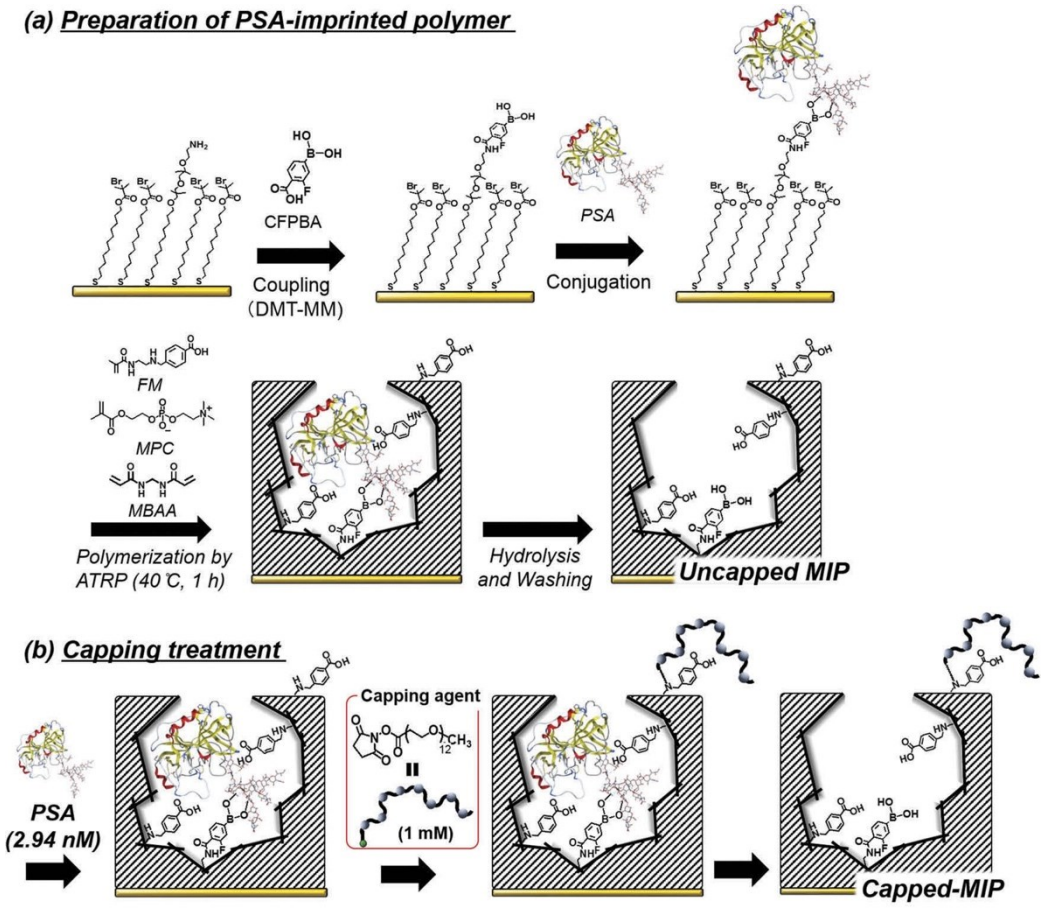

Scheme 2.7 Synthesis of molecularly imprinted polymer with conjugated PSA on the gold-coated SPR sensor chip (a) and the following post imprinting modification with the poly(ethylene glycol)-based capping agent (b). [Matsumoto et al., 2019]

As mentioned above**,** molecularly imprinted polymers (MIPs) are a great potential powerful recognition material for detection of protein with high sensitivity and specificity. Hence, MIPs have greatly advanced in biosensing technologies for food analytical applications because their quality is comparable to natural antibodies, which are popularly used in applications of food analysis. Currently, several MIPs-based sensors include quartz crystal microbalance (QCM), surface plasmon resonance (SPR), electrochemical, and optical sensors have been expanding developed in the areas of food analysis, as they are cost effective, easy preparation, cost production and high stability as stated in Figure 2.7.[24]

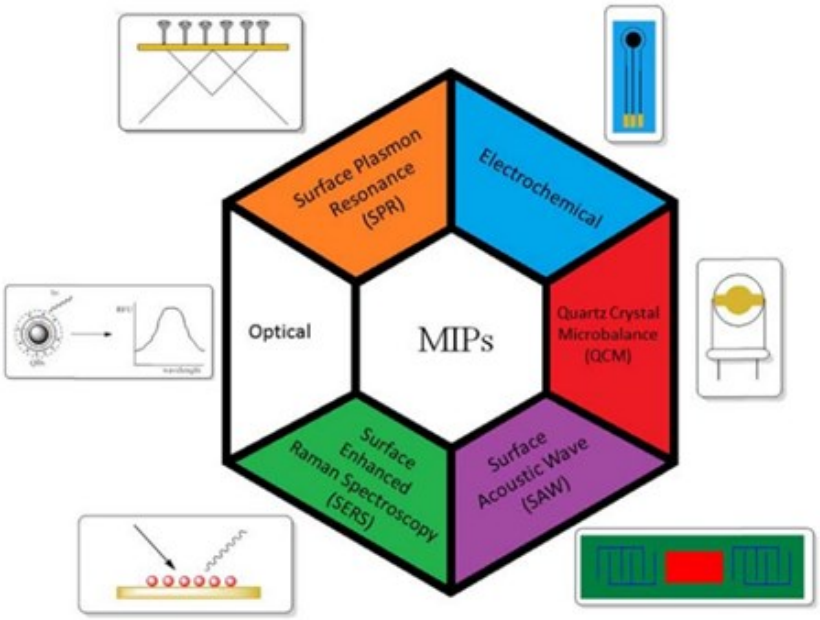

Figure 2.7 Schematic illustration of applications of MIPs-based sensor for food analysis. Reprinted from [Ashley et al., 2017]

2.3.1 MIPs recognition for protein targets

Tretjakov et al., (2013) developed a surface molecularly imprinted polymers (SIPs) thin films for recognition of human immunoglobin IgG using polydopamine (PDA) controlled electrodeposition on QCM based sensor. The IgG template was covalently immobilized on a gold electrode, was then performed electrodeposition of a nm-thin film of PDA. After removal of template molecule, the rebinding of IgG was demonstrated using a flow injection QCM sensor. The developed SIPs with a film thickness of around 17 nm capable of IgG showed good affinity and selectivity presented by imprinting effect of 1.66 and the binding constant of 296

nM.[25] In another interesting study also reported by Tretjakov and coworkers (2016), the integration of MIPs film capable of human IgG with Surface Acoustic Wave (SAW) sensing platform was first developed for detection of IgG. After covalent immobilization of IgG on the SAW chips, the ultrathin polymeric films were performed with surface imprints of IgG (IgG-MIPs). Then, the IgG-MIPs was integrated with SAW sensing via facial electrochemical synthesis approach as seen in Scheme 2.8. Under the optimum of film thickness (11 nm), the IgG-MIPs based sensor exhibited high selectivity for detection of IgG by the imprinting factors toward IgG in the range of 2.8-4, while their recognition efficiencies showed more better than that of the interfering proteins, IgA and HSA. The results indicated that the developed MIPs-based SAW sensor provided an efficient method for cost effective fabrication of biosensor for biological sample analyses.[26]

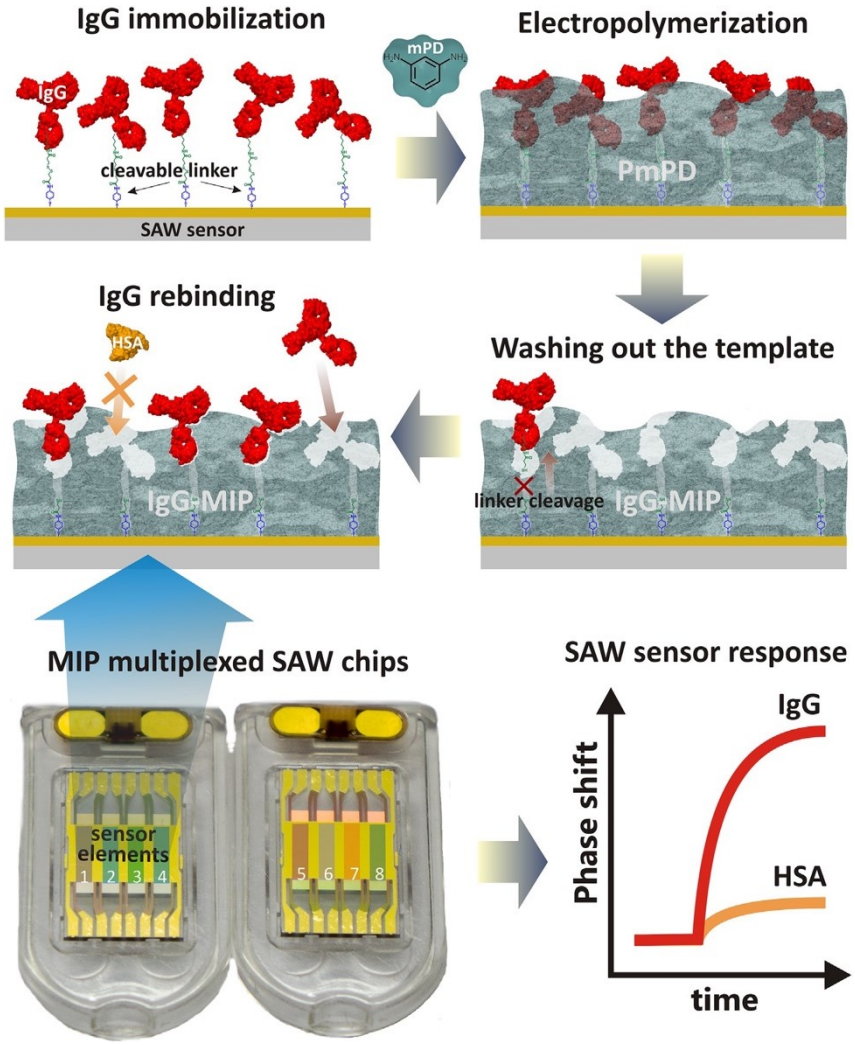

Scheme 2.8 Schematic illustration of preparation of IgG-MIPs based SAW sensor. Reprinted from [Tretjakov et al., 2016]

In a study conducted by Li and colleagues (2016), the surface protein imprinted hydrophilic core-shell particles capable of porcine serum albumin (PSA) using a metal chelating method was demonstrated. Firstly, the MIPs were immobilized on silica beads using copper (II) chelating interaction, and the free radical polymerization was performed at 25 °C using 2-hydroxyethyl methacrylate and methacrylic acid as the hydrophilic functional monomers. The imprinted cavities of 5 μm was left on the PSA-imprinted core- shell particles (MIPs) after removal of template and copper ion as shown in Scheme 2.9. The evaluate the binding affinity and selectivity of MIPs core-shell particles, the chromatographic analysis was performed by HPLC. The novel developed MIPs capable of PSA showed high selectivity and affinity toward the PSA even in presence of the competitive protein owing to the recognition sites located on the hydrophilic polymer shell. This confirmed that the protein imprinted materials could be a great potential for protein separation application.[27]

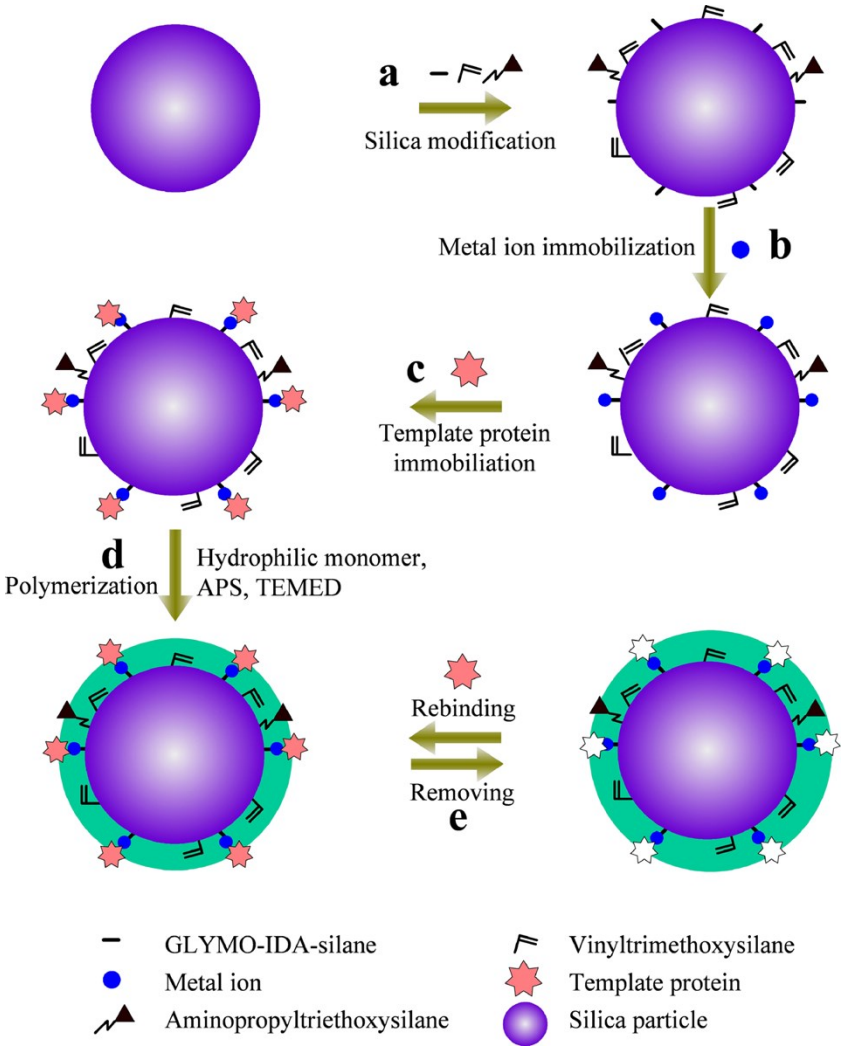

Scheme 2.9 Schematic representation of preparation of surface imprinted core-shell particles capable of PSA with metal chelating. Reprinted from [Li et al., 2016]

Bertolla and colleagues (2017), developed the solvent-responsive molecularly imprinted poly(acrylamido)-derivative nanogels (PAD-nanoMIP) capable human serum transferrin (HTR). The developed PAD-nanoPIM showed their bifunctional characters of selectively binding toward HTR and responsive to solvent, where both characteristics were proven compatible to MALD-TOF-MS targeted protein analysis as seen in Figure 2.8. Under MALDI-TOF-MS analytical platforms, the PAD-nanoMIP exhibited a fast and easy protocol with no restraint of the nanomaterial, and provided strong affinity and selectivity toward HTR even in real serum samples.[28]

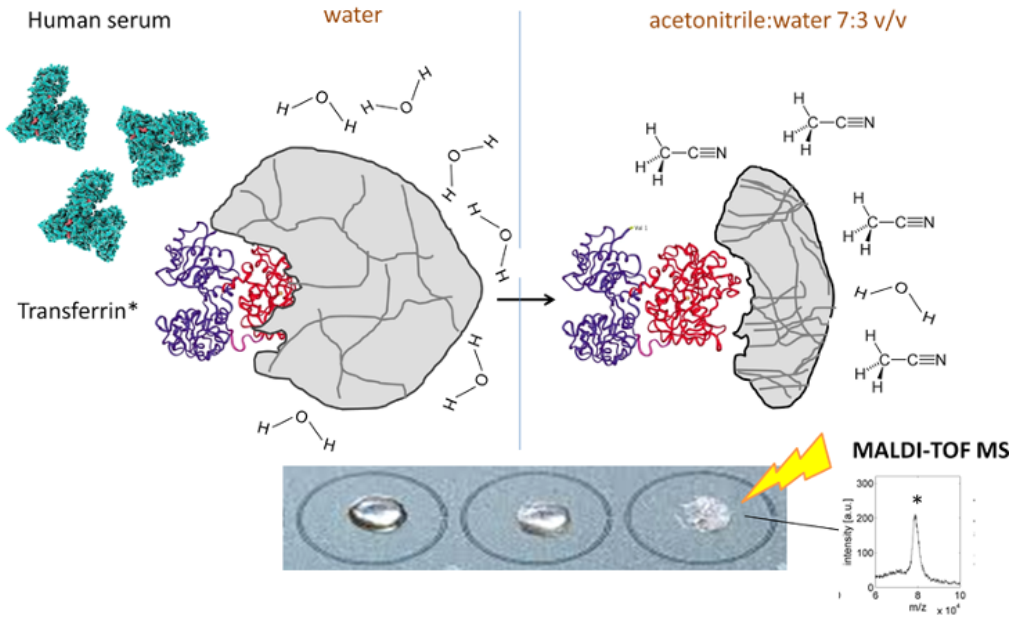

Figure 2.8 A novel solvent-responsive transferrin-imprinted nanogels/MALDI MS method for targeted protein analysis. Reprinted from [Bertolla et al., 2017]

Qin et al., 2018 prepared a novel dual-template epitope imprinting polymer coated on magnetic carbon nanotubes (MCNTs@D-EMIP) for highly specific recognition of porcine serum albumin (PSA) via dual-template epitope imprinting, metal chelation imprinting and distillation-precipitation polymerization (DPP). As seen in Scheme 2.10, the MCNTs@D-EMIPs were prepared using DPP method, where C-terminal peptides and N-terminal peptides of PSA were selected as templates, Zinc acrylate and N-isopropylacrylamide were used as functional monomers and cross-linker, respectively. Firstly, the template epitopes were immobilized on magnetic carbon nanotube by metal chelation and six-membered ring formed with zinc acylate. In their study, the MCNTs@D-EMIPs was prepared in only 30 min, which was faster than that of the other polymerizations. Then, the rebinding experiment was

performed by UV-vis spectroscopy and HPLC to evaluate the adsorption capacity of proteins. This method showed high affinity and specificity presented by its adsorption amount and imprinting factor of 45.05 mg/g and 4.50, respectively. In another important study was also reported by Qin and colleagues (2018), the new type of thermosensitive MCNTs@D-EMIP for simultaneous recognition of human serum albumin (HSA) and transferrin (Trf) via the same procedures as above was developed. The results showed that this method exhibited high affinity and selectivity for recognition of protein targets even in the real blood serum samples. Moreover, the MCNTs@D-EMIP presented a thermosensitive property to realize temperature-controlled recognition and release of target proteins. Integrating with HPLC platform, MCNTs@D-EMIP has a great potential to be a recognition material for application in protein separation areas.[29-30]

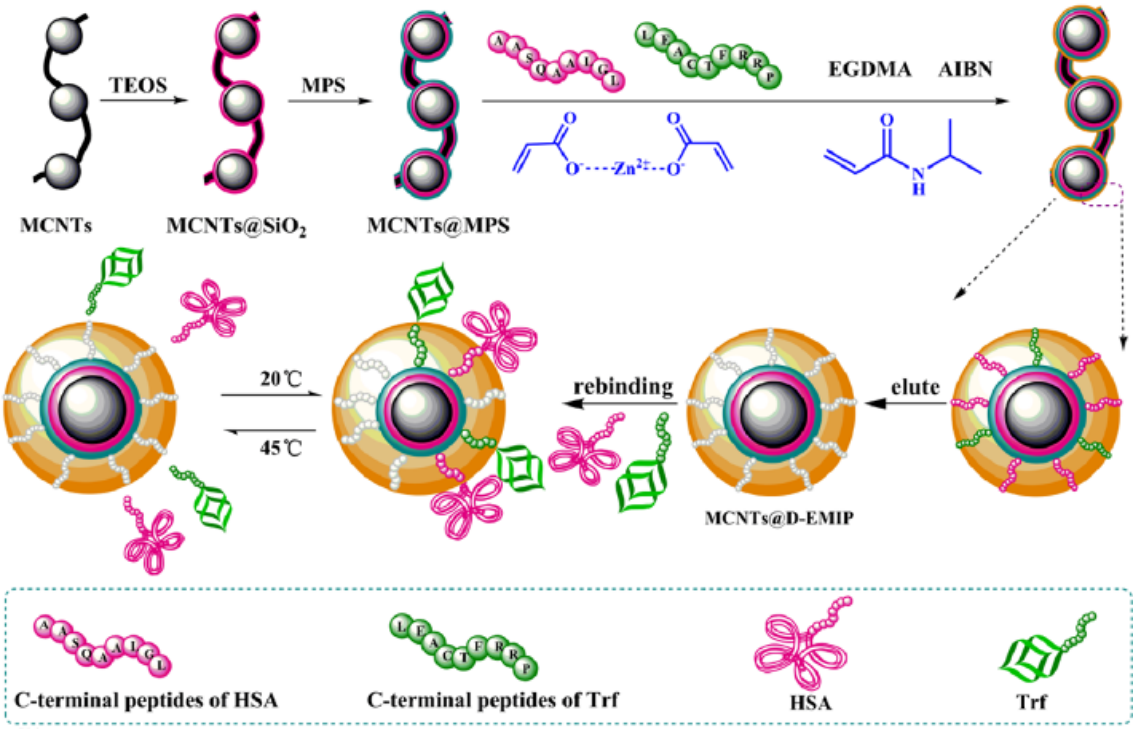

Scheme 2.10 Schematic illustration of preparation MCNTs@D-EMIP via dual-template epitope imprinting, metal chelation imprinting and distillation-precipitation polymerization (DPP). Reprinted with modified from [Qin et al., 2018]

In another interesting study published by Sun and Zhong (2018), a novel strategy for preparing MIPs fabricated using Pickerling emulsions stabilized solely by denatured casein nanoparticles (DCP) was developed for selective recognition of bovine hemoglobin (BHb). In their study, they developed MIPs capable of protein based on DCPs-stabilized Pickerling

emulsions for fabrication for the first time. Before dopamine polymerization, the DCPs were prepared using acidification and heat denaturation followed by establishing them as emulsifier for oil-in-water Pickering emulsions. After polymerization and removal of template protein, more imprinted cavities were exposed on the surface of the polymeric materials as shown in Scheme 2.11. This method showed high affinity and excellent selectivity for recognition of BHb with easy regeneration for recycling, allowing more feasibility to be a new method for protein purification and separation.[31]

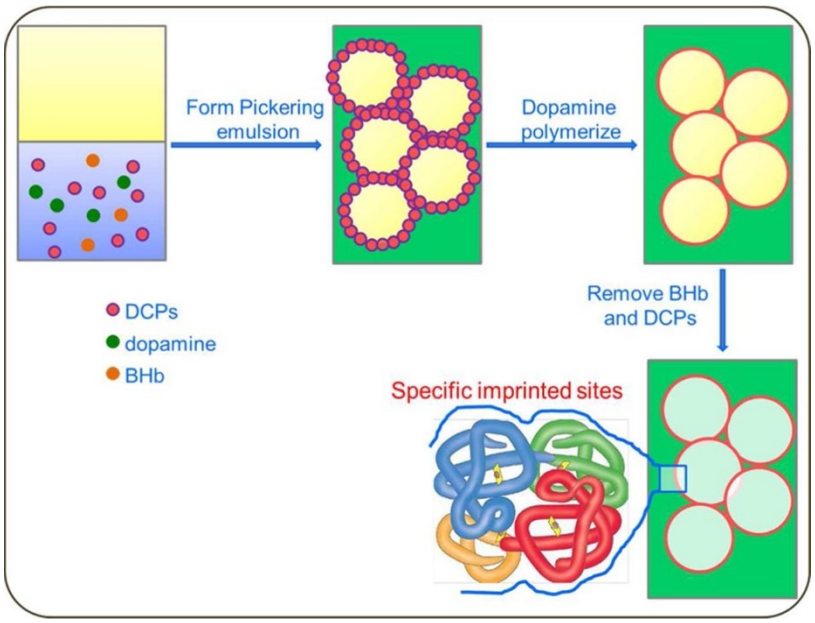

Scheme 2.11 Schematic representation of the preparation of MIPs based on a denatured casein nanoparticle (DCP)-stabilized Pickering emulsion capable of BHb bovine hemoglobin. Reprinted from [Sun and Zhong et al., 2018]

In a reported study, Li et al., (2019) developed a new approach for preparation of highly sensitive and selective hybrid Aptamer-MIPs for recognition of target proteins. In this study, aptamer was used as ligand, and immobilized into a gold thin-layer coated for conjugation of template protein as glycoprotein alkaline phosphatase (ALP) and controlling surface imprinting via dopamine polymerization as seen in Scheme 2.12. After removal of templated protein, an aptamer-MIPs exhibited excellent affinity and selectivity for recognition of ALP presented by low cross-reactivity of 3.2-5.6% and a dissociation constant of 1.5 nM. Moreover, the developed aptmer-MIPs based on a plasmonic immunosandwish assay (PISA) was reliable to detect of ALP even in real human serum samples.[32]

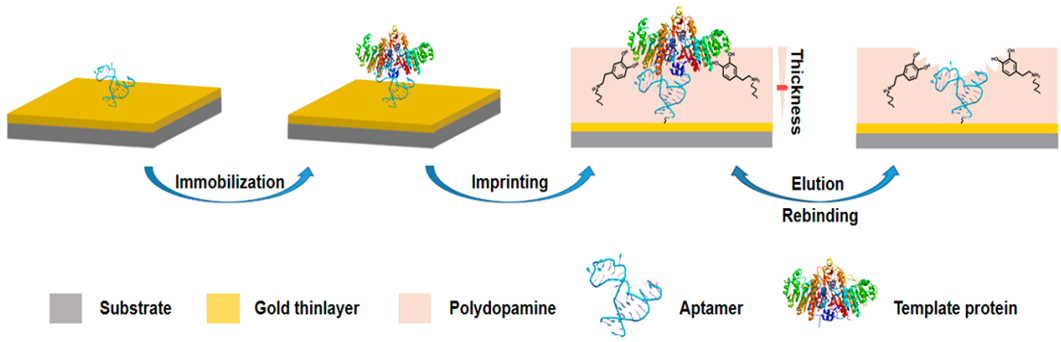

Scheme 2.12 Schematic overview of the preparation of hybrid aptamer-MIPs for recognition of glycoprotein alkaline phosphatase. Reprinted from [Li et al., 2019]

Kitayama and Isomura (2020), developed a gas-stimuli responsive MIP particle for recognition of protein targets using switchable functional monomer for the first time. The MIP particles were prepared in core-shell-type MIPs particles, where 2-diethylaminoethyl methacrylate was used as a gas-responsive functional monomer (DEAEMA) with CO_2- and N_2-responsive interaction sites, using emulsifier-free emulsion polymerization followed by seeded polymerization in aqueous solution as shown in Figure 2.9. After the removal of template molecule, the binding property of the MIP particles toward HSA and the reference proteins was investigated by micro BCA assay, which was performed to determine the protein concentration in the supernatant of incubated MIP particles with protein targets. The developed MIP particles exhibited good affinity for recognition of HSA over the reference proteins such as IgG, Cytochrome, and Lysozyme. The results indicated that MIP particles can be more suitable application in protein separation areas owing to their high usability, low cost, and low toxicity.[33]

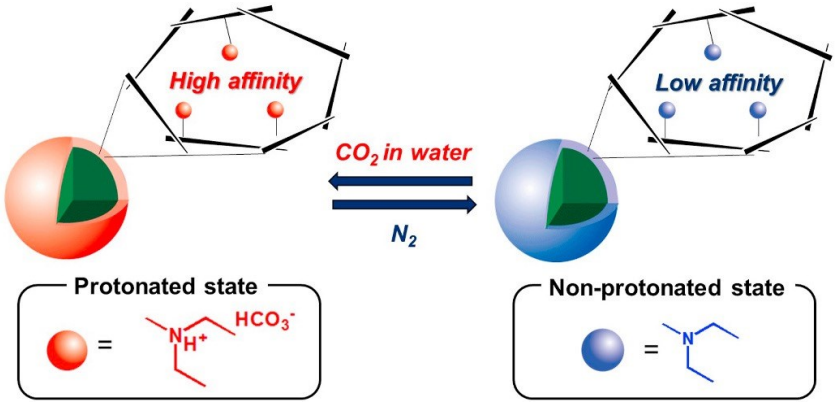

Figure 2.9 Preparation of Mild-gas-stimuli-responsive core-shell MIP particles synthesized. Reprinted from [Kitayama and Isomura et al., 2020]

In a recent study reported by Piloto and colloquies (2021), the integration of MIPs with Quantum dots (QDs) for recognition of the cardiac biomarker myoglobin (Myo) was developed. The MIPs were prepared using Myo as a template molecule, acrylamide as a functional monomer and bisacrylamide as a cross-linker. After conjugation of MIPs with QDs, the imprinted cellulose membrane (HEC/MIP@QDs) was performed by assembly of the cellulose with MIP@QDs as seen in Figure 2.10. The binding response was evaluated by fluorescent quenching of the imprinted membrane occurred with increasing of concentration of target protein (Myo). This method provided a portable, flexible, and robust substrate to detect of Myo with high sensitivity and selectivity presented by low detection limit of 3.08 pg/mL and an imprinting factor of 1.65, respectively. The results confirmed that the HEC/MIP@QDs have a great potential to be applied in clinical analysis areas.[34]

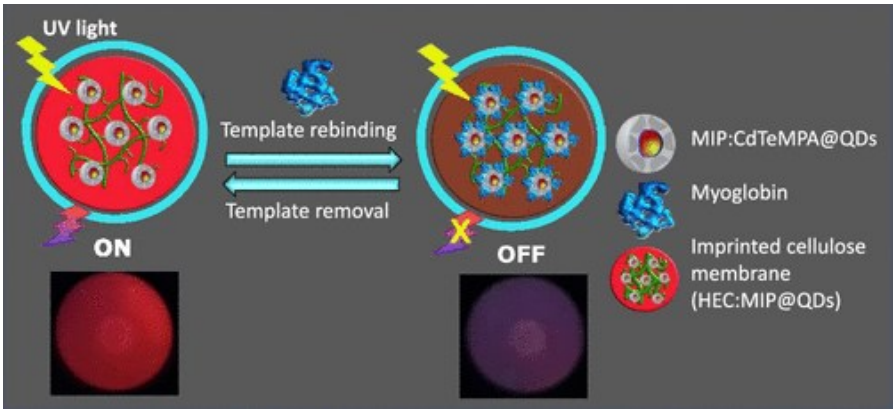

Figure 2.10 Schematic illustration of the assembly of the imprinted cellulose membrane. Reprinted from [Piloto et al., 2021]

2.3.2 Post-imprinting modifications (PIM)

Deng et al., (2013) developed a simple selective fluorescent molecularly imprinted polymers sensing for recognition of Lysozyme (Lys) using molecular imprinting and post-imprinting modification methods (F-Lys-MIPs). The developed sensor was prepared by grafting MIPs onto the surface of multi-wall carbon nanotubes, followed by conjugation of fluorescein isothiocyanate (FITC) via post-imprinting method. Then the binding properties of F-Lys-MIPs toward Lys were evaluated by fluorescence quenching as shown in Scheme 2.13. The proposed sensor exhibited good selectivity for detection of Lys over the competitive proteins such as hemoglobin (HB), bovie serum albumin (BSA), and cytochrome C (Cyt C).[35]

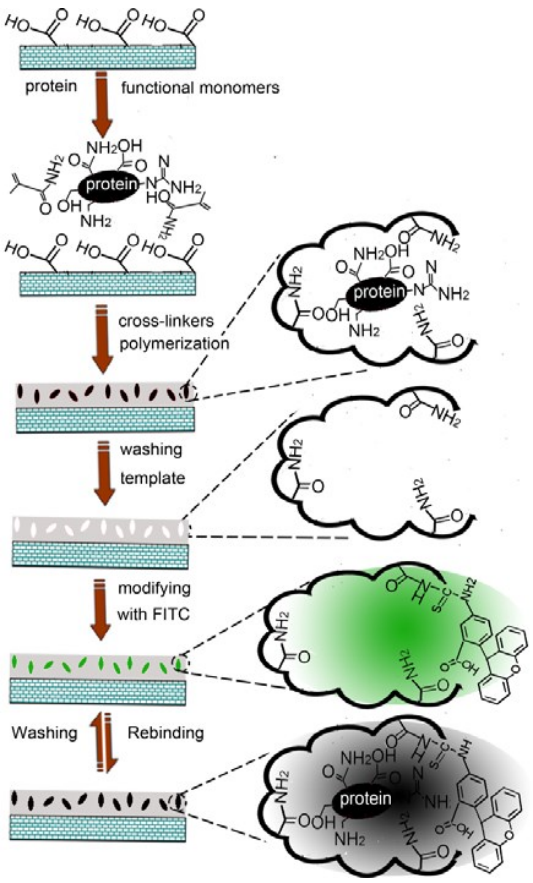

Scheme 2.13 Schematic representation of the preparation of fluorescent MIPs for protein recognition. Reprinted from [Deng et al., 2019]

In another interesting study reported by Sunayama et al., (2014), developed a novel approach of preparation of fluorescent MIPs capable of Lysozyme (F-MIPs) via molecular imprinting followed by the two-step post imprinting chemical modification (PIMs). MIPs were prepared by copolymerization of 4-[2-(N-methacrylamido)ethyl-aminomethyl] benzoic acid (MABA) (Figure 2.11), which composes of benzoic acid for interaction with template proteins and a secondary amine for post-imprinting modifications, acrylamide, and N,N-methylenebis-acrylamide in the presence of Lys. After removal of template protein, two-step post imprinting modification was firstly performed by capping treatment with *p*-isothiocyanatophenyl α-D-mannopyranoside (MITC) to block exposed amine group, followed by introduction of FITC into the imprinted cavities via covalent bonding as a second post-imprinting modification step (MITC-capped-F-MIPs) (Scheme 2.14). The protein binding was evaluated by fluorescence and surface plasmon resonance (SPR) measurements. The results showed that MITC-capped-F-MIPs exhibited high affinity for recognition of Lys.[36] And another important study also reported by Sunayama and colleagues (2018), developed a method to regulate the intrinsic

protein binding activity of lysozyme-imprinted polymers using in cavity-PIMs. The ({[2-(2-methacrylamido)-ethyldithio]-ethylcarbamoyl}-methoxy)acetic acid (MDTA), which includes a disulfide linkage for PIMs, and carboxy group to interact with lysozyme, was used as a functional monomer for MIPs preparation. After copolymerization with cross-linker and removing of template protein, the various functional groups include carboxy, sulfonate, amino, and oligo-ethylene oxide, were introduced to the exposed thiol groups via a disulfide exchange reaction as shown in Scheme 2.15. Then the protein binding and selectivity toward Lys was evaluated by SPR. The results concluded that the modification of lysozyme-imprinted cavities can regulate the protein binding activity, allowed them to be a potential powerful method to develop MIPs for protein with high sensitivity.[37]

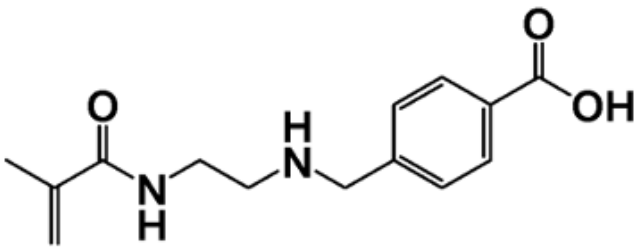

Figure 2.11 Chemical structure of MABA as a functional monomer. Reprinted with modified from [Sunayama et al., 2021]

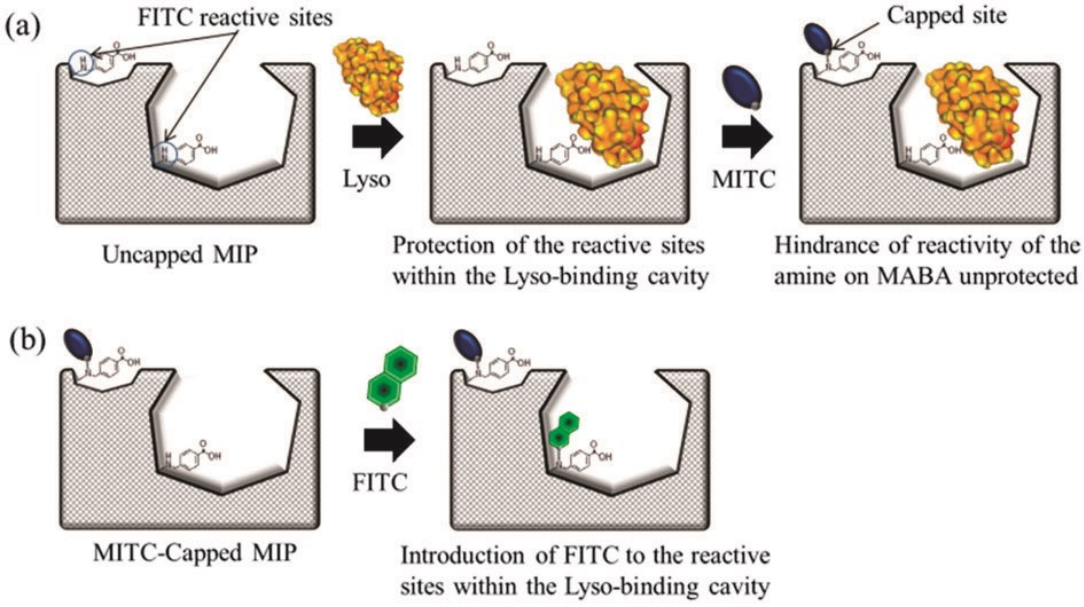

Scheme 2.14 Schematic representation of the preparation of fluorescent MIPs for protein recognition. Reprinted from [Sunayama et al., 2014]

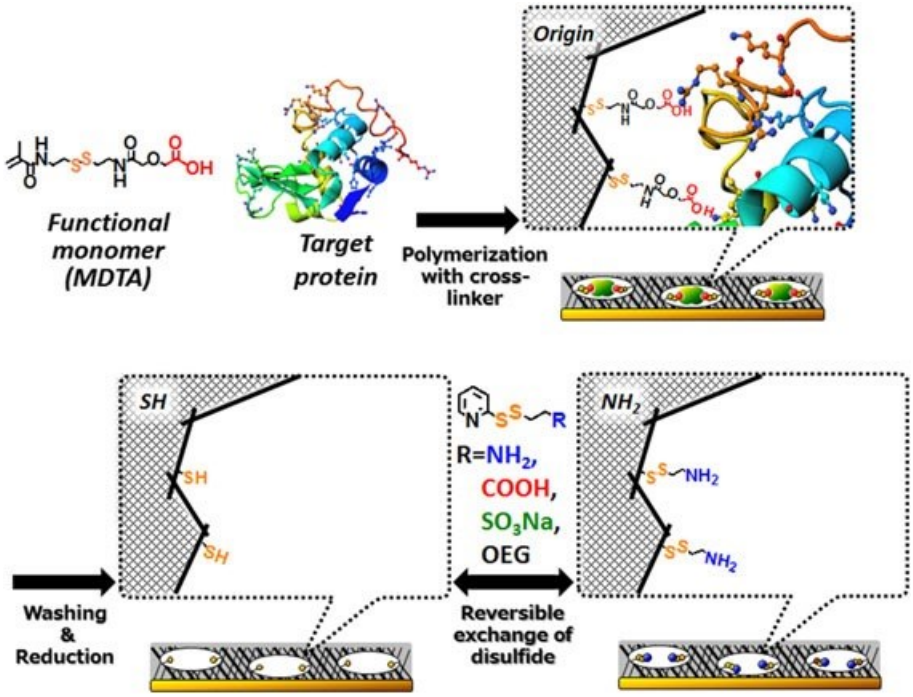

Scheme 2.15 Schematic representation of the preparation of Lys-imprinted polymer via post-imprinting modifications to exchange functional groups within the imprinted cavity. Reprinted from [Sunayama et al., 2018]

Lu et al., (2019), developed a highly sensitive fluorescent MIPs capable of bisphenol A (BPA) via post-imprinting modification based on multilevel mesoporous silica (p-MIFPs). After preparation of multilevel mesoporous-structured BPA-imprinted polymers (MIPs) using doping method, the template BPA was eluted from them by acid ethanol, and the quantum dots QDs and carbon dots (CDs) were then conjugated onto the large pore of MIPs by condensation reaction to form p-MIFPs as seen in Scheme 2.16. In their study, the sensitivity of p-MIFPs was higher than that of the fluorescent MIPs, which were prepared using the doping method (d-MIFPs). Moreover, the developed method was completely applied to detection of BPA in water samples with high recovery rate from 96.4% to 102.0% and acceptable %RSD of 4.1%. The results confirmed that post-imprinting modification is an effective method for improvement the sensitivity of MIFPs.[38]

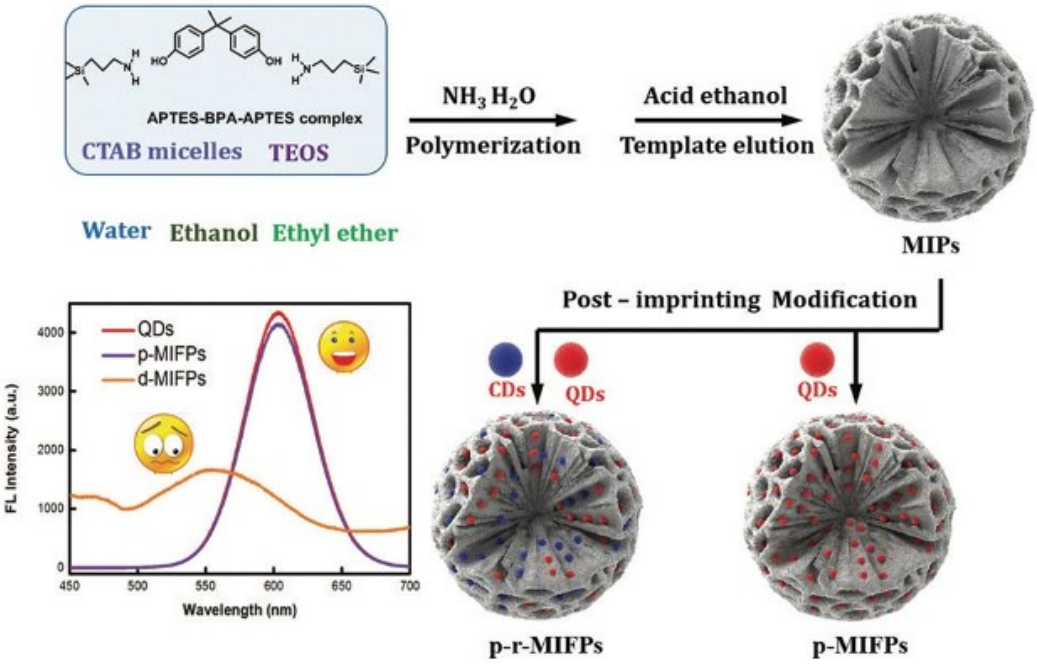

Scheme 2.16 Schematic illustration of the preparation of MIPs using the post-imprinting modification strategy. Reprinted from [Lu et al., 2019]

In another interesting study published by Morishige and colleagues (2019), developed a sensitive and selective MIPs nanocavities via molecular imprinting and PIM for recognition of α-fetoprotein (AFP) as a glycoprotein marker for hepatocellular carcinoma dieses. After immobilization of AFT on the mixed self-assemble monolayer (mixed SAM) formation, the surface-initiated atom transfer radical polymerization was performed via activators generated by electron transfer. And then two synergetic orthogonal binding sites in the imprinting cavity were created by the removal of AFP with reduction and hydrolysis method followed by introduction of fluorescent dye into nano cavities by PIM as shown in Scheme 2.17. This method exhibited high sensitivity and selectivity for AFP over the other reference proteins presented by low detection limit of 3.9 pM in diluted human serum.[39]

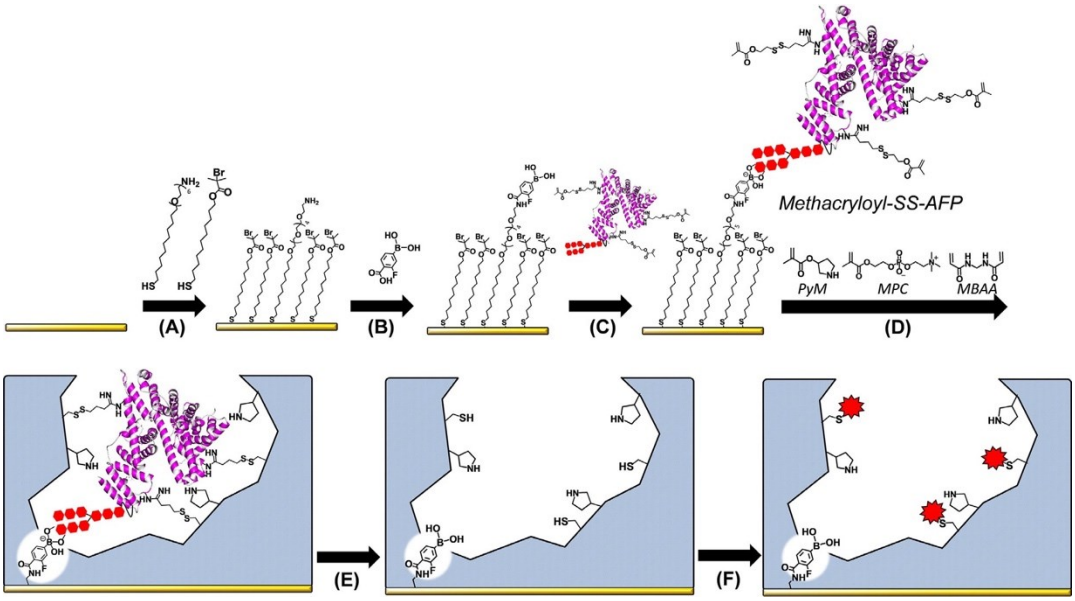

Scheme 2.17 Schematic overview of the preparation of AFP-imprinted thin layer using molecular imprinting and PIMs. Reprinted from [Morishige et al., 2019]

In a recent study reported by Saeki et al., (2020), developed fluorescent molecularly imprinted nanocavities possessing orthogonal dual interaction sites using molecular imprinting and sequential multistep post-imprinting for the detection of prostate cancer biomarker (PSA). In this study, a newly designed multi-functionalised PIM reagent (PIR), which has an interaction site and dual reaction sites for PIMs, allowed to introduce multiple functions including interaction sites and fluorescent reporter groups. Then the surface-initiated atom transfer radical polymerization was performed followed by removing of the template protein, leading to create multi-binding sites for 1st PIM and 2rd PIM by conjugation of PIR and fluorescence reporter, respectively as indicated in Scheme 2.18. This method showed highly sensitive and selective detection of PSA. Moreover, the new sequential PIM method using PIR can potentially prepare various sophisticated artificial molecular recognition materials.[40]

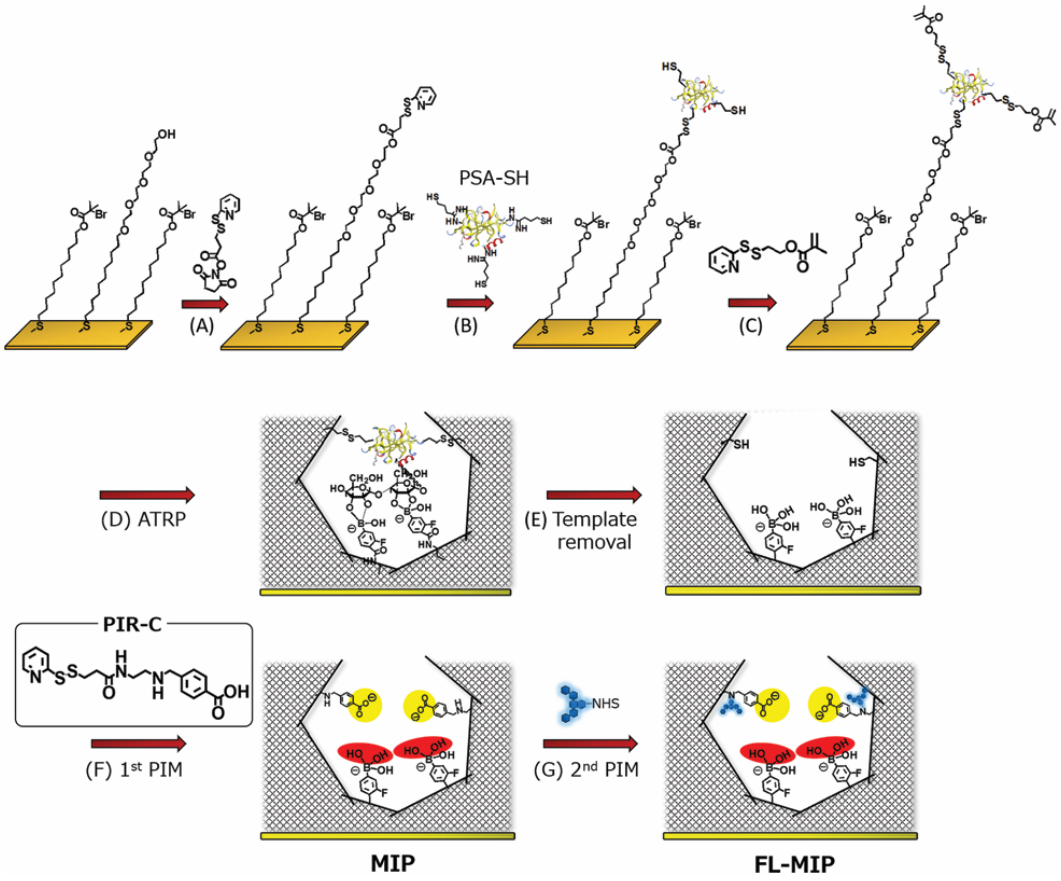

Scheme 2.18 Schematic illustration of the procedure of MIPs thin layer using molecular imprinting and fluorescent reporting groups via PIMs. Reprinted from [Saeki et al., 2020]

2.3.3 Development of MIPs-based sensor in food analysis

Currently, there are several MIP-based mimetic sensors using MIPs as a selectively artificial recognition materials for application in food area analyses including food safety, food control, and food quality. Normally, the MIPs were used as a sorbents of molecularly imprinted solid phase extractions (MISPEs) method for extraction, purification, and concentration of interest compounds in complex food matrix samples. For decade, the MIP-based sensors were rapidly developing due to their more excellent sensitivity, high specificity, fast detection, simple operation and cost-effective than that of conventional analytical methods for detection of target molecules in food analysis as shown in Table 2.5.[41]

Table 2.5 Representation of development of MIPs-based sensor in food analysis. Reprinted with modified from [Song et al., 2014]

Transduction scheme	Analyte	Functional monomer	MIP preparation procedure	Sample
UV-visible spectroscopy and EIS	Cholesterol	MAA	UV-initiated radical	Aqueous
Diffraction intensity	Diethylstilbestrol	7.5:1 MMA/AM	Thermoradical	Food
CL	Fenvalerate	AM	Thermoradical	Fruits and vegetables
SERS	BPA	Triethoxysilane template complex (BPA-Si)	Sol-gel process	Beverage
SPR	Chlorpyrifos	Dopamine	Oxygen	Apple
FD	PAHs	MAA	Thermoradical	Milk
FD	Lysozyme	$(NH_4)_2TiF_6$	Liquid-phase deposition	Proteins
DP	Oxytetracycline	Prussian blue	Electrochemical	Milk
FD	Penicillin G	MAA	Thermoradical	Milk
CV and DPV	Melamine	MAA	Thermoradical	Milk
BELISA method	Metolcarb	Acrylamide	Thermoradical	Apple juice
Chronoamperometry	Hydroquinone	MAAM	UV-initiated radical	Water
EIS	BPA	BPA-terthiophene and carbazole	Electrochemical	Aqueous
DPV	2,4-Dichlorophenol	MAA	Thermoradical	Tap water
DPASV	L-Aspartic acid	NAPD	ATRP	Pharmaceutics
Potentiometry	Chlorpyrifos	MAA	Thermoradical	—
Potentiometry	BPA	BIS-DMA	Thermoradical	Drinking bottles
Potentiometry	Clenbuterol	MAA, MMA	Thermoradical	Pig urine
CV	Horseradish peroxidase	AM, APB	Oxidative	Proteins
QCM	BHb, Tryp	NHMA, NiPAm	Catalyzed	Proteins
QCM	L-Nicotine	MAA	Thermoradical	Saliva
QCM	Melamine	Bis(2,2′-bithienyl)-benzo-[18-crown-6]methane	Electrochemical	—
Impedometric detection	Desmetryn	AMPS	UV-initiated radical	Drinking water
Interdigitated capacitance	Hevein allergenic proteins	6:2 MAA:NVP	Thermoradical and oxidative	Latex rubber

Anirudhan et al., (2017), developed a novel magnetic molecularly imprinted polymers (MMIPs) for recognition of melamine in application of protein separation. The melamine, 2-acrylamido-2-methylpropane sulfonic acid (AMPS), N,N”-methylenebisacrylamide (MBA) potassium persulfate (KPS) were used as a template molecule, functional monomer, cross-linker and initiator, respectively, for copolymerization using surface imprinting on vinyltrimethoxysilane coated Fe_3O_4 (Fe_3O_4-VTMS) as seen in Scheme 2.19. After the removal of template molecule. the binding investigations of the MMIPs toward melamine was evaluated by HPLC-UV-visible spectroscopy, which was performed to determine melamine concentration in the supernatant of incubated MMIPs with target molecules. This method exhibited good affinity and fast detection for detection of melamine in milk samples. The results indicated that the MMIPs is a promising solid phase extraction of melamine from complex matrices with good selective, rapid, and efficient preconcentration.[42]

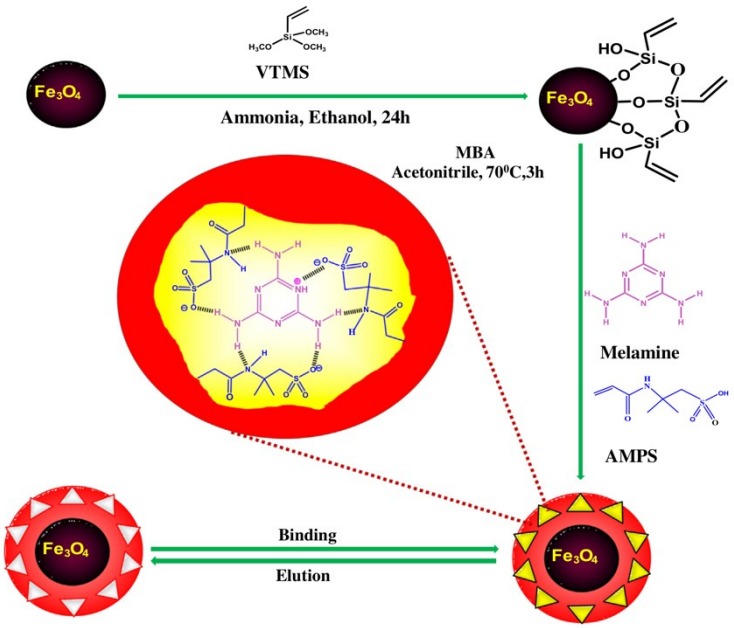

Scheme 2.19 Schematic illustration of the preparation of MMIPs. Reprinted from [Anirudhan et al., 2017]

In an interesting reported by Ashley et al., (2018), they have developed MIP-based SPR sensor for detection of α-Casein as a milk allergen molecular marker. The MIP nanoparticles were prepared by a solid-phase imprinting method, and were then immobilized on gold surface via covalent bonding as a sensitive and selective MIP-based SPR sensor for α-casein detection as shown in Figure 2.20. This method exhibited a good affinity and selectivity for detection of α-casein achieving a detection limit of 0.127 ppm, where the performance of developed sensor was comparable to that of commercial ELISA kits. Therefore, this proposed sensor is potential to detect milk allergen in food processing samples for food safety and food control.[43]

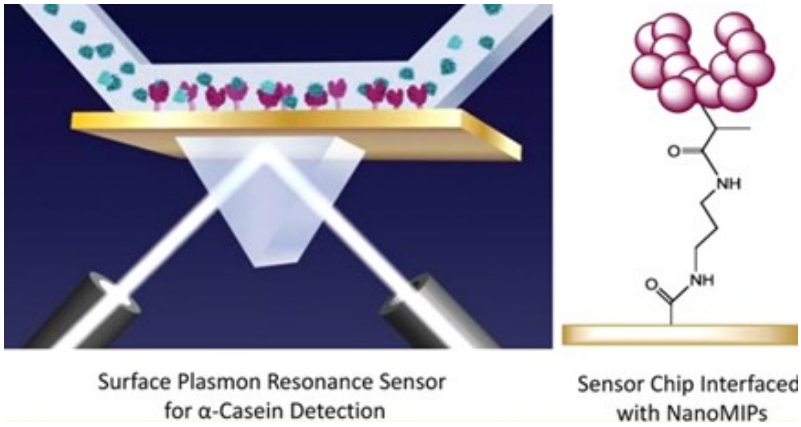

Scheme 2.20 Schematic illustration of MIP-based SPR sensor. Reprinted from [Ashley et al., 2018]

In a recent study published by Aguilar and colleagues (2020), a selective molecularly imprinted polymer (MIP) was developed for detection of tetracycline (TC) in milk samples. The MIPs were prepared using methacrylic acid as a functional monomer, ethylene glycol dimethacrylate as a cross-linker, persulphate as an initiator for precipitation polymerization method. After removal of the template molecule, the rebinding of MIPs toward TC was investigated using surface plasmon resonance-based sensor as seen in Scheme 2.21. The developed MIPs-based sensor showed high affinity and selectivity for detection of TC in milk samples. The results indicated that the proposed sensor provided a potential significant method to develop MIP-based sensor for detection of several contaminants in complex samples for food analysis.[44]

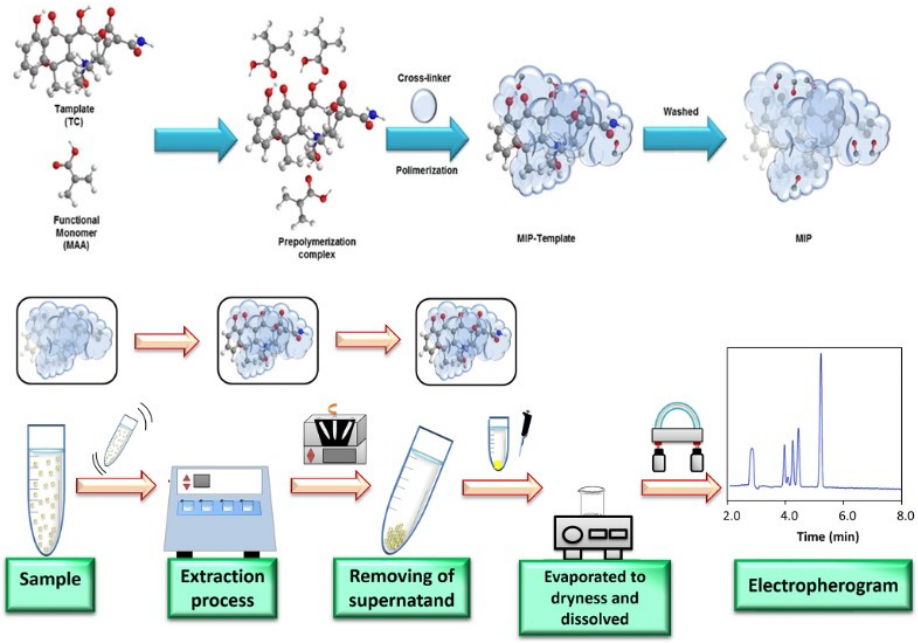

Scheme 2.21 Schematic illustration of MIP-based SPR sensor. Reprinted from [Aguilar et al., 2018]

The literature reviews showed that the authentication of halal food products using an accuracy, simple, and rapid analytical methods is very important for global halal food industry. To overcome the drawbacks of using natural receptors, MIPs as a selectively artificial receptor is considered as the novel advance biosensors for detection of pork contamination in halal food analysis. I believe that the MIPs-based sensors is a great potential powerful method to detect pork contamination for halal food control. From the best of our knowledge, the development of MIP-based sensors for halal food analysis has not been reported. In this dissertation, i have first attempted to develop and evaluate the feasibility of MIP-NGs to be a reliable candidate method for applications in halal food control.

2.4 Reference

(1) Pew Research Center, **2017**, "The Changing Global Religious Landscape".

(2) Nurrachmi, R. *TIFBR,* **2017**, 11 (1), 39-56.

(3) Hassan, N. *Seminar UICW*, **2014.**

(4) Abdul-Rahman, M.S. The Qur'an with tafsir ibn Kathir; MSA Publication Limited; Herne Hill: London, **2017**.

(5) The Food and Agriculture Organization (FAO), **2021**, "The FAO Meat Price Index".

(6) Sakalar, E.; Kaynak, A. *Int. J. Food Prop.* **2016**, 19, 31–40.

(7) Lee, S.Y.; Kim, M.J.; Hong, Y.; Kim, H.Y. *Food Control* **2016**, 66, 53-61.

(8) Al-Kahtani, H.A.; Ismail, E.A.; Ahmed, M.A. *Food Chemistry* **2017**, 219, 54-60.

(9) Cai, Y.; He, Y.; Lv, .R.; Chen, H.; Wang, Q.; Pan, L. *PLoS ONE* **2017**, 12 (8), 181949.

(10) Amaral, J.S.; Santos, G.; P.P.Oliveira, M.B.; Mafra, I. *Food Control* **2017**, 72, 53-61.

(11) Kuswandi, B.; Gani, A.T.; Kristiningrum, N.; Ahmed, M. *Sens. Transducers.* **2017**, 208 (1), 7-13.

(12) Cahyadi, M.; Wibowo, T.; Pramono, A.; Abdurrahman, Z.H. *Food Sci. Anim. Resour.* **2020**, 40 (4), 628-635.

(13) Lim, S.A.; Ahmed, M.U. *Food Chemistry* **2016**, 206, 197-203.

(14) Kuswandi, B.; Gani, A.T.; Ahmed, M. *Food Biosci.* **2017**, 19, 1-6.

(15) Madli, J.; Fatimi, I.EL.; Seddaoui, N.; Amine, A. *Food Chemistry* **2018**, 255, 380-389.

(16) Thienes, C.; Masiri, J. *J. AOAC* ***Int.*** **2018**, 101(3), 817-823.

(17) Pan, X.D; Chen, J.; Chen, Q.; Huang, B.F; Han, J.L. *RSC Adv.* **2018**, 8, 11157-11162.

(18) Han, F.; Huang, X.; Aheto, J.H.; Zhang, D.; Feng, F. *Food* **2020**, 9, 193.

(19) Wackerling, J.; Schirhagl, R. *Anal. Chem*. **2016**, 88, 250-261.

(20) Wuiff, G.; Sarhan, A. *Angew. Chem. Int. Ed. Engl.* **1972**, 11, 341.

(21) Takeuchi, T.; Kitayama, Y.; Sasao, R.; Yamada, T.; Toh, K.; Matsumoto, Y.; Kataoka, K. *Angew. Chem., Int. Ed*. **2017**, 56, 7088− 7092.

(22) Verheyen, E.; Schillemans, J.P.; Wijk, M.V.; Demeniex, M.A.; Hennink, W.E.; Van Nostrum, C.F. *Biomaterials* **2011**, 32, 3008− 3020.

(23) Matsumoto, H.; Sunayama, H.; Kitayama, Y.; Takano, E.; Takeuchi, T. *Sci. Technol. Adv. Mater.* **2019**, 20 (1), 305-312.

(24) Ashley, J.; Shahbazi, M.A.; Kant, K.; Chidambara, V.A.; Wolff, A.; Bang, D.D.; Sun, Y. *Biosen. Bioelectron.* **2017**, 91, 606-615.

(25) Tretjakov, A.; Syritski, V.; Reut, J.; Boroznjak, R.; Volobujeve, O.; Öpik, A. *Microchim. Acta.* **2013**, 180, 1433-1442.

(26) Tretjakov, A.; Syritski, V.; Reut, J.; Boroznjak, R.; Öpik, A. *Analytica. Chimica. Acta.* **2016**, 902, 182-188.

(27) Li, Q.; Yang, K.; Li, S.; Liu, L.; Zhang, L.; Liang, Z.; Zhang, Y. *Microchim. Acta.* **2016**, 183, 345-352.

(28) Bertolla, M.; Cenci, L.; Anesi, A.; Ambrosi, E.; Tagliaro, F.; Vanzetti, L.; Guella, Graziano.; Bossi, A.M. *ACS Appl. Mater. Interfaces* **2017**, 9, 6908−6915.

(29) Qin, Y.P.; Wang, H.Y; He, X.W.; Li, W.U.; Zhang, Y.K. *Talanta* **2018**, 185, 620-627.

(30) Qin, Y.P.; Wang, H.Y; He, X.W.; Li, W.U.; Zhang, Y.K.. *ACS Appl. Mater. Interfaces* **2018**, 10, 9060−9068.

(31) Sun, Y.; Zhong, S. *Anal. Bioanal. Chem.* **2018**, 410, 3133–3143.

(32) Li, W.; Zhang, Q.; Wang, Y.; Ma, Y.; Guo, Z.; Liu, Z. *Anal. Chem.* **2019**, 91 (7), 4831-4837.

(33) Kitayama, Y.; Isomura, M., *Polymer* **2020**, 203, 122781.

(34) Piloto, A.M.L; Ribeiro, D.S.M.; Rodrigues, S.S.M.; santos, J.L.M.; Sampaio, P.; Sales, G. *Acs Appl. Bio. Mater.* 2021, xx, xxx-xxx.

(35) Deng, Q; Wu, J.; Zhai, X.; Fang, G.; Wang, S. *Sensors* **2013***,* 13, 12994-13004.

(36) Sunayama, H; Ohya, T.; Takeuchi, T. *Chem. Commun.* **2014**, 50, 1347.

(37) Sunayama, H; Kitayama, Y.; Takeuchi, T. *J Mol Recognit.* **2018***,* 31, 2633.

(38) Lu, H; Wei, D.; Zheng, R. Xu, S. Analyst **2019***,* 144, 6283.

(39) Morishige, T.; Takano, E.; Sunayama, H; Kitayama, Y.; Takeuchi, T. *ChemNanoMat.* **2019**, 5, 224 – 229.

(40) Saeki, T.; Takano, E.; Sunayama, H; Kitayama, Y.; Takeuchi, T. *J. Mater. Chem. B,* **2020**, 8, 7987.

(41) Song, X.; Xu, S.; Chen, L; Wei, Y.; Xiong, H. *J. APPL. POLYM. SCI.* **2014**, 131 (16), 40766.

(42) Anirudhan, T.S.; Christa, J.; Deepa, J.R. *Food Chemistry* **2017**, 227, 85–92.

(43) Ashley, J.; Shukor, Y.; D`Aurelio R.; Trinh, L.; Rodgers, T.; Temblay, J.; Pleasants, M.; Tothill, I.E. *ACS Sen.* **2018**, 3, 418-424.

(44) Aguilar, J.F.F.; Miranda, J.M.; Rodriguez J.A.; Paez-Hernandez, M.E.; Ibarra, I.S. *J. Polym. Res.* **2020**, 27, 176.

Chapter 3

A Label-Free Molecularly Imprinted Nanogels Capable of Porcine Serum Albumin- based QCM Sensor for Detection of Pork Contamination

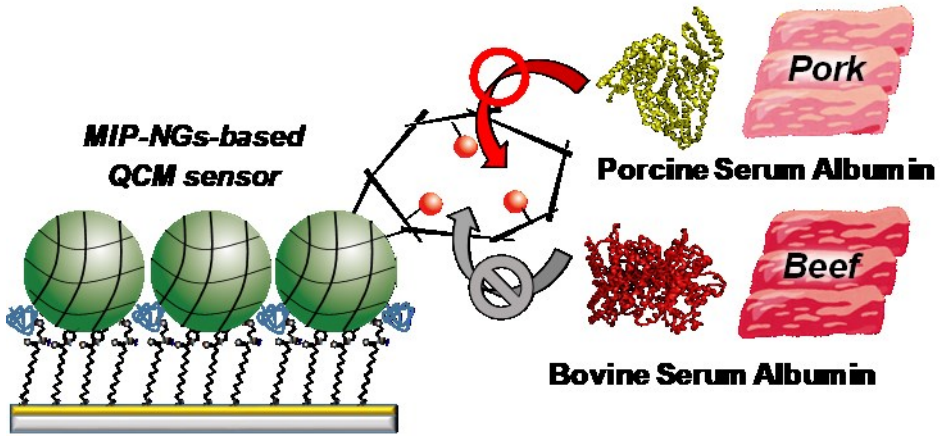

A Label-Free Molecularly Imprinted Nanogels Capable of Porcine Serum Albumin- based QCM Sensor for Detection of Pork Contamination

3.1 Introduction

Porcine serum albumin (PSA) is presented in blood serum of pig (*Sus scrofa*), and it plays critical roles in biological systems such as carrier proteins in blood, carrier of fatty acids and transport innumerable exogenic and endogenic ligands including as a significant allergen from pork. In addition, PSA is also found in all secretions and every tissue of pig. The conformational structure of serum albumin is more stable and very flexible due to their structure consists of α-helix proteins with many of disulfide bridges,[1] resulting in easy to bind with several types of ligands for molecular imprinting process. Currently, many research groups have successfully prepared a variety of selective molecularly imprinted polymers (MIPs) using PSA as a template molecule. Therefore, PSA is a great potential as a protein template for synthesis of MIPs to evaluate the authenticity in halal food control.

Issues of food authenticity are rapidly expanding owing to religious, economic, and cultural concerns. Particularly, a specific type of meat is unacceptable for some populations owing to religious concerns. Within 15 years, the Muslim population is expected to represent around 30% of the world's population; thus, the global halal food industry is currently the fastest-growing consumer segment in the world.[2] The Muslim halal rule requires food products be free from pork and its derivatives. However, for reducing the cost of food production, manufacturers mix pork into food products instead of beef because pork is less expensive than beef.[3] Thus, powerful, easy, and accurate analytical methods for detection of pork derivatives are important to provide the authenticity of halal products, especially in raw meat. For decade, there are numerous analytical methods available for detecting pork contamination in meat products, and the two molecular biomarkers generally used for analyses are proteins and DNA.[4−13] Particularly, protein-based detection methods using immune-based techniques with porcine serum albumin (PSA), such as an enzyme-linked immunosorbent assay (ELISA), and label-free immunosensors have been developed for the detection of pork contamination in meat

products.[14–18] However, these methods, utilizing immune-based techniques, need cumbersome procedures and high budgets for using monoclonal antibodies.

Molecularly imprinted polymers (MIPs) are alternative materials to monoclonal antibodies[19–32] to recognize PSA for the detection of pork contamination in halal meat products. To date, MIPs for protein recognition have been widely applied in many fields[33] such as drug delivery,[34–37] separation,[38–43] and sensors[44–53] owing to their selective recognition capability, high stability, and low cost of production. MIPs for protein recognition are synthesized by forming a polymer around a template protein with functional monomers, comonomers, and cross-linkers to create specific binding cavities, which are complementary in shape, size, and spatial arrangement to the template proteins. The recognition of target proteins by MIPs is based on the steric matching and intermolecular interactions such as hydrophobic and electrostatic interactions, such as the antigen−antibody interaction.[54] Currently, MIP nanoparticles for the detection of proteins are being developed. Their characteristics are close to those of monoclonal antibodies with a few binding sites per unit, high specificity, and rapid interaction with the target protein.[55–57]

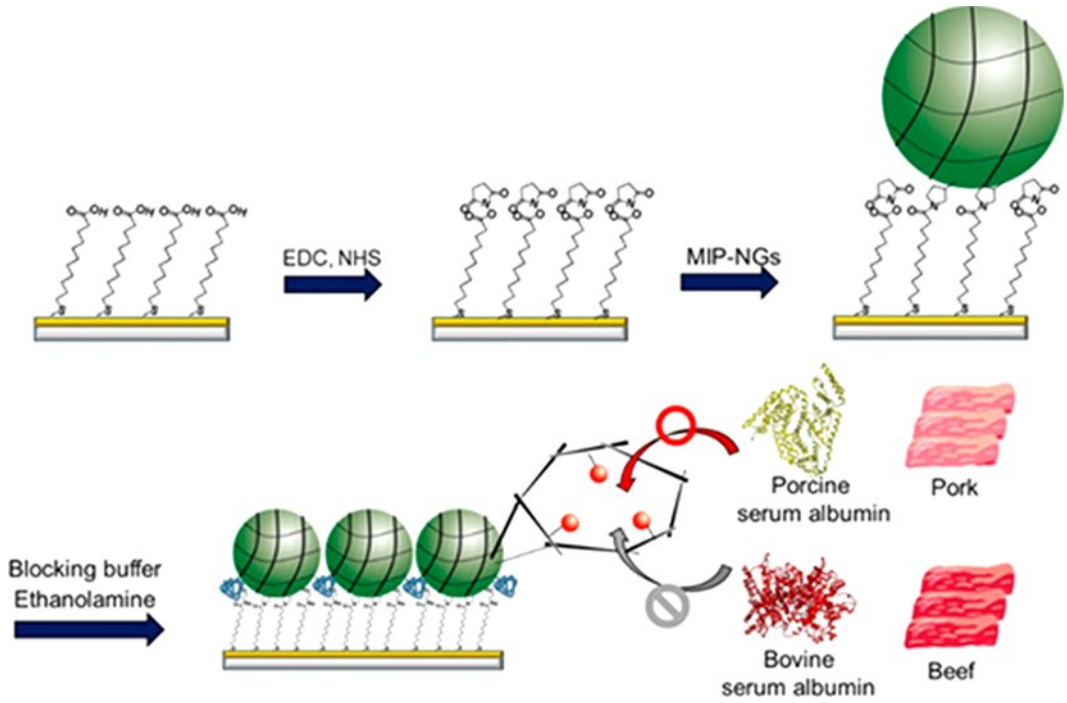

Scheme 3.1 Preparation of MIP-NGs-Based QCM Sensor for PSA Detection.

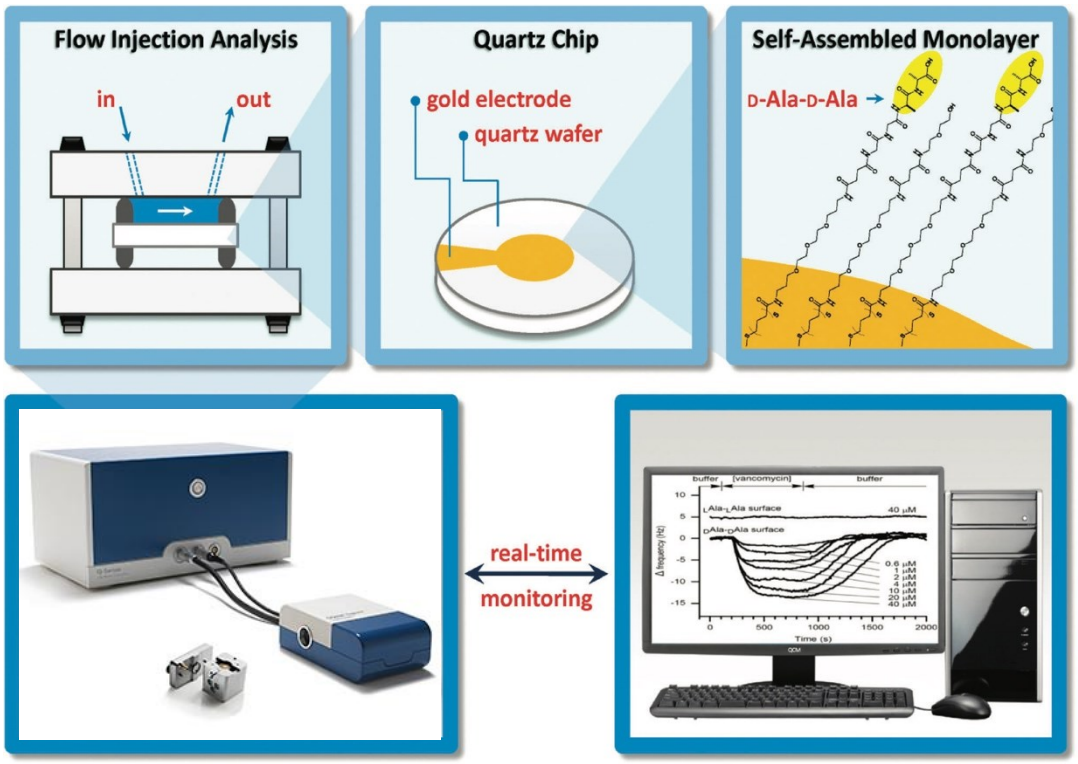

Scheme 3.2 Schematic overview of a QCM system. Reprinted with modified from [Cheng et al., 2012]

To date, there have been no reports of MIP-based sensors for pork contamination in halal raw meats. In this current work, I aimed to prepare molecularly imprinted nanogels (MIP-NGs) for highly specific recognition of PSA by emulsifier-free precipitation polymerization and develop the quartz crystal microbalance (QCM) sensor with MIP-NGs for the sensitive detection of PSA (Scheme 3.1). QCM is a label free technique (Scheme 3.2),[58] which can be detect the target molecules based on the measurement of small mass changes on the sensor chip with sub-nanogram detection capabilities. Currently, QCM was used for protein recognitions in applications of MIPs-based QCM sensor because of their selectivity, high accuracy, sensitivity, and stability.

MIP-NGs were prepared with a partially modified method previously reported for stealth nanocarriers for drug delivery,[36] (Scheme 3.3) where ion-exchange chromatography was employed to effectively remove the template PSA in the purification step.

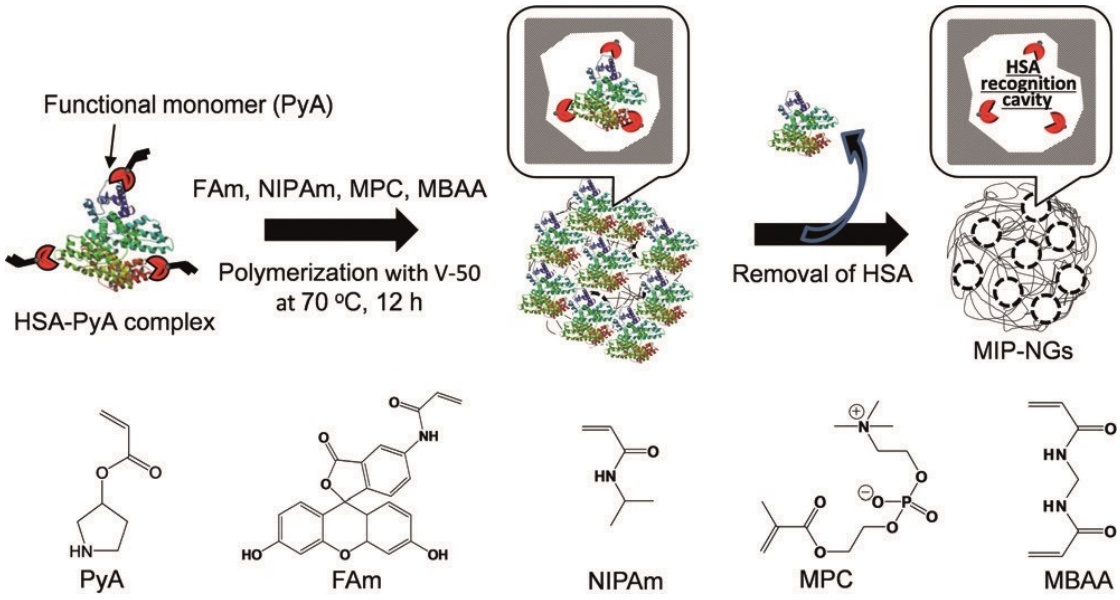

Scheme 3.3 Schematic representation of the preparation of MIP-NGs for human serum albumin (HSA) via emulsifier-free precipitation polymerization. Reprinted from [Takeuchi et al., 2017]

The possibility of detection of pork contamination in halal raw meat was investigated by following two approaches: (i) recovery test of PSA spike in real beef extract, and (ii) detection of extracted proteins derived from beef and pork meats. Furthermore, the detection limit of pork contamination was also investigated using real beef meat extracts.

3.2 Experimental Section

3.2.1 Reagents and Materials

Albumins from pig (PSA), bovine (bovine serum albumin, BSA), human (human serum albumin, HSA), goat (goat serum albumin, GSA), sheep (sheep serum albumin, SSA) and rabbit (rabbit serum albumin, RSA), ethanolamine, N-hydroxysuccinimide (NHS), 11-mercaptoundecanoic acid (MUA), and DEAE–Sephadex A-50 were purchased from Sigma-Aldrich (MO, USA). N- Isopropyl acrylamide (NIPAm), and N,N'-methylenebisacrylamide (MBAA) were purchased from Nacalai Tesque Co. (Kyoto, Japan). 2,2'-Azobis(2-methylpropionamidine) dihydrochloride (V- 50) and ethanol were purchased from Wako Pure Chemical Industries, Ltd. (Osaka, Japan). 2- Methacryloyloxyethylphosphorylcholine (MPC)

was purchased from NOF Corporation (Tokyo, Japan). The QCM sensor chips (QSX 301 Gold) were purchased from Biolin Scientific (Q-sense, Sweden). The Micro BCA Protein Assay Kit and the Protein–Free (PBS) blocking buffer were purchased from Thermo Fisher Scientific (MA, USA). 1-(3-Dimethylaminopropyl)-3- ethylcarbodiimide (EDC) were purchased from Tokyo Chemical Industries (Tokyo, Japan). Fluorescein acrylamide (FAm) and pyrrolidyl acrylate (PyA) were prepared by using my previously reported procedures.[35, 69]

3.2.2 Instrumentation

The fluorescence spectra were measured using an F-2500 fluorescence spectrophotometer (Hitachi High-Technologies, Tokyo, Japan). The UV-Vis measurements were carried out using a V-560 spectrophotometer (JASCO Ltd., Tokyo, Japan). The particle size distribution was carried out using a DLS system Zetasizer Nano ZS (Malvern Instruments Ltd., Malvern, U.K.). The QCM measurements were carried out using a QCM-D (Q-sense, Sweden). TEM images were observed by JEM-1230 (JEOL. Ltd).

3.2.3 Circular Dichroism Spectra of PSA

Circular dichroism spectra were measured for PSA (13.2 mg/mL) dissolved in 10 mM PBS (pH 7.4, 140 mM, 100 mL) before and after the incubation at 70 °C for 12 h (the polymerization condition) at 25 °C by J-725K spectrometer (JASCO, Tokyo, Japan). The CD spectra between 200-255 nm were collected.

3.2.4 Preparation of MIP-NGs

PSA (13.2 mg), pyrrolidyl acrylate (PyA) (42 mg, 0.3 mmol) as a functional monomer, fluorescein acrylamide (FAm) (4 mg, 0.01 mmol) as a fluorescent monomer, 2-methacryloyloxyethyl phosphorylcholine (MPC) (59 mg, 0.2 mmol) and N-isopropylacrylamide (NIPAm) (407 mg, 3.6 mmol) as comonomers, N,N′-methylenebis(acrylamide) (MBAA) (30.8 mg, 0.2 mmol) as a cross-linker, and V-50 (217 mg) as an initiator were dissolved in 10 mM phosphate buffer (pH 7.4). After degassing by N2/ vacuum cycles, an emulsifier-free precipitation polymerization was carried out at 70 °C for 12 h. Nonimprinted polymer nanogels (NIP-NGs) were also prepared under the same conditions without template PSA. After the polymerization, the obtained NGs were purified by ion-exchange chromatography. DEAE Sephadex A-50 was packed into a column (size 10 cm × 1.0 cm I.D.), and 10 mM Tris-buffer (pH 7.4) was used as the eluent. The dispersed NGs in 10 mM Tris-buffer pH 7.4 (1 mL) were injected into the packed column, and fractions (1.5 mL) were

collected. Fluorescence spectroscopy was used to collect the fractions of NGs and to confirm the removal of protein template from NGs. NIP-NGs were also purified by the same procedure. The particle size distribution of obtained NGs both before and after purification was measured by DLS. To estimate a removal rate of PSA from MIP-NGs, fluorescence intensities of tryptophan residues of PSA in MIP-NGs were measured at λem: 350 nm (λex: 280 nm) before and after the purification by ion-exchange chromatography for 300 μg/mL of MIP-NGs. The removal rate was calculated from the following eq 1.

$$\text{Removal rate (\%)} = \frac{\lambda_{em,\ before} - \lambda_{em,\ after}}{\lambda_{em,\ before}} \times 100 \quad \textbf{(1)}$$

3.2.5 TEM Observation of MIP-NGs and NIP-NGs

First, the solvent containing the purified MIP-NGs and NIP-NGs was exchanged by pure water using ultrafiltration (Amicon Ultra 10 kDa). The aqueous dispersion was poured on a carbon-coated Cu-grid and dried. The Cu-grid was then inverted on an aqueous solution of 1 wt % potassium Eu-encapsulated Preyssler-type phosphotungstate (Wako Pure Chemical Industries, Osaka, Japan). The samples were then dried, and TEM images were observed.

3.2.6 Preparation of MIP-/NIP-NGs-Based QCM Sensor Chips

After rinsing with ethanol, a gold-coated QCM sensor chip was dried with N_2. The QCM gold sensor chip was cleaned by UV−O_3 treatment for 20 min and set in an in- house made Teflon holder with a cylindrical cell (7 mm × 10 mm I.D.). The sensor chip was incubated with an ethanol solution containing 11-mercaptoundecanoic acid (MUA) (5 mM) for 24 h at 25 °C. The QCM sensor chip was washed with 200 μL of ethanol in triplicate and 10 mM phosphate buffer (pH 7.4). For the immobilization of NGs on the QCM sensor chip, the chip was mounted on the flow module unit performed using QCM-D: the fundamental frequency was 4.95 MHz, and the frequency signal baseline was equilibrated using 10 mM phosphate buffer (pH 7.4) as a running buffer for 2 h until the frequency signal response was within ±0.5 Hz/30 min. After stabilization of the baseline, an aqueous solution containing 0.05 M N-hydroxysuccinimide (NHS) and 0.2 M 1- (3-(dimethylamino)propyl)-3-ethylcarbodiimide·HCl (EDC) was introduced for 15 min at 100 μL/min, followed by injecting 10 mM phosphate buffer (pH 7.4) containing MIP- NGs or NIP-NGs (100, 300, and 500 μg/mL) for various flow times (10, 20, 30, and 40 min) at 100 μL/min. The frequency change values of immobilized NGs ($\Delta F_{\text{immobilization}}$) on the QCM sensor chips were measured from

differences in frequency signal response at 10 min after nanogel injection. After immobilization, the blocking of the chip surface was performed by injecting protein-free (PBS) blocking buffer solution for 15 min, followed by 1 M ethanolamine aqueous solution (pH 8.5) for 15 min, where the flow rate was 100 μL/ min.

3.2.7 Monitoring of the Immobilization of MIP-NGs on QCM and SPR Sensor Chips and the Fluorescence Measurements on the Surfaces of MIP-NGs-Immobilized Substrate

The immobilization procedure of MIP-NGs was performed on a QCM (Figure S5) and SPR (Figure S6) sensor chips. The SPR measurement was conducted using Biacore 3000 (GE Healthcare Japan, Tokyo, Japan). The fluorescence intensity of MIP-NGs-immobilized substrates was measured (Figure S7) using an IX73 fluorescent microscope (×100, extinction wavelength 460−495 nm, fluorescence wavelength > 510 nm) with U-HGLGPS light source (Olympus, Tokyo, Japan) and Zyla SCMOS CCD camera (Andor Technology, Belfast, U.K.).

3.2.8 Binding and Selectivity Experiments by QCM

The binding experiments toward MIP-/NIP-NGs-based QCM sensor chips were conducted in 0, 10, 100, 500, 1000, and 2000 μg/mL of PSA dissolved in 10 mM phosphate buffer (pH 7.4) by setting a flow rate of 100 μL/min at 25 °C. The protein samples were injected into the NGs-based QCM sensor chip for 15 min at 100 μL/min. After injection of 10 mM PBS for 10 min at 100 μL/min, the frequency change values of protein binding ($\Delta F_{binding}$) were measured from the frequency signal response. The adsorption of the protein target toward immobilized NGs on the QCM sensor chip was evaluated by $\Delta F_{binding}/\Delta F_{immobilization}$.

To investigate the selectivity of MIP-NGs and NIP-NGs for PSA recognition, the other serum albumins from five different animals including bovine, human, goat, sheep, and rabbit (BSA, HSA, GSA, SSA, and RSA) dissolved in 10 mM phosphate buffer (pH 7.4) were used as competitive proteins. The protein concentration was determined to be 1000 μg/mL. The selectivity factor was calculated from the following eq 2.

$$\text{Selectivity factor} = \frac{(\Delta F_{binding}/\Delta F_{immobilization})_{Reference}}{(\Delta F_{binding}/\Delta F_{immobilization})_{PSA}} \quad (2)$$

where $(\Delta F_{binding}/\Delta F_{immobilization})_{Reference}$ and $(\Delta F_{binding}/\Delta F_{immobilization})_{PSA}$ values were obtained from reference proteins and PSA, respectively.

3.2.9 Curve Fitting of Binding Isotherms

The affinity constant for PSA was estimated by curve fitting using DeltaGraph 5.4.5v. The fitting equation is shown below eq 3.

$$Y = [(1 + KG + KH) - \sqrt{(1 + KG + KH) - 4K^2HG}] \times \frac{D}{2KG} \quad (3)$$

The equation is used with the affinity constant for 1:1 complex formation, where Y is Adsorption ($\Delta F_{binding}/\Delta F_{immobilization}$), K is an affinity constant, H is found by fitting raw data to a theoretical curve, G is a PSA concentration, and D is the maximum bound amount of PSA.

3.2.10 Multiple Sequence Alignments of Animal Serum Albumin

The amino acid sequences of animal serum albumins from The National Center for Biotechnology Information (NCBI) sequence database (PSA; NP_001005208.1, BSA; CAA76847.1, HSA; AAA98797.1, GSA; XP_005681801.1, SSA; NP_001009376.1 and RSA; NP_001075813.1) were aligned using Clustal W (2.1) multiple sequence alignments program.[70]

3.2.11 Preparation of Meat Extracts and Measurement of Protein Concentration

The meat samples (pork and beef) were purchased from a local supermarket. The extraction of protein from meat samples was performed as follows: 1 g of meat samples was mixed with 5 mL of the extraction buffer (10 mM phosphate buffer, pH 7.4) and then homogenized for 1 min (10 000 rpm), followed by centrifugation for 30 min at 4 °C (16000 g). The clear supernatant was separated and filtered through a 0.2 μm filter three times. The meat extracts were stored at −20 °C until use.

3.2.12 Preparation of Spiked Sample for Recovery Test

The various dilution factors of beef extract solutions (0, 1, 10, 100, 1000 and 10 000 fold) were prepared using 10 mM phosphate buffer (pH 7.4), and the binding experiment was performed using the MIP-NGs-based QCM sensor chip. The undiluted and diluted extract samples were injected into the MIP-NGs- based QCM sensor for 15 min at 100 μL/min, then

ΔFbinding values were measured from the frequency signal response after injection of 10 mM PBS for 10 min.

After determination of the appropriate dilution factor for the binding experiment of the spiked sample in real meat extract, the different concentrations of PSA (0−2000 μg/mL) were added to the beef extract solution, and the binding experiments of PSA dissolved in diluted real meat extract were demonstrated. The experimental conditions were the same as described above in Binding and Selectivity Experiments by QCM. Recovery rates were estimated from the following eq 4.

$$\text{recovary rate}(\%) = \frac{(\Delta F_{\text{binding}}/\Delta F_{\text{immobilization}})_{\text{spiked sample}}}{(\Delta F_{\text{binding}}/\Delta F_{\text{immobilization}})_{\text{buffer}}} \quad (4)$$

where $(\Delta F_{\text{binding}}/\Delta F_{\text{immobilization}})_{\text{spiked sample}}$ and $(\Delta F_{\text{binding}}/\Delta F_{\text{immobilization}})_{\text{buffer}}$ values were obtained from the PSA binding experiments in the spiked sample and in buffer solution, respectively.

3.2.13 Extracted Protein Detection from Real Meats

After measuring the protein concentration of the meat extracts from both beef and pork, the extracts were diluted to final protein concentrations of 0, 20, 40, 60, and 80 μg/mL. The diluted meat extracts containing different total protein concentrations were injected into the MIP-NGs-based QCM sensor chip, and the frequency signal response was measured. The measurement conditions were as described above in Binding and Selectivity Experiments by QCM.

3.2.14 Detection of Pork Adulteration in Halal Beef Samples

Pork contaminated beef samples were prepared by mixing pork extract solution to beef extract solution in the concentration range of 0.1, 1, 10, and 50 (% v/v). The extract solutions containing 100% pork and 100% beef were used as positive and negative controls, respectively. Various pork contaminated beef samples (0, 0.1, 1, 10, 50, and 100 (%v/v)) were injected into the MIP-NGs-based QCM sensor chip, and then the frequency signal response was measured and adsorption amount calculated. The measurement conditions were as described above in Binding and Selectivity experiments by QCM.

3.3 Results and Discussions

3.3.1 Preparation of MIP-NGs for PSA

PSA was used as a target for the synthesis of MIP-NGs for the detection of pork contamination. The MIP-NGs were prepared by emulsifier-free precipitation polymerization in the buffered solution, where PSA and PyA were used as a template molecule and a functional monomer interacting with PSA via electrostatic and hydrophobic interaction, respectively. NIPAm and MBAA were used as a comonomer and cross-linking agent, respectively, for the preparation of the polymer matrix. MPC was also copolymerized as a hydrophilic and biocompatible comonomer to control the particle size and lower critical solution temperature.

CD spectra showed that PSA maintained its original secondary structure after incubation in the polymerization conditions, indicating that the PSA template was not denatured during polymerization (Figure 3.1). Fluorescent labeling was also performed using FAm, and the elution of MIP-NGs was easily found, confirming the separation from PSA in the chromatographic purification step. Furthermore, the immobilization of MIP-NGs on the gold-coated substrate was verified using fluorescent microscopy.

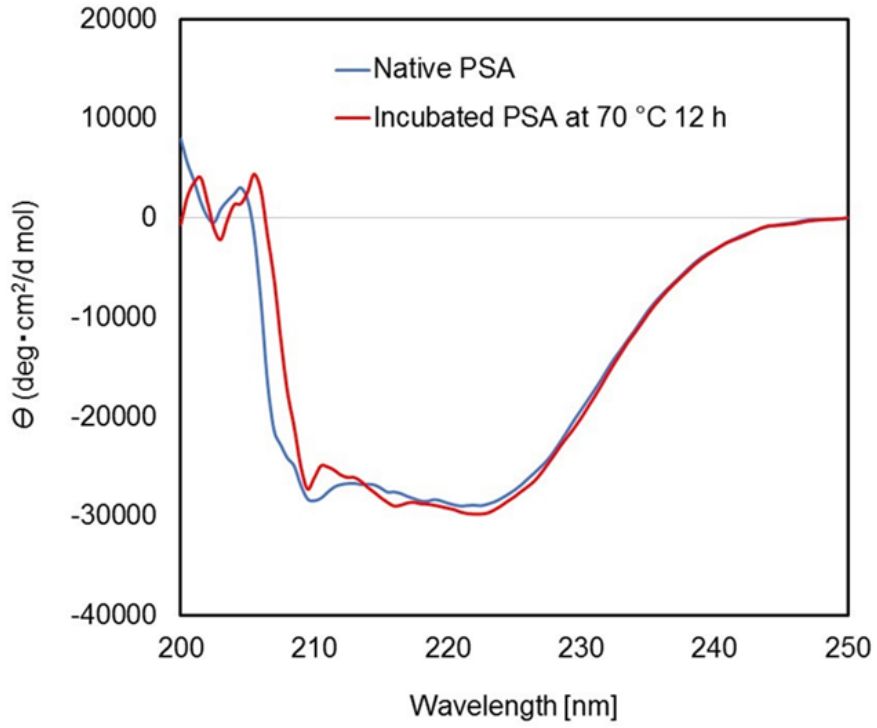

Figure 3.1 CD spectra of PSA (2 μM in 10 mM phosphate buffer, pH 7.4) before (blue line) and after incubation (red line) at 70 °C for 12 h.

After polymerization, obtained MIP-NGs were purified by ion-exchange chromatography to remove template PSA (Figure 3.2). Fluorescence intensities of tryptophan residues of PSA at λem: 350 nm before and after purification by ion-exchange chromatography were 103.10 and 8.11, respectively. From these values, the removal rate of PSA was estimated to be approximately 92%, indicating almost all PSA was removed from the NGs by the anion exchange of materials with electrostatic interaction (Figure 3.3). This removal rate was higher than that in the previous work (86%),[35] resulting in not only an increase in binding capacity but also an increase in binding cavities possessing stronger affinity to PSA than those generated from weakly PSA bound (easily removable) sites.

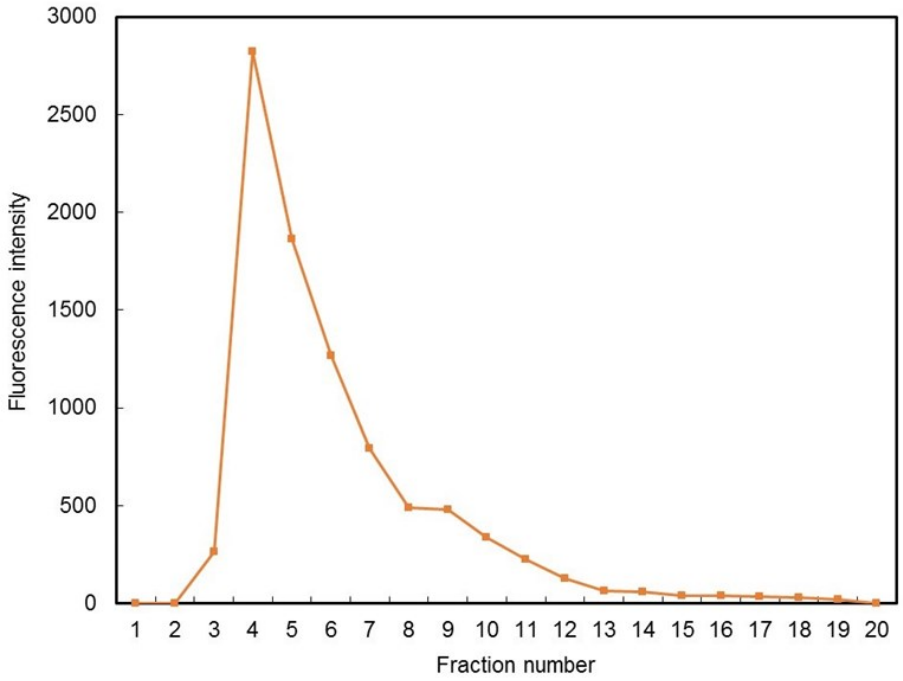

Figure 3.2 A typical chromatogram of MIP-NGs with the fluorescence intensities of FAm in MIP- NGs (λ_{ex}: 491 nm at λ_{em}: 530 nm) after the purification by ion-exchange chromatography (DEAE- Sephadex).

TEM analysis showed spherical morphologies for MIP-NGs (Figure 3.4a) and NIP-NGs (Figure 3.4b). The particle size of purified MIP-NGs was approximately 16 nm whereas for purified NIP-NGs prepared in the same manner except for PSA it was approximately 20 nm (Figure 3.5). The Z-average particle size of MIP-NGs after purification by ion-exchange chromatography (approximately 16 nm) was smaller than in the previous purification (approximately 27 nm), and zeta potentials were increased from 8.62 to 9.49 mV, indicating that the template PSA was successfully removed from the NGs. It is worth noting that the

particle size before (approximately 20 nm) and after purification (approximately 18 nm) was not much different for NIP-NGs.

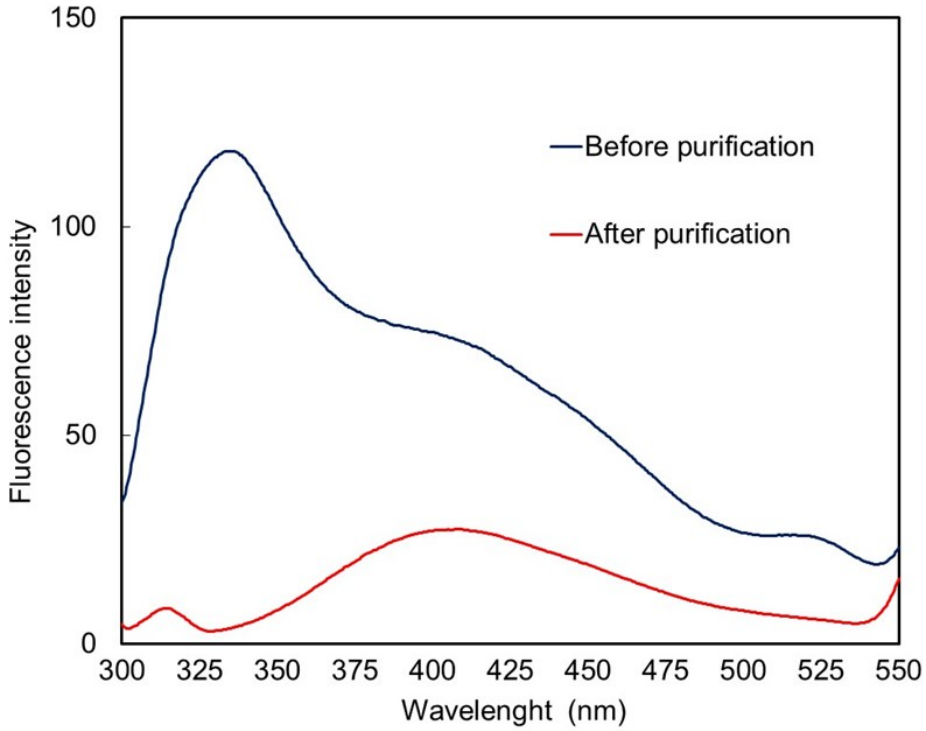

Figure 3.3 Fluorescence spectra (λ_{ex}: 280 nm) for MIP-NGs before and after the purification by ion-exchange chromatography. The concentration of obtained MIP-NGs was 300 μg/mL. PSA: porcine serum albumin

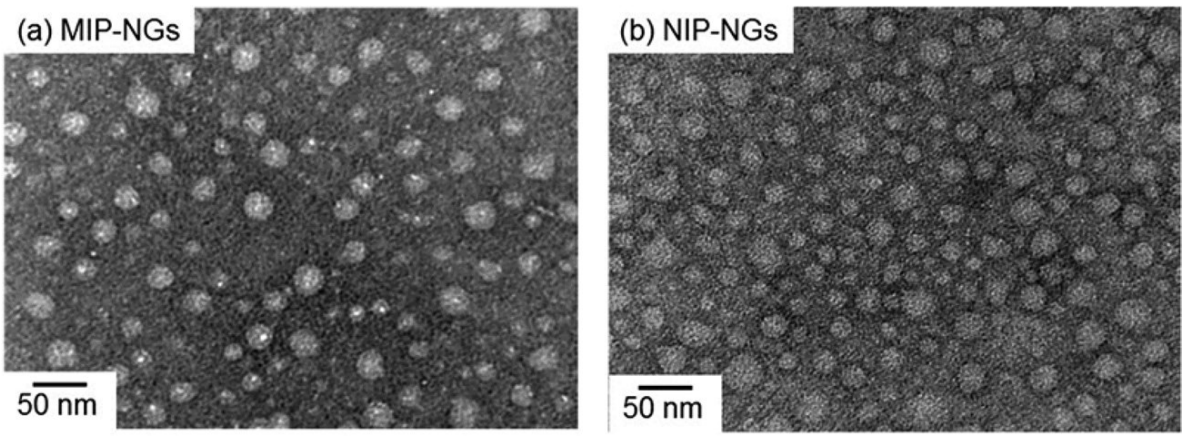

Figure 3.4 TEM images of MIP-NGs (a) and NIP-NGs (b) after purification using ion-exchange chromatography.

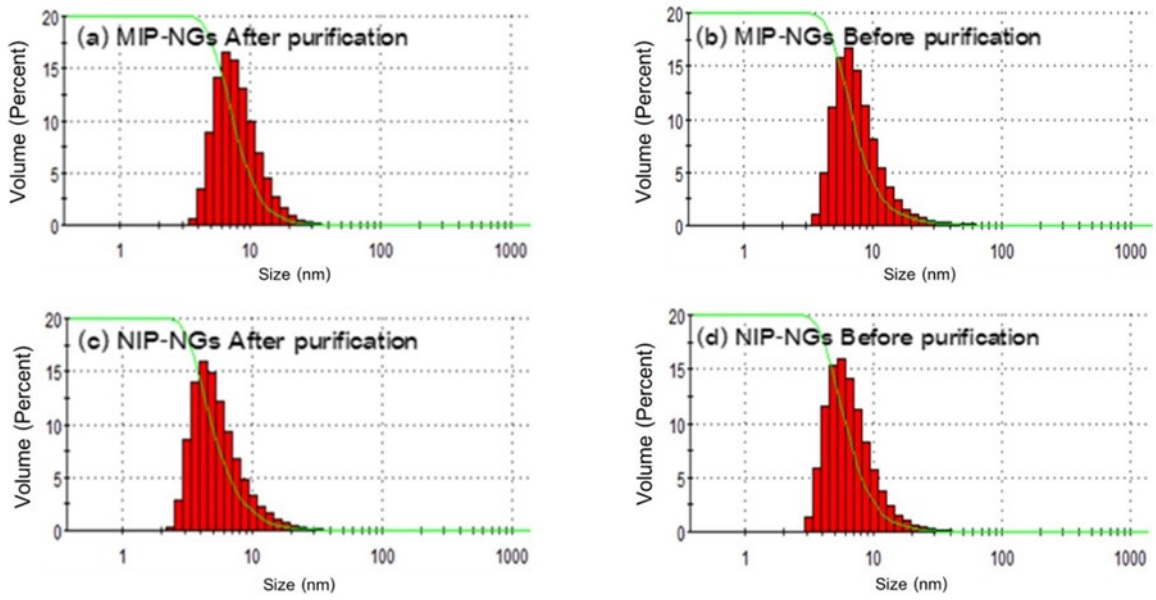

Figure 3.5 Particle size distributions of MIP-NGs and NIP-NGs before and after the purification by ion-exchange chromatography measured by DLS. (a): MIP-NGs after purification; Z-average particle size: 16 nm (b): MIP-NGs before purification; Z-average particle size: 27 nm (c): NIP- NGs after purification; Z-average particle size: 18 nm (d): NIP-NGs before purification; Z-average particle size: 20 nm.

3.3.2 QCM Experiments

The QCM sensor is the simplest type of piezoelectric sensing device offering label-free detection based on the change in mass.[59–63] The immobilization of obtained NGs onto the QCM sensor chips was performed using self-assembled monolayers (SAM) of MUA followed by an amine coupling reaction with NHS and EDC. After the coupling reaction, obtained NGs were immobilized on the QCM sensor chip via the covalent bond between secondary amine groups on the NGs and the carboxylic group on the SAM. The frequency signal response was decreased after injection of MIP-NGs into QCM sensor chips, indicating the increase in mass on the QCM sensor chip as a result of immobilization of MIP-NGs (Figure 3.6). The control NIP- NGs, which were immobilized under the same conditions as MIP-NGs, gave a similar degree of ΔFimmobilization and the same characteristics in signal response as MIP-NGs.

The immobilization of MIP-NGs was also confirmed using surface plasmon resonance (SPR) with the same SAM-formed gold surface, where the ΔRU value increased after injecting MIP-NGs (Figure 3.7). Fluorescence from the copolymerized FAm was detected from the MIP-NGs-immobilized substrate (Figure 3.8). These results indicate the successful immobilization of MIP-NGs onto the gold-coated substrates.

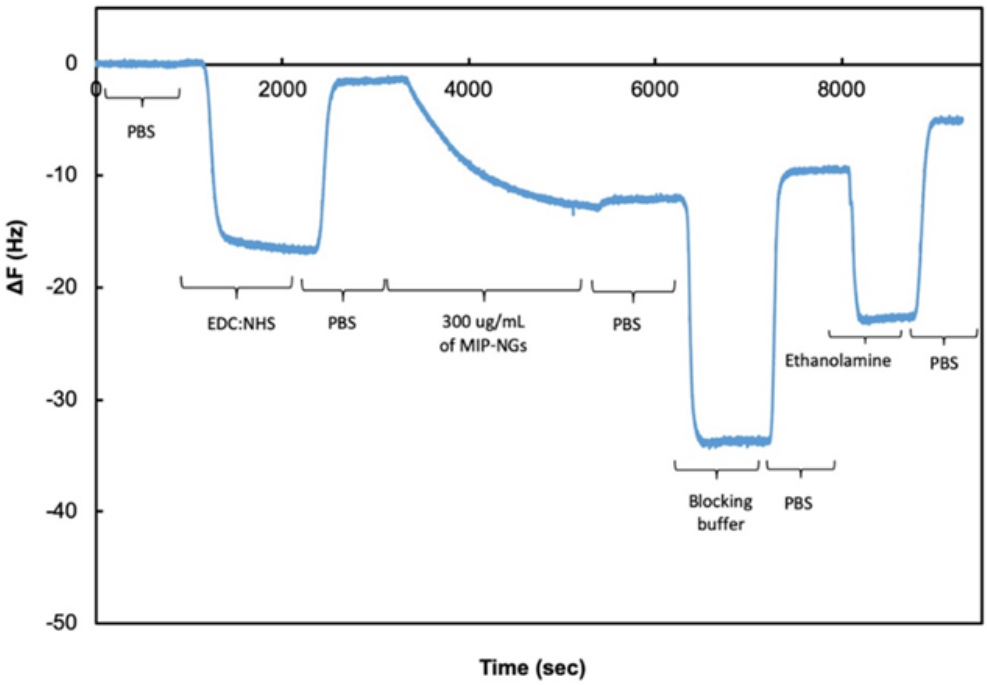

Figure 3.6 A typical QCM sensorgram for the MIP-NGs immobilization process to the sensor surface.

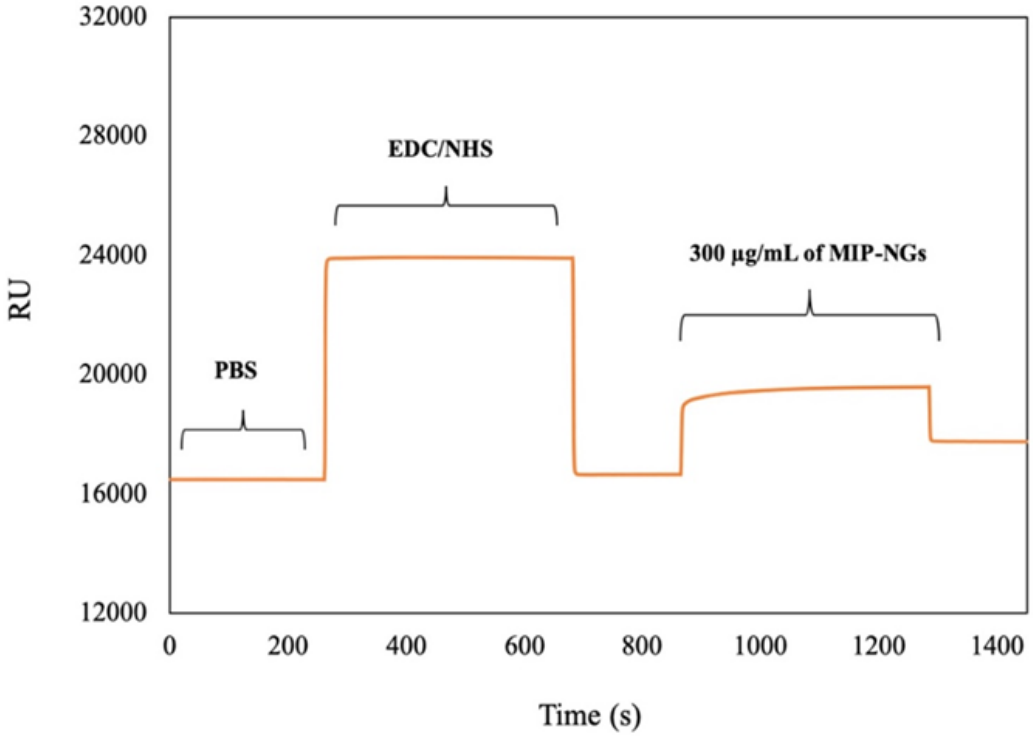

Figure 3.7 A typical SPR sensorgram for the MIP-NGs immobilization process to the sensor surface.

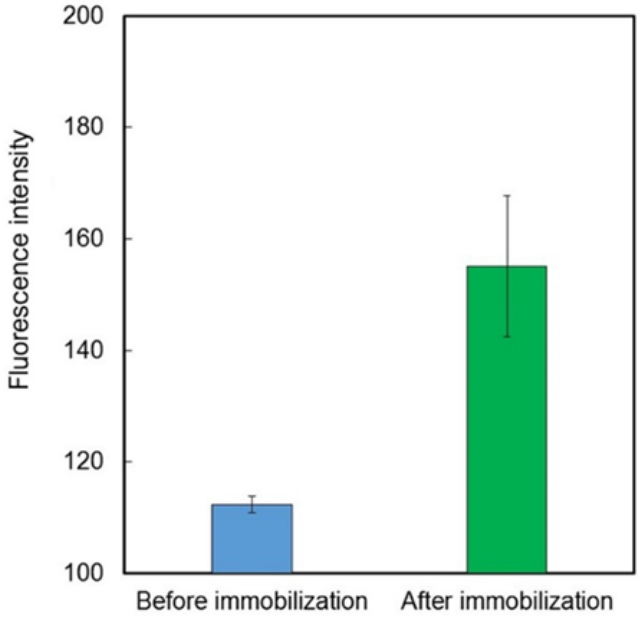

Figure 3.8 Fluorescence intensity (estimated from fluorescent microscopy) of gold-coated glass substrate before (blue) and after (green) the immobilization of MIP-NGs.

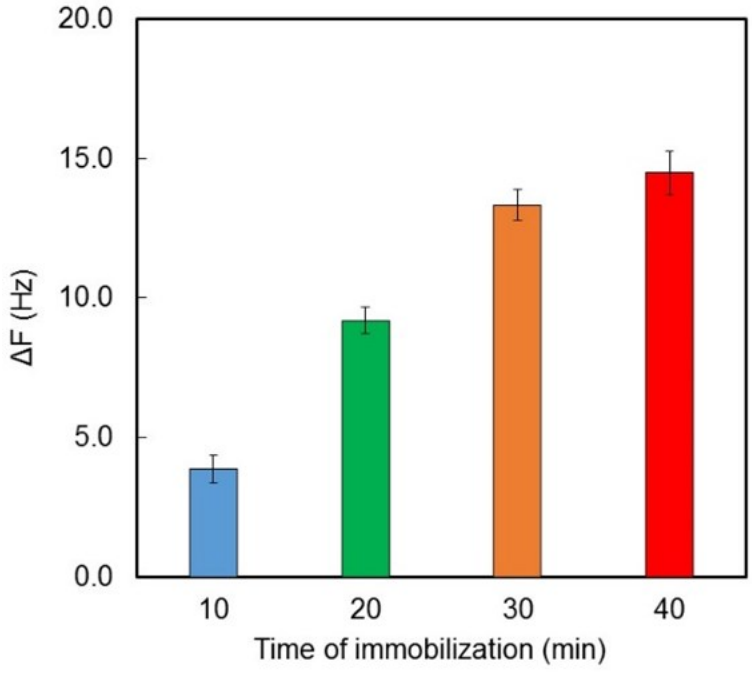

Figure 3.9 Effect of the immobilization time on the amount of immobilized MIP-NGs on the QCM chips. The concentration of MIP-NGs added was 500 μg/mL. The experiments were conducted in triplicate.

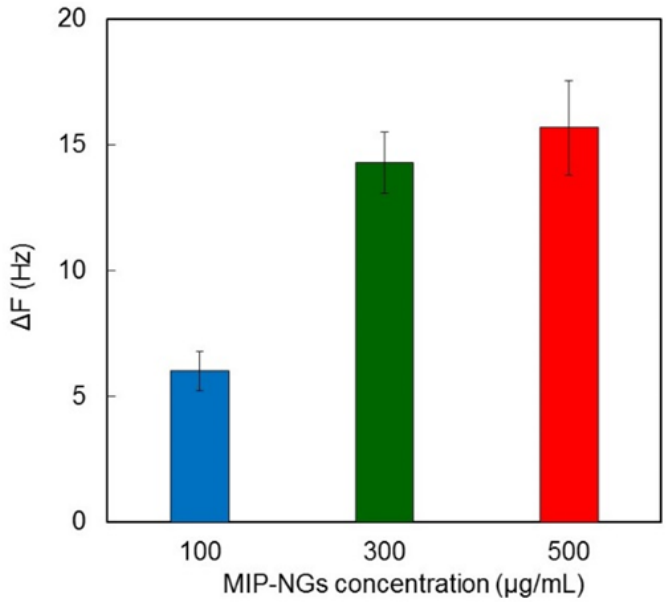

Figure 3.10 Effect of the concentration of MIP-NGs on the amount of immobilized MIP-NGs on the QCM chips. The immobilization time was 30 min. The experiments were conducted in triplicate.

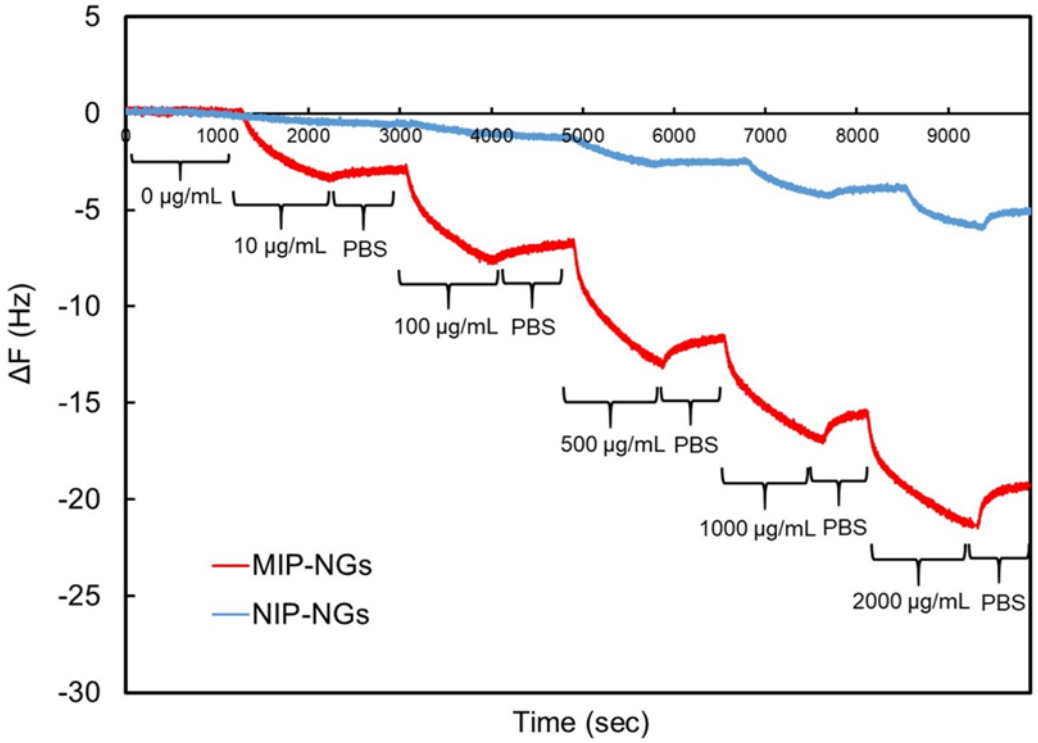

Figure 3.11 Typical sensorgrams in the MIP-NGs immobilized (red) and NIP-NGs immobilized (blue) QCM by injecting PSA (0-2,000 μg/mL).

The optimization of immobilization conditions for MIP-NGs was further demonstrated with different immobilization times and concentrations of MIP-NGs using QCM. The ΔF value was almost constant at 30 min, when the interaction time changed from 10 to 40 min (Figure 3.9). Furthermore, the ΔF values toward 300 and 500 μg/mL of MIP-NGs were similar to those of the 30 min immobilization (Figure 3.10). Therefore, 300 μg/mL of MIP-NGs and 30 min incubation time were used for the immobilization conditions.

The PSA recognition capability of MIP-/NIP-NGs-based QCM sensor chips was investigated. The adsorption of PSA increased notably with the increasing PSA concentration in the samples, which shows concentration dependent binding of the MIP-NGs-based QCM sensor chip (Figure 3.11). The PSA adsorption value ($\Delta F_{binding}$ /$\Delta F_{immobilization}$) on MIP-NGs was significantly higher than that of NIP-NGs (Figures 3.12).

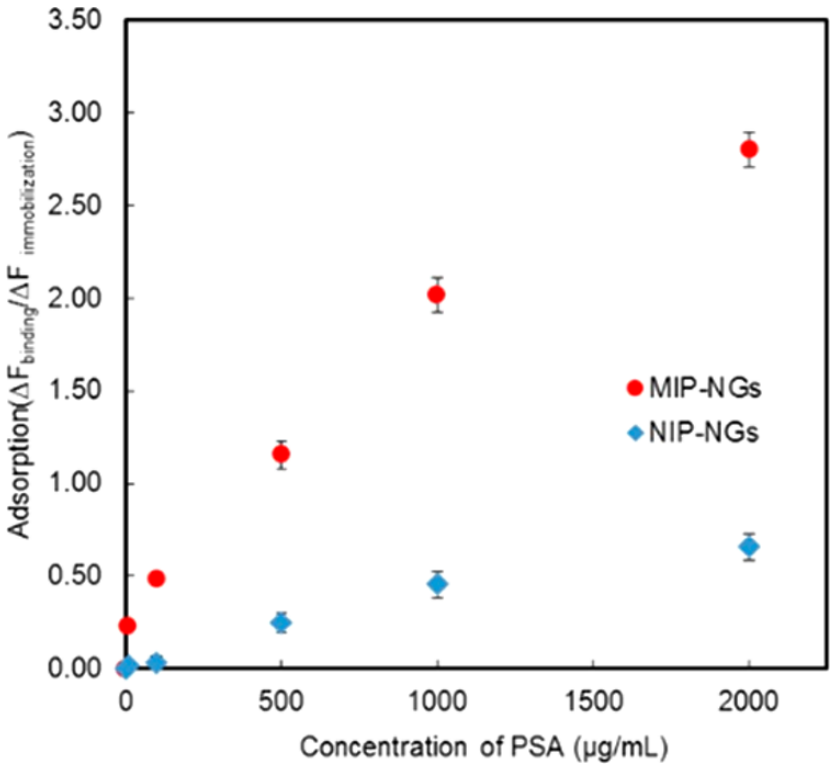

Figure 3.12 PSA binding behavior to MIP-NGs (circles) and NIP-NGs (diamonds). Various concentrations of PSA (0−2000 μg/mL) were injected into the NGs-based QCM sensor. Error bars were obtained from triplicate experiments.

Furthermore, MIP-NGs showed a higher binding affinity ($K_a = 6.7 \times 10^7\ M^{-1}$) than NIP-NGs ($K_a = 3.0 \times 10^7\ M^{-1}$), indicating the affinity of PSA to MIP-NGs was increased via the molecular imprinting process (Figure 3.13). I evaluated the analytical performance of the MIP-

NGs-based QCM sensor. The response time of the sensor was estimated to be 10 min in accordance with 90% of the final value after injection of 10 µg/mL PSA (Figure 3.14). The limit of detection of PSA for the MIP-NGs-based QCM sensors was calculated according to 3SD/m (m = slope of the linear part of the binding behavior, SD = standard deviation for a value of 0 µg/mL PSA) and was found to be 12 µg/mL (Figure 3.15). The sensitivity was higher than that of previously reported MIP-based detection methods with HPLC (sub-mg/mL),[31,64,65] although less than electrochemical immunosensors (0.5 pg/mL) and SPR detections (19.8 ng/mL).[15,66] Sensitivity is apparently dependent on the detection devices employed. In practical use, the sensitivity of the MIP-NGs-based QCM sensor is sufficient to detect contaminated PSA. To study the long-term stability of the sensor, the binding of PSA (10−1000 µg/mL) before and after storage at 4 °C for 60 days was investigated. Both binding behaviors were shown to be similar (Figure 3.16).

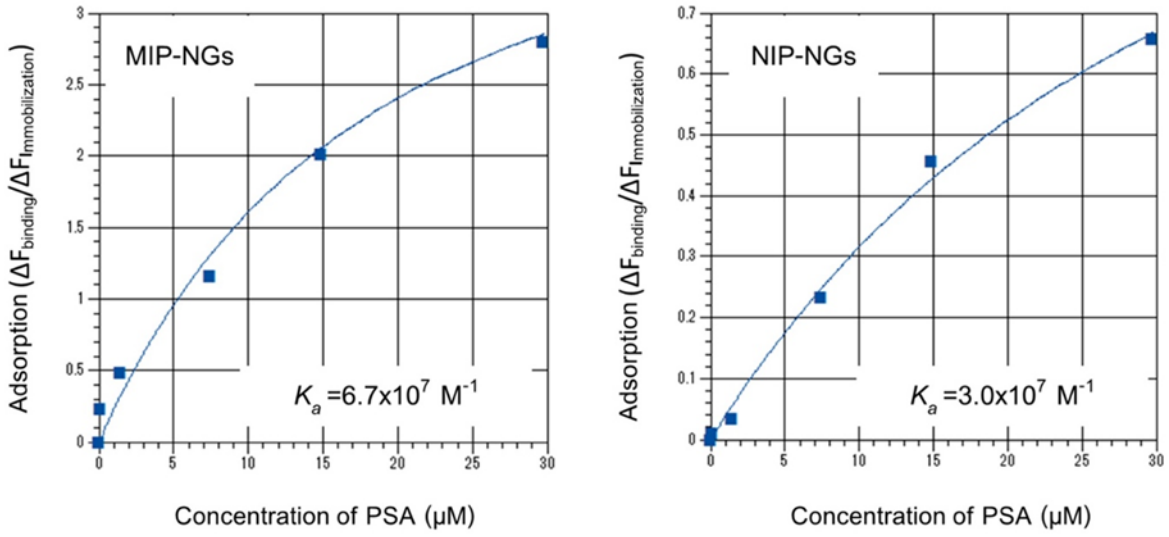

Figure 3.13 Affinity constants (K_a) for the binding of PSA to MIP-NGs and NIP-NGs, estimated from the QCM measurements data.

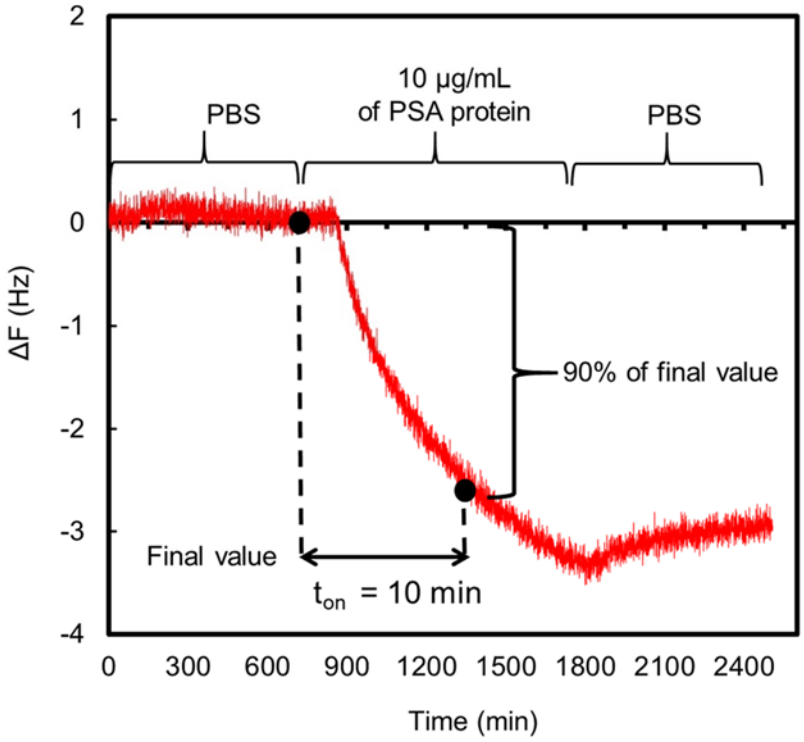

Figure 3.14 Response of MIP-NGs-based QCM sensor to 10 μg/mL of PSA.

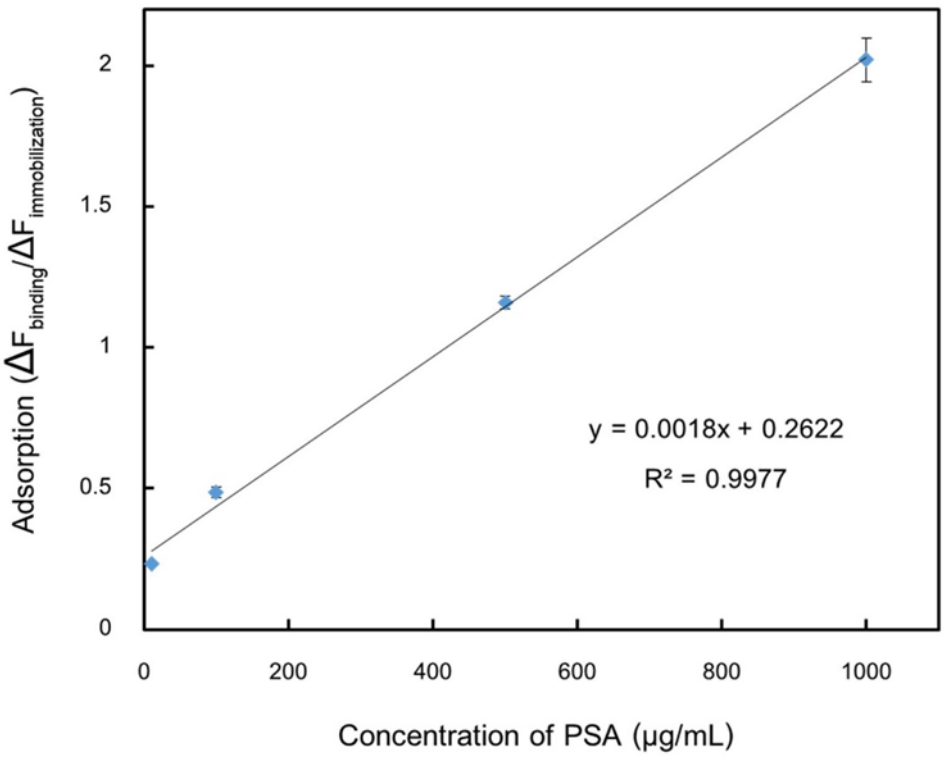

Figure 3.15 A calibration curve of PSA at a range of 10 to 1,000 μg/mL, (R2: 0.9977).

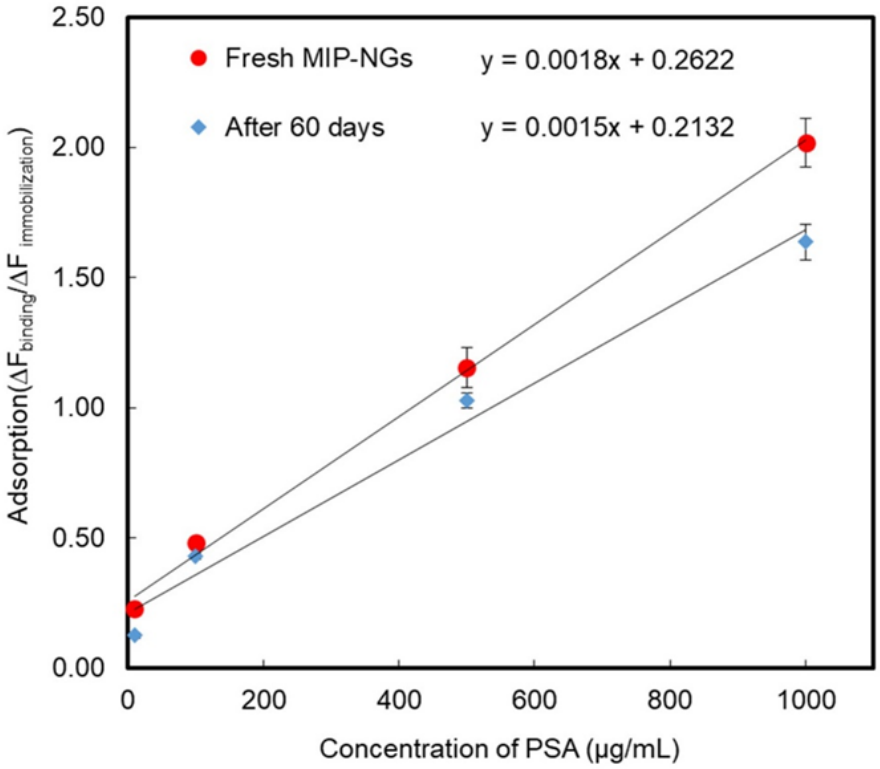

Figure 3.16 Calibration curves of PSA (10-1000 μg/mL) for the MIP-NGs-based QCM sensor before (fresh sample) and after 60 days at 4 °C. The experiments were conducted in triplicate.

Selectivity for PSA is also important for pork contamination sensor in real meat extracts. To investigate the selectivity of MIP-NGs for PSA, the binding behaviors of PSA and five reference serum albumins including BSA, HSA, GSA, SSA, and RSA were investigated, where the homologies of amino acid sequence to PSA were 80, 76, 78, 78, and 74%, respectively (Figure 3.17 and Table 3.1). The adsorption of PSA on MIP-NGs was significantly higher than those of competitive proteins at every concentration, and the binding behaviors of competitive proteins were similar (Figure 3.18). The selectivity factors of these reference proteins; BSA, HSA, GSA, SSA, and RSA at 1000 μg/mL were estimated to be 0.11, 0.09, 0.12, 0.15, and 0.11, respectively, confirming that the MIP-NGs had highly selective binding for PSA (Figure 3.19a). However, it is difficult to confirm why the present MIP-NGs exhibited high selectivity. In terms of the properties of the C-terminal regions such as the amino acid sequences and the number of charged amino acids, PSA is very different from other albumins (Figure 3.17). The terminal regions seem to be more flexible and easily interact with MIP-NGs. This might affect the high selectivity developed in the present MIP. Furthermore, an anthracene derivative was reported to show different behaviors in the binding to PSA, BSA, HSA, SSA, and RSA.[65] A therapeutic agent, pinostrobin, also exhibited differences in hydrophobic

interaction-based binding behaviors to PSA, BSA, HSA, GSA, SSA, and RSA.[66] Therefore, the properties of the C-terminal region and the hydrophobic region on PSA might influence the selectivity. In contrast, PSA selectivity was not observed in NIP-NGs, where the selectivity factors of BSA, HSA, GSA, SSA, and RSA at 1000 μg/mL were estimated to be 1.00, 1.41, 1.14, 0.83, and 1.46, respectively (Figure 3.19b). Thus, the PSA recognition nanocavities of MIP-NGs were successfully formed by the molecular imprinting process.

```
Goat            MKWVTFISLLLLFSSAYSRGVFRRDTHKSEIAHRFNDLGEENFQGLVLIAFSQYLQQCPF
Sheep           MKWVTFISLLLLFSSAYSRGVFRRDTHKSEIAHRFNDLGEENFQGLVLIAFSQYLQQCPF
Bovine          MKWVTFISLLLLFSSAYSRGVFRRDTHKSEIAHRFKDLGEEHFKGLVLIAFSQYLQQCPF
Pig             MKWVTFISLLFLFSSAYSRGVFRRDTYKSEIAHRFKDLGEQYFKGLVLIAFSQHLQQCPY
Human           MKWVTFISLLFLFSSAYSRGVFRRDAHKSEVAHRFKDLGEENFKALVLIAFAQYLQQCPF
Rabbit          MKWVTFISLLFLFSSAYSRGVFRREAHKSEIAHRFNDVGEEHFIGLVLITFSQYLQKCPY
                **********:**************:::***:****:*:**: * .****:*:*:**:**:

Goat            DEHVKLVKELTEFAKTCVADESHAGCDKSLHTLFGDELCKVATLRETYGDMADCCEKQEP
Sheep           DEHVKLVKELTEFAKTCVADESHAGCDKSLHTLFGDELCKVATLRETYGDMADCCEKQEP
Bovine          DEHVKLVNELTEFAKTCVADESHAGCEKSLHTLFGDELCKVASLRETYGDMADCCEKQEP
Pig             EEHVKLVREVTEFAKTCVADESAENCDKSIHTLFGDKLCAIPSLREHYGDLADCCEKEEP
Human           EDHVKLVNEVTEFAKTCVADESAENCDKSLHTLFGDKLCTVATLRETYGEMADCCAKQEP
Rabbit          EEHAKLVKEVTDLAKACVADESAANCDKSLHDIFGDKICALPSLRDTYGDVADCCEKKEP
                ::*.***.*:*::**:******  .*:**:* :***::* :.:**: **::**** *:**

Goat            ERNECFLKHKDDSPDLPKLK-PEPDTLCAEFKADEKKFWGKYLYEVARRHPYFYAPELLY
Sheep           ERNECFLNHKDDSPDLPKLK-PEPDTLCAEFKADEKKFWGKYLYEVARRHPYFYAPELLY
Bovine          ERNECFLSHKDDSPDLPKLK-PDPNTLCDEFKADEKKFWGKYLYEIARRHPYFYAPELLY
Pig             ERNECFLQHKNDNPDIPKLK-PDPVALCADFQEDEQKFWGKYLYEIARRHPYFYAPELLY
Human           ERNECFLQHKDDNPNLPRLVRPEVDVMCTAFHDNEETFLKKYLYEIARRHPYFYAPELLF
Rabbit          ERNECFLHHKDDKPDLPPFARPEADVLCKAFHDDEKAFFGHYLYEVARRHPYFYAPELLY
                ******* **:*.*::* :  *:  .:*  *: :*: *  :****:**********:

Goat            YANKYNGVFQECCQAEDKGACLLPKIETMREKVLASSARQRLRCASIQKFGERALKAWSV
Sheep           YANKYNGVFQECCQAEDKGACLLPKIDAMREKVLASSARQRLRCASIQKFGERALKAWSV
Bovine          YANKYNGVFQECCQAEDKGACLLPKIETMREKVLTSSARQRLRCASIQKFGERALKAWSV
Pig             YAIIYKDVFSECCQAADKAACLLPKIEHLREKVLTSAAKQRLKCASIQKFGERAFKAWSL
Human           FAKRYKAAFTECCQAADKAACLLPKLDELRDEGKASSAKQRLKCASLQKFGERAFKAWAV
Rabbit          YAQKYKAILTECCEAADKGACLTPKLDALEGKSLISAAQERLRCASIQKFGDRAYKAWAL
                :*  *:  : ***:* **.*** **:: :. :   *:*::**:***:****:** ***::
```

Figure 3.17 The conversation rating by Clustal W multiple sequence alignment of serum albumin from goat, sheep, bovine, pig, human and rabbit. (* = the most conserved alignment position, : = the moderate conserved alignment position and, . = the least conserved alignment position).

Table 3.1 The aligned score of PSA to the other animal serum albumins.

Sequence of animal serum albumin	Aligned. Score
PSA : BSA	80.0659
PSA : HSA	75.6178
PSA : GSA	78.4185
PSA : SSA	78.2537
PSA : RSA	73.8056

Note: PSA= porcine serum albumin, BSA= bovine serum albumin, HSA= human serum albumin, GSA= goat serum albumin, SSA= sheep serum albumin and RSA= rabbit serum albumin.

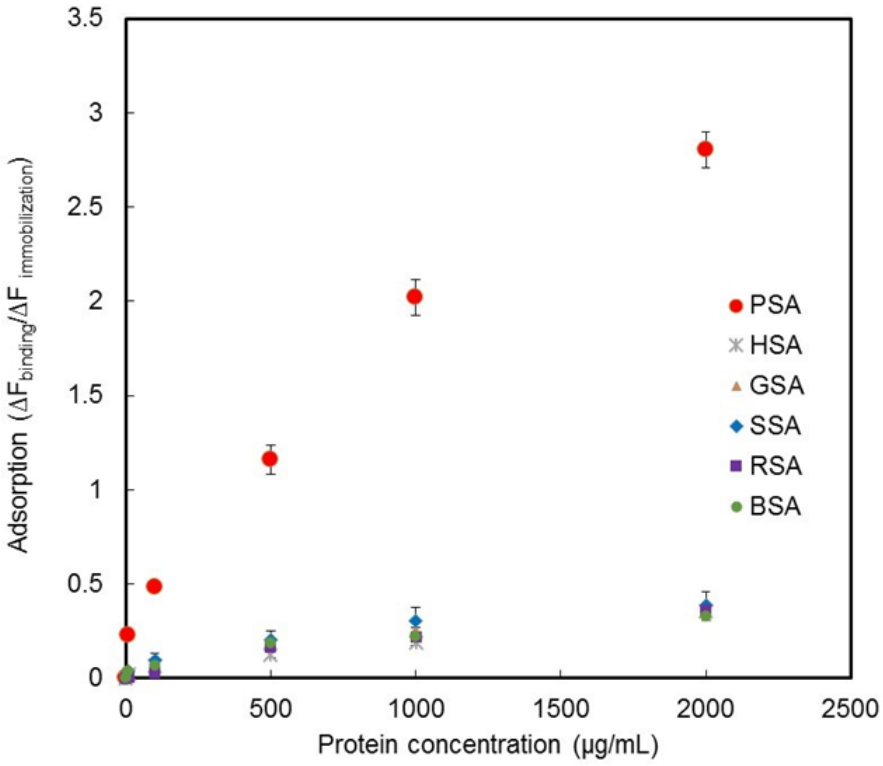

Figure 3.18 Binding isotherms of porcine serum albumin (PSA), bovine serum albumin (BSA), human serum albumin (HSA), goat serum albumin (GSA), sheep serum albumin (SSA), and rabbit serum albumin (RSA) for MIP-NGs-immobilized QCM sensor chip. The error bar of standard deviation was obtained by triplicate experiments.

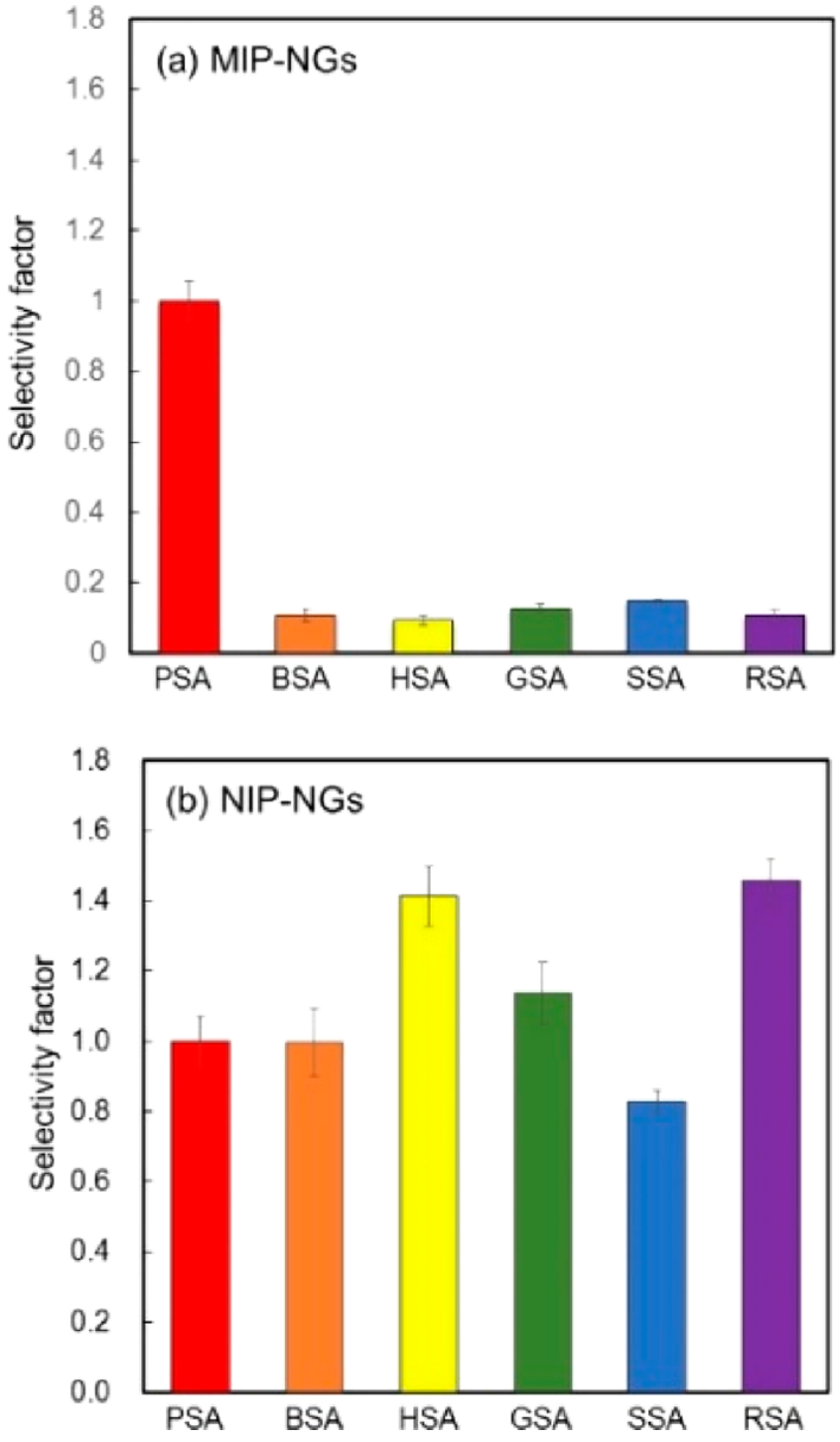

Figure 3.19 Selectivity factor of MIP-NGs (a) and NIP-NGs (b) for PSA and the five competitive serum albumins BSA, HSA, GSA, SSA, and RSA. The concentration was 1000 μg/mL. Error bars were obtained from triplicate experiments.

The dilution factor is important to reduce the matrix interference effects in real samples while investigating the binding behavior of MIP-NGs for PSA in real meat extract samples. Therefore, the beef extract samples (8.68 mg/mL) were diluted in 10 mM phosphate buffer (pH 7.4) with a range of dilution factors (x) between 1−10 000. Protein adsorptions of MIP-NGs using undiluted and 10-fold diluted samples were much higher than those of the blank sample (PBS buffer) owing to the effects of the interference matrix of the real beef extract samples (Figure 3.20). On the other hand, $\Delta F_{binding}/\Delta F_{immobilization}$ value change after the injection of 100-, 1000-, and 10 000-fold diluted samples was much smaller than those of undiluted and 10-fold diluted samples. In addition, the signal from the 100-fold diluted sample matrix ($\Delta F_{binding}/\Delta F_{immobilization}$: approximately 0.024) was small enough for PSA detection ($\Delta F_{binding}/\Delta F_{immobilization}$: approximately 0.25 at 10 μg/mL), indicating that 100-fold dilution was appropriate for analyzing real meat extract samples.

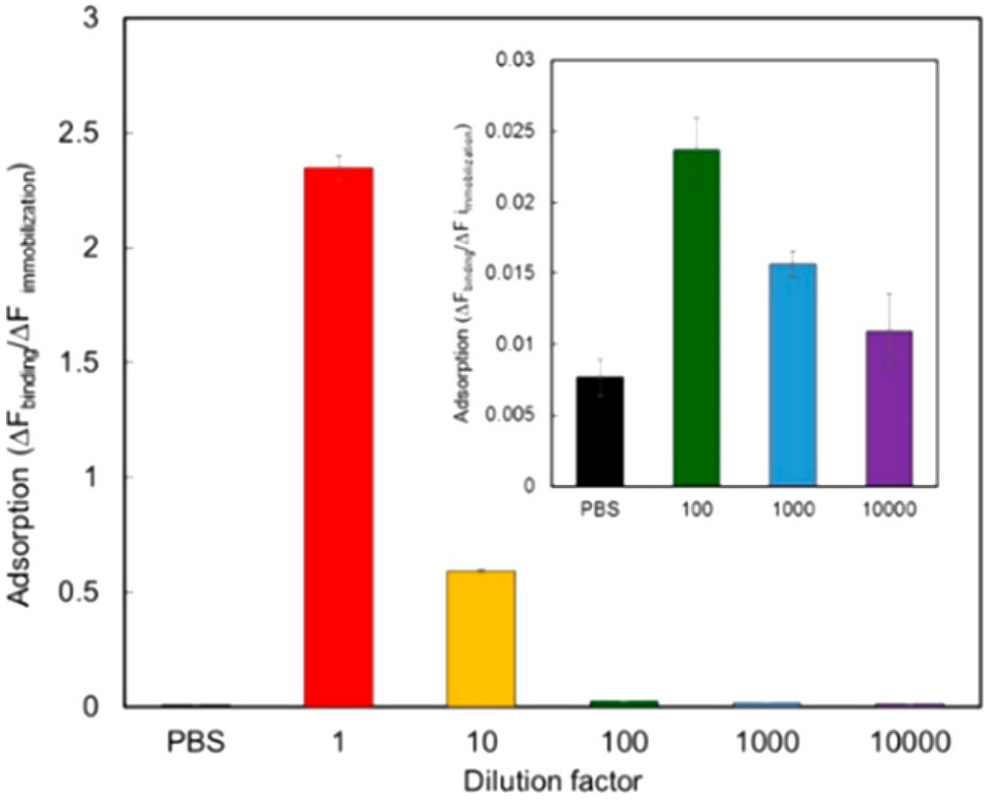

Figure 3.20 Adsorption amount of extracted proteins in PBS and 1-, 10-, 100-, 1000-, 10000-fold diluted beef extract samples to MIP-NGs. Original protein concentration in beef meat extract determined by Micro BCA assay: 8.68 mg/mL. Error bars were obtained from triplicate experiments.

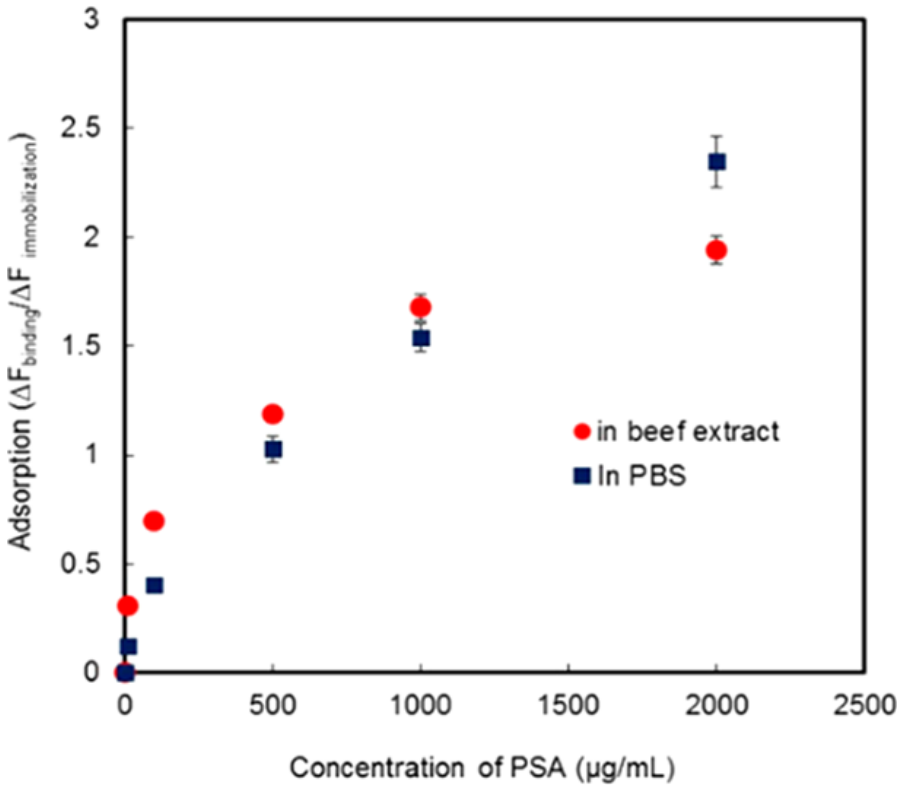

Figure 3.21 Binding behaviors of PSA in 10 mM phosphate buffer solution (pH 7.4) (squares) and the 100-fold diluted beef extract (circles) for MIP-NGs. Error bars of standard deviation were obtained from triplicate experiments.

Table 3.2 The result of recovery rate for determination of PSA in spiked samples (n=3).

Spiked samples (μg/mL)	Measured concentration (μg/mL)	Recovery (%)	RSD* (%)
10	12.8	128.00	3.9
100	120.7	120.70	3.1
500	489.0	97.80	3.6
1000	830.0	83.00	2.5

*Relative standard deviation

Then the spiked samples were prepared by adding various concentrations of PSA into the 100-fold diluted beef extract. The binding behavior of PSA-spiked beef extracts to MIP-NGs is comparable to that of the buffer solution (Figure 3.21). From these binding profiles, the recovery rates were estimated to be from 83% to 128% with acceptable relative standard deviation (2.5−3.9%) (Table 3.2). These results indicate that the MIP- NGs can recognize the target protein PSA even in the diluted real meat extracts.

3.3.3 Detection of Pork Adulteration in Halal Beef Samples

The binding profiles for the proteins derived from pork and beef extracts as positive and negative controls, respectively, were investigated by using the MIP-NGs-based QCM sensor chip for the detection of pork contamination in real beef meat extracts (Figure 3.22). The protein concentration in both extracts were measured by micro BCA assay (Figure 3.23 and Table 3.3). The protein solutions were diluted to various concentrations, and these samples were injected into the sensors. More than six times higher adsorption signals were detected for extracts derived from pork meat than that of beef extracts, confirming that the MIP-NGs successfully detect extracted protein derived from pork meats.

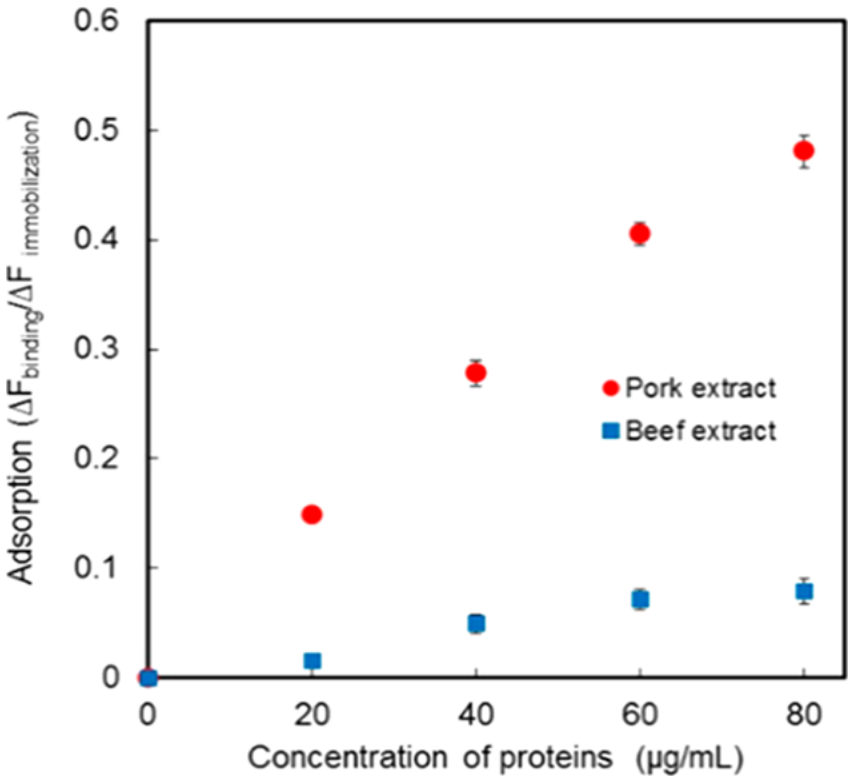

Figure 3.22 Binding behaviors of extracted proteins from pork meat as a positive control (circles) and beef meat as a negative control (squares) using the MIP-NGs-based QCM sensor. Error bars were obtained from triplicate experiments.

Finally, to study the feasibility of the developed MIP-NGs- based QCM sensor for the detection of pork contamination in halal meat samples, the beef extract samples containing different levels of pork (0, 0.1, 1, 10, 50, and 100 (% v/v)) were prepared by mixing 100-fold diluted pork extract with 100-fold diluted beef extract solution. For 0.1% (v/v) contamination, the adsorption signal was similar to that of control (PBS). For 1% (v/v), a significant adsorption signal was observed with nonoverlapping error bars for 0 and 0.1% of pork contamination levels, indicating that the detection limit of pork contamination was estimated to be 1% using the MIP- NGs-based QCM sensor (Figure 3.24).

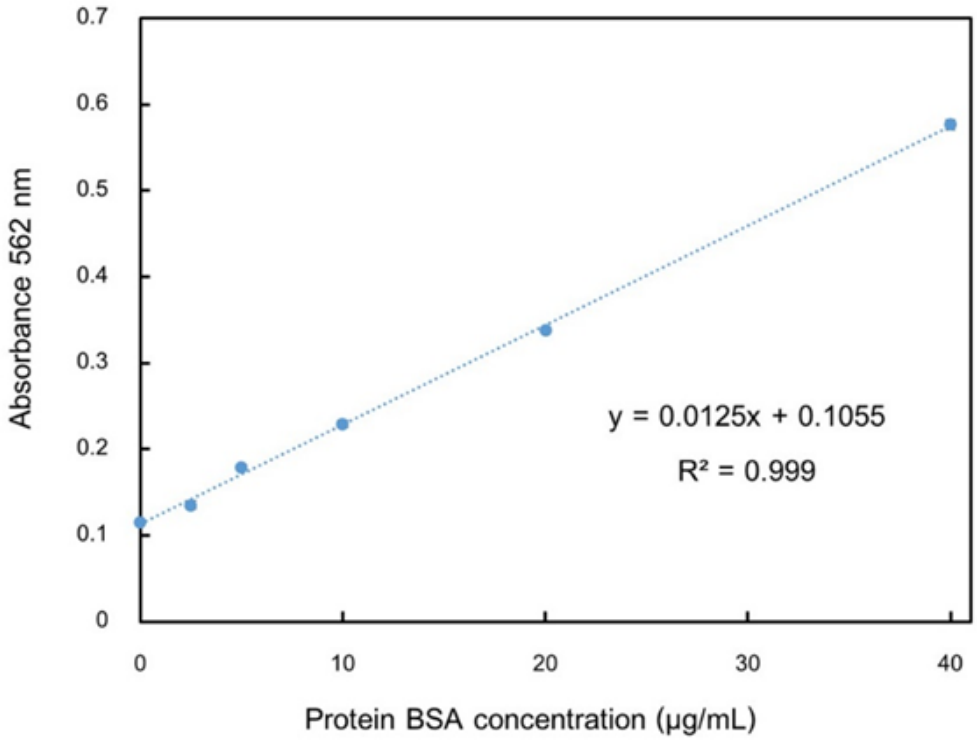

Figure 3.23 BSA protein standard curve. The absorbance at OD 562 (nm) was determined for a range of BSA protein standards from 0-40 µg/mL (R2=0.999).

Table 3.3 The total protein concentration of meat extracts.

Sample	Protein concentration (mg/mL)
Pork extract	10.48
Beef extract	8.68

In general, the manufacturers mix pork with beef at a high level to save costs, because pork is less expensive than beef. Consequently, the detection limit of 1% was acceptable for the recognition of pork contamination in raw meat extract samples. Thus, an acceptable detection limit for pork adulteration was achieved in this study owing to the high selectivity of PSA induced by the molecular imprinting process and to the high sensitivity of the MIP-NGs-based QCM sensor (LOD: 12 μg/ mL). These results show that the developed MIP-NGs-based QCM sensor has great potential for the detection of pork contamination in halal raw beef.

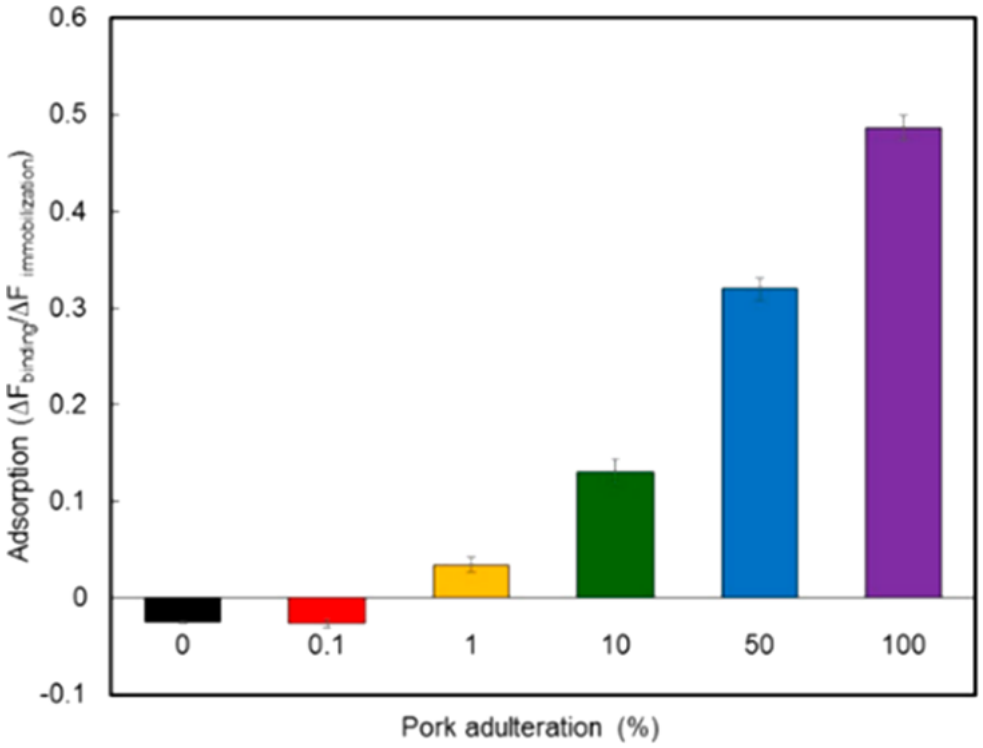

Figure 3.24 Adsorption amounts of various concentrations of pork contamination in beef extract samples to MIP-NGs. Error bars were obtained from triplicate experiments.

3.4 Conclusions

In this study, MIP-NGs capable of detecting PSA contamination in real meat extract samples for halal food control were successfully developed for the first time. The MIP-NGs showed high potential as the molecular recognition elements on the QCM sensor for specific detection of PSA. The present study achieved high selectivity of MIP-NGs for PSA when compared to five different animal serum albumins (BSA, HSA, GSA, SSA, and RSA) with very low selectivity factors (0.09− 0.15). Furthermore, the PSA recognition capability was shown even

in the real meat extract sample, and the high recovery rates of PSA (83−128%) were achieved from PSA spiked beef extract. Finally, the developed MIP-NGs-based QCM sensor detected pork contamination in beef extract samples as low as 1% (v/v). Thus, the developed sensor provides a new and simple approach to detect pork contamination in halal raw meat samples with high selectivity and reliability using MIP-Gs as artificial molecular recognition materials.

3.5 References

(1) Peters, T., Jr. All about albumin: Biochemistry, genetics, and medical applications; Academic Press: California, San Diego.**1996.**

(2) Izberk-Bilgin, E.; Nakata, C. C. *Bus. Horiz*. **2016**, 59, 285−292.

(3) Al-Jowder, O.; Kemsley, E. K.; Wilson, R. H. *Food Chem*. **1997**, 59, 195−201.

(4) Girish, P.; Anjaneyulu, A.; Viswas, K.; Anand, M.; Rajkumar, N.; Shivakumar, B.; Bhaskar, S. *Meat Sci*. **2004**, 66, 551−556.

(5) Aida, A.; Che Man, Y. B.; Wong, C.; Raha, A.; Son, R. *Meat Sci*. **2005**, 69, 47−52.

(6) Ofori, J. A.; Hsieh, Y. H. P. J. Agric. *Food Chem*. **2007**, 55, 5919− 5924.

(7) Asensio, L.; Gonzaĺez, I.; García, T.; Martín, R. *Food Control* **2008**, 19, 1−8.

(8) Kesmen, Z.; Gulluce, A.; Sahin, F.; Yetim, H. *Meat Sci*. **2009**, 82, 444−449.

(9) Ali, M. E.; Razzak, M. A.; Hamid, S. B.; Rahman, M. M.; Amin, M.; Rashid, N. R. *Food Chem*. **2015**, 177, 214−224.

(10) Al-Kahtani, H. A.; Ismail, E. A.; Asif Ahmed, M. *Food Chem*. **2017**, 219, 54−60.

(11) Amaral, J. S.; Santos, G.; Oliveira, M. B. P. P.; Mafra, I. *Food Control* **2017**, 72, 53−61.

(12) Kang, S. S. N.; Lee, H. G.; Kim, H. *LWT-Food Sci. Technol*. **2018**, 97, 697−702.

(13) Skouridoua, V.; Tomasob, H.; Rauc, J.; Bashammakhd, A. S.; El-Shahawid, M. S.; Alyoubid, A. O.; O'Sullivana, C. K. *Food Chem*. **2019**, 287, 354−362.

(14) Liu, L.; Chen, F. C.; Dorsey, J. L.; Hsieh, Y.-H. P *J. Food Sci*. **2006**, 71, 1−6.

(15) Lim, S. A.; Ahmed, M. U. *Food Chem*. *2016*, 206, 197−203.

(16) Kuswandi, B.; Gani, A. A.; Ahmad, M. *Food Biosci*. **2017**, 19, 1− 6.

(17) Thienes, C. P; Masiri, J.; Benoit, L. A; Barrios-Lopez, B.; Samuel, S. A; Cox, D. P;8 Dobritsa, A. P; Nadala, C.; Samadpour, M. *J. AOAC Int*. **2018**, 101, 817−823.

(18) Mandli, J.; El Fatimi, I.; Seddaoui, N.; Amine, A. *Food Chem*. **2018**, 255, 380−389.

(19) Sellergren, B. Molecularly Imprinted Polymers: Man-Made Mimics of Antibodies and Their Applications: Analytical Chemistry; Elsevier: Amsterdam, **2001**.

(20) Komiyama, M.; Takeuchi, T.; Mukawa, T.; Asanuma, H. Molecular Imprinting: from Fundamentals to Applications; Wiley-VCH: Weinheim, **2003**.

(21) Yan, M.; Ramström, O. Molecularly Imprinted Materials: Science and Technology; Marcel Dekker: New York, **2005**.

(22) Takeuchi, T.; Hishiya, T. *Org. Biomol. Chem*. **2008**, 6, 2459− 2467.

(23) Chen, L.; Xu, S.; Li, J. Chem. Soc. Rev. 2011, 40, 2922−2942.

(24) Haupt, K. Molecular Imprinting; Springer-Verlag: Berlin, 2012.

(25) Seung-Woo, L.; Kunitake, T. Handbook of Molecular Imprinting -Advanced Sensor Applications; Pan Stanford Publishing: Singapore, **2013**.

(26) Schirhagl, R. *Anal. Chem*. **2014**, 86, 250−261.

(27) Takeuchi, T.; Hayashi, T.; Ichikawa, S.; Kaji, A.; Masui, M.; Matsumoto, H.; Sasao, R. *Chromatography* **2016**, 37, 43−64.

(28) Chen, L.; Wang, X.; Lu, W.; Wu, X.; Li, *J. Chem. Soc. Rev*. **2016**, 45, 2137−2211.

(29) Komiyama, M.; Mori, T.; Ariga, K. *Bull. Chem. Soc. Jpn*. **2018**, 91, 1075−1111.

(30) Qin, Y. P.; Jia, C.; He, X. W.; Li, W. Y.; Zhang, Y. K. *ACS Appl. Mater. Interfaces* **2018**, 10, 9060−9068.

(31) Qin, Y. P.; Wang, H. Y.; He, X. W.; Li, W. Y.; Zhang, Y. K. *Talanta* **2018**, 185, 620−627.

(32) Dong, X.; et al. *Polym. Int*. **2019**, 68, 955−963.

(33) BelBruno, *J. Chem. Rev*. **2019**, 119, 94−119.

(34) Zhang, K. L.; Guan, X. J.; Qiu, Y. X.; Wang, D. D.; Zhang, X. Y.; Zhang, H. X. *Appl. Surf. Sci*. **2016**, 389, 1208−1213.

(35) Trotta, F.; Caldera, F.; Cavalli, R.; Soster, M.; Riedo, C.; Biasizzo, M.; Balzano, F.; Brunella, V.; Uccello Barretta, G. *Expert Opin. Drug Delivery* **2016**, 13, 1671−1680.

(36) Takeuchi, T.; Kitayama, Y.; Sasao, R.; Yamada, T.; Toh, K.; Matsumoto, Y.; Kataoka, K. *Angew. Chem., Int. Ed*. **2017**, 56, 7088− 7092.

(37) Yoshida, A.; Kitayama, Y.; Kiguchi, K.; Yamada, T.; Akasaka, H.; Sasaki, R.; Takeuchi, T. *ACS Appl. Bio. Mater*. **2019**, 2, 1177− 1183.

(38) Liu, J.; Yang, K.; Deng, Q.; Li, Q.; Zhang, L.; Liang, Z.; Zhang, Y. *Chem. Commun*. **2011**, 47, 3969−3971.

(39) Li, Q. R.; Yang, K. G.; Liu, J. X.; Zhang, L. H.; Liang, Z.; Zhang, Y. K. *Microchim. Acta* **2013**, 180, 1379−1386.

(40) Ma, Y.; Pan, G. Q.; Zhang, Y.; Guo, X. Z.; Zhang, H. Q. *Angew. Chem*. **2013**, 52, 1551−1554.

(41) Yang, K.; Liu, J.; Li, S.; Li, Q.; Wu, Q.; Zhou, Y.; Zhao, Q.; Deng, N.; Liang, Z.; Zhang, L.; Zhang, Y. *Chem. Commun*. **2014**, 50, 9521−9524.

(42) Takimoto, K.; Takano, E.; Kitayama, Y.; Takeuchi, T. *Langmuir* **2015**, 31, 4981−4987.

(43) Saeki, T.; Sunayama, H.; Kitayama, Y.; Takeuchi, T. *Langmuir* **2019**, 35, 1320−1326.

(44) Zhang, W.; Liu, W.; Li, P.; Xiao, H.; Wang, H.; Tang, B. *Angew. Chem., Int. Ed*. **2014**, 53, 12489−12493.

(45) Zhou, J.; Gan, N.; Li, T.; Hu, F.; Li, X.; Wang, L.; Zheng, L. *Biosens. Bioelectron*. **2014**, 54, 199−206.

(46) Takeuchi, T.; Mori, T.; Kuwahara, A.; Ohta, T.; Oshita, A.; Sunayama, H.; Kitayama, Y.; Ooya, T. *Angew. Chem., Int. Ed*. **2014**, 53, 12765−12770.

(47) Guo, T.; Deng, Q. L.; Fang, G. Z.; Liu, C. C.; Huang, X.; Wang, S. *Biosens. Bioelectron*. **2015**, 74, 498−503.

(48) Kuwata, T.; Uchida, A.; Takano, E.; Kitayama, Y.; Takeuchi, T. *Anal. Chem*. **2015**, 87, 11784−11791.

(49) Wackerlig, J.; Lieberzeit, P. A. *Sens. Actuators, B* **2015**, 207, 144−157.

(50) Chen, L.; Wang, X.; Lu, W.; Wu, X.; Li, *J. Chem. Soc. Rev*. **2016**, 45, 2137−2211.

(51) Gui, R.; et al. *Biosens. Bioelectron*. **201**8, 100, 56−70.

(52) Yang, Q.; et al. *Biosens. Bioelectron*. **2018**, 112, 54−71.

(53) Cenci, L. *Talanta* **2018**, 178, 772−779.

(54) Whitcombe, M. J.; Chianella, I.; Larcombe, L.; Piletsky, S. A.; Noble, J.; Porter, R.; Horgan, A. *Chem. Soc. Rev*. **2011**, 40, 1547− 1571.

(55) Zeng, Z.; Hoshino, Y.; Rodriguez, A.; Yoo, H.; Shea, K. *J. ACS Nano* **2010**, 4, 199−204.

(56) Caceres, C.; Canfarotta, F.; Chianella, I.; Pereira, E.; Moczko, E.; Guerreiro, A.; Piletska, E.; Esen, C.; Whitcombe, M. J.; Piletsky, S. *Analyst* **2016**, 141, 1405−1412.

(57) Cenci, L.; Andreetto, E.; Vestri, A.; Bovi, M.; Barozzi, M.; Iacob, E.; Busato, M.; Castagna, A.; Girelli, D.; Bossi, A. M. *J. Nanobiotechnol*. **2015**, 13, 51−65.

(58) Cheng, C.I.; Chang, Y.P.; Chu, Y.H. *Chem. Soc. Rev.,* **2012**, 41, 1947–1971.

(59) Fang, G.; Wang, H.; Yang, Y.; Liu, G.; Wang, S. *Sens. Actuators, B* **2016**, 237, 239−246.

(60) Karaseva, N.; Ermolaeva, T.; Mizaikoff, B. Sens. Actuators, B 2016, 225, 199−208.

(61) Horikawa, R.; Sunayama, H.; Kitayama, Y.; Takano, E.; Takeuchi, T. *Angew. Chem., Int. Ed*. **2016**, 55, 13023−13027.

(62) Phan, N. V. H.; Sussitz, H. F.; Ladenhauf, E.; Pum, D.; Lieberzeit, P. A. *Sensors* **2018**, 18, 180.

(63)Pirincçi,S.S.;Ertekin,Ö.;Laguna,D.E.;Özen,F.S.;Öztürk, Z. Z.; Öztürk, S. *Sensor*s **2018**, 18, 1161.

(64) Liu, J.; Deng, Q.; Tao, D.; Yang, K.; Zhang, L.; Liang, Z.; Zhang, Y. *Sci. Rep*. **2015**, 4, 5487.

(65) Li, Q. R.; Yang, K. G.; Liu, J. X.; Zhang, L. H.; Liang, Z.; Zhang, Y. K.; Li, S. *Microchim. Acta* **2016**, 183, 345−352.

(66) Wang, W.; Zhu, X.; Teng, S.; Xu, X.; Zhou, G. *J. AOAC* Int. **201**8, 101, 1868−1872.

(67) Nishijima, M.; Goto, M.; Fujikawa, M.; Yang, C.; Mori, T.; Wada, T.; Inoue, Y. *Chem. Commun*. **2014**, 50, 14082.

(68) Feroz, S. R.; Sumi, R. A.; Malek, S. N. A.; Tayyab, S. *Exp. Anim*. **2015**, 64, 101−108.

(69) Inoue, Y.; Kuwahara, A.; Ohmori, K.; Sunayama, H.; Ooya, T.; Takeuchi, T. *Biosens. Bioelectron.* **2013**, 48, 113– 119.

(70) Jeanmougin, F.; Thompson, J. D.; Gouy, M.; Higgins, D. G.; Gibson, T. J. *Trends Biochem Sci*. **1998**, 23, 403-405.

Chapter 4

Development of Fluorescent Molecularly Imprinted Nanogels Sensing via Molecular Imprinting and Post-Imprinting Modification for Pork Contamination Detection

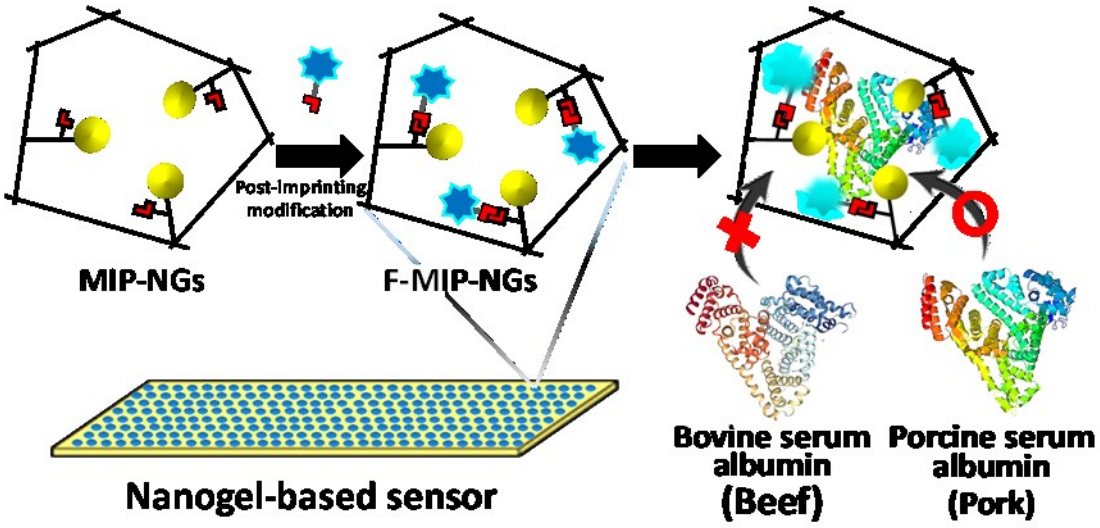

Development of Fluorescent Molecularly Imprinted Nanogels Sensing via Molecular Imprinting and Post-Imprinting Modification for Pork Contamination Detection

4.1 Introduction

The halal food industry is important worldwide, owing to the wide distribution of Muslims (Izberk-Bilgin and Nakata, 2016).[1] Halal food products must be free from non-halal materials, including alcohol, blood, and pork. Nevertheless, many Muslims are concerned that halal meat products might be contaminated with pork or pork derivatives, which are prohibited for Muslims to consume. The contamination of beef products by pork is a cost advantage for manufacturers because pork costs less than beef (Al-Jowder et al., 1997).[2] Thus, there is a need for tools to ensure that beef is free from pork contamination. These tools must involve highly effective analytical methods, with high sensitivity, rapid detection, and good specificity for detecting pork contamination in halal meats. Currently, immune-based techniques using specific interactions between antigens and antibodies are most widely used to detect pork contamination in halal meat products (Liu et al., 2006; Lim and Ahmed, 2016; Kuswandi et al., 2017; Mandli et al., 2018).[3-6] These methods need sophisticated equipment and procedures, including natural receptors (antibodies), which have high cost and low stability.

Molecularly imprinted polymers (MIPs) are effective alternatives to synthetic receptors (plastic antibodies). MIPs are simple to prepare, have high stability, and are effective alternatives to monoclonal antibodies (Komiyama et al., 2004; Haupt, 2012; Schirhagl, 2014; Takeuchi et al., 2016, 2017). [7-11] MIPs for the recognition of animal serum albumins such as human serum albumin (HSA), bovine serum albumin (BSA), and porcine serum albumin (PSA) have been developed and show good specificity and selectivity for their target proteins (Liu et al., 2015; Li et al., 2016; Qin et al., 2018a, 2018b; Xiangzhi et al., 2019; Morishita et al., 2020).[12-17] Currently, many researchers are working on the preparation of nanoparticle MIPs to bring their characteristics closer to those of natural antibodies and produce high specificity and fast interaction with the protein targets (Zeng et al., 2010; Cenci et al., 2015; Caceres et al., 2016).[18-20] The fluorescence-based sensors have been produced using molecular imprinting technology to create rapidly acting MIPs which are highly sensitive to target molecules (Li et al., 2007; Inoue et al., 2013; Murase et al., 2016; Qian et al., 2018; Luo et al., 2019).[21-25]

However, high background fluorescence levels are frequently apparent when functional monomers and fluorescence monomers are co-polymerized to create binding cavities and polymer matrices. Post imprinting modification (PIM) is an effective method for reducing the background by introducing fluorescent reporter molecules into the cavities of MIPs (Sunayama et al., 2010, 2014, 2016; Horikawa et al., 2016; Takeuchi and Sunayama, 2018; Morishige et al., 2019) [26-31] (Scheme 4.1).

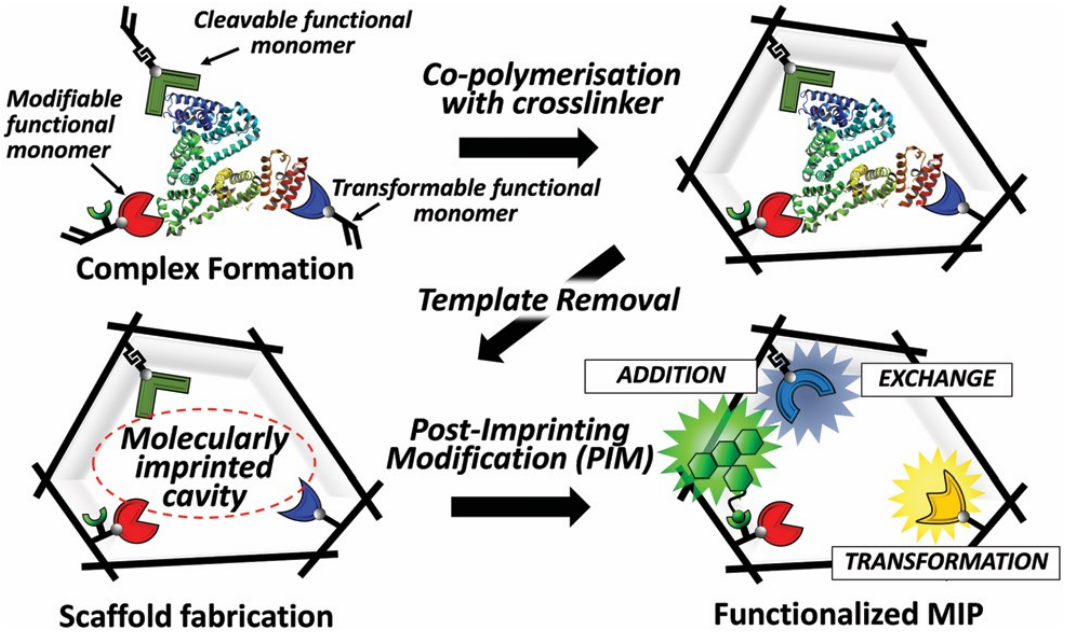

Scheme 4.1 Schematic overview of the preparation of MIPs via molecular imprinting and post-imprinting modification. Reprinted from [Takeuchi and Sunayama, 2018]

Recently, I have successfully developed MIP fluorescence-based sensors for intact exosomes by molecular imprinting and PIM. These sensors have extremely high sensitivity (6 pg/mL) and very fast detection of target exosomes (<10 min) (Mori et al., 2019)[32] (Scheme 4.2). Therefore, the post-imprinting introduction of fluorescent dye into specific cavities of MIPs could create rapidly acting MIP-based sensors and potentially improve their sensitivity to detect pork contamination in halal meat products.

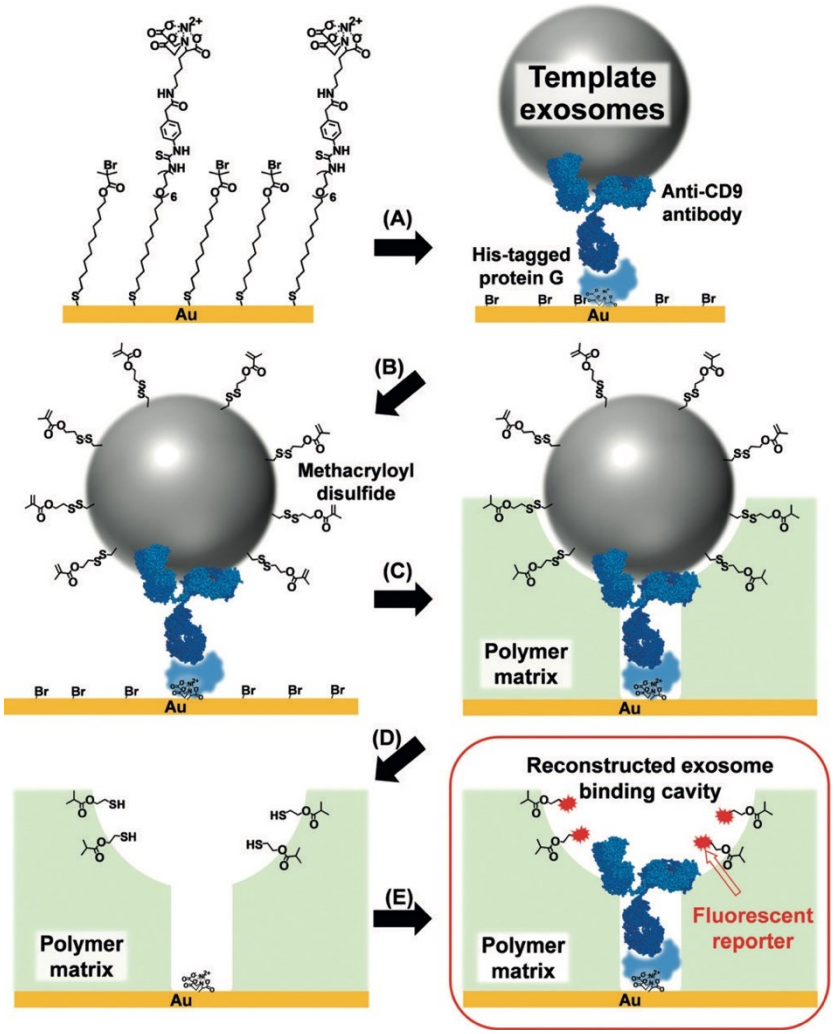

Scheme 4.2 Schematic representation of the preparation of MIP fluorescence-based sensors for intact exosomes by molecular imprinting and PIM. Reprinted from [Mori et al., 2019]

MIP-based sensors are generally used to detect chemical and biological target compounds (Gan et al., 2014; Takeuchi et al., 2014; Guo et al., 2015; Chen et al., 2016; Rijun et al., 2018; Lucia et al., 2018).[33-38] My previous study was the only one to develop MIP-nanogels (MIP-NGs) targeting PSA to detect pork contamination in halal raw meats (Cheubong et al., 2020),[39] where i prepared MIP-NGs by emulsifier-free precipitation polymerization, with pyrrolidyl acrylate used as a functional monomer, and demonstrated their use as MIP-NGs based a quartz crystal microbalance (QCM) sensors for the detection of PSA in halal meat extracts. The MIP-NGs based QCM sensor provided high selectivity for PSA compared to other animal serum albumins, but the sensitivity was considerably lower than that of immunosensors (Scheme 4.3).

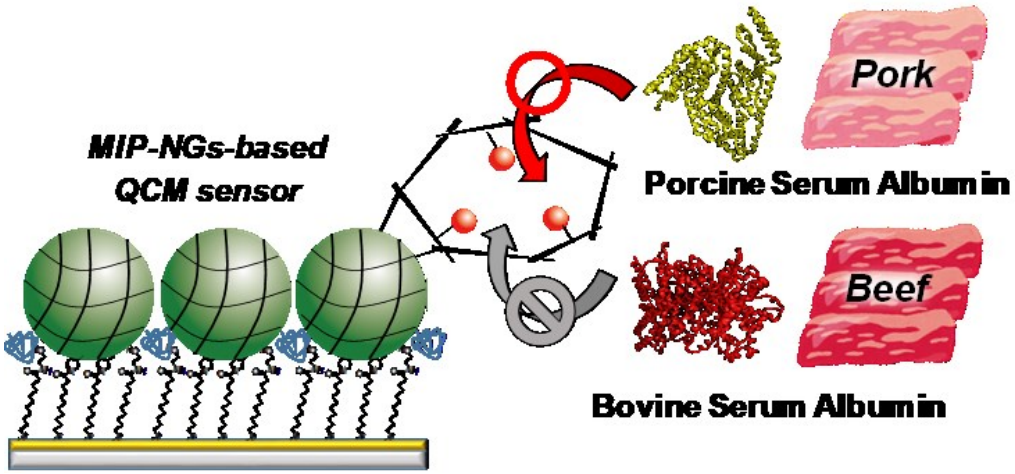

Scheme 4.3 Schematic overview of the preparation of MIPs via molecular imprinting and post-imprinting modification. Reprinted from [Cheubong et al., 2020]

In the current work, i aimed to combine the advantages of good affinity and selectivity of MIP-NGs with PIM for the development of highly sensitive MIP-NGs fluorescence-based sensors, using 4-[2-(*N*- methacrylamido) ethylaminomethyl] benzoic acid (MABA) as a functional monomer and ATTO 647N as a fluorescent dye introduced via PIM (Scheme 4.4). I successfully prepared a MIP-NGs fluorescence-based sensor with high sensitivity and selectivity for rapid PSA detection of pork contamination in halal meat extract samples for the first time.

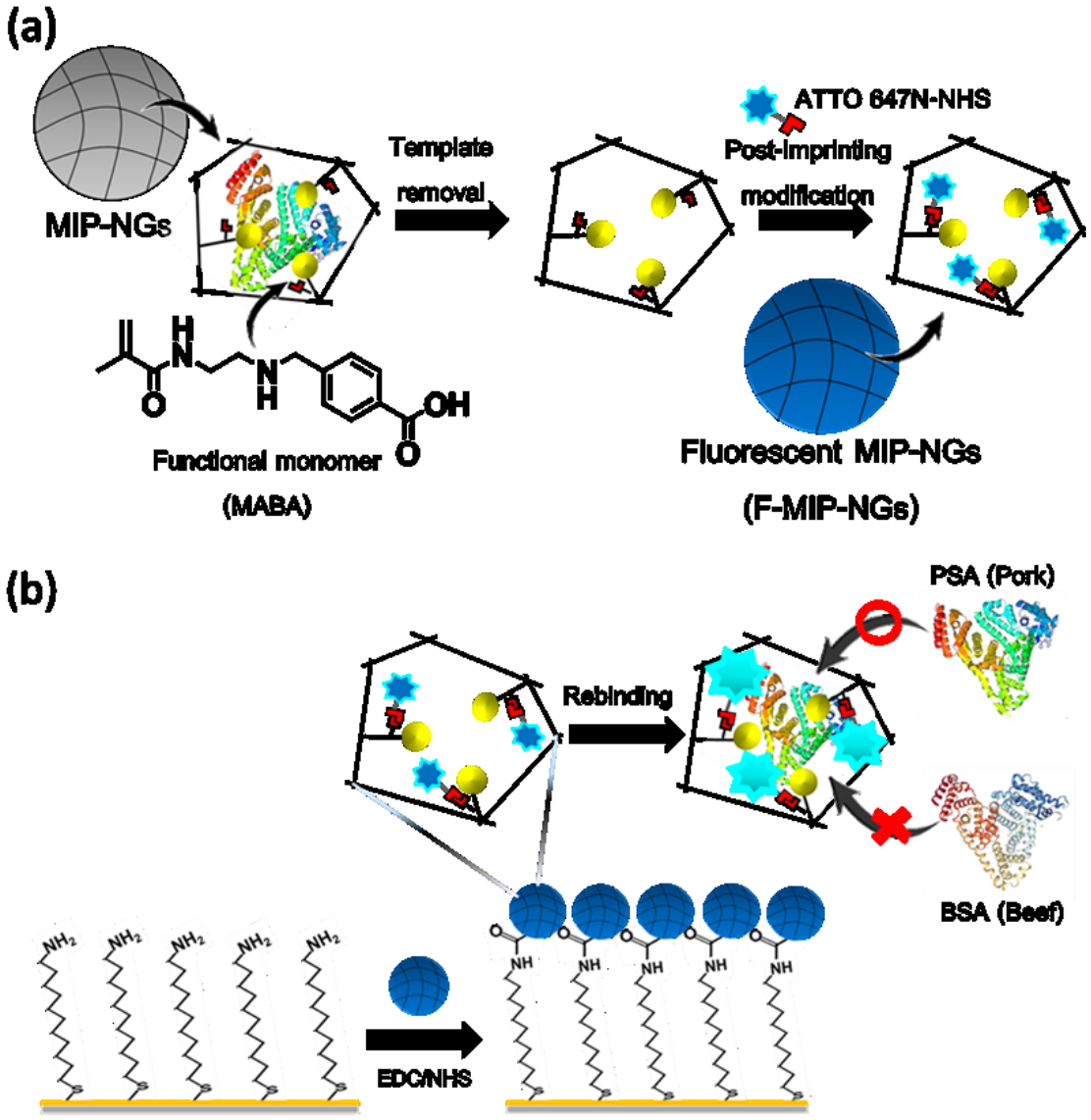

Scheme 4.4 Schematic illustration of the preparation of fluorescent MIP-NGs (F-MIP-NGs) (a), and the binding of PSA detection by the fluorescence-based sensor (b).

4.2 Experimental Section

4.2.1. Reagents and materials

Albumins from the pig (porcine serum albumin, PSA), human (human serum albumin, HSA) and bovine (bovine serum albumin, BSA), Transferrin (Trf), Lysozyme (Lyz),11-Amino-1-undecanethiol hydro- chloride (AUT), *N*-hydroxysuccinimide (NHS) and DEAE–Sephadex A- 50 were purchased from Sigma-Aldrich (MO, USA). *N*-Isopropyl acryl- amide (NIPAm) and *N,N*′-methylenebisacrylamide (MBAA) were pur- chased from Nacalai Tesque

Co. (Kyoto, Japan). Sephadex G-100 was purchased from GE Healthcare (Tokyo, Japan). Ethanol (EtOH), Dimethyl sulfoxide (DMSO) and 2,2′ -azobis (2-methylpropionamidine) dihydrochloride (V-50) were purchased from Wako Pure Chemical Industries, Ltd. (Osaka, Japan). 2-Methacryloyloxyethylphosphorylcho- line (MPC) was purchased from NOF Corporation (Tokyo, Japan). 1- (3-Dimethylaminopropyl)-3-ethylcarbodiimide hydrochloride (EDC) was purchased from Tokyo Chemical Industries (Tokyo, Japan). The Micro BCA Protein Assay Kit, the Protein–Free (PBS) blocking buffer and sulfo-NHS acetate were purchased from Thermo Fisher Scientific (MA, USA). ATTO 647N NHS-ester was purchased from ATTO-TEC GmbH (Siegen, Germany). SpeedSTAR HS DNA polymerase and CycleavePCR 6 Meat Species Identification Kit were purchased from TaKaRa Bio Inc. (Shiga, Japan). The mixtures of primers and FAM-labelled probe in the kit were used for real-time PCR. MABA were prepared using a previously reported procedure (Sunayama et al., 2010, 2014).[26-27]

4.2.2. Instrumentation

The fluorescence spectra were measured using an F-2500 fluorescence spectrophotometer (Hitachi High-Technologies, Tokyo, Japan). The particle size distribution and the zeta potential were carried out using a Dynamic Light Scattering (DLS) system Zetasizer Nano ZS (Malvern Instruments Ltd., Malvern, U.K.). The morphology of the MIP-NGs was characterized by a Transmission electron microscope (TEM) using JEM-1230 (JEOL. Ltd., Tokyo, Japan). The fluorescence intensities were measured using a custom-made liquid handling robot equipped with a fluorescence microscope (System Instruments Co. Ltd., Tokyo, Japan) (Mori et al., 2019; Takano et al., 2019).[32,40]

4.2.3 Preparation of MIP-NGs

MIP-NGs were prepared using emulsifier-free precipitation poly-merization method. In brief, PSA (13.2 mg, 0.2 μmol), MABA (78.6 mg, 0.3 mmol) as a functional monomer, MPC (59 mg, 0.2 mmol) and NIPAm (407 mg, 3.6 mmol) as a comonomer, MBAA (30.8 mg, 0.2 mmol) as a cross-linker, and V-50 (217 mg) as an initiator were dissolved in 10 mM phosphate buffer (pH 7.4) containing 140 mM NaCl (PBS) (50 mL). After degassing by N2/vacuum cycles, a polymerization was carried out at 70 °C for 12 h.

After the polymerization, the purification procedure was performed to purify the obtained nanogels from template protein in the two steps; size exclusion chromatography to

separate MIP-NGs and unreacted monomers by their size and ion-exchange chromatography to remove PSA from obtained NGs. First, size exclusion chromatography was performed on packed Sephadex G-100 into column (33 cm × 1.2 cm I.D.) and PBS was used as the eluent. The dispersed NGs in PBS (2 mL) were injected into the packed column and fractions (1.5 mL) were collected. Fluorescence spectroscopy was used to collect the fractions of NGs. Next, ion-exchange chromatography was performed on packed DEAE Sephadex A-50 into a column (size 10 cm × 1.0 cm I.D.) and 10 mM Tris-buffer (pH 7.4) containing 140 mM NaCl (TBS) was used as the eluent. The five collected fractions (fraction no.9–13) from size-exclusion chromatog- raphy were mixed together, and condensed by ultrafiltration with 10 kDa cut-off of Amicon ultra centrifugal filters (7500 g × 3, at 25 °C for 20 min) using TBS as a solvent. Then 1.0 mL of condensed MIP-NGs, dispersed in TBS, were injected into the packed column and fractions of 1.5 mL were collected. In order to collect the NG fractions and confirm the removal of the protein template from NGs, fluorescent measure- ments were performed for MIP-NGs at 400 nm (λ_{ex}: 280 nm) and for protein at 350 nm (λ_{ex}: 280 nm). Non-imprinted polymer nanogels (NIP-NGs) were prepared with the same condition as MIP-NGs without template and purified by the same procedure. The particle size distribution of obtained MIP-NGs and NIP-NGs both before and after purification was measured by DLS. To estimate a removal rate of PSA from MIP-NGs, fluorescence intensities of tryptophan residues of PSA in MIP-NGs were measured at λem: 350 nm (λex: 280 nm) before and after the purification by ion-exchange chromatography for 300 μg/mL of MIP-NGs. The removal rate was calculated from the following eq 1.

$$\text{Removal rate (\%)} = \frac{\lambda_{em,\ before} - \lambda_{em,\ after}}{\lambda_{em,\ before}} \times 100 \quad \textbf{(1)}$$

4.2.4 Preparation of fluorescent MIP-NGs (F-MIP-NGs) from MIP-NGs via PIM

The purified MIP-NGs and NIP-NGs (500 μg/mL, 1000 μL) were incubated with 5 μL of 10 mg/mL ATTO 647N NHS-ester in DMSO at 25 °C for 2 h. After incubation, the unreacted fluorescent dye was removed by Amicon ultra centrifugal filters with a 10 kDa cut-off (7500 g x 3, at 25 °C for 20 min) and washed by PBS. To confirm the successful of introducing fluorescent dye into MIP-NGs and NIP-NGs, the fluorescence intensity of ATTO 647N both before and after post-imprinting modification were measured by fluorescence spectroscopy (λex: 646 nm and λem: 664 nm).

4.2.5 Morphology of F-MIP-NGs and fluorescent NIP-NGs (F–NIP-NGs)

The morphology of obtained F-MIP-NGs and F–NIP-NGs was observed using TEM. For TEM sample preparation, solvent of purified NGs was changed to pure water using ultrafiltration (Amicon Ultra 10 kDa). The dispersions were dried on carbon-coated Cu-grid. Then, the Cu-grid inverted on 1 wt% potassium Eu-encapsulated Preyssler-type phosphotungstate (Wako Pure Chemical Industries, Osaka, Japan) aqueous solution, then the sample was dried. TEM observation was performed using JEM-1230 (JEOL. Ltd).

4.2.6 Preparation of MIP-NGs-based fluorescent sensor

4.2.6.1 Immobilization of F-MIP-NGs on gold-coated sensor chip

After rinsing with ethanol, a 4.3 × 9.8 mm of gold-coated sensor chip, coated with Ti (5 nm thickness) and Au (165 nm thickness), was dried with N_2. The sensor chip was cleaned by UV-O_3 treatment for 20 min and dipped in ethanol solution containing AUT (1.0 mM) for 24 h at 25 °C to form a self-assembled monolayer (SAM). After the reaction, the gold-coated sensor chip was washed with ethanol and pure water triplicate. For the immobilization of F-MIP-NGs on the gold-coated sensor chip, 100 μL of an aqueous solution containing 0.05 M NHS and 0.2 M EDC was dropped onto the gold-coated sensor chip and incubated for 60 min. After rinsing with water, 100 μL of PBS containing F-MIP-NGs or F–NIP-NGs (10, 50, 100, 200 and 400 μg/mL) for various incubation time (30, 60, 90, 120 and 180 min) were dropped onto modified gold-coated sensor chips. After immobilization, the blocking of the chip surface was performed by dropping 100 μL of 10 mM sulfo-NHS acetate aqueous solution for 30 min, followed by dropping 100 μL of Protein–Free (PBS) blocking buffer solution for 30 min. The fluorescence intensity values of immobilized NGs on the gold-coated sensor chips were measured using fluorescence microscope. The fluorescence intensity change values of immobilized NGs (F_0) on the gold-coated sensor chips were measured from differences in fluorescence intensity before and after immobilization of NGs into the gold-coated sensor chips ($F_0 = F_{\text{immobilized NGs}} - F_{\text{only substrate}}$). In additional, the QCM experiment was also performed to confirm the successful immobilization of NGs on gold-coated sensor chip. F–NIP-NGs were also immobilized on the gold-coated sensor chips in the same manner.

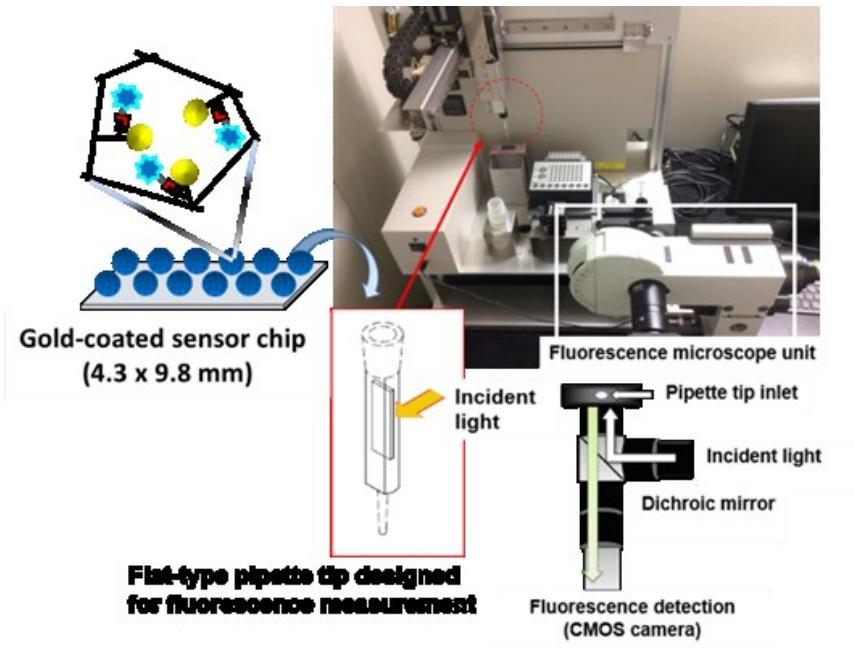

Figure 4.1 Photograph and illustration of the custom-made liquid handling robot equipped with a fluorescence microscope, and the flat-type pipette tip designed for detection of fluorescence.

4.2.6.2 Monitoring of the PIM-treatment in MIP-NGs Immobilized on Gold-coated Sensor Chip

The QCM measurement was conducted using a QCM-D (Q-sense, Sweden). The same procedure was performed to immobilize F-MIP-NGs onto the QCM sensor chip for QCM measurements and fluorescence measurements with the immobilization process onto the gold senser chip. The chip was mounted on the flow module unit performed using QCM-D (Q-Sense, Sweden), the fundamental frequency 4.95 MHz, and PBS as a running buffer.

4.2.6.3 Fluorescence detection of PSA

The fluorescence detection experiments for binding and selectivity of NGs for PSA were performed using a custom-made liquid handling robot equipped with fluorescence microscope (Figure 4.1) (Mori et al., 2019; Takano et al., 2019). The gold-coated sensor chip on which F-MIP-NGs or F–NIP-NGs were immobilized was inserted into a designed flat-type pipette tip, after then the binding experiments were performed using the following steps. (1) The flat-type pipette tips were settled on the tip rack, which were captured with a robot arm. (2) A protein concentration of PSA (0, 0.25, 0.5, 1, 2, 3, 5, 10, 20, 40, 80 and 160 nM) in PBS were aspirated into the flat-type pipette tip (150 µL). (3) The protein samples were incubated for (0.5, 1, 2, 5 and 10 min) at 25 °C and then discharged. (4) After PBS (150 µL) was aspirated, the robot arm

was moved into the detection port to capture the image and to measure the fluorescence intensity by Zyla 5.5 sCMOS camera (Andor Technology Ltd, Belfast, UK) equipped with a fluorescence turret (BX3-URA, Olympus, Tokyo, Japan) in each sample. The measurements were conducted in triplicate, and ten different regions of interests (ROIs) were selected in each chip. objective lens, 5 × (LMPLFLN5X, Olympus, Tokyo, Japan); exposure time, 0.1 sec; light source, mercury lamp (HGLGPS-SET, Olympus, Tokyo, Japan); Bandpass filters (Cy5TM), 604–644 nm for excitation and 672–712 nm for emission. The fluorescence intensity change values of protein binding (F) towards the immobilized NGs sensor chips were measured from differences in fluorescence intensity before and after incubation of PSA into the gold-coated sensor chips ($F = F_{\text{incubated PSA}} - F_{\text{only substrate}}$). Then the relative fluorescence intensity of binding experiments was calculated from this equation $(F - F_0)/F_0$, where F_0 and F are the fluorescence intensity change values of the immobilized NGs and protein binding, respectively. To investigate the selectivity of F-MIP-NGs and F–NIP-NGs for PSA recognition, 10 nM of the reference proteins including HSA, BSA, Trf and Lyz dissolved in PBS were used as reference proteins. The relative fluorescence intensity was then calculated by equation as describe above.

4.2.6.4 Curve Fitting of Binding Isotherms

The affinity constant for PSA was estimated by curve fitting using DeltaGraph 5.4.5v. The fitting equation is shown below eq 2.

$$Y = [(1 + KG + KH) - \sqrt{(1 + KG + KH) - 4K^2HG}] \times \frac{D}{2KG} \quad (2)$$

The equation is used with the affinity constant for 1:1 complex formation, where Y is Adsorption (ΔFbinding/ΔFimmobilization), K is an affinity constant, H is found by fitting raw data to a theoretical curve, G is a PSA concentration, and D is the maximum bound amount of PSA.

4.2.6.5 The long-term stability

To study the stability of the sensor, F-MIP-NGs were immobilized on gold-coated sensor chip under the optimized conditions as describe above in the immobilization section, and then the sensor chips were kept at 4 °C until use. The binding experiments of 10 nM of PSA dissolved in PBS toward the kept sensor chip in the day of 1, 3, 7, 14, 30, 45, and 60 were individually measured. The quantity of PSA binding toward F-MIP- NGs was monitored by detecting the fluorescence intensity as describe above in the fluorescence detection section.

4.2.6.6 Meat extract samples and protein extraction

The meat extract samples were prepared from two different raw meat samples (pork and beef, purchased from a local supermarket). The extraction of protein was performed as follows: the meat samples were chopped separately. A portion of 1 g was weighted and mixed with 5 mL of the extraction buffer (PBS), then homogenized using a benchtop homogenizer, Polytron PT 1600 E (Kinematica AG, Luzern, Switzerland) for 2 min (10,000 rpm), followed by centrifugation for 30 min at 4 °C (3 × 16,000 g). The clear supernatant was separated and filtered through a 0.2 μm PTFE filter (DISMIC-13HP, Toyo Roshi Kaisha Ltd., Tokyo, Japan) three times, and then the protein concentration of the meat extract samples from both beef and pork were measured using Micro BCA Assay. The meat extract samples were kept at − 20 °C until use.

4.2.6.7 Recovery study on the sensor

To evaluate the appropriate dilution factor of beef extracts for the PSA binding experiments in real meat extract samples, the various dilution factors of beef extract and PBS (1, 10, 100, 500 and 1000 folds) were spiked with 10 nM of PSA dissolved in PBS. The binding experi- ments were performed using F-MIP-NGs immobilized gold-coated sensor chip, which was inserted into a designed flat-type pipette tip and settled on a custom-made liquid handling robot equipped with fluorescence microscope. The fluorescence intensity was measured as describe above in the fluorescence detection section. Then the binding experiment of the spiked sample was performed at the appropriate dilution factor of beef extract in previous experiment, the different concentrations of PSA (0–160 nM) were added to the beef extract solution, and the binding experiments of PSA dissolved in diluted real meat extract were demonstrated under the experimental conditions as describe above in the fluorescence detection section. Recovery rates were estimated from the following eq 3,

$$Recovery\ rates(\%) = \frac{(Relative\ fluorescence\ intensity)_{spikedsample}}{(Relative\ fluorescence\ intensity)_{buffer}} \mathbf{x}\ 100 \qquad \mathbf{(3)}$$

where $(\text{Relative fluorescence intensity})_{\text{spiked sample}}$ and $(\text{Relative fluorescence intensity})_{\text{buffer values}}$ were obtained from the PSA binding experiments in spiked sample and in buffer solution, respectively.

4.2.7 Detection of pork contamination in beef extract samples

To confirm the feasibility of proposed sensor to detect pork contamination in real beef extract samples, the contaminated beef extract samples with pork were prepared by mixing pork extract and beef extract for four concentration range of 0.01, 0.1, 1 and 10 wt%. The uncontaminated beef extract and original pork extract were used as negative and positive controls, respectively. Then the contaminated beef samples (0.01, 0.1, 1 and 10 wt%) and control samples (100 wt% beef extract and 100 wt% pork extract) were incubated into F-MIP-NGs immobilized gold-coated sensor chip, and the fluorescence intensity was measured and the relative fluorescence intensity was calculated. The measurement conditions were as described above in the fluorescence detection section.

4.2.8 Real-time PCR for detecting pork contamination in beef extract samples

To detect pork contamination in PBS and beef extract samples by a real-time PCR system using microfluidic technology (Furutani et al., 2016),[41] the meat samples were prepared in the same manner as describe in meat extract samples section without filtration step to avoid a loss of contained DNA during the filtration; 1% pork contamination in PBS and beef extract. The PCR mixture consisted of 2.25 µL of DNase-free water, 1.25 µL of 10 × Fast Buffer I (including 3 mM $MgCl_2$), 1.0 µL of 2.5 mM dNTP mixture, 5.0 µL of primers and probe mixture, 0.25 µL of RNaseH, 0.25 µL of 5 U/µL of SpeedSTAR HS DNA polymerase, and 2.5 µL of meat extract. The real-time PCR reaction was 96 °C for 10 sec (activation of SpeedSTAR HS DNA polymerase), fifty cycles of amplification at 96 °C of 5 sec (denaturation), and 57 °C for 15 sec (annealing and extension).

4.3 Results and Discussions

4.3.1 Preparation of F-MIP-NGs

The synthesis of F-MIP-NGs capable of detecting PSA as a marker of pork contamination in halal meat extracts was completed in two steps. First, emulsifier-free precipitation polymerization was used to prepare MIP-NGs in PBS. MABA was used as the functional monomer, which non-covalently interacted with PSA via hydrophobic and electrostatic interactions. The NG particle size was controlled using MPC as a hydrophilic and biocompatible co-monomer. I previously reported that under polymerization conditions similar to those in the current study, the secondary structure of PSA was not denatured when maintained at 70 °C for 12 h (Cheubong et al., 2020). After polymerization, the obtained MIP-

NGs were first purified using size-exclusion chromatography followed by ion-exchange chromatography (Fig. 4.2a and 4.2b). This two-step purification procedure purified the MIP-NGs from the unreacted monomers and free PSA, showing a sharp peak in the chromatogram of the MIP-NGs (fraction No. 15 in Fig. 4.2b). The high removal rate of PSA (94%) confirmed the effectiveness of this two-step purification procedure in collecting the pure fraction and removing all PSA molecules from the polymer matrix (Fig. 4.3). The two-step purification of MIP-NGs in the current study showed a higher removal rate of the template protein than that achieved using one-step purification via size-exclusion chromatography (86%) or ion-exchange chromatography (92%), as described in my previous reports (Takeuchi et al., 2017; Cheubong et al., 2020). The particle size and zeta potential of MIP-NGs before and after purification were investigated using DLS. As shown in Fig. 4.4, the obtained NGs exhibited good monodispersity, and no coagulation was observed under the polymerization conditions. The Z-average particle size of the purified MIP-NGs, at approximately 25 nm, was smaller than that of the unpurified MIP-NGs. The zeta potential of the purified MIP-NGs increased from − 0.51 to 3.3 mV, indicating that the template PSA, a negatively charged protein, was successfully removed from the NGs after the two-step purification. The Z-average particle size of NIP-NGs, which were prepared using the same procedure in the absence of PSA, was approximately 20.7 nm and the zeta potential before and after purification—2.4 and 1.9 mV, respectively—was not significantly different (Table 4.1). These results confirmed that MIP-NGs and NIP-NGs were completely synthesized using the emulsifier-free precipitation polymerization method and successfully purified using two-step purification with size-exclusion and ion exchange chromatography.

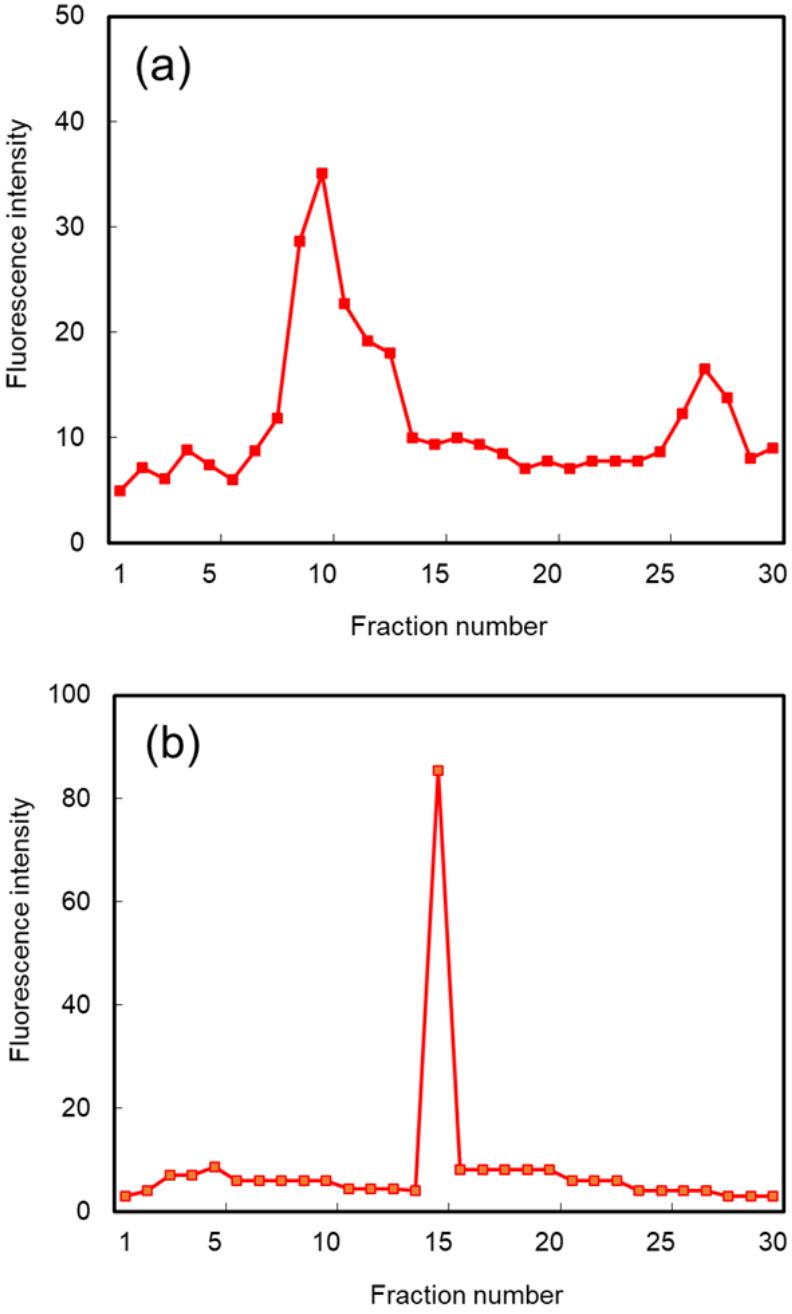

Figure 4.2 The chromatogram of purified MIP-NGs, (a) measured from the fluorescence intensities of MABA in MIP-NGs at (λ_{ex}: 280 nm at λ_{em}: 400 nm) after first purification by size exclusion chromatography and (b) after second purification by ion-exchange chromatography (DEAE-Sephadex).

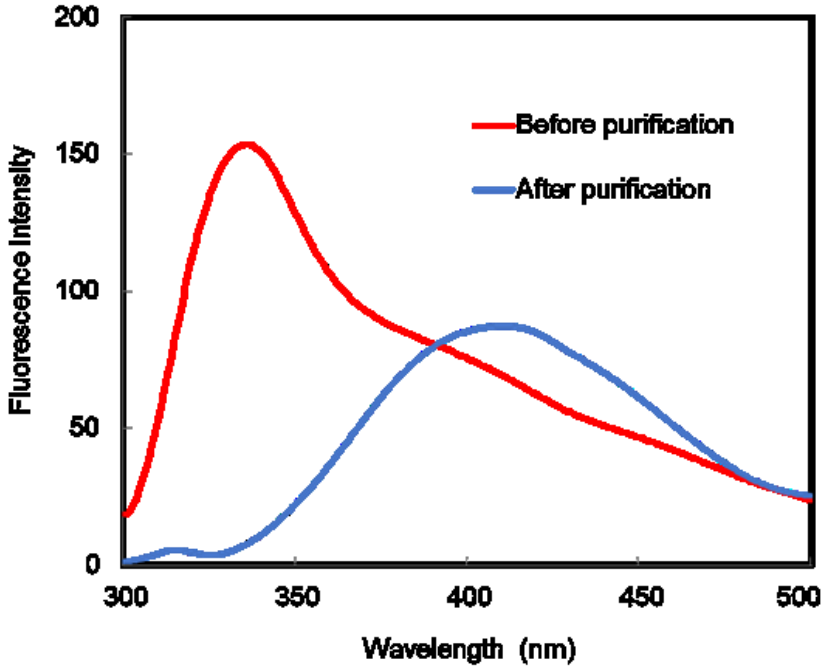

Figure 4.3 Fluorescence spectra at λ_{ex}: 280 nm of tryptophan residues in PSA before and after purification by two-steps purification. Fluorescence intensities of tryptophan residues of PSA at λ_{em}: 350 nm before and after purification were 152.7 and 10.0, respectively. The concentration of obtained MIP-NGs before and after purification was 500 µg/mL. PSA: Porcine serum albumin

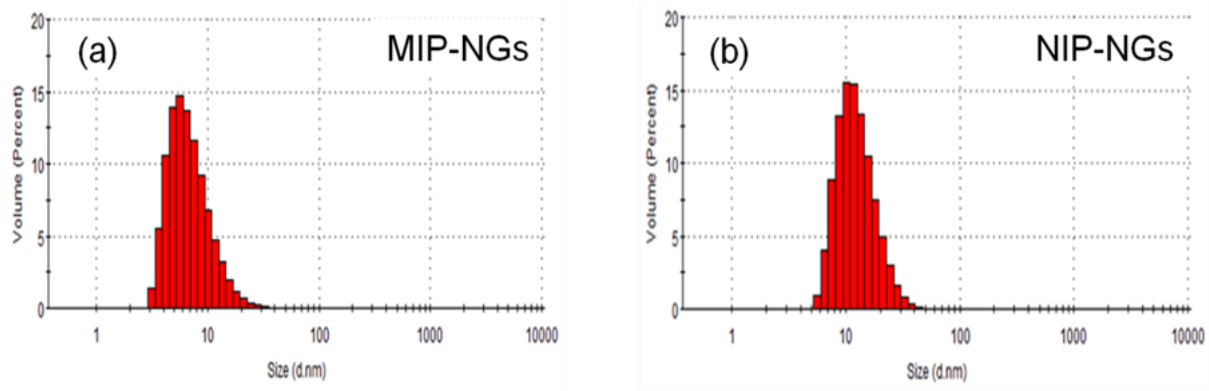

Figure 4.4 Particle size distributions of MIP-NGs and NIP-NGs after purification by size exclusion chromatography and ion-exchange chromatography determined by DLS. (a): MIP-NGs after purification; Z-average particle size: 25 nm (b): NIP-NGs after purification; Z-average particle size: 21 nm.

Table 4.1 Characterization of the obtained particle size distribution of MIP-NGs and NIP-NGs.

Characteristics	MIP-NGs		NIP-NGs	
	Before purification	After purification	Before purification	After purification
Z-average (d.nm)	32	25	62	21
PdI	0.52	0.52	0.51	0.43
Zeta potential (mV)	-0.51	3.3	2.5	1.9

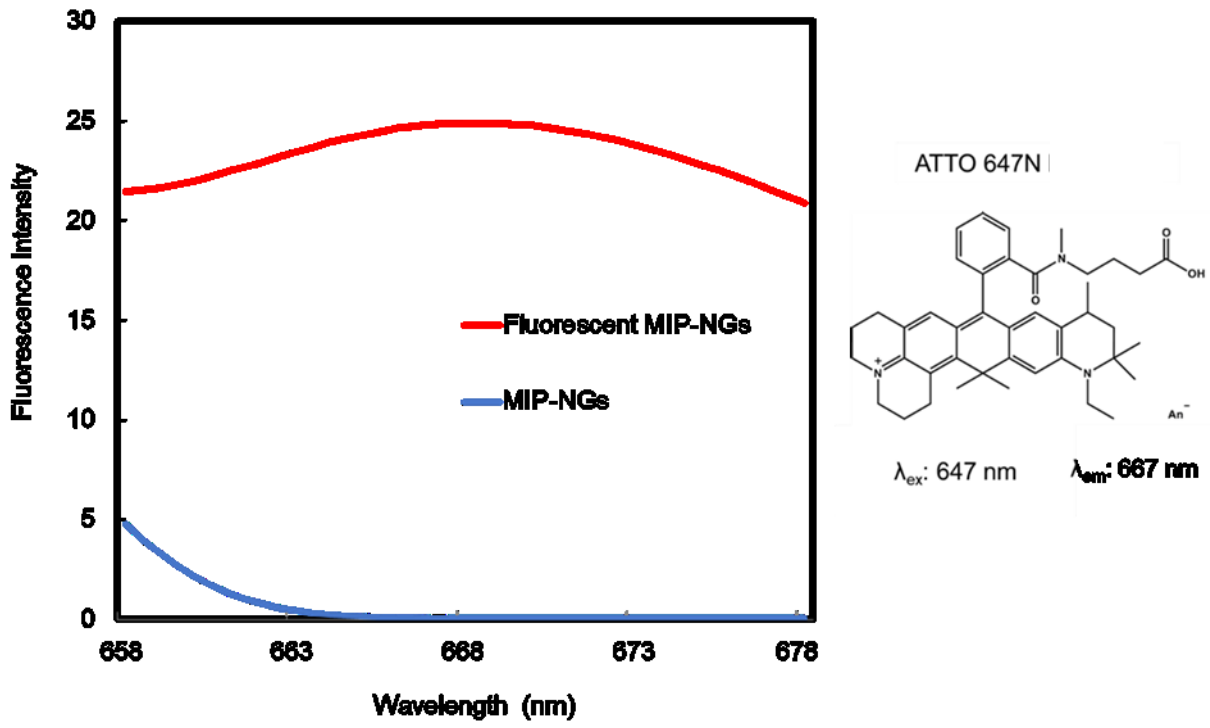

Figure 4.5 Fluorescence intensity of the ATTO 647N NHS-ester in MIP-NGs before and after incubation (λ_{ex}: 647 nm and λ_{em}: 667 nm).

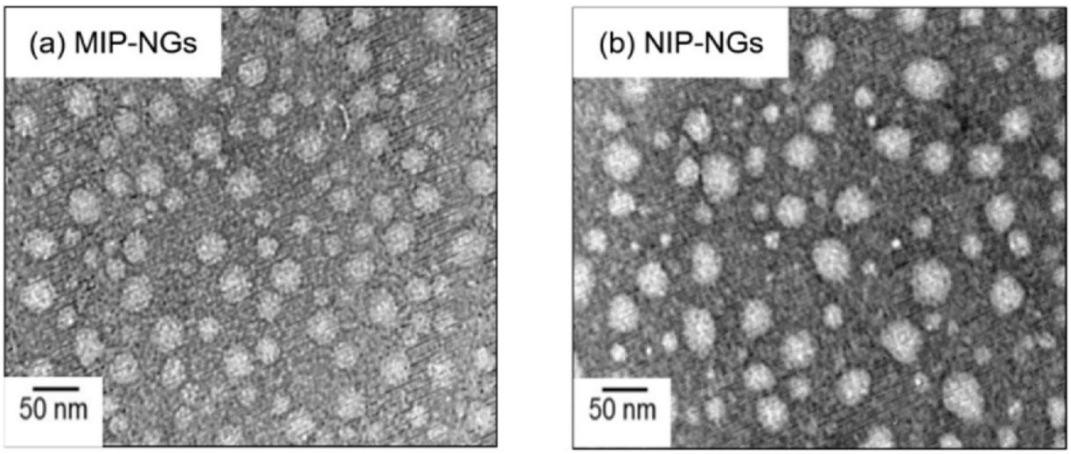

Figure 4.6 Transmission electron microscopy images of MIP-NGs (a) and NIP-NGs (b) after the introduction of ATTO 647N NHS-ester for post-imprinting modifications (F-MIP-NGs and F–NIP-NGs).

In the second step, ATTO 647N was used as the fluorescent reporter molecule for the PIM of MIP-NGs via conjugation between ATTO 647N and the secondary amino group within the PSA-imprinted nanocavity. After incubating MIP-NGs with ATTO 647N NHS ester, the fluorescence intensity of ATTO 647N in the F-MIP-NGs and untreated MIP-NGs was measured at 25 °C at an excitation wavelength of 647 nm. The maximum peak was observed at a wavelength of 668 nm. The fluorescence spectrum of ATTO 647N was observed in the F-MIP-NGs, but not in the untreated MIP-NGs (Figure 4.5), confirming that ATTO 647N was successfully introduced into the secondary amino group of MIP-NGs. A fluorescence peak at around 668 nm was also observed for F–NIP-NGs. The characterization of the fluorescent NGs using TEM revealed spherical morphologies of F-MIP-NGs and F–NIP-NGs (Figure 4.6), which were related to the DLS results of F-MIP-NG and F–NIP-NG characterization. Furthermore, it was also observed that the morphologies of the fluorescent NGs remained intact in both size and shape after PIM.

4.3.2 Immobilization of F-MIP-NGs on gold-coated sensor chips

The F-MIP-NG-based sensors were prepared by immobilizing the fluorescent NGs on gold-coated sensor chips. The immobilization was achieved by the covalent conjugation of the primary amino groups on the SAM to the carboxyl groups on the fluorescent NGs and confirmed using a custom-made liquid-handling robot equipped with a fluorescence microscope. Subsequently, the fluorescence intensity derived from the introduced ATTO 647N

was recorded. The images of the gold surfaces with immobilized F-MIP-NGs were found to exhibit many differences from those of non-immobilized gold chips (Figure 4.7), indicating successful immobilization. F-MIP-NG immobilization was also confirmed using a QCM and the same gold surface as used in AUT modification. Here, the signal response frequency was decreased after F- MIP-NG injection into the QCM sensor chips (Figure 4.8). These results provided supporting evidence for the successful immobilization of F-MIP-NGs on the modified gold-coated sensor chips.

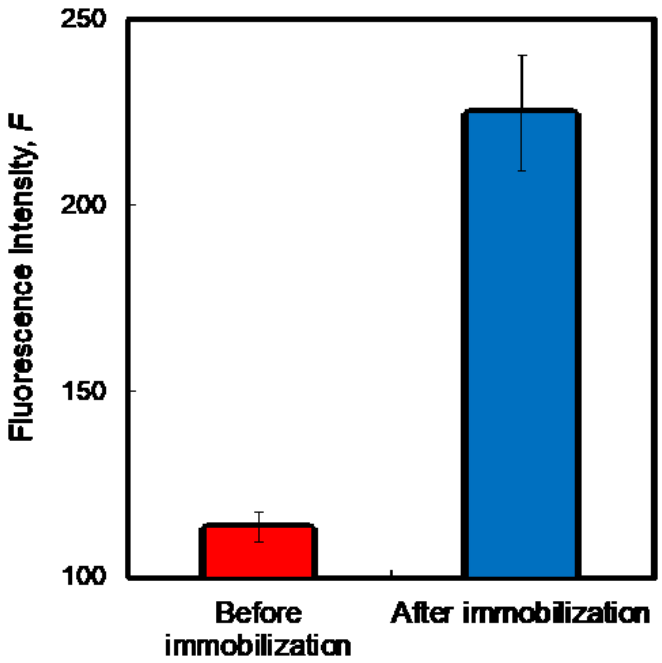

Figure 4.7 Fluorescence intensity of the gold-coated glass substrate before (red) and after (blue) the immobilization of F-MIP-NGs.

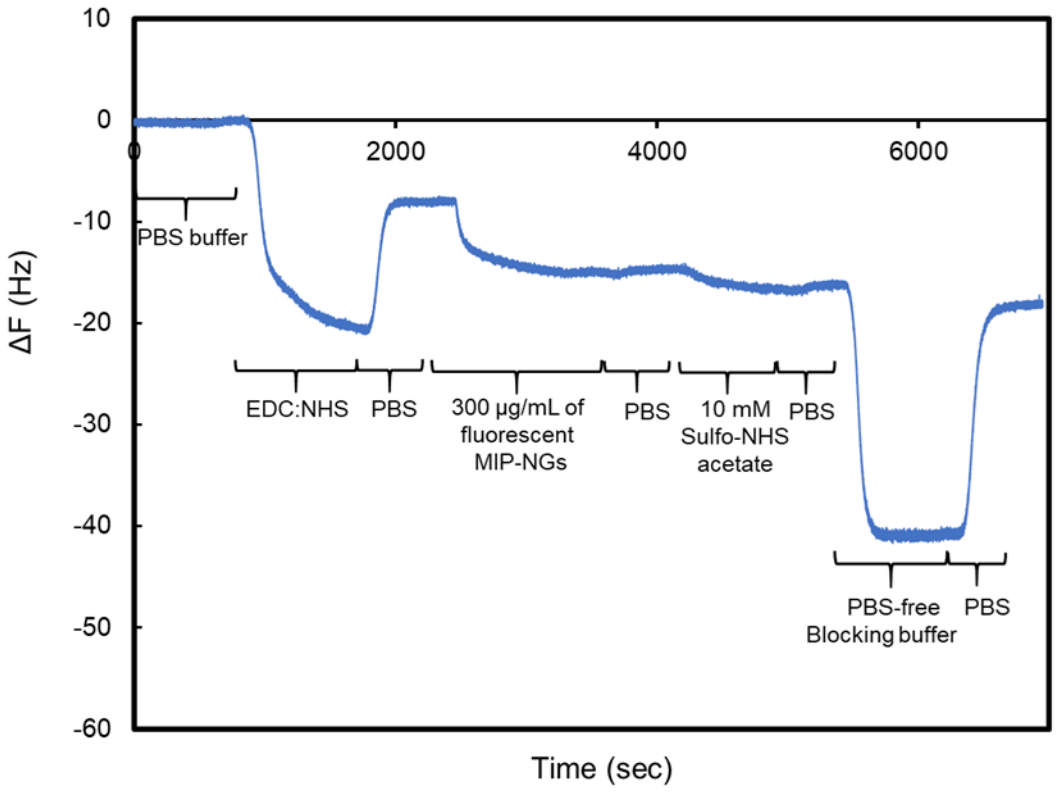

Figure 4.8 Sensorgram of QCM for immobilization of F-MIP-NGs to QCM sensor chip surface.

4.3.3 Optimization of NG concentration, immobilization time, and binding time

To create a highly sensitive F-MIP-NG-based sensor for PSA detection, i investigated the optimization of three parameters using the custom-made liquid handling robot equipped with a fluorescence microscope (10 nM PSA). First, F-MIP-NG concentration was optimized by testing five concentrations (10, 50, 100, 200, and 400 µg/mL); the 100 µg/mL concentration was ultimately selected because it provided a higher fluorescence intensity with a smaller amount of F-MIP-NG than the other two concentrations, 200 and 400 µg/mL (Figure 4.9a). The immobilization times of F-MIP-NGs were measured, and the relative fluorescence intensity achieved at the 60 min immobilization time point showed complete immobilization (Figure 4.9b). Upon increasing the immobilization time to over 60 min, the responses obtained were slightly different. Thus, an F-MIP-NG concentration of 100 µg/mL and an immobilization time of 60 min were selected as the optimal immobilization conditions for further experiments. Finally, several incubated PSA binding times were optimized under the chosen immobilization conditions. The 2 min binding time produced the highest response, and no significant changes were observed when the binding time was increased to over 2 min (Figure 4.9c). Therefore, a

binding time of 2 min was selected as the ideal binding experiment conditions. The proposed sensor rapidly detected PSA binding at a sensor time of 0.5 min, at which point the binding response reached over 63.2% of the total response value. This result was considerably faster than that determined in my previous work (7 min) (Cheubong et al., 2020).

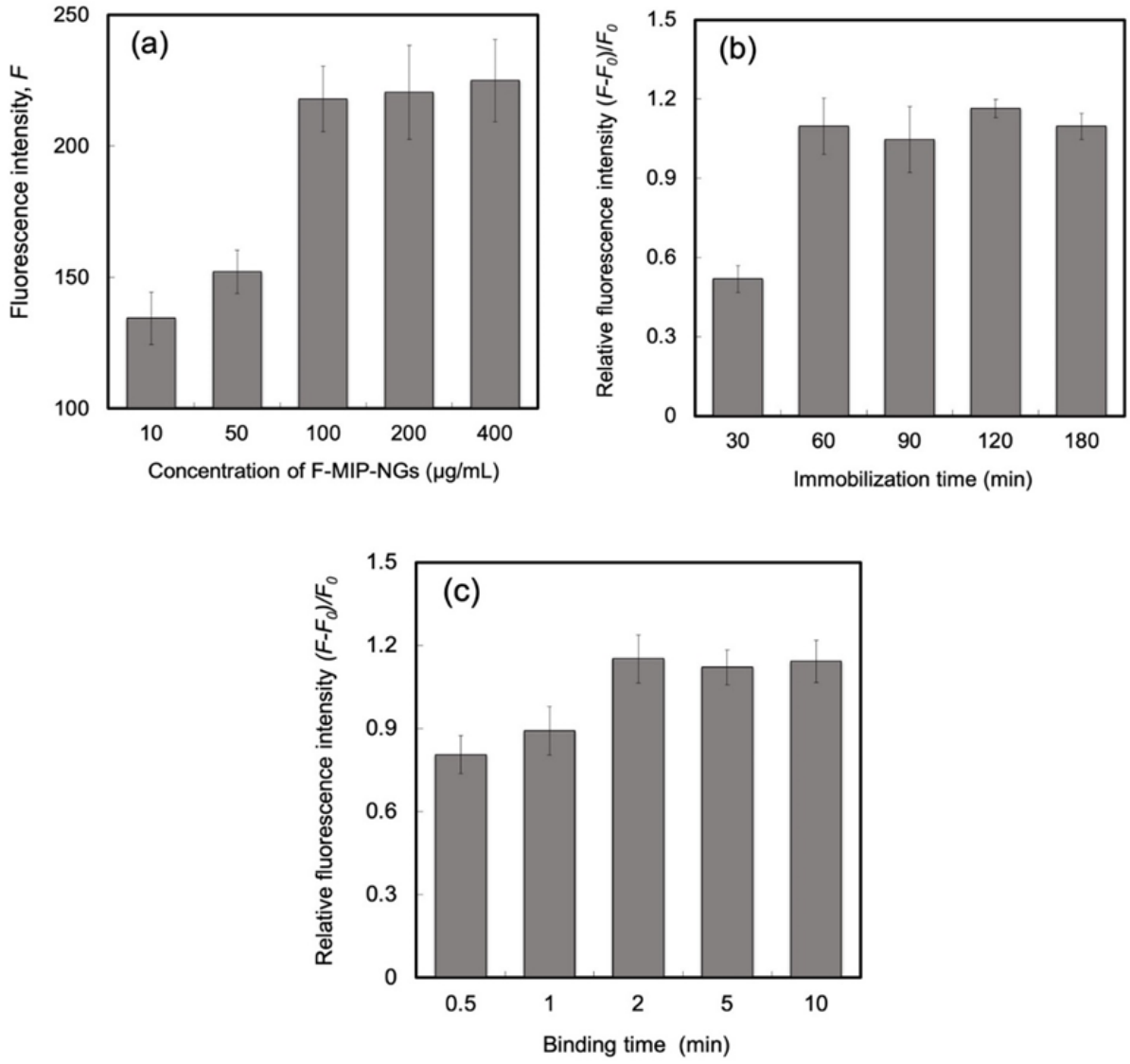

Figure 4.9 Optimization of the experimental conditions. (a) F-MIP-NGs of different concentrations were immobilized on gold-coated sensor chips. (b) Different incubation times were tested for complete immobilization of F-MIP-NGs on gold-coated sensor chips. (c) Different porcine serum albumin binding times for the F-MIP-NGs immobilized on gold-coated sensor chips were tested. The error bars were obtained from triplicate experiments.

4.3.4 Analytical performance of the F-MIP-NG-based sensor

To evaluate the performance of the proposed sensor, several features were investigated under optimal conditions.

4.3.4.1 Calibration curve, linearity range, and limit of detection (LOD)

The relative fluorescence intensity of the F-MIP-NG-immobilized gold-coated sensors after incubation with different concentrations of PSA exhibited a typical calibration curve, as shown in Figure 4.10, with a linear range of 0.25–5 nM. The LOD of PSA for the F-MIP-NG-immobilized gold-coated sensor was calculated according to 3 SD/m, where m was the slope of the linear part of the binding behaviour, and SD was the standard deviation for 0 nM PSA. The LOD was found to be 40 pM (2.5 ng/mL). The sensitivity of the proposed sensor was 5000 times higher than that of my previous MIP-NG-immobilized QCM sensor, for which the LOD was only 12 μg/mL (Cheubong et al., 2020). The proposed sensor also showed higher sensitivity than previously reported MIP-based detection methods using high performance liquid chromatography (LOD: sub mg/mL) (Liu et al., 2015; Li et al., 2016; Qin et al., 2018a, 2018b) and immune sensors based on surface plasmon resonance (SPR) detection (19.81 ng/mL) (Wang et al., 2018).[42] These results confirmed that the sensitivity of the MIP-NG-based sensor was successfully increased via PIM of the ATTO dye introduced into the imprinted cavity of MIP-NGs. On the contrary, the sensitivity of the proposed sensor was less than that of an electrochemical immunosensor, which exhibited the highest sensitivity for the detection of PSA, at 0.5 pg/mL (Li et al., 2016). However, the MIPs are inexpensive and easy to prepare and highly stable, unlike expensive and unstable natural antibodies, rendering the proposed system an easy-to-use system that is amenable for biosensing markets.

4.3.4.2 Binding affinity of the sensor

The binding affinities (K_a values) of PSA to F-MIP-NGs and F–NIP- NGs immobilized on gold-coated sensor chips were evaluated. The relative fluorescence intensities of PSA showed concentration dependent binding to the F-MIP-NGs immobilized on the gold-coated sensor chips, such that the binding isotherm gradually increased with increasing PSA concentration in the solutions. The response values of F–NIP-NGs were significantly lower than that of MIP-NGs at every PSA concentration (Figure 4.11). As in the case of previously reported fluorescent MIPs (Sunayama et al., 2010, 2014), this phenomenon could be due to the formation of high affinity binding cavities conjugated with ATTO 647N in F-MIP-NGs. The binding affinity of PSA to F-MIP-NGs was calculated to be $1.61 \times 108\ M^{-1}$, which was higher

than that of F–NIP-NGs (K_a = 4.06 × 107 M^{-1}) (Figure 4.12). These results indicated that the affinity of PSA for F-MIP-NGs increased due to the molecular imprinting process.

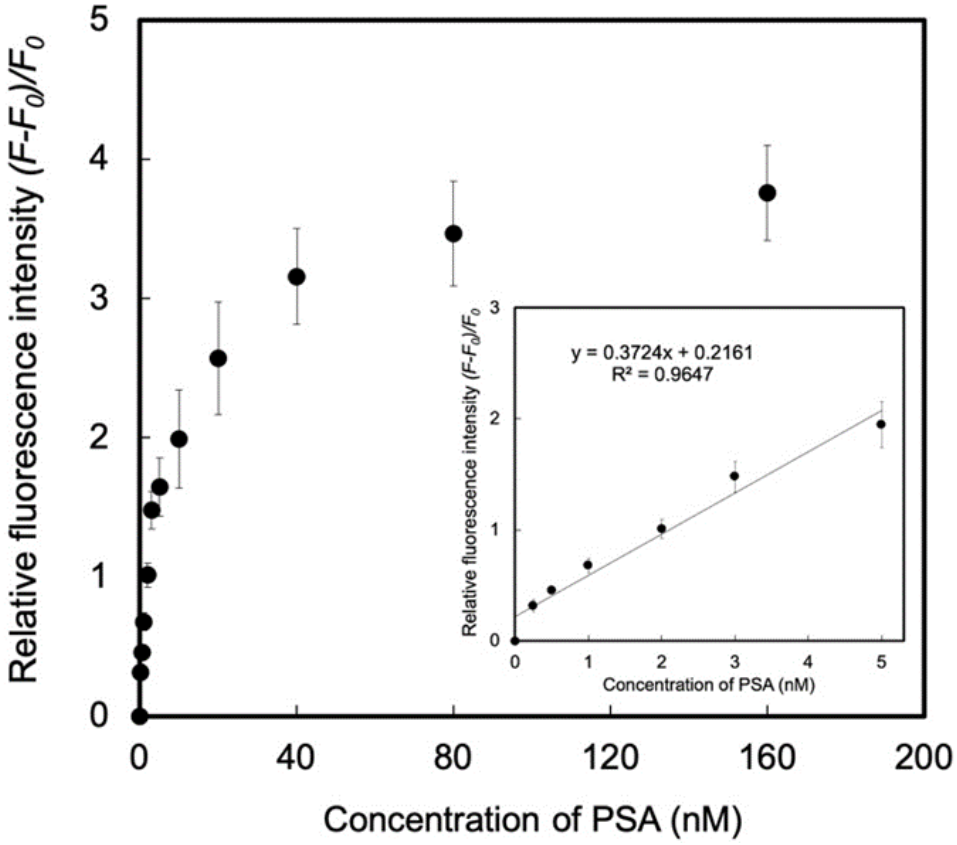

Figure 4.10 The binding isotherm of F-MIP-NGs to PSA (0-160 nM) shows a linear calibration range of 0.25–5 nM (r^2 = 0.9647). The error bars were obtained from triplicate experiments.

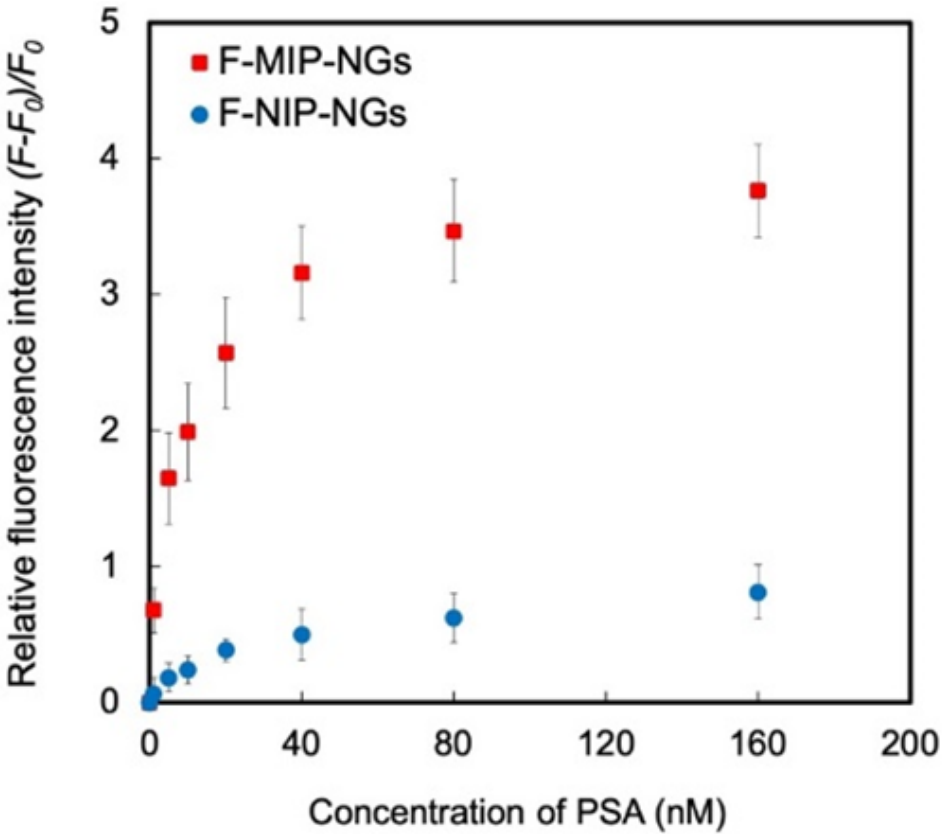

Figure 4.11 Binding behaviour of PSA to F-MIP-MGs (red squares) and F–NIP-NGs (blue circles). PSA of various concentrations (0–160 nM) was incubated on NGs- immobilized gold-coated sensors. The error bars were obtained from triplicate experiments.

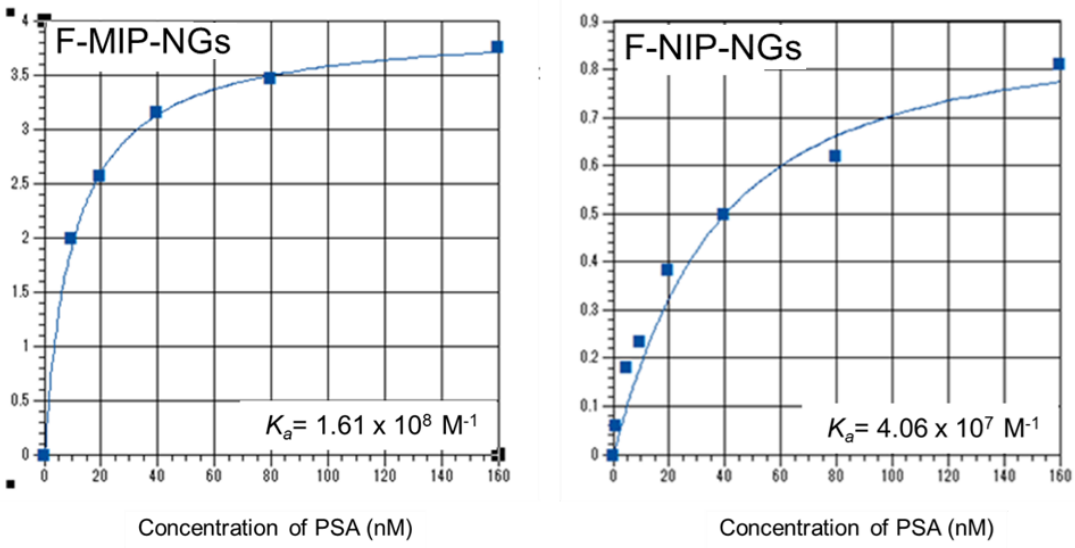

Figure 4.12 Affinity constants (K_a) for the binding of PSA to F-MIP-NGs and F-NIP-NGs, estimated from the relative fluorescence intensity measurements data.

4.3.4.3 Selectivity of the sensor

To evaluate the selectivity of the F-MIP-NG for PSA, the fluorescence intensities of PSA and potentially interfering proteins, including HSA, BSA, Trf, and Lyz, which bind to F-MIP-NGs and F–NIP-NGs, were measured, and the relative fluorescence intensities were calculated. The relative fluorescence intensities of the interfering proteins were significantly lower than that of PSA at a similar protein concentration (10 nM), confirming that F-MIP-NGs exhibited high selectivity for PSA (Figure 4.13a). The responses of the two animal serum albumins, HSA and BSA, which are homologous to PSA, were higher than those of Trf and Lyz due to the similarities in the amino acid sequences, isoelectric points (pI = 5.1), and molecular weights (Mw = 68 kDa) of the animal serum albumins to those of PSA. The lowest imprinting factor was obtained for Lyz, which has a different amino acid sequence (net positive charge in PBS), molecular weight (14.4 kDa), and pI (10.7) compared to those of PSA, indicating that the higher PSA selectivity of F-MIP-NGs was driven by two specific properties of PSA: 1) the amino acid sequences of the terminal (Cheubong et al., 2020) and hydrophobic (Nishijima et al., 2014; Feroz et al., 2015)[43-44] regions relative to those of other animal serum albumins, and 2) the different sizes and net charges of the proteins under experimental conditions. PSA selectivity was not, however, observed for F–NIP-NGs. The responses to F–NIP-NGs of all the proteins investigated were much smaller than that of F-MIP-NGs (Figure 4.13b). Thus, these results suggested that the PSA-specific recognition nanocavities of F-MIP-NGs were formed by the molecular imprinting process, and ATTO 647N was successfully introduced into the nanocavities via the PIM treatment.

4.3.4.4 Precision and stability of the sensor

To evaluate the precision of the proposed sensor, i demonstrated the reproducibility of SAM preparation and NG immobilization using seven different F-MIP-NGs immobilized on gold-coated sensor chips for 10 nM PSA detection and then calculated the relative standard deviation (%RSD). The reproducibility of the sensor was found to be acceptable (% RSD = 6.2) (Table 4.2).

The stability of the proposed sensor was evaluated by measuring the relative fluorescence intensity of 10 nM PSA for F-MIP-NGs immobilized on gold-coated sensor chips after storage at 4 °C for 60 d. After storage for 45 d, the relative fluorescence intensity remained at over 80% of the initial value (day 1) for 10 nM PSA (Figure 4.14a), whereas the response decreased to 58% of the initial value after 60 d of storage. Thus, these results indicated the long-term stability of the sensor to be 45 d.

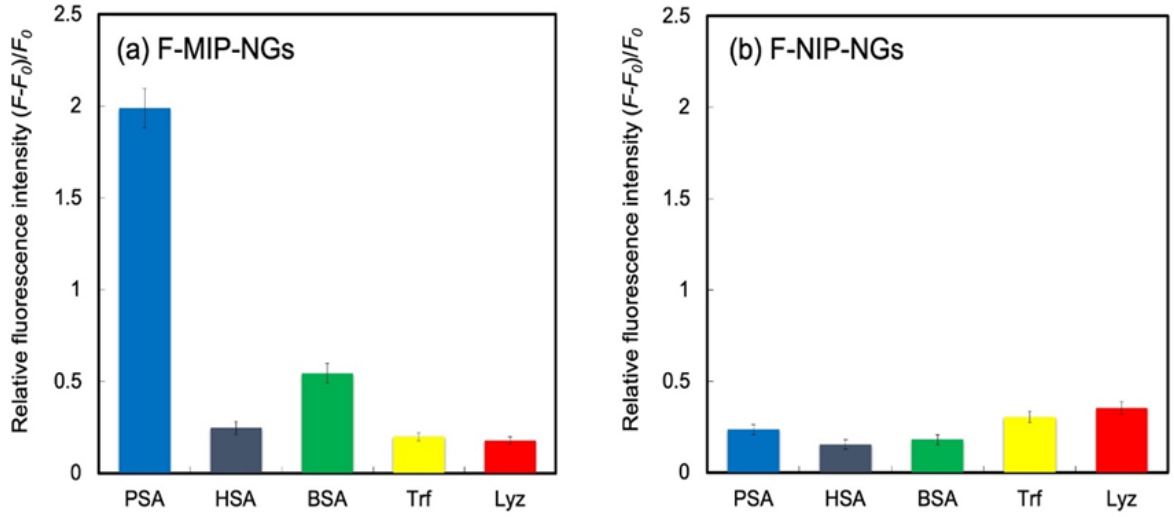

Figure 4.13 Relative fluorescence intensities of F-MIP-NGs (a) and F–NIP-NGs (b) for PSA and four competitive proteins: human and bovine serum albumins (HSA and BSA), transferrin (Trf), and lysozyme (Lyz). The protein concentrations were 10 nM. The error bars were obtained from triplicate experiments.

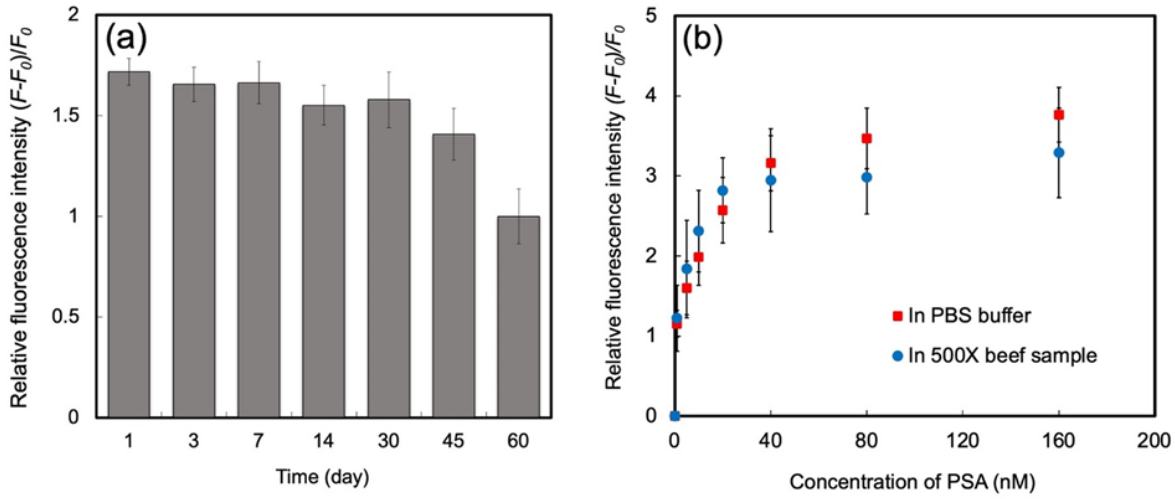

Figure 4.14 Analytical performance of the F-MIP-NG- based sensor. (a) Long-term stability of the proposed sensor determined by measuring the relative fluorescence intensity of porcine serum albumin (PSA) for fluorescent molecularly imprinted polymer nanogels (F-MIP-NGs). PSA concentration was 10 nM. (b) PSA binding behaviour towards fluorescent molecularly imprinted polymer nanogels (F-MIP-NGs) in PBS (red squares) and 500-fold-diluted beef extract (blue circles). The error bars were obtained from triplicate experiments.

Table 4.2 The result of the reproducibility of F-MIP-NGs–immobilized on the gold-coated sensor chips for determination of 10 nM PSA. The relative standard deviation (%RSD) was calculated from seven triplicate experiments (n=7).

Replicate (Time)	Relative fluorescence intensity $(F\text{-}F_0)/F_0$
1	1.7527
2	1.5110
3	1.7176
4	1.5100
5	1.6036
6	1.7760
7	1.6232
Average	**1.6420**
SD	**0.1016**
% RSD	**6.190**

4.3.4.5 Recovery study of the sensor

The choice of appropriate dilution factor was an important consideration for reducing matrix interferene effects when real meat extract binding experiments were performed. After the protein extraction from the meat samples, the protein concentrations of both the beef and pork extracts were measured using the Micro BCA Protein Assay (Figure 4.15 and Table 4.3). The beef extract samples (12.21 mg/mL of total protein concentration) were diluted in PBS with a range of dilution factors (x) (1–1000) and then spiked with 10 nM PSA in preparation for the binding experiments. The relative fluorescence intensities of PSA binding to F- MIP-NGs in undiluted and 10-fold diluted samples were very different from that of the blank sample, which consisted only of PBS buffer, due to the interference matrix effects of the real beef extract samples, indicating that PSA binding to F-MIP-NGs was interrupted by the interference matrix in real samples (Figure 4.16). The responses after in- cubation with PSA added to 100-, 500-, and 1000-fold diluted samples were much higher than those after incubation with PSA added

to the undiluted and 10-fold diluted samples. The values for the 500- and 1000-fold diluted sample matrices were not significantly different from that of the blank sample diluted with PBS, confirming that the dilution factors of the 500- and 1000-fold diluted samples did not suffer from the matrix effect on PSA detection. Thus, a 500-fold dilution of the beef extracts was suitable for PSA detection in real meat extract samples. The accuracy of the proposed sensor was investigated using a recovery test by adding various PSA concentrations to 500-fold diluted beef extract.

As seen in Figure 4.14b, the binding isotherm of the spiked beef extracts to F-MIP-NGs was the same as that of PBS buffer. Based on Table 4.4, the recovery range for PSA was 93–116%. These results indicated that F- MIP-NGs displayed high accuracy in recognizing the target protein PSA, even in real meat extract samples.

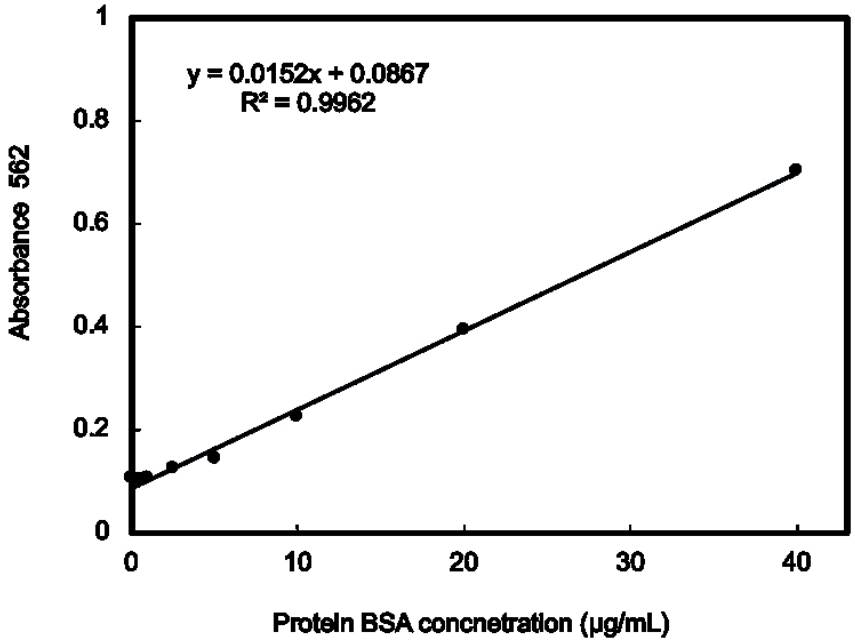

Figure 4.15 BSA protein standard curve. The absorbance at OD 562 (nm) was determined for a range of BSA protein standards from 0-40 μg/mL (r^2=0.9962).

Table 4.3 The total protein concentration of meat extracts.

Sample	Protein concentration (mg/mL)
Pork extract	15.74
Beef extract	12.21

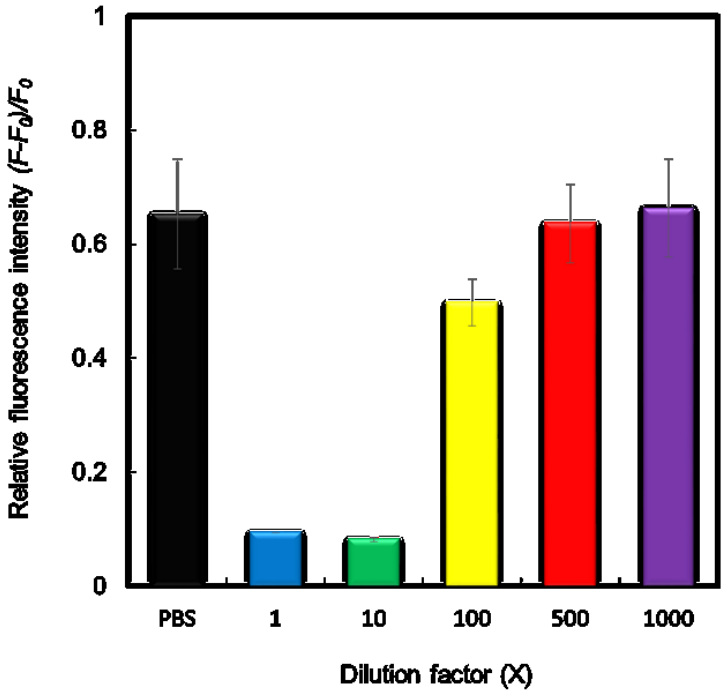

Figure 4.16 The relative fluorescence intensities of spiked 10 nM of PSA into diluted beef extract samples (PBS, 1, 10, 100, 500 and 1,000-fold dilutions) binding to F-MIP-NGs. Original protein concentration in beef meat extract determined by Micro BCA assay: 12.21 mg/mL. Error bars were obtained from triplicate experiments.

Table 4.4 The result of recovery rate for determination of PSA in spiked samples (n=3).

Spiked samples (nM)	Measured concentration (nM)	Recovery (%)
1	1.06	106.03
5	5.74	114.79
10	11.63	116.28
20	21.93	109.66
40	37.31	93.28

4.3.5 Detection of pork contamination in beef extract samples

To study the feasibility of the proposed sensor, simulated pork contaminated beef extract samples were prepared by mixing diluted pork extract and beef extract solutions in ranges of 0, 0.01, 0.1, 1, 10, and 100 wt%. At 0 and 0.01 wt% contamination, the response signals were similar to those of the PBS-only control, with overlapping error bars. For 0.1 wt% contaminated pork in the beef extract samples, significant response signals were observed, with non-overlapping error bars for the pork contamination levels, indicating that the detection limit of pork contamination for the F-MIP-NG-based sensor was approximately 0.1 wt%, where the beef extract was used as the negative control, as the similar response signal was observed for the PBS-only control (Figure 4.17). These results indicated the potentiality of the proposed sensor for commercial use, as the detection limit of 0.1 wt% is significantly efficient for identifying pork contamination in raw beef samples, which is generally contaminated with high levels of pork for cost reduction purposes and consequent business advantages. Compared to my previously developed MIP-NG-based QCM sensor, the F-MIP-NG- based sensor was more sensitive for detecting pork contamination (1 wt %; 100-fold dilution sample), even in 500-fold diluted meat extract samples. The sensitivity of the F-MIP-NG-based sensor developed in this work for the detection of pork contamination in real meat samples was comparable to that of the sandwich enzyme-linked immunosorbent assay (ELISA; 0.1% w/w) (Liu et al., 2006), immunosensor (0.1% w/w) (Kuswandi et al., 2017), and ELISA/immunoassay (0.1%) (Mandli et al., 2018).

To confirm the effectiveness of my fluorescence-based sensor for the detection of pork contamination in beef extract samples, real-time PCR of PBS and beef extracts with 1 wt% pork contamination was conducted. As shown in Fig. 6b, pork contamination in PBS (samples 1–3) could be detected at Ct values of 34.4, 37.5, and 38.1, respectively, but pork contamination in the beef extract samples appeared to be negative. This observation might be due to PCR inhibition by components in the raw beef extracts. These results confirmed the advantage of my sensor, which not only possessed high sensitivity, selectivity, and stability but was also able to detect pork contamination in halal meat extracts for halal food control.

The comparatively lower sensitivity of the proposed sensor compared to that of the champion data of other PSA sensors and the long-term stability of 45 d could be the technical limitations encountered for its commercial use. However, the proposed sensor system, which was constructed using the MIP-NGs, synthetic polymer materials is capable of molecular recognition and signalling the binding events following a simpler preparation method than the tedious and time-consuming procedure required for natural antibodies. Moreover, the

monomers used for preparing the MIP-NGs are commercially available and can be obtained easily, rendering the proposed system as an affordable system to be used in the biosensing markets. Furthermore, the stability of the proposed sensor could be improved by using a more stable fluorescent dye during the PIM of MIP-NGs.

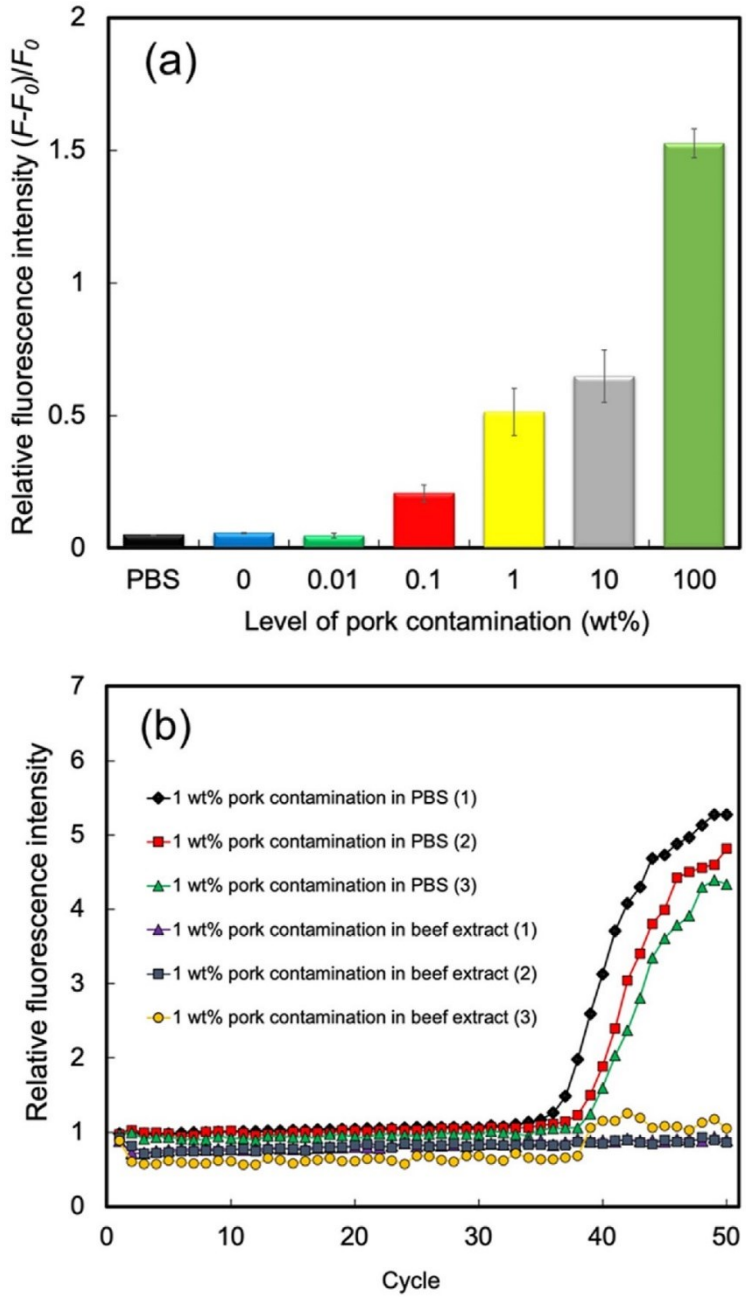

Figure 4.17 Relative fluorescence intensities of pork contamination of various concentrations in beef extract samples (0–100 wt%) to F-MIP-NGs (a). The error bars were obtained from triplicate experiments; The real-time results (Ct-value) of 1 wt% pork contamination in PBS and beef extract samples (b). The real-time PCR was repeated three times.

4.4 Conclusions

In this study, F-MIP-NGs capable of PSA recognition were successfully constructed using molecular imprinting technology and PIM, and their performance in both simulated and real samples of pork contamination was demonstrated. The F-MIP-NGs exhibited a highly sensitive fluorescence response towards PSA with a low LOD (40 pM), reflecting their potential as fluorescence-based sensors for PSA detection. Additionally, i observed high selectivity of F-MIP-NGs for PSA, compared to four different interfering proteins (HSA, BSA, Trf, and Lyz). The sensor showed excellent performance in terms of response time (rapid detection in 30 s), repeatability (%RSD = 6.2), and stability (45 d) for PSA detection. High recovery rates of PSA (93–116%) from PSA-spiked real beef extract samples were obtained. A detection limit for pork contamination was as low as 0.1 wt% in the pork-contaminated beef extract samples was also achieved. My proposed sensor is the first F- MIP-NG-based method for detecting PSA as a marker for pork contamination in halal food extracts providing a new, rapid, fluorescence-based detection method. The proposed sensor is easy to prepare compared to natural antibodies and incurs a low cost demonstrating its potential to detect pork contamination in halal raw meat extracts with high sensitivity and selectivity. Therefore, this easy and rapid sensing system would be a powerful tool for food analysis.

4.5 References

(1) Izberk Bilgin, E.; Nakata, C.C. *Bus. Horiz*. **2016**, 59, 285–292.

(2) Al Jowder, O.; Kemsley, E.K.; Wilson, R.H. *Food Chem*. **1997**, 59, 195–201.

(3) Liu, L.; Chen, F.C.; Dorsey, J.L.; Hsieh, Y.H.P. *J. Food Sci*. **2006**, 71, 1–6.

(4) Lim, S.A.; Ahmed, M.U. *Food Chem*. **2016**, 206, 197–203.

(5) Kuswandi, B.; Gani, A.A.; Ahmad, M. *Food Biosci.* **2017**, 19, 1–6.

(6) Mandli, J.; Fatimi, I.E.; Seddaoui, N.; Amine, A. *Food Chem*. **2018**, 255, 380–389.

(7) Komiyama, M.; Takeuchi, T.; Mukawa, T.; Asanuma, H. Molecular Imprinting. Wiley, Weinheim. **2004**.

(8) Haupt, K. Molecular Imprinting. Springer, Berlin. **2012**.

(9) Schirhagl, R. *Anal. Chem*. **2014**, 86, 250–261.

(10) Takeuchi, T.; Hayashi, T.; Ichikawa, S.; Kaji, A.; Masui, M.; Matsumoto, H.; Sasao, R.; *Chromatography* **2016**, 37, 43–64.

(11) Takeuchi, T.; Kitayama, Y.; Sasao, R.; Yamada, T.; Toh, K.; Matsumoto, Y.; Kataoka, K. *Angew. Chem. Int. Ed*. **2017**, 56, 7088–7092.

(12) Liu, J.; Deng, Q.; Tao, D.; Yang, K.; Zhang, L.; Liang, Z.; Zhang, Y. *Sci. Rep*. **2015**, 4, 5487.

(13) Li, Q.R.; Yang, K.G.; Liu, J.X.; Zhang, L.H.; Liang, Z.; Zhang, Y.K.; Li, S. *Microchim Acta* **2016**, 183, 345–352.

(14) Qin, Y.P.; Jia, C.; He, X.W.; Li, W.Y.; Zhang, Y.K. *ACS Appl. Mater. Interfaces* **2018**, 10, 9060–9068.

(15) Qin, Y.P.; Wang, H.Y.; He, X.W.; Li, W.Y.; Zhang, Y.K. *Talanta* **2018**, 185, 620–627.

(16) Xiangzhi, D.; Yong, M.; Chunping, H.; Baoliang, Z.; Hepeng, Z.; Qiuyu, Z. *Polym. Int*. **2019**, 68, 955–963.

(17) Morishita, T.; Yoshida, A.; Hayakawa, N.; Kiguchi, K.; Cheubong, C.; Sunayama, H.; Kitayama, Y.; Takeuchi, T. *Langmuir* **2020**, 36, 10674–10682.

(18) Zeng, Z.; Hoshino, Y.; Rodriguez, A.; Yoo, H.; Shea, K.J *ACS Nano*. **2010**, 4, 199–204.

(19) Cenci, L.; Andreetto, E.; Vestri, A.; Bovi, M.; Barozzi, M.; Iacob, E.; Busato, M.; Castagna, A.; Girelli, D.; Bossi, A.M. *J. Nanobiotechnol*. **2015**, 13, 51–65.

(20) Caceres, C.; Canfarotta, F.; Chianella, I.; Pereira, E.; Moczko, E.; Guerreiro, A.; Piletska, E.; Esen, C.; Whitcombe, M.J.; Piletsky, S. *Analyst* **2016**, 141, 1405–1412.

(21) Li, J.; Kendig, C.E.; Nesterov, E.E. *J. Am. Chem. Soc*. **2007**, 129, 15911–15918.

(22) Inoue, Y.; Kuwahara, A.; Ohmori, K.; Sunayama, H.; Ooya, T.; Takeuchi, T. *Biosens. Bioelectron***. 2013**, 48, 113–119.

(23) Murase, N.; Taniguchi, S.; Takano, E.; Kitayama, Y.; Takeuchi, T. *J. Mater. Chem. B*. **2016**, 4, 1770–1777.

(24) Qian, Y.; Jinhua, L.; Xiaoyan, W.; Hailong, P.; Hua, X.; Lingxin, C. *Biosens. Bioelectron.* **2018**, 112, 54–71.

(25) Luo, L.; Zhang, F.; Chen, C.; Cai, C. *Anal. Chem*. **2019**, 91, 15748–15756.

(26) Sunayama, H.; Ooya, T.; Takeuchi, T. *Biosens. Bioelectron*. **2010**, 26, 458–462.

(27) Sunayama, H.; Ooya, T.; Takeuchi, T. *Chem. Commun*. **2014**, 50, 1347–1349.

(28) Sunayama, H.; Ohta, T.; Kuwahara, A.; Takeuchi, T. *J. Mater. Chem. B.* **2016**, 4, 7138–7145.

(29) Horikawa, R.; Sunayama, H.; Kitayama, Y.; Takano, E.; Takeuchi, T. *Angew. Chem. Int. Ed*. **2016**, 55, 13023–13027.

(30) Takeuchi, T.; Sunayama, H. *Chem. Commun*. **2018**, 54, 6243–6251.

(31) Morishige, T.; Takano, E.; Sunayama, H.; Kitayama, Y.; Takeuchi, T. *ChemNanoMat* **2019**. 5, 224–229.

(32) Mori, K.; Hirase, M.; Morishige, T.; Takano, E.; Sunayama, H.; Kitayama, Y.; Inubushi, S.; Sasaki, R.; Yashiro, M.; Takeuchi, T. *Angew. Chem. Int. Ed*. **2019**, 58, 1612–1615.

(33) Gan, N.; Li, T.; Hu, F.; Li, X.; Wang, L.; Zheng, L. *Biosens. Bioelectron*. **2014**. 54, 199–206.

(34) Takeuchi, T.; Mori, T.; Kuwahara, A.; Ohta, T.; Oshita, A.; Sunayama, H.; Kitayama, Y.; Ooya, T. *Angew. Chem. Int. Ed*. **2014**, 53, 12765–12770.

(35) Guo, T.; Deng, Q.L.; Fang, Z.G.; Liu, C.C.; Huang, X.; Wang, S. *Biosens. Bioelectron*. **2015**, 74, 498–503.

(36) Chen, L.; Wang, X.; Lu, W.; Wu, X.; Li, J. *Chem. Soc. Rev*. **2016**, 45, 2137–2211.

(37) Rijun, G.; Hui, J.; Huijun, G.; Zonghua, W. *Biosens. Bioelectron*. **2018**, 100, 56–70.

(38) Lucia, C.; Chiara, P.; Paolo, B.; Bossia, A.M. *Talanta* **2018**, 178, 772–779.

(39) Cheubong, C.; Yoshida, A.; Mizukawa, Y.; Hayakawa, N.; Takai, M.; Morishita, T.; Kitayama, Y.; Sunayama, H.; Takeuchi, T. *Anal. Chem*. **2020**, 92, 6401–6407.

(40) Takano, E.; Shimura, N.; Ujima, Y.; Sunayama, H.; Kitayama, Y.; Takeuchi, T. *ACS Omega* **2019**, 4, 1487–1493.

(41) Furutani, S.; Naruishi, N.; Hagihara, Y.; Nagai, H. *Anal. Bioanal. Chem*. **2016**, 408, 5641– 5649.

(42) Wang, W.; Zhu, X.; Teng, S.; Xu, X.; Zhou, G.J. *AOAC Int* **2018**, 101, 1868–1872.

(43) Nishijima, M.; Goto, M.; Fujikawa, M.; Yang, C.; Mori, T.; Wada, T.; Inoue, Y. *Chem. Commun*. **2014,** 50, 14082–14085.

(44) Feroz, S.R.; Sumi, R.A.; Malek, S.N.A.; Tayyab, S. *Exp. Anim*. **2015**, 64, 101–108.

Chapter 5

A Sensitive Biotic/abiotic Antibody Sandwich Assay for Highly Sensitive Detection of Pork Contamination for Halal Biomarker Sensing Application

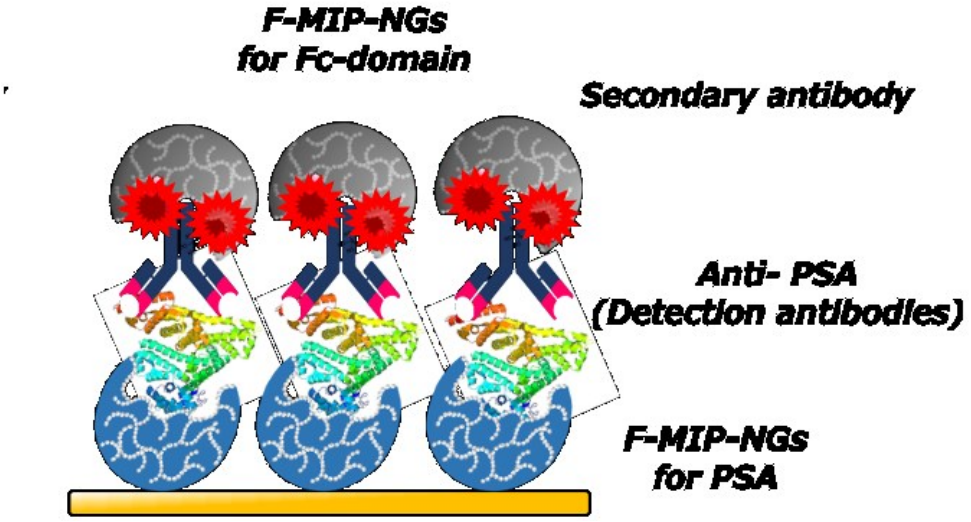

A Sensitive Biotic/abiotic Antibody Sandwich Assay for Highly Sensitive Detection of Pork Contamination for Halal Biomarker Sensing Application

5.1 Introduction

Halal biomarker sensing is increasingly developed for halal meat authentication, due to the fast growing up of global halal food market in the world.[1-2] One of the contaminant compounds commonly found in halal meat products is porcine serum albumin (PSA) from pork meat, instead of beef or any other halal meats for saving a cost.[3] This is a very serious concern of Muslim on meat products in the halal food market. Thus, the fast simple, sensitive, and selective sensing can help the manufactures to ensure that their products free from pork and ready for Muslim to consume. Currently, the immunoassays which are the popular analytical method for the detection of protein biomarker in diagnosis[4-5] and food analysis[6-7], are most common used to detect pork contamination in halal meat products for halal biomarker sensing application as a result of high sensitivity and specificity.[8-12] However, these methods are cost-intensive and time consuming, and the natural antibodies and conjugated enzymes have low stability. Furthermore, to achieve highly sensitive and selective detection of target marker protein, two or more antibodies and labeled antibodies are necessary. These specifications tended to make the above more time consuming and costly.

To overcome these drawbacks, molecularly imprinted polymers (MIPs) prepared using copolymerization of functional monomer, co-monomer, cross-linker by covalent and non-covalent binding in the present of targe molecules, have already been used as artificial antibodies alternative of natural antibodies in various application owing to their easy preparation, high stability, low-cost and cost-production.[13-18] Therefore, MIP-based sensors are considerable as promising alternatives to immunosensors for sensitive and selective detection of the protein targets.[19-23] In the last two year, the first report of using MIPs nanogels (MIP-NGs)-based quartz crystal microbalance (QCM) sensor for detection of PSA in halal meat extracts was published by my group. I prepared MIP-NGs capable of PSA by molecular imprinting with pyrrolidyl acrylate (PyA) used as functional monomer and developed MIP-NGs based-QCM sensor for detection of PSA in real meat extracts. The selectivity of this

sensor was high for PSA compared to other animal serum albumins, nevertheless the sensitivity was much lower than that of immunosensors.[24] Next year after, i have demonstrated a highly sensitive MIP-based fluorescence sensor for fast detection of pork contamination in halal meat extracts in the first time. To achieve high sensitivity for recognition of target protein, the fluorescent MIP-NGs (F-MIP-NGs) targeting PSA were developed via molecular imprinting and post-imprinting modification (PIM), where can create modifiable sites for fluorescence dye introduction in molecularly imprinted nanocavities.[25-26] Since PIM-based functionalization of imprinted cavity was targeted to functional groups on functional monomer residues located within the cavity, undesired introduction of functional groups such as fluorescent dye located outside of the cavity which induced non-specific signal and high background, would be suppressed. The F-MIP-NGs-based fluorescence sensor exhibited excellent sensitivity with limit of detection (LOD) of 2.5 ng/mL and provided a fast detection of pork contamination in meat extracts, but the comparable performance to immunosensor is still a challenge.[27]

Using conjugated secondary antibodies which recognize the specific crystallisable region (Fc domain) of immunoglobulin G (IgG) and capture primary antibodies with their antigen binding domains, is an effective key role to amplify the signal and to increase the sensitivity for detection of target molecules in immunoassays. Nowadays, a several immunosensor formats with different secondary antibody labels such as enzyme immunosensor, radioimmonosensor, chemiluminescent immunosensor and fluorescent immunosensor have been developed because of providing significant increase in sensor signal responses.[28] The production of antibodies labelled with fluorescent dye, radioisotopes, biotin, avidin and enzymes where maintain the intrinsic molecular recognition ability of antibody, are still challenging. In contrast, synthetic polymer-based MIP can be easily labelled using the PIM strategy. From my best knowledge, MIPs was widely used to be alternative antibodies instead of natural antibodies for protein recognition in MIP-based sensor, but have not been reported yet to use MIPs as secondary antibody mimics for sensor signal amplification. Some previous reports of different imprinting techniques indicated that MIPs for whole IgG or Fc domain were most promising as artificial antibodies for application in protein purification and biosensor due to their selective recognition and sensitive detection of target molecules.[29-32] Moreover, imprinting of Fc domain exhibited strong binding for IgG of both human and goat.[33] Their characteristics are close to those of secondary antibodies with a specific recognition for different antibodies owing to their conserved regions. Thus, Fc domain provided a high potential ability as a template molecule for synthesis of MIPs with specific to antibodies.

Recently, my group was successfully synthesized the MIP-NGs targeting Fc-domain by precipitation polymerization as a stealth nanocarriers with specific adsorption of IgG. The Fc-MIP-NGs had a good recognition capability for IgG, resulting that regulating the protein corona formed on the Fc MIP-NGs.[34] This inspired us to explore a novel sensitive MIP-based sensor of close to conventional immunoassay using fluorescent Fc-MIP-NGs as conjugated secondary antibody mimics with increased signal responses of pork contamination detection.

Herein, i present a novel biotic/abiotic antibody sandwich assay based on fluorescent Fc-MIP-NGs capable of Fc domain as a fluorescent secondary antibody mimic for fast detection of pork contamination in halal meat extracts. First, the fluorescent Fc F-MIP-NGs were prepared via molecular imprinting and PIM, where the 4-(2-Methacrylamidoethyl aminomethyl) phenylboronic acid (FMB)[35] was used as a functional monomer with a modifiable site for PIMs and ATTO 647N NHS was introduced as fluorescent reporter dye into the Fc domain-imprinted cavity (Figure 5.1). Second, the fluorescent signaling ability of prepared fluorescent Fc-MIP-NGs was investigated using Fc domain, deglycosylated Fc domain, whole IgG and albumin. Finally, biotic/abiotic antibody sandwich assay was demonstrated where previously reported PSA-imprinted polymer nanogels were used for capturing target PSA[27], anti-PSA antibody was used as a primary antibody and fluorescent Fc-MIP-NGs were used as a secondary antibody. Then, the sensitivity, selectivity, accuracy, stability, and recovery, as well as the feasibility of the proposed sandwich assay in detecting of pork contamination for halal meat sensing applications were evaluated. (Scheme 1).

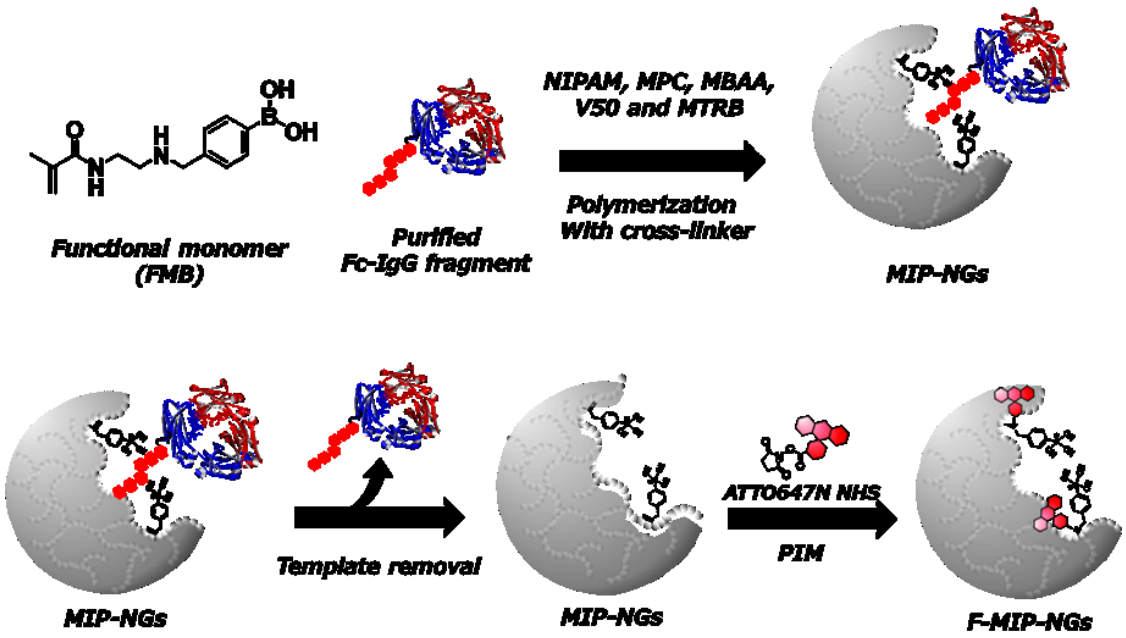

Figure 5.1 Schematic illustration of the preparation of flurescent Fc-MIP-NGs via emulsifier-free precipitation polymerization and PIM

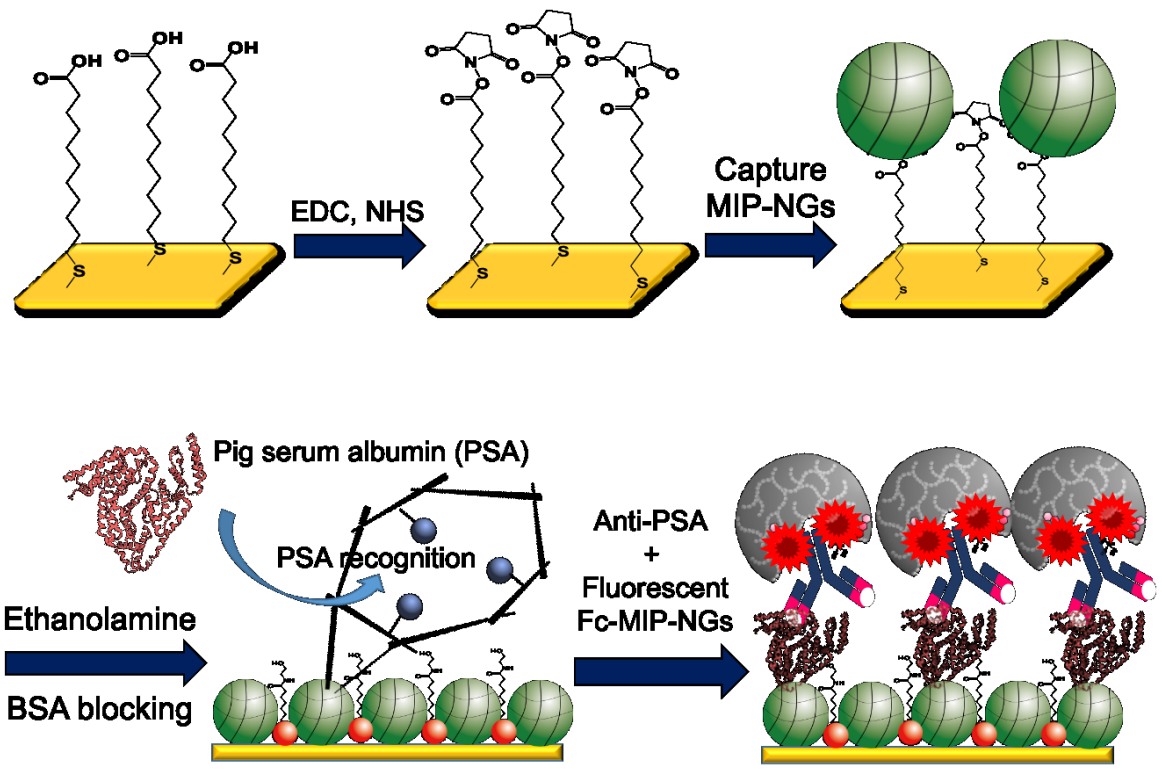

Scheme 5.1 Schematic representation of demonstration of biotic/abiotic antibody sandwich assay for detection of pork contamination in halal meat extracts.

5.2 Experimental Section

5.2.1. Reagents and materials

Human immunoglobulin G (IgG), human serum albumin (HSA), porcine serum albumin (PSA), bovine serum albumin (BSA), goat serum albumin (GSA), cheep serum albumin (CSA), rabbit serum albumin (RSA), Lysozyme (Lyz), Papain, 11-mercaptoundecanoic acid (MUA), N-hydroxysuccinimide (NHS), ethanolamine, sodium dodecyl sulphate (SDS), DEAE–Sephadex A- 50, and HitrapTM Protein A HP were purchased from Sigma-Aldrich (MO, USA). L-Cysteine, ethylenediamine tetra-acetate (EDTA), N-Isopropyl acryl- amide (NIPAm) and N,N′-methylenebisacrylamide (MBAA) were purchased from Nacalai Tesque Co. (Kyoto, Japan). Sephadex G-100 was purchased from GE Healthcare (Tokyo, Japan). Ethanol (EtOH), Dimethyl sulfoxide (DMSO) and 2,2′-azobis (2-methylpropionamidine) dihydrochloride (V-50) were purchased from Wako Pure Chemical

Industries, Ltd. (Osaka, Japan). 2-Methacryloyloxyethylphosphorylcho- line (MPC) was purchased from NOF Corporation (Tokyo, Japan). 1- (3-Dimethylaminopropyl)-3-ethylcarbodiimide hydrochloride (EDC) was purchased from Tokyo Chemical Industries (Tokyo, Japan). The Protein–Free (PBS) blocking buffer and Methacryloxyethyl Thiocarbamoyl Rhodamine B (MTRB) were purchased from Thermo Fisher Scientific (MA, USA). ATTO 647N NHS-ester was purchased from ATTO-TEC GmbH (Siegen, Germany). Bio-safe Coomassie G-250 was purchBio-Rad Laboratories, Inc. (Japan). PNGase F PRIME TM glycosidase was purchased from Funakoshi Co., Ltd. (Japan). The Pig Albumin ELISA Kit (E101-110) and polyclonal antibody of pig serum albumin (Anti-PSA) was purchased from Bethyl Laboratories, Inc. (Montgomery, USA). The HiTrap™ Protein A HP column, 1 ml from GE Healthcare, GmbH, Germany). MIP-NGs capable of PSA were prepared using a previously reported procedure (Cheubong et al., 2020).[24] FMB as a functional monomer were synthesized using a previously reported procedure (Saeki et al., 2020).[35]

5.2.2. Instrumentation

The particle size distribution and the zeta potential were measured using a Dynamic Light Scattering (DLS) system Zetasizer Nano ZS (Malvern Instruments Ltd., Malvern, U.K.). The protein concentration was measured using NanoDrop™ One UV-Vis Spectrophotometer (Thermo Fisher Scientific, Inc., USA). The fluorescence spectra were obtained using an F-2500 fluorescence spectrophotometer (Hitachi High-Technologies, Tokyo, Japan). The fluorescence intensities were carried out by custom-made liquid handling robot equipped with a fluorescence microscope (System Instruments Co. Ltd., Tokyo, Japan). SDS-PAGE was performed using AE-6500 (ATTO, Tokyo, Japan) as electrophoresis tank with PowerPac Basic Power Suply (Bio-Rad, California, USA) with e-PAGEL (ATTO, Tokyo, Japan) as polyacrylamide gel. The absorbance at 450 nm of ELISA assay were measured using a Perkin Elmer Wallac Envision 2100 Multilabel Microplate Reader (PerkinElmer, Inc., Waltham, MA, USA)

5.2.3 Preparation of Template Fc Domain and Deglycosylated Fc Domain.

Papain digestion of antibodies was carried out with a partially modified method to the previous reports.[36] Human IgG molecules were digested with papain to obtain Fc domain at 37 ºC for 24 h. After digestion, the mixture solution was filtered using Amicon ultra centrifugal filters with a 10 kDa cut-off (7500 g x 3, at 25 °C for 20 min) for desalting and buffer exchanging to 20 mM phosphate buffer pH 7.0 as a binding buffer for purification process. The IgG fragments were first purified by ultrafiltration with 100 kDa cut-off (7500 g x 3, at 25 °C

for 20 min) to separate Fc domain (~50 kDa) from whole IgG (~150 kDa). The collected solution was next purified through HiTrapTM Protein A HP 1 mL, and was analyzed by the sodium dodecyl sulphate–polyacrylamide gel electrophoresis (SDS-PAGE) to evaluate the size of purified Fc domain. The purified Fc domain were freeze-dried for further use.

Regarding degylcosylated Fc domain preparation, the obtain Fc domain was incubated with 20 µL of 2 mg/mL of PNGase F PRIME TM glycosidase to produce deglycosylated Fc domain at 37 °C for 30 min. Then the solution mixture was purified and anaylzed by same condition as above.

5.2.4 Preparation of Fluorescent Fc-MIP-NGs and NIP-NGs.

FMB was synthesized as reported previously.[35] Briefly, Fc domain (2.5 mg, 50 nmol) as a template molecule, FMB (15.7 mg, 0.06 mmol) as a functional monomer, MTRB (0.42 mg, 0.63 µmol) as a fluorescence monomer, MPC (3.7 mg, 0.012 mmol) and NIPAm (102 mg, 0.9 mmol) as a comonomer, MBAA (7.71 mg, 0.05 mmol) as a cross-linker, and V-50 (54.2 mg, 0.2 mmol) as an initiator were dissolved together in 10 mM carbonate buffer containing of 2% dimethyl sulfoxide (pH 9.2, 25 mL). Then, the nanogel was synthesized by emulsifier free precipitation polymerization at 50 °C for 12 h. After polymerization, the solvent of the obtained nanogels was exchanged with 10 mM phosphate buffer saline, PBS (140 mM of NaCl, pH 7.4) using ultrafiltration with 10 kDa cut off (7500×g, 20 min 3 times), and the collected nanogels were incubated with SDS aqueous solution (40 mg/mL, 1 mL) for 5 min at 25 °C. The template removal process was performed via two-step purification with size exclusion chromatography followed by anion exchange chromatography as reported previously. Finally, further purification to remove SDS was carried out using PD-10 column (desalt column), the collected fractions (2.5 mL) was applied to the PD-10 column and eluted by 10 mM PBS) (3.5 mL). In order to collect the NG fractions fluorescent measurements were measured for Fc-MIP-NGs at 575 nm (λ_{ex}: 548 nm of MTRB as a fluorescence monomer). Non-imprinted polymer nanogels (NIP-NGs) were prepared and purified using a similar procedure as MIP-NGs without template. The particle size distribution of obtained MIP-NGs and NIP-NGs both before and after purification was obtained by DLS.

Fluorescent Fc-MIP-NGs were prepared using in-cavity PIM method with ATTO 647N NHS-ester as a fluorescence reporter. The obtained MIP-NGs (500 µg/mL, 1000 µL) were incubated with 5 µL of 10 mg/mL ATTO 647N NHS-ester in DMSO at 25 °C for 2 h. The unreacted fluorescent dye was then removed by Amicon ultra centrifugal filters with a 10 kDa cut-off (7500 g x 3, at 25 °C for 20 min) and washed by PBS. To confirm the successful of

fluorescent dye conjugation in cavity of MIP-NGs, the fluorescence intensity of ATTO 647N both before and after post-imprinting modification were measured by fluorescence spectroscopy (λex: 646 nm and λem: 664 nm). Fluorescent NIP-NGs were prepared using a similar in-cavity PIM method as MIP-NGs.

5.2.5 Fluorescence Measurements of Fc Domain.

The gold-coated sensor chip (4.3 × 9.8 mm) coated with Au (165 nm thickness), and Ti (5 nm thickness) was washed by pure water and ethanol. The sensor chip was then dried with N_2 and cleaned by UV-O_3 treatment for 20 min. The sensor chip was incubated in ethanol solution containing of 11-mercaptoundecanoic acid (MUA) (1.0 mM) for 24 h at 25 °C to make a self-assembled monolayer (SAM) on the surface. After washing the gold-coated sensor chip with ethanol and pure water, 100 µL of an aqueous solution containing 0.05 M N-hydroxysuccinimide (NHS) and 0.2 M 1- (3-(dimethylamino) propyl)-3-ethylcarbodiimide· HCl (EDC) was dropped onto the gold-coated sensor chip and incubated for 120 min. After rinsing with water, 100 µL of PBS containing fluorescent Fc-MIP-NGs or fluorescent NIP-NGs (100 µg/mL) were dropped onto modified gold-coated sensor chips for 60 min. After immobilization, the blocking process was performed by dropping of 1 M ethanolamine aqueous solution (pH 8.5, 100 µL) for 30 min, followed by dropping of Protein–Free (PBS) blocking buffer solution for 30 min (100 µL).

The fluorescence measurements for binding and selectivity of NGs for Fc domain were performed using a custom-made liquid handling robot equipped with fluorescence microscope (Figure 5.2).[27] The sensor chip on which fluorescent Fc-MIP-NGs or fluorescent NIP-NGs were immobilized was inserted into a designed flat-type pipette tip, and the binding experiments were then investigated via the following procedures. Firstly, the flat-type pipette tips were settled on the tip rack, which were captured with a robot arm. Next, a PBS containing of Fc domain (0, 10, 50, 100, 200, 400, 800 and 1,600 nM) were introduced into the flat-type pipette tip (150 µL). followed by incubation for 2 min at 25 °C. Finally, after discharging the solution, the PBS (150 µL) was introduced, and the robot arm was moved into the detection port to capture the image and to measure the fluorescence intensity by Zyla 5.5 sCMOS camera (Andor Technology Ltd, Belfast, UK) equipped with a fluorescence turret (BX3-URA, Olympus, Tokyo, Japan) in each sample. The experiments were performed in triplicate, and sixth different regions of interests (ROIs) were collected in each chip. objective lens, 5 × (LMPLFLN5X, Olympus, Tokyo, Japan); exposure time, 0.1 sec; light source, mercury lamp (HGLGPS-SET, Olympus, Tokyo, Japan); Bandpass filters (Cy5TM), 604–644 nm for

excitation and 672–712 nm for emission.

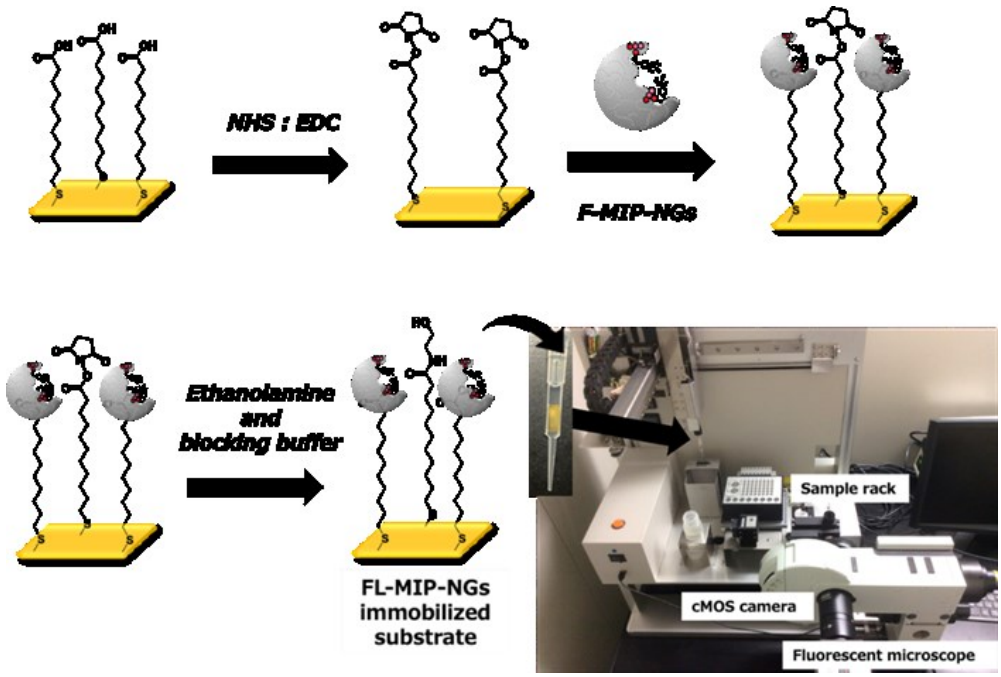

Figure 5.2 Schematic overview of the preparation of MIP-NGs sensing chip for Fc domain.

The fluorescence intensity change values of immobilized NGs (F_0) on the gold-coated sensor chips and protein binding (F) towards the immobilized NGs sensor chips were investigated using fluorescence microscope, and measured from differences in fluorescence intensity before and after immobilization of NGs ($F_0 = F_{\text{immobilized NGs}} - F_{\text{only substrate}}$) and differences in fluorescence intensity before and after incubation of Fc domain into the gold-coated sensor chip ($F = F_{\text{incubated PSA}} - F_{\text{only substrate}}$), respectively. The relative fluorescence intensity of binding experiments was then calculated from this equation $(F - F_0)/F_0$, where F_0 and F are the fluorescence intensity change values of the immobilized NGs and protein binding, respectively. To evaluate the selectivity of fluorescent Fc-MIP-NGs and fluorescent NIP-NGs for Fc domain, 100 nM of the reference proteins including whole IgG, deglycosylated Fc domain and PSA dissolved in PBS were used as competitive proteins.

5.2.6 Preparation of Immobilized Capture MIP-NGs on the Gold-coated Sensor Chip.

The surface modification of SAM on the gold coated sensor chip was prepared in the same manner as described above. After the reaction, an aqueous solution containing 0.2 M EDC and 0.05 M NHS was dropped and incubated for 120 min. Next, 100 μg/mL of the MIP-NGs capable of PSA prepared by emulsifier-free precipitation polymerization method with PyA as a functional monomer according to my reported previously,[24] was immobilized on the gold coated sensor chip for 60 min as a capture NGs for PSA. After washing with pure water, the blocking process was performed by dropping of 1 M ethanolamine aqueous solution (pH 8.5, 100 μL) for 30 min, followed by dropping of various blocking reagents (PBS, Protein free PBS-blocking buffer, 0.1% and 0.5% (w/v) BSA and 0.5% (w/v) skimmed milk) for 60 min (100 μL). Finally, the gold coated sensor chip with immobilized capture MIP-NGs were washed with pure water and ready to evaluate the optimization of assay conditions.

5.2.7 Fluorescence Detection of the Developed sandwich assay for PSA.

The fluorescence detection experiments for binding and selectivity of biotic/abiotic antibody sandwich assay for PSA were investigated using a custom-made liquid handling robot equipped with fluorescence microscope. The biotic/abiotic antibody sandwich assay was prepared by the following procedures. (1) The immobilization of the capture MIP-NGs for PSA and blocking process of selected blocking reagent were performed the manner as described above. (2) During the blocking process, the cocktail solution was prepared by mixing equal volume of PBS containing of Ant-PSA (0.01, 0.1, 1, 5 and 10 μg/mL) with various concentrations of fluorescent MIP-NGs (1, 10, 50, 100 and 200 μg/mL) followed by incubation for 30 min. The reaction was then added by various final concentration of PSA (0-100 nM and 1 nM PSA for optimization condition), followed by incubation for 30 min. (3) After washing of sensor chip with pure water, the premixed cocktail solution was dropped on the gold coated sensor chip with immobilized capture MIP-NGs, and was incubated for (1, 5, 10, 20, 30 and 60 min). (4) After washing with pure water (3 x 500 μL), and PBS (3 x 500 μL), the sensor chip was inserted into a designed flat-type pipette tip, followed by introducing of 150 μL PBS, and the robot arm was moved into the detection port to capture the image and to measure the fluorescence intensity under the condition of SIC as described above. Then, the relative fluorescence intensity of binding experiments was calculated by this equation (F – F0)/F0, where F0 and F are the fluorescence intensity of before and after incubation, respectively. To investigate the selectivity of the developed sensor for PSA, 10 nM of the reference proteins

including BSA, GSA, SSA and RSA dissolved in PBS were added to the cocktail solution as competitive proteins.

5.2.8 Stability of Capture MIP-NGs Immobilized on the Sensor Chip.

To evaluate the stability of the developed sensor, the sensor chips with immobilized capture MIP-NGs for PSA were prepared as described above and the sensor chips were then kept at 4°C until use. The individual fluorescent detections of 1 nM PSA for the kept sensor chips in the day of 1, 3,7,15 and 30 days were measured under the optimization conditions. The quantity of stability was evaluated using the relative fluorescent intensity compared to the first day preparation.

5.2.9 Preparation of Meat Extract Samples.

The meat extract samples were prepared from three different raw meat samples (beef and Lamb as a halal meat, and pork as non-halal meat purchased from a Japanese local supermarket). The raw meat samples were chopped separately. A portion of 1 g was weighted and mixed with 5 mL of the extraction buffer (PBS), then homogenized using a benchtop homogenizer, Polytron PT 1600 E (Kinematica AG, Luzern, Switzerland) for 2 min (10,000 rpm), followed by centrifugation for 30 min at 4 °C (3 X 16,000 g). The clear supernatant was collected and filtered through a 0.2 µm PTFE filter (DISMIC-13HP, Toyo Roshi Kaisha Ltd., Tokyo, Japan) three times. The filtered solutions of meat extract samples were then measured the total protein concentration at the absorbance of a protein solution at 280 nm (A280) using NanoDrop One UV/Vis Spectrophotometers. The meat extract samples were then kept at -20 °C until use.

5.2.10 Recovery Study of the Developed Sensor.

To investigate the recovery of the developed sensor in real meat extract samples, the appropriate dilution factor of beef extracts (1, 10, 100 and 500 folds) for the PSA binding experiments, were spiked with 1 nM of PSA dissolved in PBS. Under the proper dilution factor of real meat extracts, the binding experiment of the spiked sample was performed for PSA concentrations range of 0-100 nM using the optimized condition as described above, then the recovery rates were calculated from the following equation,

$$\text{Recovery rates}(\%) = \frac{(\text{Relative fluorescence intensity})_{spikedsample}}{(\text{Relative fluorescence intensity})_{buffer}} \text{ x } 100$$

where (Relative fluorescence intensity)$_{\text{spiked sample}}$ and (Relative fluorescence intensity)$_{\text{buffer}}$ values were obtained from the PSA binding experiments in spiked sample and in buffer solution, respectively.

5.2.11 Pork Contamination Detection in Halal Meat Extract Samples.

To evaluate the feasibility for detection of pork contamination in halal meat extract samples (beef and lamb meat extract samples) using the biotic/abiotic antibody sandwich assay based on fluorescent Fc-MIP-Nga as artificial fluorescent secondary antibody, the contaminated halal meat extract samples with pork were prepared by mixing pork extract and halal meat extracts for five concentration ranges of 0.001, 0.01, 0.1, 1 and 10 wt%. Then the contaminated halal meat extract samples (0.001, 0.01, 0.1, 1 and 10 wt%) and 100 wt% halal beef and lamb extracts as a negative control, and 100 wt% pork extract as a positive control were added to the cocktail solution of anti-PSA and fluorescent Fc-MIP-NGs, followed by dropping on the capture MIP-NGs immobilized gold-coated sensor chip under the optimization condition as described above. The fluorescence intensities were then measured and the relative fluorescence intensity was calculated using the conditions as described above.

5.2.12 ELISA for Detection of Pork Contamination in Halal Meat Extract Samples.

The Pig Albumin ELISA Kit (E101-110: Bethyl Laboratories) was based on a sandwich ELISA assay and colorimetric method detection with 3.30 h analysis time. The contaminated halal meat extract samples for detecting pork contamination via the ELISA kit were prepared the same manner as described above. After stop the reaction, the absorbance at 450 nm of yellow products was measured using microplate reader.

5.3 Results and Discussions

5.3.1 Preparation of fluorescent Fc-MIP-NGs.

To prepare the Fc domain as a template molecule for synthesis of fluorescent MIP-NGs, the Human IgG (Mw ~ 150 kDa, pI 6.6-7.2) was incubated at 37 °C for 24 h with PBS containing of papain to cleavage of a hinge region and reducing agent (cysteine) to increase the enzyme activity (Figure 5.3a).[36] The mixtures solution was then filtered using ultrafiltration of 100 kDa to separate the Fc domain (Mw ~ 50 kDa) from the whole IgG. The filtered of the obtained Fc and Fab domain was then purified using HiTrap^{TM} Protein A HP 1 mL column which is a high affinity for the Fc-region of IgG, followed by collecting of fractions after injection of elution buffer. As seen in Figure 5.4, only the fraction no.15 exhibited the absorbance of protein at 280 nm, confirming that the purification method was a high affinity to Fc domain and easy elution at low pH of citrate buffer pH 3.5. To obtaine the deglycosylated Fc domain, the purified Fc domain was incubated with PNGase F PRIME ^{TM} glycosidase at 37 °C for 30 min to cleavage the sugar chain on the Fc domain (Figure 5.3b).[37] The purified Fc domain and deglycosylated Fc domain were confirmed by SDS-PAGE. The sample buffer was prepared as follows; Tris (hydroxymethyl) aminomethane 3 g, Glycine 14.4 g, and SDS 1 g were dissolved in 1 L of pure water. The elution buffer was prepared as follows; Bromophenol blue (BPB) 1 mg, SDS 400 mg, and Glycerol 2 mL were dissolved in 0.5 M Tris-HCl buffer (pH 6.8) (2.5 mL), and the solution was then diluted by 5.5 mL of pure water. To evaluate the protein size using SDS-PAGE, the 50 µL of sample solution (100 µg/mL) and 50 µL sample buffer were mixed together and incubated at 85 °C for 5 min. After incubation, the mixed sample was injected to 12.5% cross-linked polyacrylamide gel for SDS-PAGE. Then the SDS-PAGE was carried out by 20 mA for 70 min followed by washing with pure water triplicate on shaker and staining using the bio-safe Coomassie G-250 stain solution for 1 h at room temperature with slowly shaking. On the SDS-PAGE (Figure 5.5) digested human IgG samples (lane 4-5) were composed by three polypeptide derived from whole human IgG as M_r ~ 150 kDa, Fc or Fb fragments as M_r ~ 50 kDa, and small polypeptide fragment as M_r ~ 25 kDa, respectively. After first purification through protein A column, the purified samples (lane 6-7) were composed by two polypeptide chains. The larger polypeptide chain was expected as Fc-IgG fragment with M_r ~50 kDa but the smaller polypeptide chain remained occurring on gel resulting from impurity of sample. Therefore, the second purification was performed to get high purity of Fc domain. As seen in lane 8 and 9, only polypeptide chain as Fc-domain (~50

kDa) was observed, confirming the high purity of Fc domainn to be obtained with second purification using HiTrap^{TM} Protein A HP column. The shift in the mobility of the band (lane 10-11) confirmed the successful deglycosylation of Fc domain to be a deglycosylated Fc-domain, allowing them to use in further experiments.

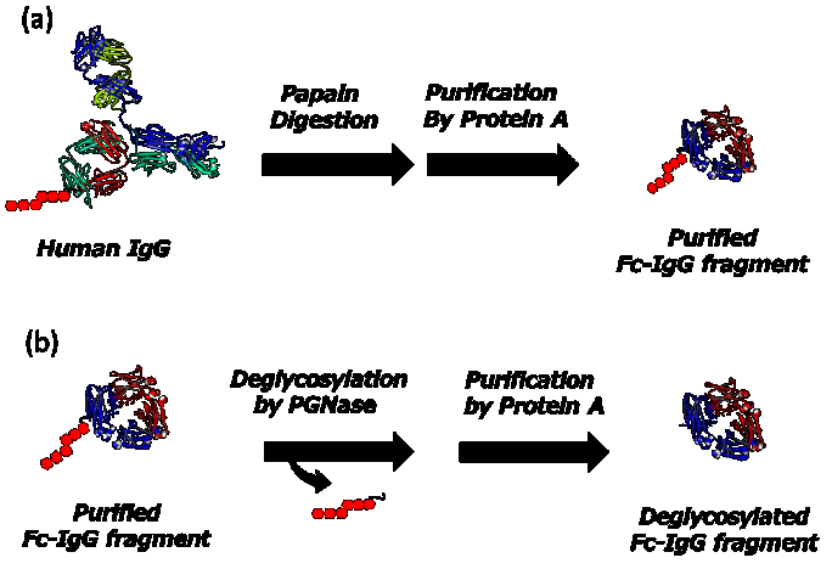

Figure 5.3 Schematic representation of (a) preparation of Fc domain using papain digestion and purification through HitrapTM Protein A HP 1 mL, and (b) preparation of deglygosylated Fc domain using PGNase.

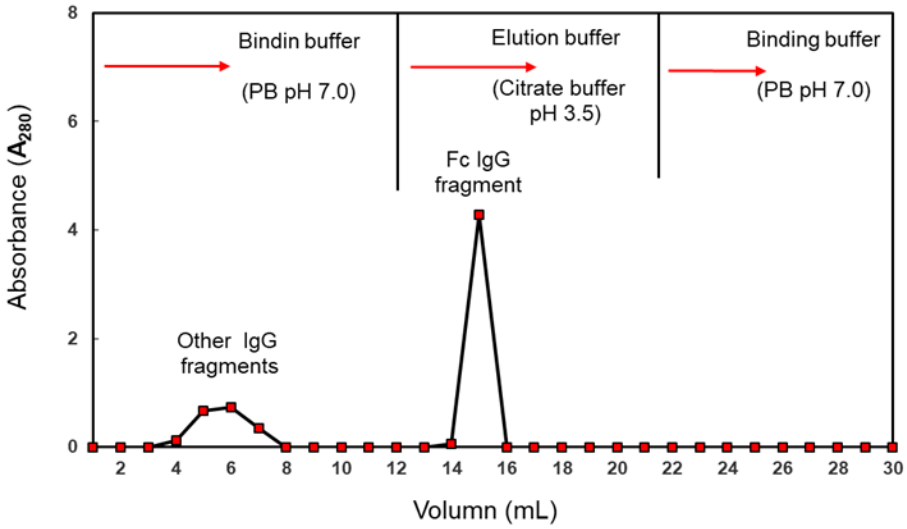

Figure 5.4 A typical chromatogram of purification of Fc domain with syringe operation. Absorbance at 280 nm was measured by Nanodrop. under the condition as follows; syringe operation, elution buffer as 0.1 M sodium citrate, pH 3.5, approximate flowrate as 1 mL/min.

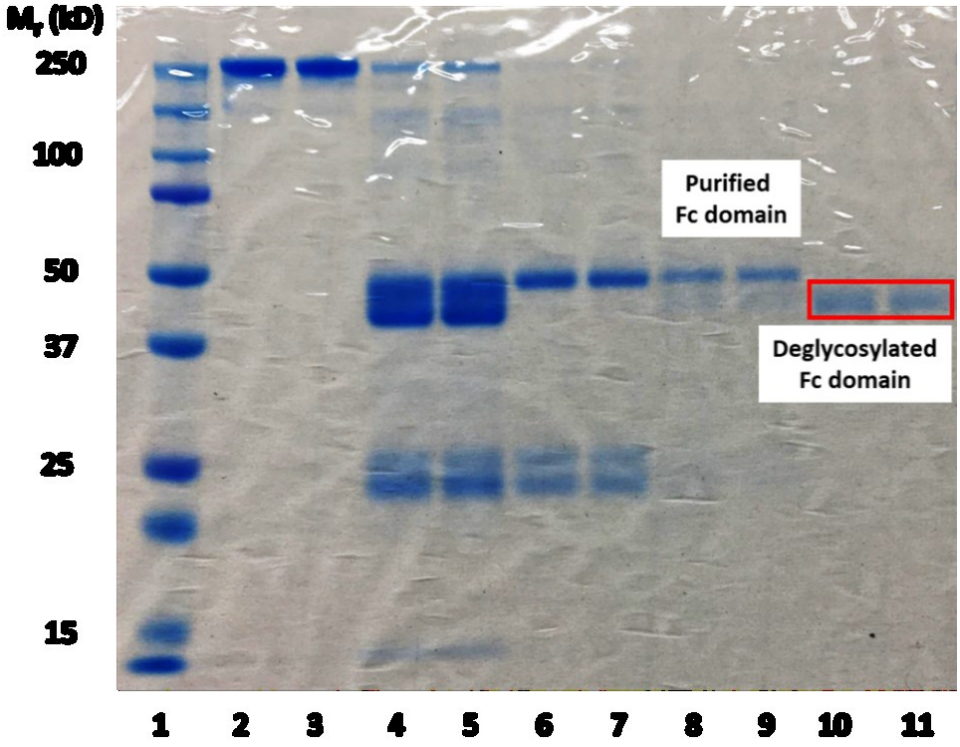

Figure 5.5 SDS-PAGE analysis of purified Fc domain. Lane 1: Protein marker (Bio-Rad), Lane 2-3: IgG, Lane 4-5: Digested IgG, Lane 6-7: 1st purified Fc domain, Lane 8-9: 2rd purified Fc domain and Lane 10-11: purified deglyocosylated Fc domain.

The synthesis of fluorescent Fc-MIP-NGs as an artificial secondary antibody capable of Fc domain for biotic/abiotic antibody sandwich assay application was developed. FMB was used as the functional monomer, which can bind to Fc domain glycan via covalently boronate ester and can bind to template molecules via non-covalently interacted with via electrostatic and hydrophobic interactions. Under the polymerization condition, the CD spectra of template molecule maintained its original secondary structure, as the result of the Fc domain template was not denatured during polymerization (Figure 5.6). After polymerization, the obtained NGs were purified by two steps purification method using size exclusion chromatography to separate MIP-NGs and unreacted monomers by their size and ion-exchange chromatography to remove template molecule from obtained NGs as reported previously (Figure 5.7).[27] The removal rate of Fc domain was more than 80%, where was comparable to that of my two previously reported, [24,27] confirming the potential ability of NGs for rebinding with target molecule (Figure 5.8). The particle size and zeta potential of NGs before and after purification were investigated using DLS. As seen in Figure 5.9, the obtained NGs provided a good

monodispersity, and no coagulation was observed under the polymerization conditions, according to my previous studies on the characterization of NGs by a transmission electron microscope (TEM) showed that the morphology of the NGs prepared via emulsifier-free precipitation polymerization with the different functional monomer provided the same spherical morphologies.[24] Moreover, the morphologies of the fluorescent NGs after PIM by introducing of fluorescent dye remained intact in both size and shape.[27] The particle size of the Fc-MIP-NGs and Fc-NIP-NGs were estimated to be 21 nm and 18 nm, respectively. These results concluded that Fc-MIP-NGs and Fc-NIP-NGs were successfully synthesized using emulsifier-free precipitation polymerization method and perfectly purified using two-step purification with size-exclusion and ion exchange chromatography.

For post-imprinting modification, the Fc-MIP-NGs and NIP-NGs were incubated with ATTO 647N as the fluorescent reporter molecule for conjugation by the secondary amino group within the imprinted nanocavity of NGs. The fluorescence intensity of ATTO 647N in the fluorescent Fc-MIP-NGs, NIP-NGs and untreated NGs was then investigated at an excitation wavelength of 647 nm and, observed a maximum peak as a wavelength of 668 nm. The fluorescence spectrum of ATTO 647N were founded only in the florescent Fc-MIP-NGs and fluorescent NIP-NGs (Figure 5.10), suggesting that the conjugation of fluorescent reporter into the secondary amino group of NGs via in-cavity PIM was successfully demonstrated.

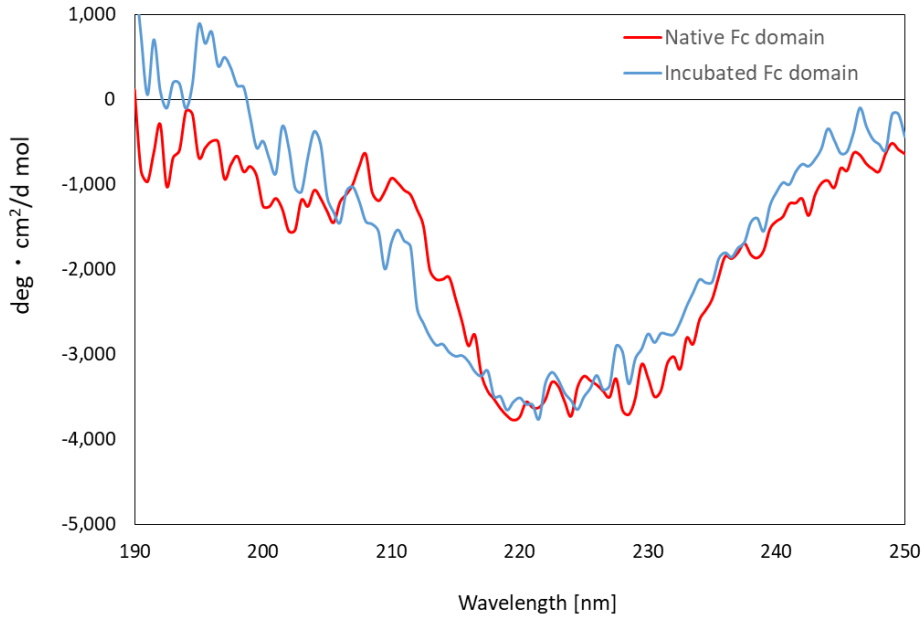

Figure 5.6 CD spectra of Fc domain (100 nM in 10 mM phosphate buffer, pH 7.4) native (red line) and after incubation (blue line) at 50°C for 12 h.

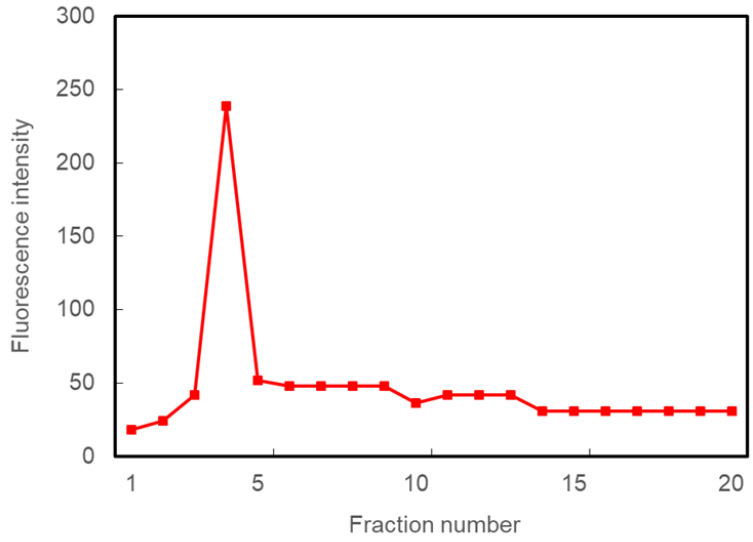

Figure 5.7 A typical chromatogram of MIP-NGs with the fluorescence intensities of MTRB in MIP-NGs (λ_{ex}: 548 nm at λ_{em}: 570 nm) after two steps purification by size exclusion (Sephadex-G100) and ion-exchange chromatography (DEAE-sephadex).

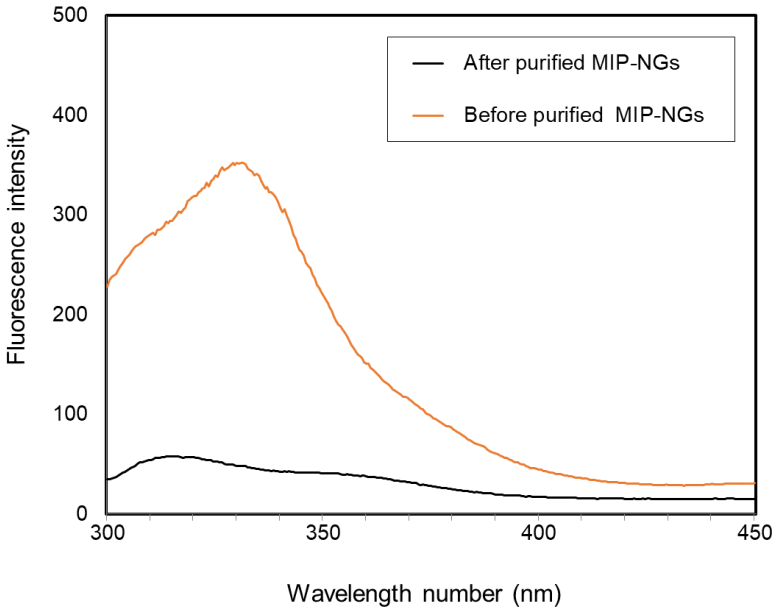

Figure 5.8 Fluorescence spectra at λ_{ex}: 280 nm of tryptophan residues in MIP-NGs for Fc domain before and after purification by two-steps purification. Fluorescence intensities of tryptophan residues of Fc domain at λ_{em}: 350 nm before and after purification were 218 and 41, respectively. The concentration of obtained MIP-NGs before and after purification was 500 µg/mL.

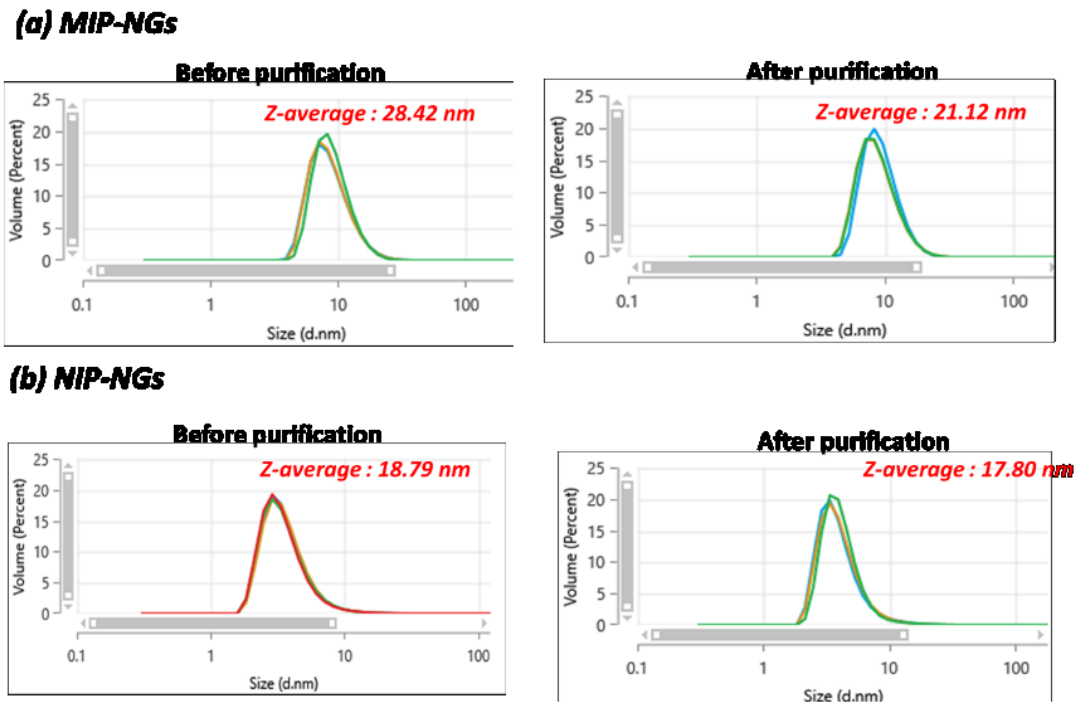

Figure 5.9 Particle size distributions of MIP-NGs and NIP-NGs after purification by size exclusion chromatography and ion-exchange chromatography determined by DLS. (a): MIP-NGs after purification; Z-average particle size: 21 nm (b): NIP-NGs after purification; Z-average particle size: 18 nm.

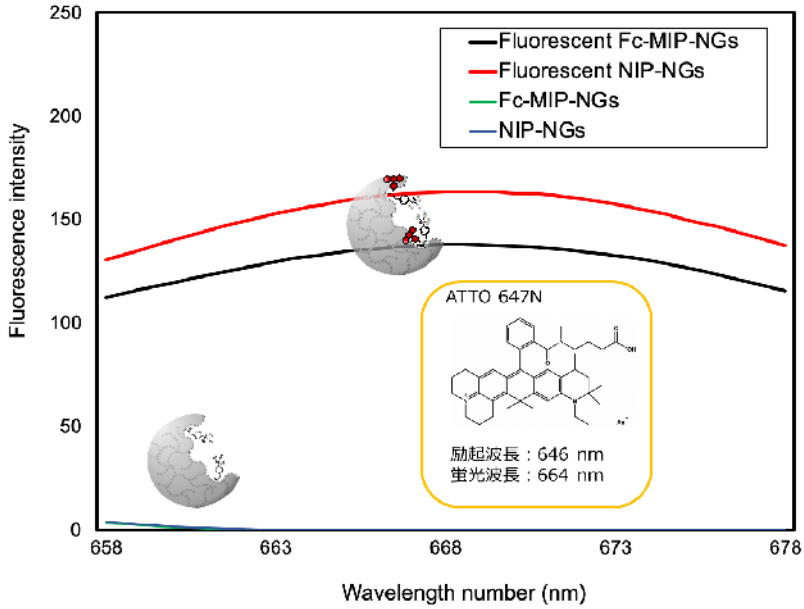

Figure 5.10 Fluorescence intensity of the ATTO 647N NHS-ester in MIP-NGs and NIP-NGs after PIM treatment (λex: 647 nm and λem: 668 nm).

5.3.2 Binding Affinity and Selectivity of Fluorescent Fc-MIP-NGs-based.

The binding affinity and selectivity of fluorescent Fc-MIP-NGs were investigated using a custom-made liquid handling robot equipped with fluorescence microscope on the gold-coated sensor chip with immobilized fluorescent Fc-MIP-NGs. As seen in Figure 5.11, the fluorescence intensity derived from the introduced ATTO 647N in nanocavities of F-MIP-NGs increased after immobilization, indicating that the fluorescent Fc-MIP-NGs were successfully immobilized onto the gold-coated sensor chip. After incubation with different concentrations of Fc domain, the relative fluorescence intensity of the sensor chip increased with concentration of Fc domain. In contrast, NIP-NGs for Fc domain provided lower signal responses than that of fluorescent Fc-MIP-NGs in every concentration (Figure 5.12). The apparent binding affinities (K_a values) of fluorescent Fc-MIP-NGs toward Fc domain were demonstrated from the binding isotherms. The relative fluorescence intensities of Fc domain for fluorescent Fc-MIP-NGs showed a higher binding affinity ($K_a = 6.20 \times 10^7\ M^{-1}$) than F-NIP-NGs ($K_a = 6.15 \times 10^6\ M^{-1}$) for Fc domain (Figure 5.13). These results indicated that the nano-cavity capable of Fc domain binding and transducing the binding event into fluorescent changes was successfully created in the polymer nano-gels by molecular imprinting and PIMs

The relative fluorescence intensities of fluorescent NGs towards Fc domain and competitive proteins, including deglycosylated Fc domain, whole IgG and PSA at 100 nM were investigated to evaluate the selectivity. The selectivity factors of fluorescent Fc-MIP-NGs towards these competitive proteins; deglycosylated Fc domain, whole IgG and PSA were estimated to be 0.49, 0.67 and 0.25 respectively. The selectivity factors of the competitive proteins were lower than that of Fc domain, indicating that fluorescent Fc-MIP-NGs provided high selectivity for Fc domain (Figure 5.15a). The signal responses of deglycosylated Fc doamin, where the glycan was depleted from polypeptide chain, and whole IgG for fluorescent Fc-MIP-NGs were higher than that of PSA, suggested that the MIP-NGs can bind Fc domain of IgG selectively. The apparent K_a values of fluorescent Fc-MIP-NGs towards deglycosylated Fc domain and whole IgG were estimated to be $3.02 \times 10^7\ M^{-1}$ and $5.06 \times 10^7\ M^{-1}$ (Figure 5.14), respectively. The K_a value toward deglycosylated Fc domain was half of that of glycosylated Fc domain indicating that interaction between FMB residues and sugar chain on Fc domain is important for specific recognition. Furthermore, these Ka values were higher than that of NIP-NGs, indicating that functional monomer, FMB can interact with not only sugar chain moiety but also polypeptide moiety on Fc domain. In contrast, Fc domain selectivity was not observed in fluorescent NIP-NGs, where the selectivity factors of deglycosylated Fc

domain, whole IgG and PSA at 100 nM were estimated to be 0.76, 2.37 and 1.51, respectively (Figure 5.15b).

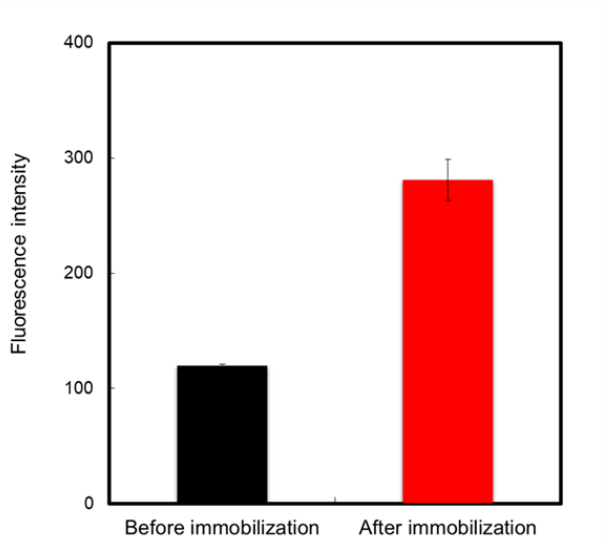

Figure 5.11 Fluorescence intensity of the gold-coated glass substrate before (red) and after (blue) the immobilization of F-MIP-NGs.

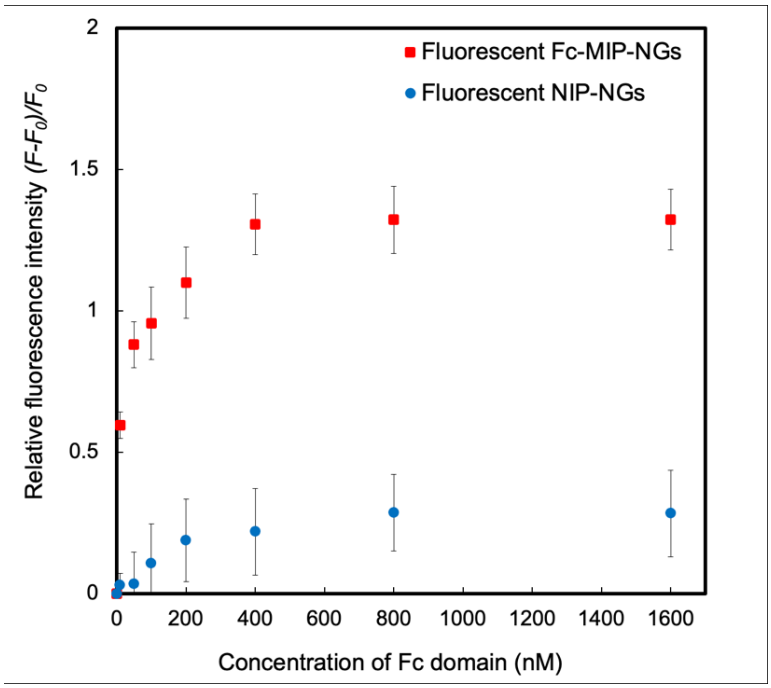

Figure 5.12 The binding isotherms of fluorescent Fc-MIP-MGs and fluorescent NIP-NGs for Fc domain. The various concentrations of Fc domain (0–1,600 nM) was incubated on NGs-immobilized gold-coated sensors. The error bars were obtained from triplicate experiments.

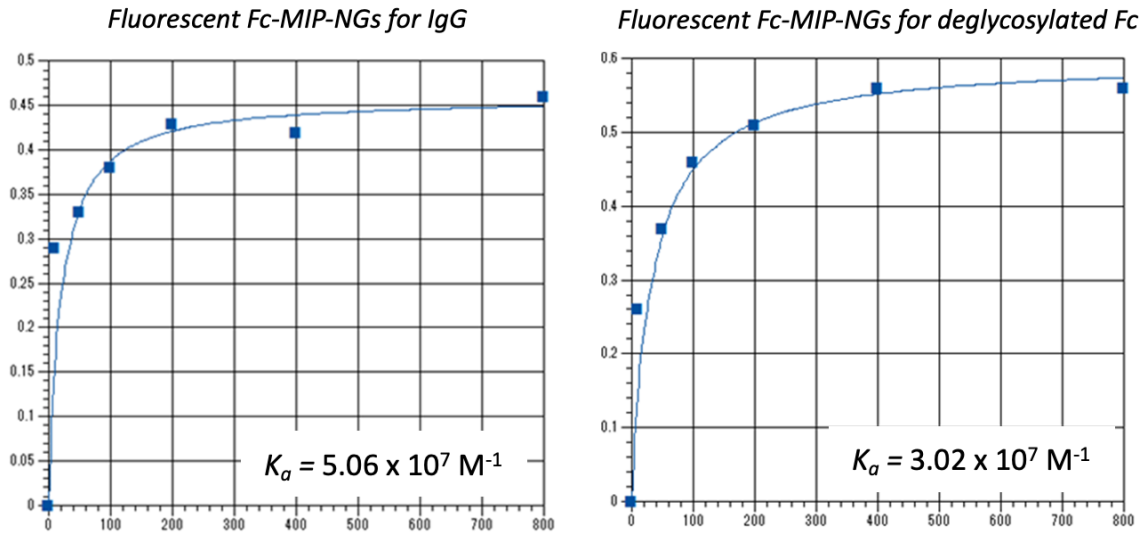

Figure 5.13 Affinity constants (Ka) for the binding of Fc doamin to fluorescent Fc-MIP-NGs and NIP-NGs, estimated from the relative fluorescence intensity measurements data.

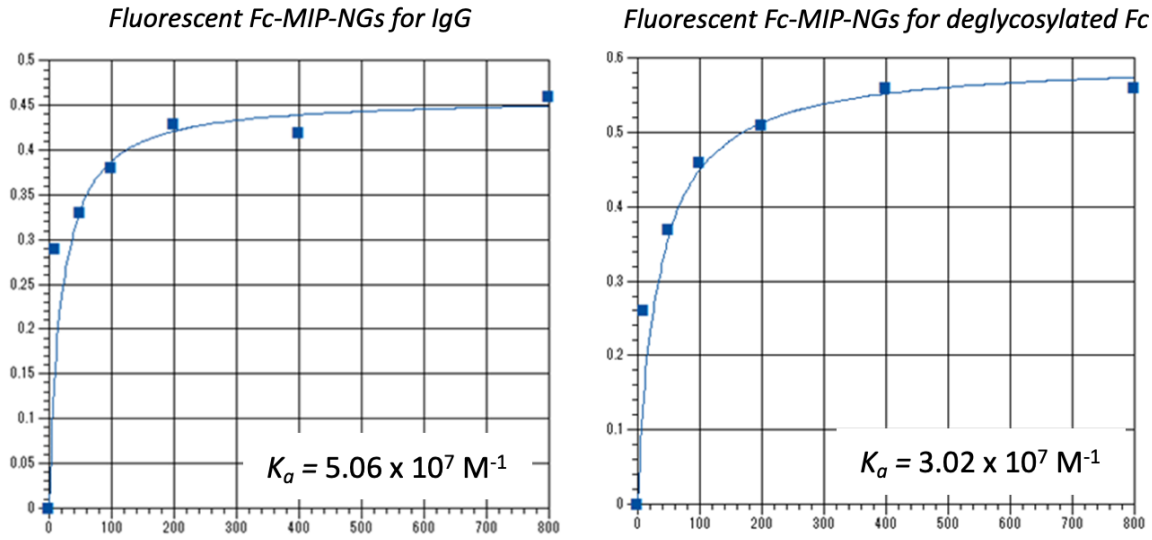

Figure 5.14 Affinity constants (K_a) for the binding of F-MIP-NGs to whole IgG and *deglycosylated Fc domain* estimated from the relative fluorescence intensity measurements data.

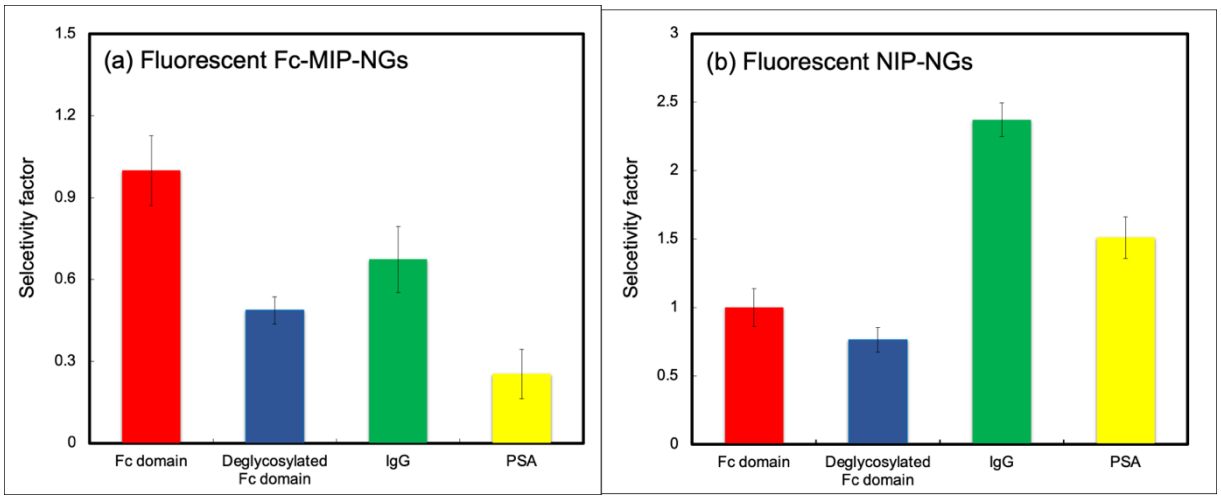

Figure 5.15 Relative fluorescence intensities of fluorescent Fc-MIP-NGs (a) and fluorescent NIP-NGs (b) for Fc domain and four competitive proteins: deglycosylated Fc domain, whole IgG and PSA. The protein concentrations were 100 nM. The error bars were obtained from triplicate experiments.

Thus, these results indicated that the Fc domain specific recognition nanocavities of fluorescent Fc-MIP-NGs were completed formed by the molecular imprinting process, and allowed ATTO 647N to introduce into the nanocavities via the PIMs. In order to develop biotic/abiotic antibody sandwich assay for detection of pork contamination, PSA could be an interfering protein of fluorescent Fc-MIP-NGs to capture anti-PSA in premix solution. However, the high selectivity for Fc domain but low selectivity for PSA provided a potential ability of fluorescent Fc-MIP-NGs to be a fluorescent secondary antibody mimic for pork contamination detection via biotic/abiotic antibody sandwich assay.

5.3.3 Optimization of Assay Conditions.

The four parameters such as the effective blocking reagents, the concentration of anti-PSA and fluorescent Fc-MIP-NGs, and the binding time were investigated using a custom-made liquid handling robot equipped with fluorescence microscope in order to find the best conditions for the developed sandwich assay.

The effect of blocking reagents was optimized by incubation of PBS, Protein free PBS-blocking buffer, 0.1% and 0.5% (w/v) BSA and 0.5% (w/v) skimmed milk for 60 min after immobilization of capture MIP-NGs. Then, the blank assay with premix solutions contained of anti-PSA and fluorescent Fc-MIP-NGs without PSA were performed to evaluate the

appropriate blocking solution. After binding under the blank, 0.5% w/v of BSA blocking reagent was finally selected because it provided the lowest relative fluorescent intensity with blank measurement (Figure 5.16). Under the appropriate blocking reagent, the different concentrations of anti-PSA in premix solution were optimized (Figure 5.17a). The highest response was found to be 0.1 μg/mL of anti-PSA, and the lowest response value was showed at high concentration of anti-PSA owing to the self-binding or overlapping of antibodies in solution. Next, the optimization of fluorescent Fc-MIP-NGs concentration for mixing with 0.1 μg/mL of anti-PSA in premix solution were evaluate (Figure 5.17b). The concentration of 100 μg/mL of fluorescent Fc-MIP-NGs was selected because it gave the greatest response with a smaller amount of fluorescemt Fc-MIP-NGs. Upon increasing of fluorescent Fc-MIP-NGs over 100 μg/mL, the response obtained was slightly different. Thus, the anti-PSA concentration of 0.1 μg/mL and fluorescent Fc-MIP-NGs concentration of 100 μg/mL were ultimately selected as an optimum condition for use in the further experiments. The several incubation times of the PSA binding under the optimized concentration of 10 nM PSA, anti-PSA and fluorescent Fc-MIP-NGs in the premix solution were optimized (Figure 5.18). The optimized binding time was determined to be 30 min because it gave the highest response with minimum incubation time. These results indicated that the proposed assay as biotic/abiotic antibody sandwich assay provided a rapid PSA detection compared to the conventional ELISA based on sandwich assay (4 h analysis time) for 8 times. To confirm the potential ability of this assay with premix solution to decrease the analysis time from 4 h to 30 min, the binding isotherm and sensitivity of step-by-step immobilization of PSA, anti-PSA and fluorescent Fc-MIP-NGs for 1 h incubation of each step with multi-washing system on the sensor chip with immobilized PSA capture MIP-NGs were investigated (Figure 5.19). The binding isotherm and sensitivity of proposed assay with step-by-step immobilization were similar to that of the premix solution immobilization. As seen in Figure 5.20, the relative fluorescence intensity of blank solution of step-by-step immobilization was higher than that of premix solution immobilization as the result of high non-specific binding with multi-steps immobilization and washing. The results, confirm that the proposed sandwich assay for PSA with the premix solution immobilization exhibited high affinity and sensitivity for PSA, and provided the rapid PSA detection compared with step-by-step immobilization frequently used in ELISA.

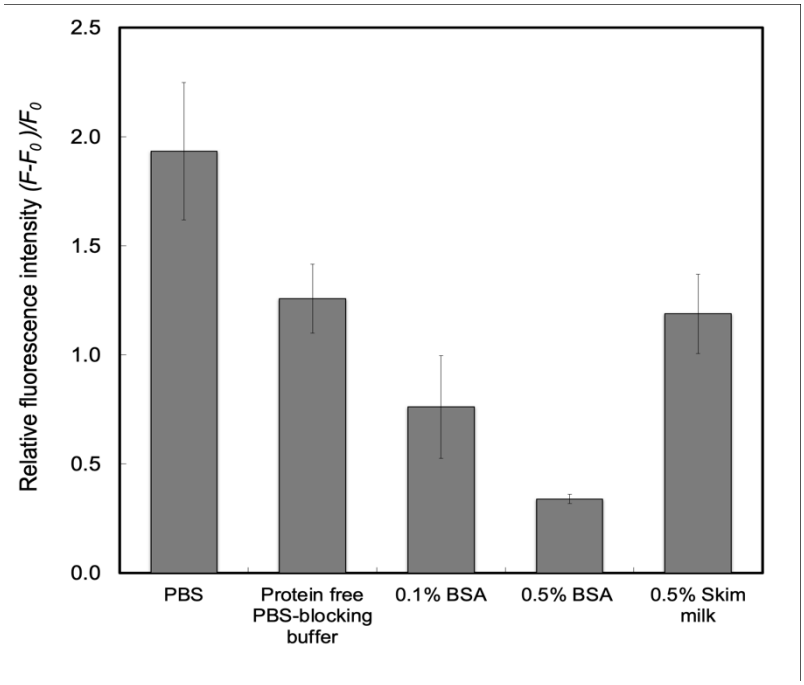

Figure 5.16 Optimization of the blocking reagents on the biomimetic immunosensor of blank (PBS) analysis. The experiments were conducted in triplicate.

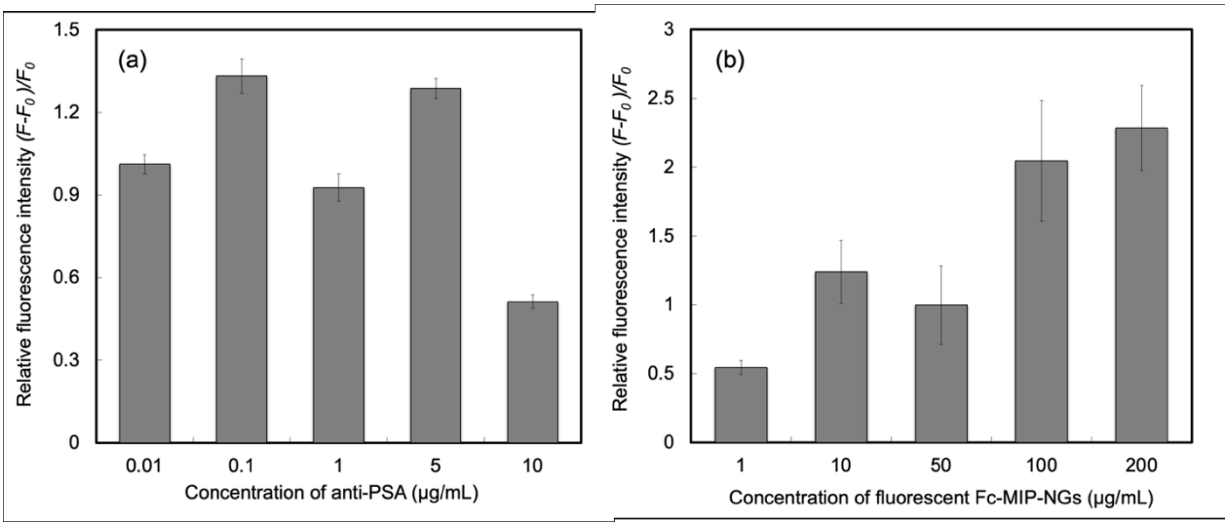

Figure 5.17 Optimization of the different concentrations of anti-PSA as a detection antibody (a). Optimization of the different concentrations of fluorescent Fc-MIP-NGs as a fluorescent secondary antibody mimic (b). The concnetration of PSA was 1 nM. The error bars were obtained from triplicate experiments.

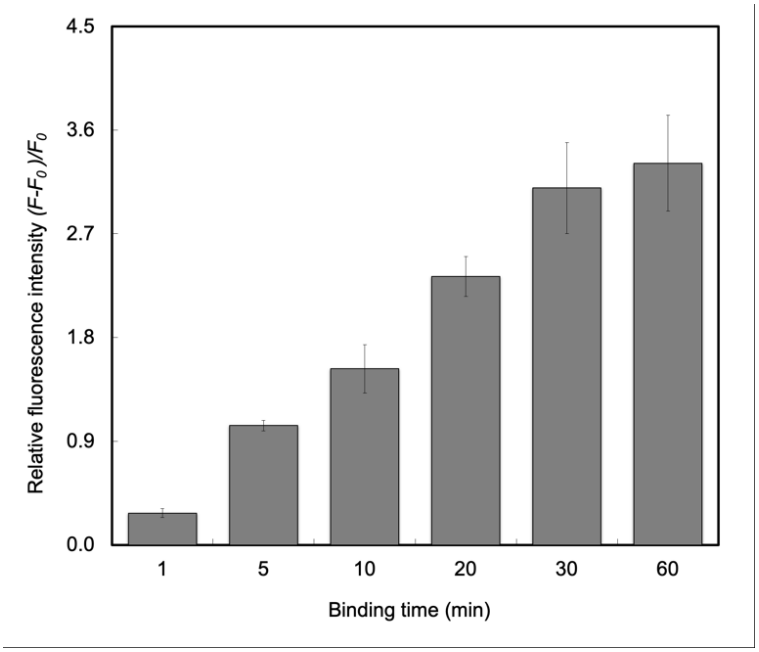

Figure 5.18 Optimization of the binding times. The concnetration of PSA was 10 nM. The error bars were obtained from triplicate experiments.

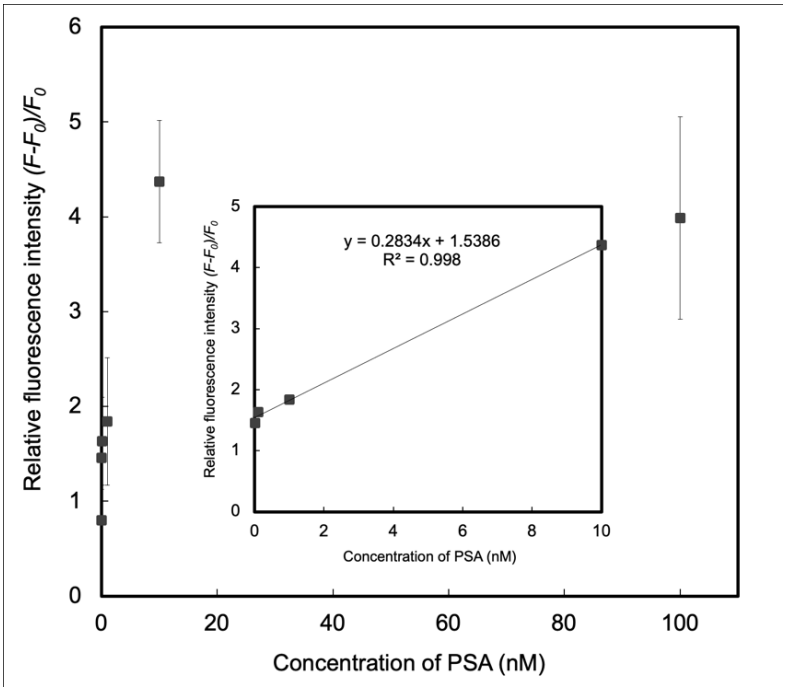

Figure 5.19 The binding isotherm of developed sensor with step-by-step immobilization for PSA (0-100 nM) shows a linear calibration range of 0.01–10 nM (r^2 = 0.998).

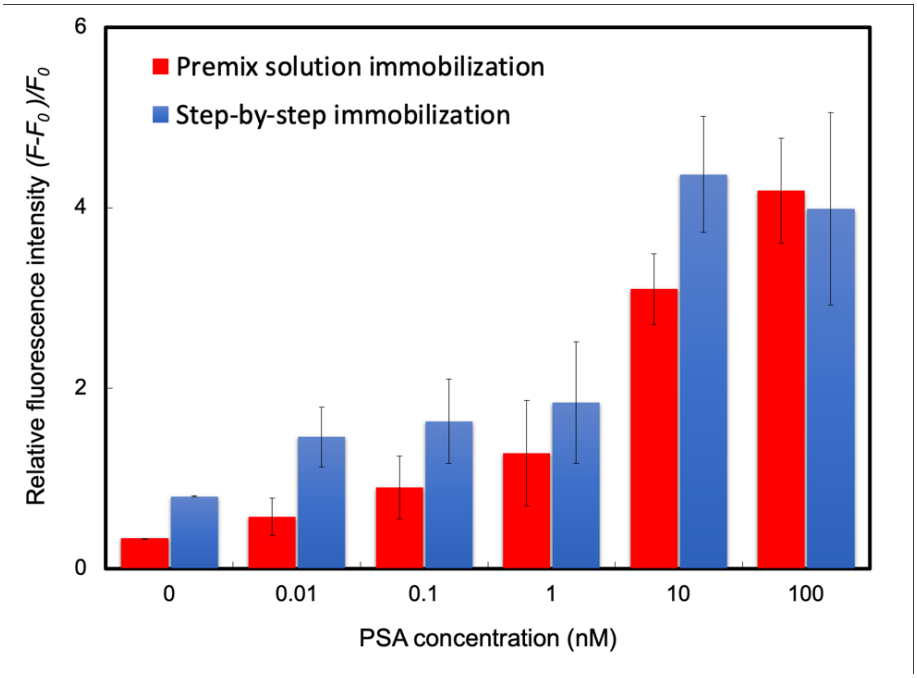

Figure 5.20 The relative fluorescence intensity of PSA binding using the premix solution immobization and step-by-step immobilization. The PSA concentration was 0-100 nM.

5.3.4 Analytical performances of Developed Sandwich Assay for PSA.

The novel biotic/abiotic antibody sandwich assay for PSA was prepared under the optimized conditions using MIP-NGs for PSA as capture antibody mimics and fluorescent Fc-MIP-NGs as fluorescent secondary mimics. In order to developed a selective assay close to the ELISA, the natural anti-PSA was required to be a detection antibody for increasing the selectivity of PSA detection. The gold-coated sensor chips immobilized with capture MIP-NGs for PSA were incubated with the premix solution of anti-PSA and fluorescent Fc-MIP-NGs in different concentration of PSA (0-100 nM), and the fluorescence intensity derived from bound fluorescent Fc-MIP-NGs on sensor chip was measured. The binding isotherm of developed assay for PSA presented a linear calibration range of 0.01–10 nM with $r^2 = 0.969$ (Figure 5.21). The limit of detection (LOD) of PSA for the develop assay was calculated according to 3 SD/m, where m was the slope of the linear part of the binding isotherm, and SD was the standard deviation for 0 nM PSA. The LOD was determined to be 10 pM (0.5 ng/mL). The sensitivity of the novel biotic/abiotic antibody sandwich assay for PSA was higher than that of those my previous MIP-NGs-based QCM sensor[24] and MIP-NGs based-fluorescent sensor.[27] This assay also showed the highest sensitivity of MIP-based sensor for PSA detection compared to the previous reports.[38-39]

The binding affinities of PSA to prepared biotic/abiotic antibody sandwich assay using

mixed fluorescent Fc-MIP-NGs and fluorescent NIP-NGs in the premix solutions were investigated (Figure 5.22a). The relative fluorescence intensity of PSA showed the concentration depending binding to the proposed assay with premix solution containing of Fc-MIP-NGs, such that the relative fluorescence intensities increased with increasing of PSA concentration in solution. On the other hand, the response of fluorescent NIP-NGs was smaller in every concentration, suggesting that the premix solution containing of fluorescent NIP-NGs had low selectivity for developed biotic/abiotic antibody sandwich assay. These results indicated that the high affinity of PSA to the proposed sensor was increased via molecular imprinting process.

To illustrate the selectivity of the PSA biotic/abiotic antibody sandwich assay, the immobilized PSA capture MIP-NGs on the gold-coated sensor chip were incubated with the premix solution containing of 10 nM PSA or four animal serum albumin (BSA, GSA, SSA and RSA) that served as potentially interference matrices, anti-PSA and fluorescent Fc-MIP-NGs. As shown in Figure 5.22b, the premix solution containing of other animal serum albumins exhibited much lower selectivity factor than that of PSA, confirming that the proposed sensor had a great selectivity for PSA. This proposed assay provided the highest selectivity for PSA detection compared with my MIP-Based sensors reported previously.[24,27] These results indicated that the selectivity of developed assay was increased by combination of using artificial PSA antibody and natural PSA antibody for capturing and detection of PSA in solution.

To evaluate the precision of the proposed assay, the reproducibility of SAM preparation, capture PSA MIP-NGs immobilization and blocking process using seven different premix solutions containing of 1 nM PSA were demonstrated. The results as shown in Table 5.1 founded that the reproducibility of developed sensor was determined to be acceptable with the relative standard deviation (%RSD) of 7.5%. The stability of the developed assay was evaluated by detection of 1 nM PSA using immobilized PSA capture MIP-NGs on the gold-coated sensor chip after the storage for 30 days at 4°C (Figure 5.23a). After 30 days incubation, the relative fluorescent intensity was not significantly different to that of the first day preparation, according to my previous study in stability of SAM formation and fluorescent MIP-NGs immobilization on the gold-coated sensor chip under the same condition reported that the fluorescent response was decreased after 45 days incubation at 4°C.[27] These results indicating that the stability of the developed sensor had a great performance of PSA detection at least for 1 month.

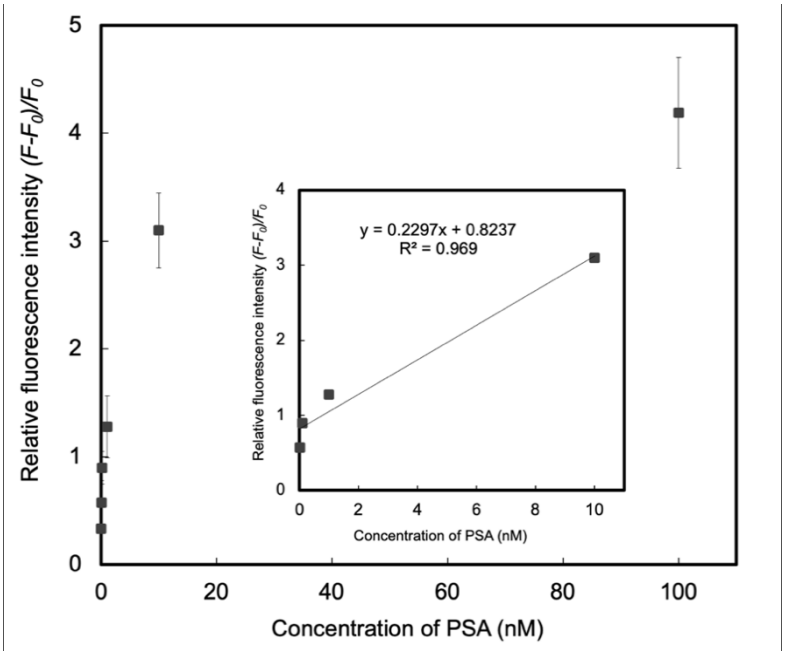

Figure 5.21 The binding isotherm of developed sensor for PSA (0-100 nM) shows a linear calibration range of 0.01–10 nM (r^2 = 0.969). The error bars were obtained from triplicate experiments.

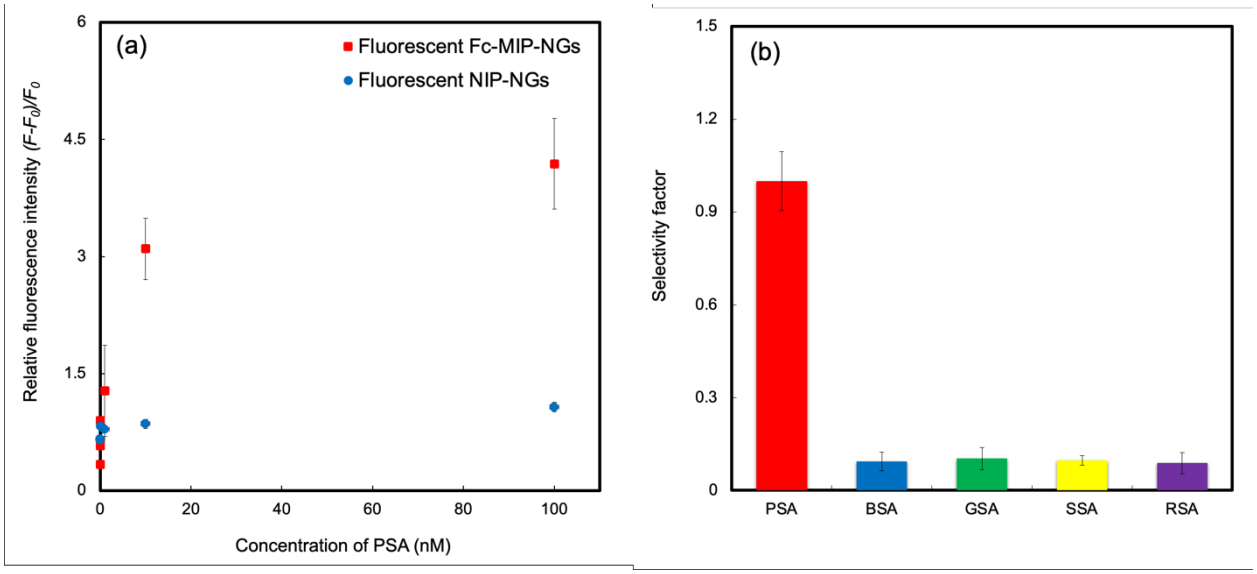

Figure 5.22 (a) The binding isotherms of developed biotic/abiotic antibody sandwich assay for PSA on the various concentrations from 0 to 100 nM. (b) The selectivity factor of developed biotic/abiotic antibody sandwich assay for PSA and four animal serum albumins (BSA, GSA, SSA and RSA) at the protein concentration of 10 nM. The error bars were obtained from triplicate.

Table 5.1 The relativec fluorescence intensities of developed sonsor for 1 nM PSA. The relative standard deviation (%RSD) was calculated from seven triplicate experiments (n=7).

Replicate (Time)	Relative fluorescence intensity $(F-F_0)/F_0$
1	0.9681
2	0.9250
3	1.0261
4	1.1439
5	1.1958
6	0.9697
7	0.9816
Average	**1.0194**
SD	**0.076**
% RSD	**7.50**

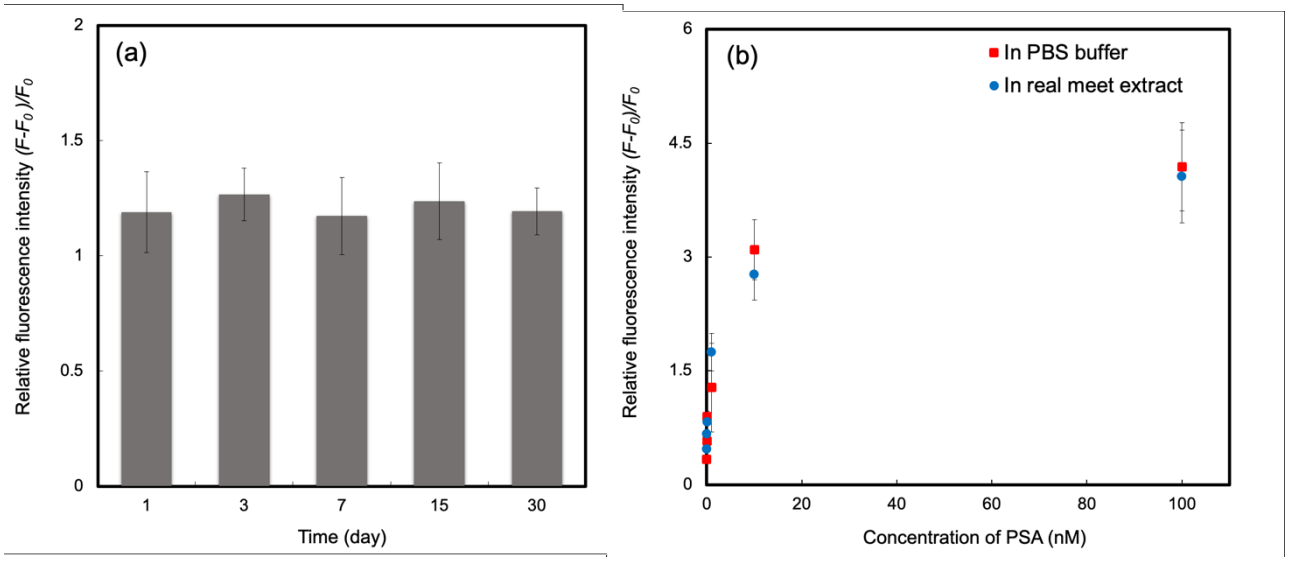

Figure 5.23 Analytical performances of developed biotic/abiotic antibody sandwich assay for PSA. (a) The stability of developed sensor and (b) PSA binding isotherms (0-100 nM) in PBS and real meat extract for developed assay. The error bars were obtained from triplicate.

Table 5.2 The total protein concentration of meat extracts were measured using NanoDrop One UV/Vis Spectrophotometers.

Sample	Protein concentration (mg/mL)
Pork extract	17.17
Beef extract	14.21
Lamb extract	17.79

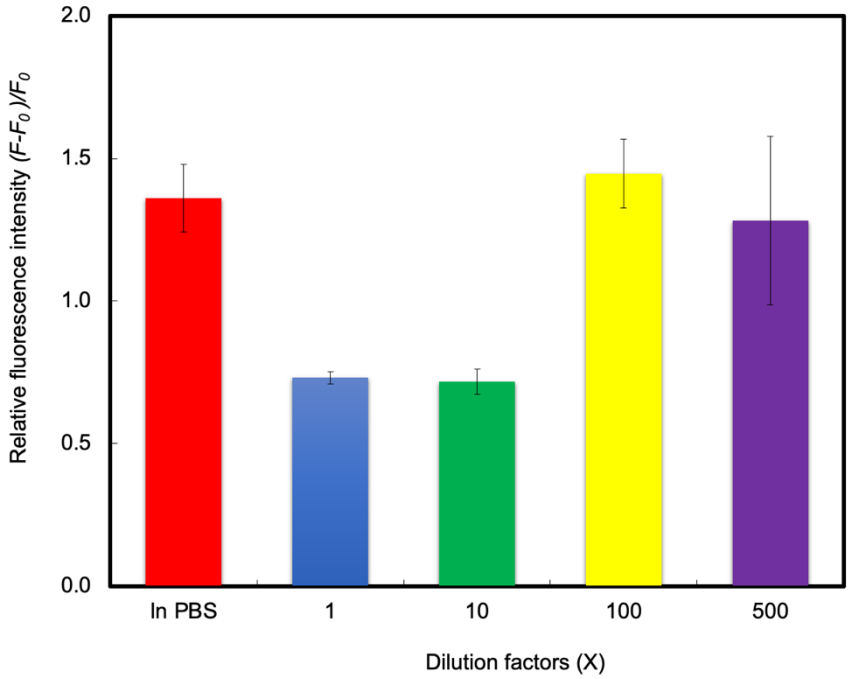

Figure 5.24 The relative fluorescence intensities of spiked 1 nM of PSA into diluted beef extract samples (PBS, 1, 10, 100 and 500-fold dilutions) binding to F-MIP-NGs. Error bars were obtained from triplicate experiments.

5.3.5 The recovery study of Developed assay

In order to detect of PSA in real meat extract samples (Table 5.2), the appropriate dilution factor of meat extract was evaluated to reduce the matrix interference effect for PSA detection. The dilution factors of real meat extract sample in PBS from 1to 500-fold were prepared for detection of 1 nM PSA using the developed assay compared to blank solution (PBS buffer). As shown in Figure 5.24, the relative fluorescence intensity of proposed assay using undiluted and 10-fold diluted were much lower than those of the blank solution due to the interference matrix effects of the real meat extract samples, suggesting that the PSA detection using the developed assay was interrupted by the matrices in meat extract samples. On the other hand, the response of 100- and 500-fold diluted meat extract samples were not significantly different from that of the blank PBS solution, confirming that the appropriated dilution factor of real meat extract sample for PSA detection using the developed assay was founded to be 100-fold dilution factor.

To illustrate the accuracy of the proposed assay, the recovery test by spiking of various concentration of PSA (0-100 nM) into 100-fold diluted meat extract samples were investigated (Figure 5.23b). The binding isotherm of spiked real meat extracts for developed assay was similar to that of PBS solution. Base on the binding profiles, the recovery rate results of developed assay as shown in Table 5.3 was determined to be 90-136%. These results implied that the developed assay exhibited high precision of PSA detection even in real meat extract. Thus, the developed biotic/abiotic antibody sandwich assay had high potential for detection of pork contamination in halal meat extracts.

Table 5.3 The result of recovery rate for determination of PSA in spiked samples (n=3).

Spiked samples (nM)	Measured concentration (nM)	Recovery (%)
0.01	0.012	116
0.1	0.092	92
1	1.36	136
10	8.95	90
100	96.93	97

5.3.5 Detection of Pork Contamination in Halal Meat Extract Samples.

Under the optimum conditions, the proposed assay was applied to detect of pork contamination in halal meat extracts samples (beef and lamb). The simulated pork-contaminated halal meat extract samples were performed by mixing diluted pork extract and halal meat extract solutions in ranges of 0, 0.001, 0.01, 0.1, 1, 10, and 100 wt%. As seen in Figure 5.25a, the fluorescent responses of the proposed sensor increased with increasing of pork contaminated levels in both of beef and lamb extract samples. However, at the response signals of 0.001% of pork contamination in both halal meat extracts were close to those of the negative controls (100% of beef and lamb extracts), with overlapping error bars. For 0.01 wt% contaminated pork in the halal meat extract samples, significant response signals were founded,

with non-overlapping error bars for the non-contaminated halal meat extract, indicating that the detection limit of pork contamination in two halal meat extracts for the proposed assay were determined to be 0.01 wt%. With very low level of pork contaminated detection of 0.01 wt%, the potentiality of the proposed assay for commercial use is significantly efficient for identifying pork contamination in halal raw meat samples, which is commonly high levels contaminated with of pork for business advantages of manufactures. Compare with my previous MIP-based methods for detection of pork contamination in meat extracts,[24,27] the biotic/abiotic antibody sandwich assay developed in this work provided increased sensitivity and selectivity. The sensitivity of the proposed assay was also higher than that of the previous developed immunoassay methods of pork contamination detection based on indirect ELISA (0.5% w/w),[40] sandwich ELISA (0.1% w/w),[41,42] lateral flow immunosensor (0.1% w/w),[43] and enzyme immunoassay (0.1%).[44], and was comparable to the highest sensitivity of pork contamination detection using immunoassay method with the same limit of detection of 0.01 wt%.[44] Moreover, the advantage of my developed assay was not only achieved high sensitivity and selectivity for detection of pork contamination in halal meat extracts but was also reduced the analysis time from 4 h, which is generally analysis time of ELISA, to 30 min.

To evaluate the effectiveness of my developed assay for the detection of pork contamination in halal meat extract samples, the immunosensor based on sandwich ELISA assay for pork contaminated halal meat extract samples was investigated as the same company. The pork contaminations in PBS buffer were conducted as a control method, and the limit of detection was determined to be 0.01 wt% (Figure 5.26a and 5.26b). As seen in Figure 5.25b, the ELISA method cannot detect pork contamination in both halal meat extract at the 0.001 wt% of simulated pork contamination. At 0.01 % of pork contamination, only pork contaminated in beef extract was observed the significantly different OD value with negative control, but was not observed in pork contaminated lamb extract. This observation might be due to the interference effect of the matrices in the raw lamb extracts. These results indicated that my developed assay provided high/comparable sensitivity to ELISA standard method for detection of pork contamination in halal meat extract with more rapid detection.

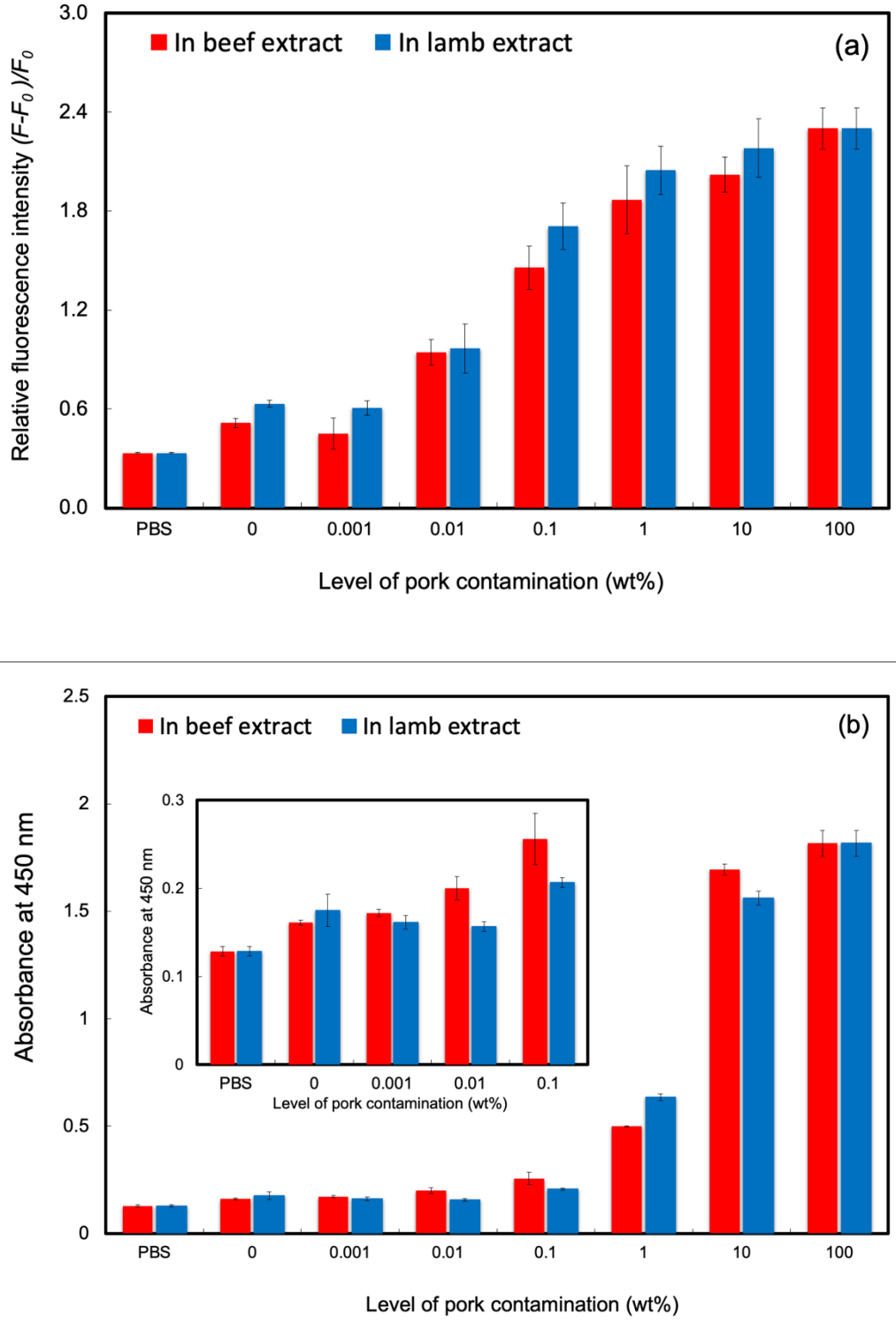

Figure 5.25 Relative fluorescence intensities to the developed assay of pork contaminated halal meat extract samples (beef and goat) in various concentrations (0–100 wt%) (a).; The absorbance at 450 nm of ELISA assay for detection of pork contamination in halal beef extract samples (b). The error bars were obtained from triplicate experiments

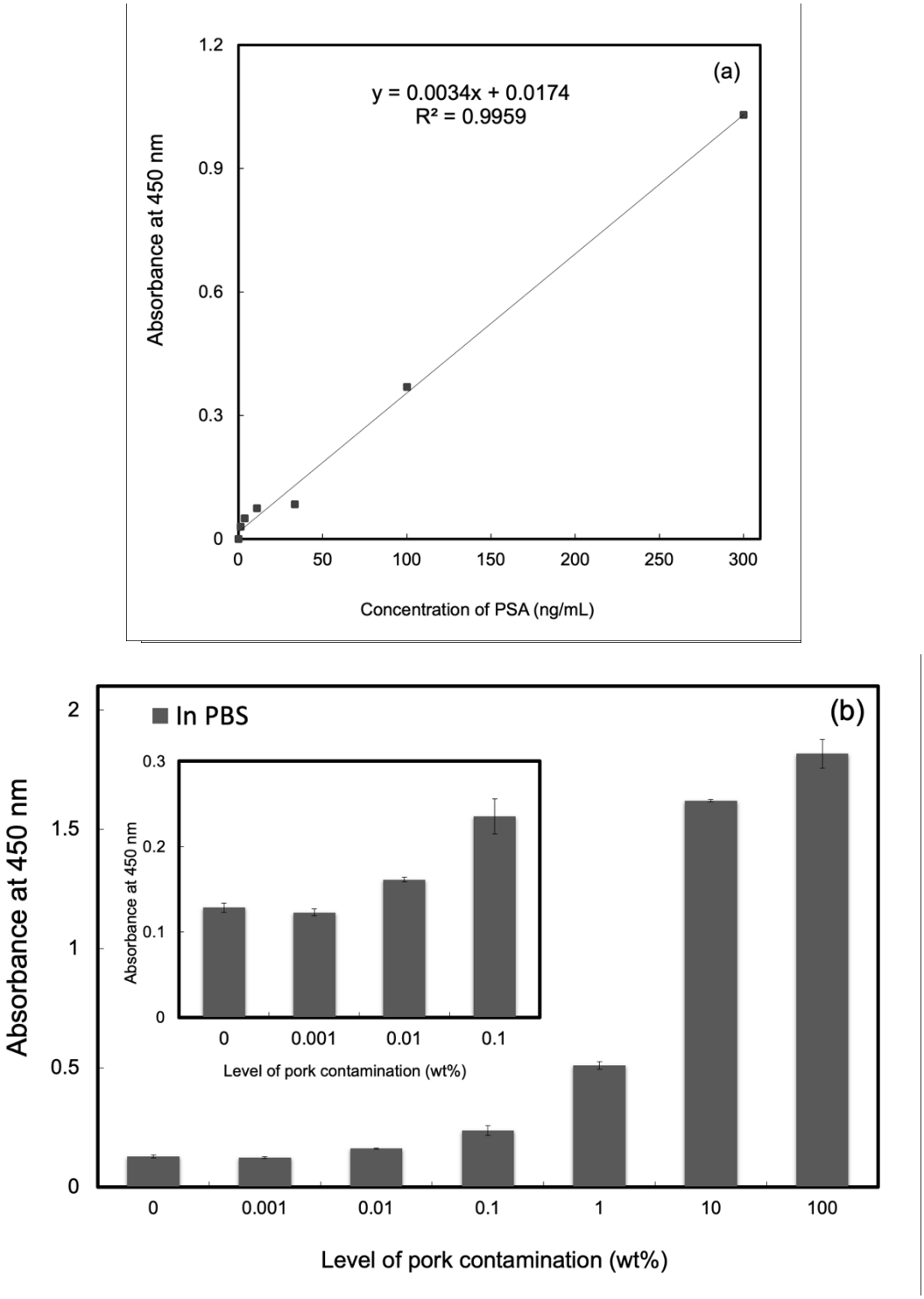

Figure 5.26 The absorbance at 450 (nm) of ELISA assay. (a) the calibration curve of determined for a range of PSA protein standards from 0-300 ng/mL (r^2=0.9959), (b) the ELISA results from various pork contamination in PBS buffer.

5.4 Conclusions

In this work, i have first used the combination of artificial antibody and natural antibody to develop a sensitive biotic/abiotic antibody sandwich assay for sensitive detection of pork contamination in halal meat extracts. Fluorescent Fc-MIP-NGs, where successfully demonstrated using molecular imprinting and PIM with high affinity and selectivity for Fc-domain, were used to be a fluorescent secondary antibody for biotic/abiotic antibody sandwich assay prepared in this work. The assay was able to increase the sensitivity and selectivity of MIP-based sensor. The developed assay exhibited a highly sensitive detection of PSA with very low LOD of 0.5 ng/mL, and excellent selectivity compared to other animal serum albumins (BSA, GSA, SSA and RSA). The good analytical performances were founded to be 30 min of analysis time, 7.5 % RSD of repeatability, >30 days of stability and 90-136% of recovery rate for PSA detection. The proposed assay allowed the fast detection of low level of pork contamination (0.01 wt%) in halal meat extract in 30 min, which was approximately faster than that of ELISA for 8 times. My developed assay has high potential ability to apply in halal biomarker sensing due to its fast detection, sensitivity, specificity, easy preparation, and low-cost demonstration. Therefore, the proposed sandwich assay would be a powerful approach to create a system for specific detection of target protein in wide areas including food analysis, food control, diagnosis and environmental analysis.

5.5 References

1) Qureshi, S.; Jamal, M.; Qureshi, M.; Rauf, M.; Syed, B.; Zulfiqar, M.; Chand, N. J Anim Plant Sci. **2012**, 2292, 79.

(2) Izberk-Bilgin, E.; Nakata, C. C. *Bus. Horiz*. **2016**, 59, 285−292.

(3) Al-Jowder, O.; Kemsley, E. K.; Wilson, R. H. *Food Chem*. **1997**, 59, 195−201.

(4) Teepoo, S.; Mhadbamrung, N.; Moonmungmee, S.; Cheubong, C. *J. Bionanosci*. **2016**, 10, 63-68.

(5) Chikkaveeraiah, B.V.; Bhirde, A.A., Morgan, N.Y.; Eden, H.S.; Chen, X. *ACS Nano*. **2012**, 6, 6546-6561.

(6) Prieto-Simón B.; Bandaru, N.M.; Saint, C.; Voelcker, N.H. *Biosens. Bioelectron*. **2015**, 67, 642-648,

(7) Oh, J.H.; Park, M.K. *Food Control* **2016**, 59, 780-786.

(8) Liu, L.; Chen, F. C.; Dorsey, J. L.; Hsieh, Y.-H. P J. *Food Sci*. **2006**, 71, 1−6.

(9) Lim, S. A.; Ahmed, M. U. *Food Chem*. **2016**, 206, 197−203.

(10) Kuswandi, B.; Gani, A. A.; Ahmad, M. *Food Biosci*. **2017**, 19, 1− 6.

(11) Thienes, C. P; Masiri, J.; Benoit, L. A; Barrios-Lopez, B.; Samuel, S. A; Cox, D. P; Dobritsa, A. P; Nadala, C.; Samadpour, M. *J. AOAC Int*. **2018**, 101, 817−823.

(12) Mandli, J.; El Fatimi, I.; Seddaoui, N.; Amine, A. *Food Chem*. **2018**, 255, 380−389.

(13) Komiyama, M.; Takeuchi, T.; Mukawa, T.; Asanuma, H. Molecular Imprinting: from Fundamentals to Applications; Wiley-VCH: Weinheim, **2003**.

(14) Haupt, K. Molecular Imprinting; Springer-Verlag: Berlin, **2012**.

(15) Schirhagl, R. *Anal. Chem*. **2014**, 86, 250−261.

(16) Takeuchi, T.; Hayashi, T.; Ichikawa, S.; Kaji, A.; Masui, M.; Matsumoto, H.; Sasao, R. *Chromatography* **2016**, 37, 43−64.

(17) Komiyama, M.; Mori, T.; Ariga, K. *Bull. Chem. Soc. Jpn*. **2018**, 91, 1075−1111.

(18) Morishita, T.; Yoshida, A.; Hayakawa, N.; Kiguchi, K.; Cheubong, C.; Sunayama, H.; Kitayama, Y.; Takeuchi, T. *Langmuir* **2020**. 36, 10674–10682.

(19) Takeuchi, T.; Mori, T.; Kuwahara, A.; Ohta, T.; Oshita, A.; Sunayama, H.; Kitayama, Y.; Ooya, T. *Angew. Chem. Int. Ed.* **2014**. 53, 12765–12770.

(20) Guo, T.; Deng, Q.L.; Fang, Z.G.; Liu, C.C.; Huang, X.; Wang, S. *Biosens. Bioelectron.* **2015**. 74, 498–503.

(21) Chen, L.; Wang, X.; Lu, W.; Wu, X.; Li, J.; *Chem. Soc. Rev*. **2016**. 45, 2137–2211.

(22) Rijun, G.; Hui, J.; Huijun, G.; Zonghua, W. *Biosens. Bioelectron.* **2018**. 100, 56–70.

(23) Lucia, C.; Chiara, P.; Paolo, B.; Bossia, A.M. *Talanta* **2018.** 178, 772–779.

(24) Cheubong, C.; Yoshida, A.; Mizukawa, Y.; Hayakawa, N.; Takai, M.; Morishita, T.; Kitayama, Y.; Sunayama, H.; Takeuchi, T. *Anal. Chem*. **2020**. 92, 6401–6407.

(25) Sunayama, H; Ohya, T.; Takeuchi, T. *Chem. Commun*. **2014**, 50, 1347.

(26) Sunayama, H; Kitayama, Y.; Takeuchi, T. *J Mol Recognit*. **2018**, 31, 2633.

(27) Cheubong, C.; Takano, E.; Kitayama, Y.; Sunayama, H.; Minamoto, K.; Takeuchi, R.; Furutani, S.; Takeuchi, T. *Biosens. Bioelectron.* **2021**. 172, 112775.

(28) Li, Y.; Sun, Y.; Beier, R.C.; Lei, H.; Gee, S.J.; Hammock, B.D.; Wang, H.; Wang, Z.; Sun, X.; Shen, Y.; Yang, J.; Xu, Z. *Trends Analyt Chem*. **2017**, 88, 25-40.

(29) Bereli, N.; Ertürk, G.; Tümer, M.A.; Say, R.; Denizli, A. *Biomed Chromatogr*. **2013** 27, 599-607.

(30) Tretjakov, A.; Syritski, V.; Reut, J.; Boroznjak, R.; Volobujeva, O.; Öpik, A. *Microchim Acta*. **2013**, 180, 1433–1442.

(31) Tretjakov, A.; Syritski, V.; Reut, J.; Boroznjak, R.; Öpik, A. *Anal Chim Acta*. **2016**, 902, 182-188.

(32) Bai, R.; Sun, Y.; Zhao, M.; Han, Z.; Zhang, J.; Sun, Y.; Dong, W.; Li, S. *Talanta* **2021**, 226, 122160.

(33) Moczko, E.; Guerreiro, A.; Cáceres, C.; Piletska, E.; Sellergren, B.; Piletsky, S.A. *J Chromatogr B Analyt Technol Biomed Life Sci*. **2019**, 1124, 1-6.

(34) Hayakawa, N.; Kitayama, Y.; Igarashi, K.; Matsumoto, Y., Takano, E.; Sunayama, H.; Takeuchi, T. *ACS Appl. Mater. Interfaces*, Revision submitted.

(35) Saeki, T.; Takano, E.; Sunayama, H; Kitayama, Y.; Takeuchi, T. *J. Mater. Chem. B*, **2020**, 8, 7987.

(36) Bennett, K.L.; Smith, S.V.; Truscott, R.J.; Sheil, M.M. *Anal Biochem*. **1997**, 245, 17-27.

(37) Kutzner, T.J.; Higuero, A.M.; Süßmair, M.; Kopitz, J.; Hingar, M.; Díez-Revuelta, N.; Caballero, G.G.; Kaltner, H.; Lindner, I.; Abad-Rodríguez, J.; Reusch, D.; Gabius, H.J. *Biochim Biophys Acta Gen Subj*. **2020**, 1864, 129449.

(38) Li, Q.R.; Yang, K.G.; Liu, J.X.; Zhang, L.H.; Liang, Z.; Zhang, Y.K.; Li, S. *Microchim Acta***. 2016**. 183, 345–352.

(39) Qin, Y.P.; Wang, H.Y.; He, X.W.; Li, W.Y.; Zhang, Y.K. *Talanta* **2018**, 185, 620–627.

(40) Chen, F.C.; Hsieh, Y.H. *J. AOAC Int*. **2000**, 83, 79-85.

(41) Liu, L.; Chen, F.C.; Dorsey, J.L.; Hsieh, Y.H. *J. Food Sci*. **2006**. 71, 1–6.

(42) Thienes, C. P.; Masiri, J.; Benoit, L. A.; Barrios-Lopez, B.; Samuel, S.A.; Cox, D. P.; Dobritsa, A. P.; Nadala, C.; Samadpour, M. *J. AOAC Int*. **2018**, 101, 817−823.

(43) Kuswandi, B.; Gani, A.A.; Ahmad, M. *Food Biosci.* **2017.** 19, 1–6.

(44) Mandli, J.; Fatimi, I.E.; Seddaoui, N.; Amine, A. *Food Chem*. **2018**. 255, 380–389.

Chapter 6

General Conclusion and Perspectives

General Conclusions and Perspectives

In this Ph.D. dissertation, i have proposed the great potential ability of molecularly imprinted polymers as selective artificial receptors for detection of pork contamination in halal food control applications through the three novel MIP-based sensors.

In the first development of MIP-based sensor, i have successfully synthesized and characterized molecularly imprinted nanogels (MIP-NGs) for highly specific recognition of porcine serum albumin (PSA) via nano-imprinting technology and emulsifier-free precipitation polymerization. The method to prepare the MIP-NGs in this study is most productive and very simple because functional monomer, co-monomer, cross-linker, and template protein can be mixed together in one-pot polymerization system. This molecular imprinting method could be applicable to other animal serum albumins. After immobilization of MIP-NGs on the QCM sensor chip through carbodiimide coupling, i have first developed and applied the MIP-NGs-based QCM sensor for greatly and specific selective detection of PSA and pork contamination in halal raw meats. The studies achieved high selectivity of MIP-NGs for PSA when compared to different animal serum albumins, confirming that the developed MIP-NGs demonstrated good selectivity for PSA. For analytical performance tests, the proposed sensor showed the high recovery rates with spiking the PSA standard into the meat extract samples, and was able to detect a level of pork adulteration in beef samples as low as 1wt%. Hence, the MIP-NGs-base sensor could provide a new advanced powerful method with reliability and high selectivity to detect pork contamination in halal raw meat samples.

Second, i have first developed a highly sensitive MIP-NGs fluorescence-based sensor for detecting PSA as a marker for pork contamination in halal food control. F-MIP-NGs were synthesized by emulsifier-free precipitation polymerization with a bivalent functional monomer as 4-[2-(N-methacrylamido)ethylaminomethyl] benzoic acid, where consists of benzoic acid moiety for interaction with template molecules and secondary amine group for conjugation of fluorescent reporter dyes. Then, the post-imprinting modification (PIM) via introduction of ATTO647N-NHS into nano-cavities of nanogels is performed to produce the fluorescence signal after the binding of protein targets. The fluorescence signal responses were measured using a fluorescence microscope in a custom-made liquid-handling robot. Under the optimized experimental conditions, the proposed sensor achieved not only good

affinity and selectivity but also high sensitivity of fluorescence response for PSA with low limit of detection (LOD: 40 pM). Furthermore, the proposed sensor showed excellent analytical performance in terms of rapid detection, repeatability, and stability for detection of PSA. Even in real meat extract samples, the high recovery rates of PSA were shown from PSA spiked beef extract. Finally, the F-MIP-NGs fluorescence-based sensor detected a very low level of pork contamination in beef extract samples as low as 0.01 wt%, ten time higher than that of previous developed QCM-based sensor. Therefore, the F-MIP-NGs-based sensor provides a new rapid fluorescence-based method to detect pork contamination in halal raw meat samples with high sensitivity, selectivity, and reliability. In applications, i believe that the fluorescent MIP-NGs as an artificial receptor can be alternative to natural antibodies for food analysis.

Third, i have first used an artificial antibody and natural antibody to develop a novel biotic/abiotic antibody sandwich assay for sensitive detection of pork contamination in halal meat extracts. The artificial antibodies used in this work are MIP-NGs targeting of PSA as a capture antibody mimic and fluorescent Fc-MIP-NGs as a fluorescent secondary antibody mimic. The fluorescent Fc-MIP-NGs were prepared by emulsifier-free precipitation polymerization with a bivalent functional monomer as 4-(2-Methacrylamidoethyl aminomethyl) phenylboronic acid (FMB), where consists of boronic acid for interaction with glycan of Fc-IgG fragment and secondary amine group for conjugation of ATTO fluorescence dyes. The proposed recognition materials provided a high sensitivity and selectivity for Fc domain, and i believed that it can be potential artificial secondary antibody for use in halal biomarker assay. Then, the developed assay was able to increase the sensitivity and selectivity of MIP-based sensor. The developed assay exhibited a highly sensitive detection of PSA with very low LOD of 0.5 ng/mL, and excellent selectivity compared to other animal serum albumins (BSA, GSA, SSA and RSA). The proposed assay allowed the fast detection of low level of pork contamination (0.01 wt%) in halal meat extract in 30 min, which was approximately faster than that of ELISA for 8 times. My developed assay has high potential ability to apply in halal biomarker sensing due to its fast detection, sensitivity, specificity, easy preparation, and low-cost demonstration.

To further extend my investigations, the proposed sensor should be applied to detect pork contamination in processed meat products, which are the most preferred halal food products in the market. This study is a first step forward in evolution of the developing advanced MIPs as MIP-based sensors for halal food control in the real-world application. The

future work may also focus on the application of F-MIP-NGs, achieved by molecular imprinting and PIM, in protein markers for human health such as HSA or IgG, for biosensor or bioimaging of therapeutics and diagnosis. Finally, i believe that the new application of MIP-based sensor can be expected by combining the specific recognition of advance molecularly imprinted materials with recent technology of biosensors such as micro array or paper-based system.

Publication list

Molecularly Imprinted Nanogels Capable of Porcine Serum Albumin Detection in Raw Meat Extract for Halal Food Control

Chehasan Cheubong, Aoi Yoshida, Yuki Mizukawa, Natsuki Hayakawa, Minako Takai, Takahiro Morishita, Yukiya Kitayama, Hirobumi Sunayama, Toshifumi Takeuchi

Analytical chemistry, 92 (9), 6401–6407, **2020**.

Molecularly Imprinted Polymer Nanogel-based Fluorescence Sensing of Pork Contamination in Halal Meat Extracts

Chehasan Cheubong, Eri Takano, Yukiya Kitayama, Hirobumi Sunayama, Kazuaki Minamoto, Ryota Takeuchi, Shunsuke Furutani, Toshifumi Takeuchi

Biosensors and Bioelectronics, 172, 112775, **2021**.

A Biotic/Abiotic Sandwich Assay for Highly Sensitive Detection of Pork Adulteration in Halal Meat Extract

Chehasan Cheubong, Hirobumi Sunayama, Eri Takano, Yukiya Kitayama, Hideto Minami, Toshifumi Takeuchi

*Submitted, **2022***

Reference publication

Molecularly Imprinted Nanogels Possessing Dansylamide Interaction Sites for Controlling Protein Corona in situ by Cloaking Intrinsic Human Serum Albumin

Takahiro Morishita, Aoi Yoshida, Natsuki Hayakawa, Kentaro Kiguchi, **Chehasan Cheubong**, Hirobumi Sunayama, Yukiya Kitayama, Toshifumi Takeuchi

Langmuir, 36 (36), 106754-10682, **2020**.

Doctor Dissertation, Kobe University
"Molecularly Imprinted Polymers-Based Sensor for Halal food Control", 161 pages

Submitted on January 21th, 2022

The date of publication is printed in cover of repository version published in Kobe University Repository Kernel.